Understanding how the chloroplasts contribute to wheat susceptibility to rust fungi

Francesca Jane Minter

A thesis submitted for the degree of Doctor of Philosophy

University of East Anglia

John Innes Centre

December 2023

This page is intentionally left blank.

Abstract

Wheat rust fungi of the *Pucciniaceae* family, including *Puccinia striiformis* f. sp*. tritici* (*Pst*), pose a significant and sustained threat to global wheat production. Previous research has shown that yield losses associated with wheat rust infection primarily result from a reduction in the photosynthetic capacity of the plant. Additionally, it is widely understood that the chloroplasts are a hub for the synthesis and release of a number of pro-defence molecules including reactive oxygen species, calcium ions and salicylic acid, making them important organelles for coordinating the immune response. However, the molecular details of how chloroplast processes are manipulated during wheat infection with rust fungi remain to be elucidated. The main objective of this project was to investigate the ways in which wheat chloroplast processes contribute to rust susceptibility. To this aim, RNA-sequencing was carried out prior to the onset of this project on *Pst*-infected wheat tissue over time, revealing that many nuclear genes encoding chloroplast-localised proteins (NGCPs) had expression patterns that correlate with resistance to *Pst* at later stages of infection. I then selected the chloroplast metallopeptidase of unknown function (*TaCPEP*), which followed this pattern of expression, for further analyses. We obtained disruption mutants from a tetraploid and hexaploid Targeted Induced Local Lesions In Genomes (TILLING) population and showed that *TaCPEP* disruption increases susceptibility to both *Pst* and *Magnaporthe oryzae* pathotype *triticum* and may reduce chlorophyll content and chloroplast size, but without affecting the rate of assimilation. This thesis provides insight into the ways in which chloroplastic processes are altered during wheat infection with *Pst* and how one gene specifically may play a key role in susceptibility.

Table of contents

List of figures

List of tables

Common abbreviations

AAA protein	ATPases associated with diverse cellular activities
ABA	Abscisic acid
Avr/avr	Avirulence (gene/protein)
BLAST	Basic Local Alignment Search Tool
BSMV	barley stripe mosaic virus
CAS	Calcium sensing receptor
CBB	Calvin Benson Bassham Cycle
CHUP1	Chloroplast Unusual Positioning 1 protein
CL1	Uncharacterised protein
CL2	Uncharacterised protein
CPEP	Uncharacterised peptidase
cROS	Chloroplastic reactive oxygen species
cTP	Chloroplast transit peptide
DEG	Differentially Expressed Gene
dpi	days post inoculation
dpvi	days post viral inoculation
ETI	Effector-triggered immunity
FtsH	Filamentous temperature sensitive H
FtsHi	Inactive filamentous temperature sensitive H
GO	Gene ontology
hpi	Hours post inoculation
HR	Hypersensitive response
JA	Jasmonic acid
KASP	Kompetitive Allele Specific PCR

MoT	*Magnaporthe oryzae* pathotype *Triticum*
MSA	Multiple sequence alignment
NGCPs	Nuclear Genes encoding Chloroplast Proteins
NHP	**N-Hydroxypipecolic acid**
NLR	Nucleotide-binding leucine-rich repeat protein
NRIP	N-receptor interacting protein
PAMP	Pathogen-associated molecular pattern (syn. Elicitor)
PCR	Polymerase chain reaction
Pgt	*Puccinia graminis* f.sp. *tritici*
PR	pathogenesis related (gene/protein)
PRK	Phosphoribulokinase
Psah2	Photosystem I reaction centre subunit VI
PsbP	Photosystem II subunit P
PsbQ1	Photosystem II subunit Q-1
PsbQ2	Photosystem II subunit Q-2
Pst	*Puccinia striiformis* f.sp. *tritici*
PSI	Photosystem I
PSII	Photosystem II
PTI	PAMP-triggered immunity
RNS	Reactive nitrogen species
ROS	Reactive oxygen species
RSC	Rubisco Small Chain
SA	Salicylic acid
SIFT	Sorting Intolerant From Tolerant
TILLING	Targeted Induced Local Lesions IN Genomes
TPM	Transcripts Per Million

VIGS	Virus-induced gene silencing

Definitions of key terms

Biotic stress: A stress caused by another living organism such as fungi, bacteria, viruses, herbivores, or parasitic plants.

Biotrophic pathogen: A pathogen that requires living host tissue to complete its life cycle.

Effector: Proteins secreted by plant-associated pests or pathogens to modulate host processes.

Effector triggered immunity (ETI): Defence response triggered by the recognition of pathogen-derived effector proteins.

Hemi-biotrophic pathogen: A pathogen that first establish a biotrophic interaction with host, then switches to a necrotrophic phase where host tissue is killed.

Homoeologues: genes in the same species derived from allopolyploidy.

Necrotrophic pathogen: A pathogen that establishes an interaction with its host whereby the host tissue is killed for nutrient acquisition.

Pathogen associated molecular pattern (PAMP): An immunogenic molecule with a conserved motif that function as ligands for plant cell surface receptors and trigger PTI.

PAMP-triggered immunity (PTI): Defence response triggered by the recognition of pathogen-associated molecular patterns.

Resistance: The extent to which the immune responses restrict pathogen colonisation or nutrient acquisition.

Susceptibility: The inability of a plant to mount sufficient immune responses to restrict pathogen growth or nutrient acquisition.

Susceptibility gene: A plant gene that manipulated by pathogens to enable growth and/or nutrient acquisition, rendering the host susceptible.

Wheat Targeted Induced Local Lesions in Genomes (TILLING) mutants: A population of EMS-mutagenised wheat plants of tetraploid variety Kronos or hexaploid variety Cadenza. Mutations in protein coding regions were identified and the consequence on protein function predicted.

Acknowledgements

Thank you to my supervisor, Professor Diane Saunders, for giving me the opportunity to begin my journey in science as an undergraduate student back in 2017, and for continuing to invest in me for seven years after. Thank you to my secondary supervisor, Nick Talbot, for contributing knowledge and guidance to my PhD, and for supporting me through six years in the Gatsby Plant Science Network.

Choosing to do a PhD was a challenge I felt ready for, but doing a PhD during a global pandemic is something none of us were prepared for. There were times it felt impossible to continue this journey, but it was the people who kept me going. Thank you to all the current and past members of the Saunders Lab who each made this undertaking a little more enjoyable every day, and for always reminding me of how exciting science can be. A huge thanks to Cassandra, Pilar, Vanessa, Nicola, and Guru for always being happy to listen, support and advise (even for years after you'd left), you were all an integral part of my formative years in science, making me the scientist I am today. Will, it was a pleasure to do this PhD journey with you, thank you for being a friend and for always being there to chat. Swathy, Ces, Sarah and Rita, thank you all for being so kind and thoughtful and for bringing new energy to my days in the lab after years of lockdowns and scheduling.

Outside of the lab, Amy, Emily, and Chloe, thank you for being the kindest university housemates and for helping me though four years of undergrad. Your continued encouragement and perspectives throughout my PhD were so valuable in helping me see the bigger picture. I am lucky to have had nearly a decade of your friendships.

To my parents and sisters (and Gus), thank you for a lifetime of support, especially for the past 8 years where the pressure and stress has been the greatest and I probably wasn't always the easiest company. For weekends by the sea, for keeping me grounded and always reminding me to take breaks. Amanda, Rob, Charlotte, and Otis, thank you for welcoming me into your family and for lovely Cambridgeshire mini-breaks. To my niece, Daisy, the most joyful three-year-old, thank you for always making me smile. Thank you for singing, dancing, laughing, and helping me see what's truly important in life.

Finally, to Joshua, my partner and best friend. Thank you for always making me laugh, especially when my PhD made me cry. I don't know if I would have made it to the end of this journey without your love, support, patience and understanding. Now, we get to decide what our future holds, and I can't wait.

1. General introduction

1.1. Fungal pathogens pose a significant threat to global wheat production

Climate change caused by human activity accounts for around 30% of the variability in the yearly yield for the most widely grown crops worldwide with trends moving towards stagnated or decreasing yields (Lobell and Field, 2007). Furthermore, the probability of simultaneous catastrophic crop failures in the main food growing regions has increased significantly since 1991 (Gaupp *et al.*, 2020). With the ever-growing requirement of our agricultural practices to minimise impact on biodiversity and contribution to the climate crisis (Abbass *et al.*, 2022; Norris, 2008) our global food systems are fragile (Mehrabi, 2020). There is a debate as to the best approach to maintain food security and increase food production. Whilst some argue that we should diversify the crops we grow, others want to prioritise research and development of existing staple food crops to increase their yields in line with the growing population (Grote *et al.*, 2021). Wheat is one of those staple food crops, and feeds 35% of the global population, providing around 20% of the daily protein and calories worldwide, making it of significant social and economic importance (Erenstein *et al.*, 2022). Wheat production faces a sustained threat from a changing environment (Pequeno *et al.*, 2021). Climate change is causing more unpredictable seasonal temperatures, rainfall and pest and disease outbreaks. Pests and diseases alone cause the annual loss of 20% of wheat produced globally and fungal pathogens specifically constitute a major group of these (Savary *et al.*, 2019).

Rust fungi including *Puccinia striiformis* f. sp. *tritici* (*Pst*), *Puccinia triticina (Pt)* and *Puccinia graminis* f. sp. *tritici* (*Pgt*) cause yellow, leaf and stem rust disease (YR/LR/SR) of wheat, respectively, and lead to combined losses of wheat equating to around $5 billion per year (Figueroa *et al.*, 2018). The primary strategies for disease control against *Pst* and *Pgt* include widespread preventative use of chemical fungicides and strategic planting of resistant wheat varieties (Carmona *et al.*, 2020; Dracatos *et al.*, 2023). However, fungicides are prohibitively expensive for many farmers in developing countries and the application of fungicides drives selection pressure for fungicide resistance (Carmona *et al.*, 2020). To promote sustainable agricultural practices, some fungicides have been banned or are being reviewed under safety concerns (Anastassiadou *et al.*, 2020; Arena *et al.*, 2018). Therefore, whilst historically *Pst* and *Pgt* have been well-controlled in major wheat-growing regions, including Western Europe, we are currently precariously positioned at risk of epidemics. This has been evidenced by the potential re-emergence of SR in the UK, as detected on both wheat in 2013 (Lewis *et al.*, 2018) and barley in 2019 (Orton *et al.*, 2019), after more than 60 years without a recorded outbreak (Lewis *et al.*, 2018). Additionally, in 2017 there was a devastating outbreak of YR in Argentina in

regions previously unaffected by the disease that spread to three million hectares of wheat field (Carmona *et al.*, 2019; Hovmøller *et al.*, 2019).

The complex life cycle of cereal rust fungi can be broadly separated into sexual and asexual phases which are completed on different host plant species, as illustrated in **Figure 1.1**. The asexual stage occurs on grasses, including wheat, making it the stage that has the potential to cause yield reduction (Schwessinger, 2017). During the asexual phase, clonal urediniospores colonise the aerial parts of wheat and other grasses (Eriksson, 1894). Upon successful entry to the plant, rust fungi form specialised feeding structures called haustoria which invaginate the plant cell membrane, creating an interface for the rust fungi to acquire host sources of carbon and secrete proteins into the plant cell to manipulate host processes to facilitate pathogenesis (Voegele and Mendgen, 2003). Studies have shown that sugar is one of the main nutrients exchanged between wheat and rust fungi upon infection which can alter the source or sink status of tissues (Lata *et al.*, 2023). Phytohormones, particularly abscisic acid (ABA), have been implicated in mediating this transition during infection by upregulating the expression of sugar transporters. Recently, it has been shown that the wheat sugar transporter genes *TaSTP3*, *TaSTP6* and *TaSTP13* are upregulated or activated in response to *Pst* (Huai *et al.*, 2019; Huai *et al.*, 2020; Huai *et al.*, 2022). Further investigation found that upregulation of *TaSTP6* is triggered by ABA, and that *Pst* promotes the accumulation of ABA to induce this response (Huai *et al.*, 2019). Not only can rust fungi hijack host sugar transporters to acquire nutrients, but the genomes of rust fungi are also known to have highly expanded metal and oligopeptide transporter families which may aid nutrient transport (Guerillot *et al.*, 2023). Although a delicate balance must be struck between acquiring nutrients and keeping host tissue viable, ultimately, wheat infected with rust fungi have low yield and produce unviable seed (Bouvet *et al.*, 2022). It is thought that reductions in photosynthetic processes in adult plants lead to this yield reduction (Chen *et al.*, 2015).

The final stage of the asexual cycle occurs when urediniospores emerge from pustules on the leaf surface. Released from these pustules are clonal urediniospores which are carried by wind currents to new plants which locally leads to cyclical infection within the same field over the growing season and global incursions of new pathogen races (Chen *et al.*, 2014). A recent study of the UK *Pst* population demonstrates the importance of both local and global spore dispersal. In this study, the authors used a Field Pathogenomics technique which involves performing RNA-seq on *Pst*-infected infected field samples (Hubbard *et al.*, 2015). It was revealed that the UK *Pst* population recently experienced a major shift to one with little genetic similarity to the historical population (Hubbard *et al.*, 2015). The authors suggest that this could have occurred due to exotic incursions from outside the UK. Whilst understanding population

dynamics over a long period of time is useful for tracing the origins and evolutionary history of the rust fungi, rapid diagnostics is required for crop protection. The Mobile And Real-time PLant disEase (MARPLE) tool developed by Radhakrishnan *et al.* (2019) enables rapid identification of *Pst* isolates in the field. This enables crop protection methods such as informed planting of resistant varieties to be implemented.

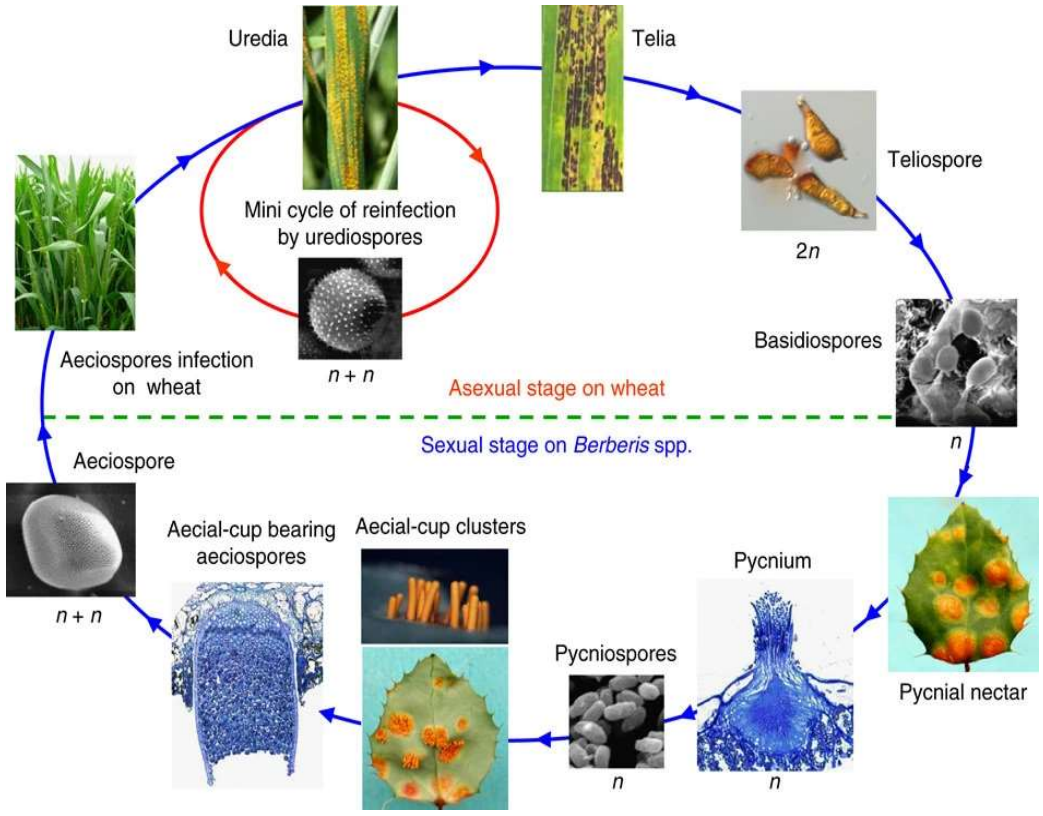

Figure 1.1. The life cycle of wheat rust fungi *Puccninia striiformis* f. sp. *tritici* (*Pst*).

The life cycle occurs in two stages on two different host plants with the asexual stage on wheat and the sexual stage on barberry. The uredia are responsible for the yield losses in wheat during the growing season, and for the widespread dispersal of spores both locally within the field, and globally via wind currents. This figure was published in Zheng *et al.* (2013) and is reused with permission from copyright holders under the Creative Commons Licence.

1.2. Molecular wheat-rust interactions

Whilst rapid advances in our understanding of the cereal rusts at the population level have been made utilising new and advancing genomic technology, elucidating the molecular responses of wheat to rust fungi has been slower. The rusts, as obligate biotrophic fungi, are unable to be artificially cultured and are recalcitrant to conventional methods of transformation (Lorrain *et al.*, 2019). These limitations have been major barriers in elucidating important determinants of host susceptibility and fungal pathogenicity. For example, avirulent effectors

(Avrs) are pathogen encoded proteins that can be recognised by host receptors to trigger resistance mechanisms (Jones and Dangl, 2006). These proteins are key for tracking populations and can accelerate the cloning and subsequent deployment of resistance genes (Vleeshouwers *et al.*, 2008). Because of the intractability of the wheat rust fungi, it was only six years ago that the first *Avrs* were cloned from *Pgt* (Chen *et al.*, 2017b; Salcedo *et al.*, 2017). However, recent advances in techniques such as virus-induced gene silencing (VIGS) and host-induced gene silencing (HIGS) have helped to study the function of fungal and plant genes *in planta* (Bakkeren and Szabo, 2020). Also, the creation of wheat genetic resources such as the TILLING (Targeted Induced Local Lesions in Genomes) mutant populations and improvements in genome editing in wheat have opened up new opportunities to address important research questions about the wheat-rust interaction (Krasileva *et al.*, 2017; Zhang *et al.*, 2016). Together these developments have accelerated the study of the wheat-rust fungi pathosystem and expanded the functional characterisation of several genes implicated in contributing to susceptibility or resistance. For example, the Rac protein TaRac6, the lipid transfer protein TaLTP3, the sugar transporter TaSTP6 and the branch chain amino acid transferase TaBCAT1 have all recently been implicated in contributing to wheat susceptibility to *Pst* (Corredor-Moreno *et al.*, 2021; Huai *et al.*, 2022; Zhang *et al.*, 2020; Zhao *et al.*, 2021). Although valuable knowledge has been contributed to the field of wheat-rust interactions, there is still more to learn about the establishment of biotrophy, host manipulation and host determinants of susceptibility.

1.3. *Magnaporthe oryzae* pathotype *Triticum* (MoT) is a hemi-biotrophic fungal pathogen that causes wheat blast

Another fungal pathogen which poses a threat to global wheat supplies is *Magnaporthe oryzae*, a hemi-biotrophic ascomycete that can cause blast disease on many grass species, including wheat (Tembo *et al.*, 2020). It is thought that *Magnaporthe oryzae* pathotype *triticum* (MoT), emerged though a host jump due to the cultivation of wheat varieties in Brazil that lacked the *RWT3* resistance genes (Inoue *et al.*, 2017). This lack of recognition of *PWT3 Avr* gene products carried in *Lolium* isolates left wheat susceptible to these isolates and resulted in wheat blast disease (Inoue *et al.*, 2017). This was also likely enabled by the close proximity of wild grasses to crops (as reviewed in Ceresini *et al.* (2019)). Wheat blast was first identified in Brazil in 1985 and devastated wheat crops within the country (Igarashi, 1986). Outbreaks within Brazil and across multiple South American countries followed (Cruz and Valent, 2017). More recently, there were outbreaks of wheat blast detected outside of South America, in Bangladesh (Callaway, 2016) and Zambia (Tembo *et al.*, 2020). This was thought to have been caused by international trade, with analysis of phylogeny and population genetics suggesting that MoT was

introduced to Bangladesh from South America (Islam *et al.*, 2016). Recent phylogenetic studies revealed that the outbreak in Zambia was likely caused by an independent introduction from South America (Latorre *et al.*, 2023). MoT can infect all aerial parts of the plant and in the field and, as a hemi-biotrophic pathogen, enters the necrotrophic stage and kills host tissue in the later stages of the life cycle (Islam *et al.*, 2016). Infection leads to disease symptoms presenting most prominently as bleached spikes that subsequently dry out or dark lesions on the leaves (Cruz and Valent, 2017). Disease in any part of the plant, at any point during plant development, leads to drastic or complete loss of grain (Goulart *et al.*, 2007). As with many fungal plant pathogens, climate change introduces uncertainty in the future spread of MoT, with changes in temperature and rainfall potentially providing the right conditions to support wheat blast in new regions (Chaloner *et al.*, 2021). Studies have shown that southeastern states in the United States may be at risk from future epidemics due to proximity to current known outbreaks, climatic conditions, and farming practices (Cruz *et al.*, 2016). With yield losses up to 100% (Singh *et al.*, 2021), it is important the farmers and crops are equipped with the means to protect themselves against wheat blast. Current efforts to prevent MoT include deploying genetic resistance, agricultural practices such as removing potential sources of inoculum and the use of fungicides (Singh *et al.*, 2021). As MoT can spread through contaminated seed, quarantine, screening and sterilisation plays a key role in controlling the spread of disease, particularly between geographical regions (Singh *et al.*, 2021). Similarly to the rust fungi, there is great potential for MoT to overcome those preventative methods, leading to the spread of disease and outbreaks in new regions (Singh *et al.*, 2021). Therefore, we need to identify and deploy new sources of resistance to provide us with multiple approaches to protect wheat against current and future epidemics caused by MoT.

1.4. The plant immune system

1.4.1. Pathogen recognition at the cell surface

As sessile organisms in a constantly changing environment, it is important that plants can sense and respond to stress. One of the major stresses that plants face is infection by pathogens (**Figure 1.2**). Unlike animals, plants do not have a circulating immune system and therefore every cell must have the capacity to detect pathogens and mount a defence against infection (Lolle *et al.*, 2020). Plants have evolved a complex and sophisticated immune system to enable this (Dodds and Rathjen, 2010). When under biotic stress, microbial pathogens and herbivores are detected by the passive or active release of immunogenic molecules, referred to as Microbe/Pathogen- or Herbivore-Associated Molecular Patterns (M/PAMPs, HAMPs,

respectively) (Barka *et al.*, 2022). Examples of PAMPs that have been used extensively to study the plant immune system against bacteria and fungi include a 22 amino acid peptide from bacterial flagellin (flg22) (Felix *et al.*, 1999) and the oligosaccharide component of the fungal cell wall (chitin) (Felix *et al.*, 1993; Shibuya *et al.*, 1993). These molecules are often referred to as elicitors, as they elicit an immune response from plants. At the plasma membrane, elicitors are recognised by Pattern Recognition Receptors (PRRs) that are grouped into receptor-like kinases (RLKs) and receptor-like proteins (RLPs), based on characteristics of the cytoplasmic portion of the receptors with RLKs, but not RLPs, possessing a cytoplasmic kinase domain (Couto and Zipfel, 2016). PRRs can function in coordination with co-receptors that are required for the recognition of elicitors and subsequent signal transduction (Xi *et al.*, 2019). Variation in the extracellular domains and interacting partners of PRRs confer the ability to recognise and respond to a diverse array of specific ligands. For example, the PRR and co-receptor pairs FLAGELLIN-SENSING 2 (FLS2)- BRI1-ASSOCIATED KINASE1 (BAK1) and LYSIN MOTIF RECEPTOR KINASE 5 (LYK5)- CHITIN-ELICITOR RECEPTOR KINASE1 (CERK1) were thought to exclusively recognise bacterial flg22 (flagellin peptide) and fungal chitin in *Arabidopsis thaliana*, respectively (Cao *et al.*, 2014; Chinchilla *et al.*, 2007). However, recent evidence suggests that CERK1 can be phosphorylated by BAK1 upon flg22 perception and that this results in defence priming against fungal pathogens (Gong *et al.*, 2019). Classically, PRR recognition of elicitors is known as Pattern-Triggered Immunity (PTI) which is thought of as a basal defence response (Jones and Dangl, 2006). In response to signal perception at the plasma membrane, signals are transduced to the nucleus to trigger defence gene expression changes primarily through the activity of calcium (Ca^{2+}), reactive oxygen species (ROS) and Mitogen-Activated Protein Kinase (MAPK) cascades (Bigeard *et al.*, 2015).

1.4.2. Intracellular pathogen recognition

Basal defence can be overcome by pathogens that have evolved ways to target and dampen components of PTI. For example, pathogens have evolved specialised proteins called effector proteins that are secreted into host cells and function in facilitating infection, as has been extensively reviewed in Toruño *et al.* (2016). Common targets of effectors are signalling components of PTI as the effectors function to disrupt basal defence responses in Effector-Triggered Susceptibility (ETS) (Dodds and Rathjen, 2010; Jones and Dangl, 2006). The functions of fungal effectors have been thoroughly explored by Figueroa *et al.* (2021). With respect to effectors from wheat rust fungi, the number characterised has increased rapidly in recent years thanks to new bioinformatic tools and analysis for the prediction of candidate effectors and technical advancements to validate and functionally characterise them (Petre *et al.*, 2016;

Sperschneider *et al.*, 2015). For example, the effectors PstGSRE1, Pst_4, Pst_5 and Pst18363 target different components of ROS signalling to promote susceptibility (Qi *et al.*, 2019; Yang *et al.*, 2020; Wang *et al.*, 2021).

Plants have evolved Nucleotide-Binding domain Leucine-Rich-Repeat receptors (NB-LRRs/NLRs) which can recognise effector proteins and mount Effector- Triggered Immunity (ETI) (Dodds and Rathjen, 2010; Jones and Dangl, 2006). Effectors can be recognised either directly or indirectly, in the apoplast or the cytosol (Selin *et al.*, 2016). Effectors that are able to be recognised by the plant are termed avirulence genes/proteins (Avrs) (Luderer and Joosten, 2001). NLRs are classified as coiled coil (CC), Toll/interleukin-1 receptor (TIR) or CC_R (CC-NLRs that contain a CC domain similar to *RESISTANCE TO POWDERY MILDEW 8*)-NLRs, depending on which domain type they possess at their N-terminal (Wang *et al.*, 2023a). ETI usually induces the hypersensitive response (HR), a type of programmed cell death that restricts pathogen growth (Balint-Kurti, 2019). In animals, it had been well known that NLRs can form multimeric 'inflammasomes' upon pathogen recognition and activation, leading to the recruitment of cell-death executing proteins that trigger an inflammatory cell death (Lamkanfi and Dixit, 2014). However, it wasn't until recently that the mechanism of plant NLR activation and activity began to be elucidated. The first multimeric 'Resistosome' was characterised for the CC-NLR HOPZ-ACTIVATED RESISTANCE 1 (ZAR1), which is able to both recognise a number of effectors from diverse pathogens and also execute cell death (Wang *et al.*, 2019b). Structural studies showed that ZAR1 forms a pentameric 'star shaped' structure that functions as an ion channel in the plasma membrane (Bi *et al.*, 2021). The influx of Ca^{2+} is accompanied by ROS production and loss of membrane integrity which is thought to contribute to HR-associated cell death (Bi *et al.*, 2021). Since the initial characterisation of the ZAR1 Resistosome, phylogenomic analysis found that resistosome formation originated early in angiosperm evolution and has been lost in multiple lineages (Adachi *et al.*, 2019; Adachi and Kamoun, 2022). Subsequently, it was found that the wheat CC-NLR Sr35 that recognises AvrSr35 from *Pgt* forms a resistosome similar to ZAR1, upon direct effector binding (Förderer *et al.*, 2022). Plants and their pathogens are engaged in an evolutionary battle whereby pathogens have evolved functionally diverse mechanisms to enable rapid evolution of new or modified effectors to evade recognition or suppress NLR activity (Wu and Derevnina, 2023). In turn, plants have evolved their own ways of maintaining robust mechanisms for detection of pathogens. For example, plants have evolved NLR networks in which functionally redundant 'helper' NLRs function with specific 'sensor' NLRs to detect and trigger immunity against diverse pathogens (Derevnina *et al.*, 2021; Wu *et al.*, 2017). It has been shown that these NLRs, and the NLRs required for cell death (NRCs), form

expansive networks that enable genetic redundancy in the plant immune system to keep up with rapidly evolving pathogens (Adachi and Kamoun, 2022).

Our understanding of the plant immune system has been transformed in recent years through characterisation of the intricacies of the signalling mechanisms at play. One of the most transformative pieces of research provided extensive evidence that the long-standing PTI-ETI dichotomy was not as clearly defined as once thought, a theory that has been previously proposed by Thomma *et al.* (2011). In seminal work it was shown that without PTI, ETI is less effective, and that ETI therein reinforces PTI, making both layers of perception vital for a robust and full immune response (Ngou *et al.*, 2021; Yuan *et al.*, 2021). Following perception of pathogens at the plasma membrane or in the cytosol, complex signal transduction pathways pass on the information from the cell surface to the nucleus, to trigger transcriptional reprogramming (Moore *et al.*, 2011). Primary signalling species include reactive oxygen species (ROS), calcium ions (Ca^{2+}) and phytohormones including salicylic acid (SA), jasmonic acid (JA) and ethylene (ET). The chloroplasts are a major player in the initiation and propagation of immune signalling molecules.

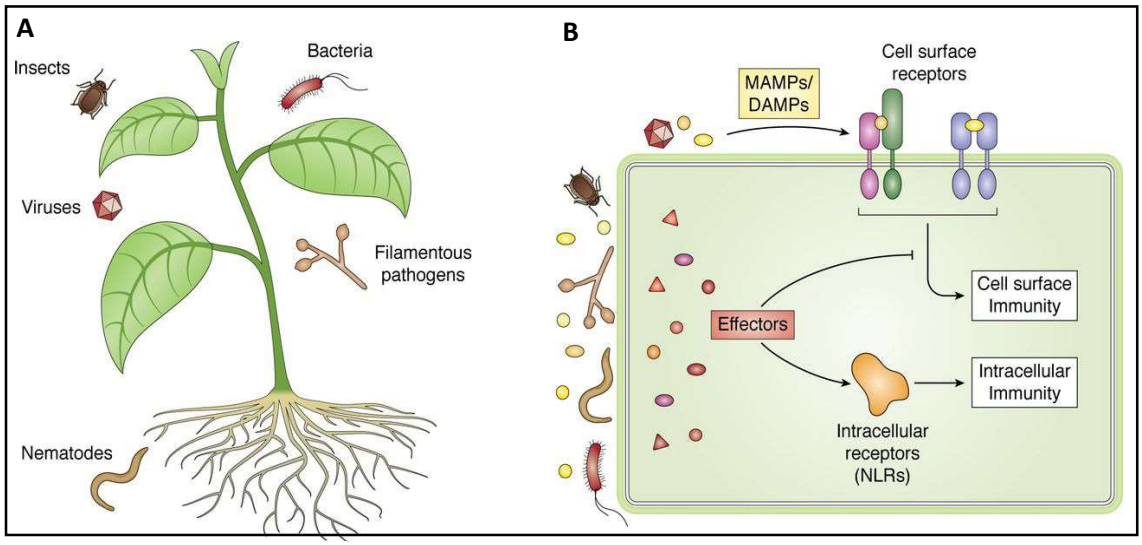

Figure 1.2 Simplified overview of the plant immune system.

(**A**) Plants face a number of pathogen threats in both the aerial parts of the plants as well as below ground. Pathogens from across kingdoms can cause disease. (**B**) Recognition of immunogenic molecules at the cell surface, such as microbe-associated molecular patterns (MAMPs)/ pathogen-associated molecular patterns (PAMPs) or effectors, leads to cell surface immunity. In the cytoplasm, recognition of effectors by intracellular receptors (NLRs) lead to intracellular immunity. These pathways are mutually potentiating and both result in transcriptional reprogramming and the initiation of the defence response. This figure was published in Bentham *et al.* (2020) and is reused with permission from copyright holders under the Creative Commons Licence.

1.5. The chloroplasts play a key role in initiating and coordinating the immune response

The chloroplasts evolved from ancient symbiotic events. Primary symbiosis occurred in one evolutionary event between a single-celled cyanobacteria and the eukaryotic heterotrophic ancestor of modern plants (Cavalier-Smith, 2000). Secondary and tertiary endosymbiotic events are also believed to have occurred between a host and free-living photosynthetic- and eukaryote-like red or green algae (Cavalier-Smith, 2002). These events led to the diversity in structure and pigment composition of chloroplasts seen in the plant kingdom today, from the phycobilin pigment in red algae to the chlorophyll a and b containing chloroplasts of land plants and green algae (Douglas, 1998). The chloroplasts are therefore an amalgamation of prokaryotic and eukaryotic- like structures and processes (Vothknecht and Soll, 2005). Over the course of evolution, the cyanobacterial genome became highly reduced, resulting in circular chloroplast genomes in angiosperms encoding a small number of genes, approximately 114 (Li and Zheng, 2018). Genes which remain encoded in the chloroplast genome are primarily responsible for transcription and translation of chloroplast-encoded genes and photosynthesis (Daniell *et al.*, 2016). It is therefore crucial that there is crosstalk between the chloroplasts and the nucleus within each cell to ensure the coordination of gene expression and protein synthesis in response to a changing environment (Jan *et al.*, 2022). The nuclear genome contains nuclear genes encoding chloroplast proteins (NGCPs) which are transcribed and translated into pre-proteins in the cytoplasm and targeted to the chloroplasts using an N-terminal chloroplast transit peptide (cTP). Chloroplast preproteins are translocated through the outer and inner membranes by the TOC and TIC supercomplexes after which they are folded and can perform their specific function within the chloroplast (Jin *et al.*, 2022; Kim *et al.*, 2022; Loudya *et al.*, 2022) .

1.5.1. The chloroplasts are sensors of environmental stress and signalling between the chloroplasts and nucleus is a vital component of the immune response

Nuclear-to-chloroplast and chloroplast-to-nuclear communication is known as anterograde and retrograde signalling, respectively (Jan *et al.*, 2022). Retrograde signalling in response to stress relies on 'operational control' signals that originate from the chloroplast and influence the expression of NGCPs (Calderon and Strand, 2021). In *A. thaliana*, the effect of disruption to retrograde signalling has been studied extensively in *genomes uncoupled* (*gun*) mutants. The consequences for retrograde signalling in *GUN* mutants was studied by inhibiting carotenoid biosynthesis or plastid translation (Susek *et al.*, 1993; Woodson *et al.*, 2011). This inhibition led to repressed expression of some NGCPs, primarily photosynthesis associated

nuclear genes (PhANGs) encoding light- harvesting complex proteins and the rubisco small chain (Susek *et al.*, 1993; Woodson *et al.*, 2011). Later studies aimed to identify the genes conferring this alteration in NGCP expression and found that most *GUN* genes were involved in tetrapyrrole biosynthesis (TPB) and heme biosynthesis, implicating metabolites in these pathway as key signals in retrograde signalling (Wu and Bock, 2021). Other molecules implicated in retrograde signalling are 3-phosphoadenosine-5-phosphate (PAP) and C-methyl-D-erythritol-2,4-cyclopyrophosphate (MEcPP) (Crawford *et al.*, 2017). Mutants defective in the PAP signalling pathway are more susceptible to both hemibiotrohic and necrotrophic pathogens due to the downregulation of salicylic acid and jasmonic acid signalling pathways (Ishiga *et al.*, 2017). MEcPP accumulates in response to abiotic and biotic stress and mediates the expression of NGCPs (Xiao *et al.*, 2012). These studies show how important and complex retrograde signalling is with the integration of multiple signals into numerous biosynthetic and phytohormone signalling pathways, to coordinate a response to environmental stress.

1.5.2. The contributions of chloroplast-derived signals to transcriptional reprogramming during immunity

Chloroplast-derived Ca^{2+} and reactive oxygen species (cROS) signals have been implicated in the early and long-term immune response (**Figure 1.3**). Alteration in Ca^{2+} pools in the chloroplast and cytoplasm is partially dependent on the thylakoid-localised Ca^{2+} -sensing receptor, CAS (Han *et al.*, 2003). *A. thaliana* mutants in *CAS* have attenuated basal defence when exposed to flg22 (Nomura *et al.*, 2012). These effects include supressed expression of *pathogenesis related* (*PR*) genes and reduced stomatal closure, which may be linked to SA biosynthesis and the expression of NGCPs (Nomura *et al.*, 2012). Recently, an effector from *Sclerotinia sclerotiorum* was found to target CAS to interfere with Ca^{2+}-mediated immune signalling and increase plant susceptibility (Tang *et al.*, 2020). This Ca^{2+} flux is perceived by, among others, calcium-dependent protein kinases which are integrated into the mitogen-activated protein kinase (MAPK) cascades, leading to the expression of immune-related genes. cROS, such as $O_2^{\cdot -}$ and H_2O_2, act downstream of Ca^{2+} and triggers unique transcriptional responses in *A. thaliana* (op den Camp *et al.*, 2003; Dietz *et al.*, 2016). Tobacco plants stably transformed with cROS-blocking flavodoxin (Fld) showed reduced cROS generation and attenuated localised cell death (LCD) against a non-host pathogen, *Xanthomonas campestris* pv. *vesicatoria* (Zurbriggen *et al.*, 2009). Further experiments in this study showed that the expression of *PR* genes and level of defence-related compounds SA and JA were unaffected in *Fld* expressing plants. These results suggest a vital role of cROS for LCD in the HR response, but with a minimal contribution to other defence signalling processes (Zurbriggen *et al.*, 2009).

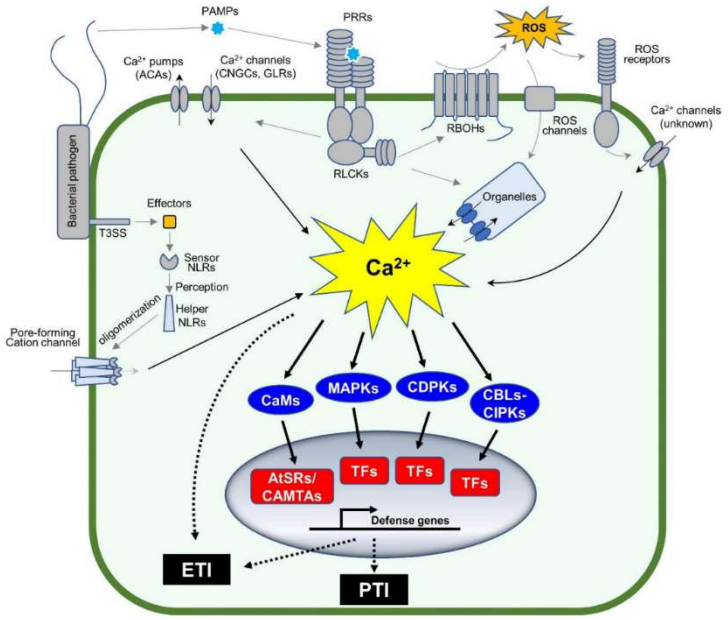

Figure 1.3 Ca^{2+} and cROS-mediated immune signalling.

Upon perception of pathogens at the cell surface, plants produce a rapid response to initiate defence strategies. Pattern Recognition Receptors (PRRs) at the cell surface recognise immunogenic molecules which leads to the opening of Ca^{2+} channels and transporters. Ca^{2+} flux is detected by calcium-dependent protein kinases which act in the immune signalling pathway to induce nuclear immunity gene expression. Ca^{2+} signalling pathways are interconnected with the appoplastic and chloroplastic ROS (cROS) signalling pathways. PAMP, pathogen-associated molecular pattern; PRR, pattern recognition receptor; RLCK, receptor-like cytoplasmic kinase; RBOH, respiratory burst ozidase homolog; ROS, reactive oxygen species; T3SS, type three secretion system; NLR, Nucleotide-binding leucine rich repeat receptor; CaM, calmodulin; MAPK, mitogen activated protein kinase; CDPK, calcium dependent protein kinase; CBL, calcineurin B-like protein; CIPK, CBL-interacting protein kinase; AtSR, *Arabidopsis thaliana* signal responsive; CAMTA, calmodulin-binding transcription activator; TF, transcription factor; ETI, effector-triggered immunity; PTI, PAMP-triggered immunity. This figure was published in Yuan *et al.* (2022) and is reused with permission from copyright holders under the Creative Commons Licence.

1.5.3. Phytohormones form an interconnected signalling complex to induce local and systemic immune responses

Plants must be able to sense and respond appropriately to the changing environment and integrate signals from numerous phytohormones to maintain optimal functions including growth, development, reproduction and immunity (as reviewed in Weyers and Paterson (2001)). Phytohormones serve a vital role in the translation of external stimuli into physiological response. For example, the phytohormones JA and SA have both been implicated in mediating the plant response to abiotic and biotic stress, and both have some or all their biosynthetic pathways localised in the chloroplasts. JA can be derived from lipids from the chloroplasts (Wang *et al.*, 2019a). JA and its derivatives are thought to contribute significantly to the plant response

to herbivores and necrotrophic pathogens (Macioszek *et al.*, 2023). This contrasts with SA which mediates responses to biotrophic and hemibiotrohic pathogens. Furthermore, there is extensive hormonal crosstalk and the interaction between SA and JA can be antagonistic (Bari and Jones, 2009). Therefore, it is important to understand how these signals function individually and together to produce an immune response. Within this piece of work, a focus was placed on understanding the wheat response to biotrophic and hemibiotrohic fungal pathogens, therefore, the role of SA during plant immunity will be explored in greater detail below.

The importance of SA in plant immunity was first documented in 1979 (White, 1979), and since then an abundance of research has uncovered the intricacies of its biosynthesis in plants, its targets and the ways in which it triggers both local and systemic resistance. SA biosynthesis is thought to occur through two major independent pathways, the isochorismate synthase (ICS) and phenylalanine ammonia-lyase (PAL) (Lefevere *et al.*, 2020). Both pathways begin with chorismate in the chloroplast. The ICS pathway is required for the synthesis of SA during immunity (Wildermuth *et al.*, 2001). In this pathway, chorismate is converted to isochorismate (IC) by ICS and transported to the cytosol by Enhanced Disease Susceptibility 5 (EDS5) (Nawrath *et al.*, 2002). Without EDS5, SA accumulates in the chloroplasts because it is unable to be transported outside into the cytosol (Serrano *et al.*, 2013). SA can be modified in numerous ways, for example by glycosylation into SA 2-O-β -D-glucoside (SAG) to form a vacuolar SA store or it can be methylated into MeSA which is highly volatile and shown to be released from plants as a signal during plant-insect interactions (Chamberlain *et al.*, 2000; Dean *et al.*, 2005). SA biosynthesis, modification and overall levels within a tissue can have far reaching consequences for several physiological processes, including immunity. For example, SA triggers local immunity by influencing the activity of the transcriptional activator non-expressor of PR gene 1 (NPR1) and transcriptional co-repressors NPR3 and NPR4 (Fu *et al*., 2012). Upon binding SA, NPR3/NPR4 are released from the promoters of defence genes whilst NPR1 binds to them, thus promoting their transcription and the activation of defence responses (Ding *et al.*, 2018a). Studies have shown that SA also induces the expression of PRRs in response to both bacterial and fungal elicitors and is required for downstream defence responses to curb pathogen growth (Tateda *et al.*, 2014). The authors hypothesised that the induction of PRRs results in a positive feedback loop, increasing the intracellular concentration of SA, also leading to increased levels in distal cells/tissues and elevated resistance in subsequent pathogen challenges. There is also experimental evidence that shows SA treatment led to the induction of genes involved in ETI including sensor and helper NLRs. Mutants in the SA biosynthetic gene *PAD4* have 20% lower levels of ETI than wildtype, as shown by quantifying the level of *Pseudomonas syringae* carrying ArRpt2 in *A. thaliana* carrying the cognate RPS2 NLR (Tsuda *et al.*, 2009). These studies highlight

the integral role of SA in local immune responses, for both PTI and ETI components of the immune system.

In addition to contributing to local immune responses in PTI and ETI, SA has also been implicated in Systemic Acquired Resistance (SAR). SAR is the occurrence of immunity in distal parts of the plant, following a primary infection which prepares the plant for future infections from the same and different pathogens (Durrant and Dong, 2004). Early studies showed that in *A. thaliana* SAR is induced in three to six hours and can continue emanating from the primary infection site for more than 6 hours (Rasmussen *et al.*, 1991). The SAR signal is thought to move acropetally via the phloem which is loaded by the apoplastic or symplastic pathway (Guedes *et al.*, 1980). Whilst SA is able to move to distal part of the plant and is required for SAR, it is not thought to be the primary signal that induces SAR (Vernooij *et al.*, 1994). It is now thought to be a coordinated effort of many chemical signals including dihydroabetinal (DA) (Chaturvedi *et al.*, 2012), pipecolic acid (pip) (Návarová *et al.*, 2012) and N-hydroxy-pipecolic acid (Hartmann *et al.*, 2018), SA and MeSA, free radicals , azelaic acid (AzA) (Jung *et al.*, 2009) and glycerol-3-phosphate (G3P) (Chanda *et al.*, 2011). The pathways for SA and N-Hydroxypipecolic acid (NHP) in SAR are interconnected and mutually potentiating (Hartmann and Zeier, 2019). The specific proteins that function in the biosynthesis of pip are explored further in Chapter 5 where components of pip biosynthesis were used as markers for SAR induction. Ultimately, the induction of SAR leads to 'priming' in which the cell is in a state ready to rapidly respond to pathogens though a heightened response to SA, the presence of PR proteins and the presence of chemical defences (Shields *et al.*, 2022). The interconnection of SA and NHP biosynthesis and function in inducing localised and systemic immunity is summarised in **Figure 1.4**.

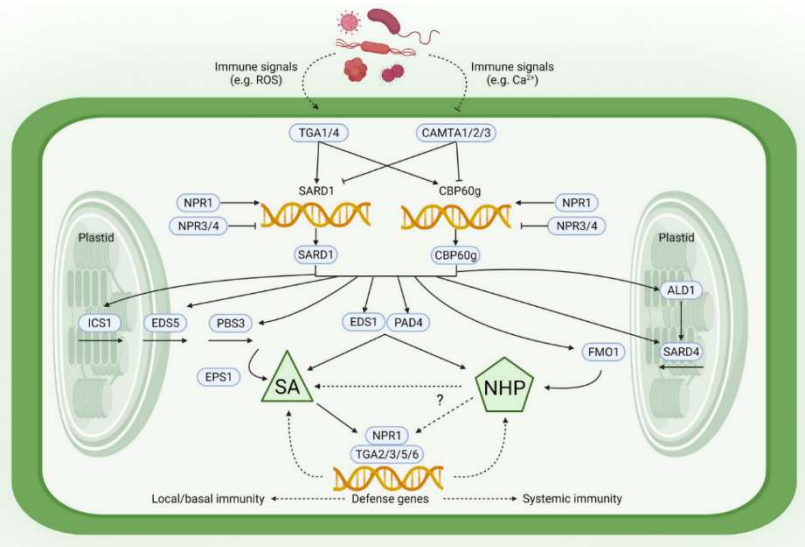

Figure 1.4 Salicylic acid (SA) and N-Hydroxypipecolic acid (NHP) are at the interface between local and systemic immunity with pathways converging on the initiation of defence gene transcription.

The perception of pathogens at the plasma membrane triggers intracellular SA and NHP signalling pathways that converge with the initiation of transcriptional responses mediated by the action of non-expressor of pathogenesis related gene 1/3/3 (NPR1/3/4), which also regulate both pathways, making them mutually potentiating. ROS, reactive oxygen species; TGA, TGACG-binding factor; CAMATA, calmodulin-binding transcription activator; SARD1/4, SAR-deficient 1/4; CBP60, calmodulin binding protein 60-like g; NPR1/3/4, non-expressor of pathogenesis related gene; ICS1, isochorismate synthase 1; EDS1/5, enhanced disease susceptibility 1/5; PBS3, avrPphB susceptible; PAD4, phytoalexin deficient4; EPS1, enhanced pseudomonas susceptibility 1; SA, salicylic acid; NHP, N-hydroxypipecolic acid; FMO1, flavin-dependent monooxygenase; TGA2/3/5/6, TGACG-binding. This figure was published in Shields *et al.* (2022) and is reused with permission from copyright holders under the Creative Commons Licence.

1.5.4. Chloroplasts are mobile and actively move to the site of pathogen invasion during infection

In addition to the chloroplasts being hubs for key signalling species such as Ca^{2+} and ROS, recent studies have also revealed the physical role the chloroplasts may play in response to pathogenic fungi. Upon exposure to stress, the chloroplasts develop stroma-filled extensions called stromules (Caplan *et al.*, 2015). Early observations showed that chloroplasts can cluster around the nucleus with their stromules nestled into grooves in the nuclear envelope (Kwok and Hanson, 2004). The roles of stromules during immunity were illuminated by studying the Tobacco mosaic virus (TMV) p50 replicase which is recognised by the *Nicotiana benthamiana* N receptor (Caplan *et al.*, 2008). The authors found that stromules are integral to innate immunity as their formation is triggered by pro-plant cell death (PCD) signals such as SA and ROS and their presence enhances PCD in *N. benthamiana* in response to TMV. N receptor interacting protein

(NRIP) and chloroplast unusual positioning 1 (CHUP1) protein were identified as key players in enabling stromules formation and chloroplast migration. NRIP moves from the chloroplast to the nucleus during infection and this accumulation is enhanced by stromules formation (Caplan *et al.*, 2008). CHUP1 is targeted to the outer membrane of the chloroplast and has actin-binding activity, suggesting a role in cytoskeletal-dependent movement of chloroplasts with *CHUP1* knock out plants having constitutive formation of stromules and enhanced PCD (Caplan *et al.*, 2015). A recent study has also shown that chloroplasts move and associate with fungal infection structures within the cell (Savage *et al.*, 2021). This work also determined that whilst the formation of stromules is dependent upon the LRR-RLK BAK1, the accumulation of chloroplasts is not. Further experiments confirmed that actin may play some role in the movement of chloroplasts around the cell (Caplan *et al.*, 2015). Recent studies suggest that microtubule structure determines the formation of stromules and actin enables anchoring (Kumar *et al.*, 2018). It is unclear whether the movement of chloroplasts to the plant-pathogen interface has evolved to benefit the pathogen by enhancing nutrient acquisition or the plant by localising pro-defence compounds to the site of infection (Savage *et al.*, 2021). Together, studies show that the chloroplasts are an integral component of the plant immune response to pathogens both in physical defence against cellular invasion and at the metabolic and transcriptomic level.

1.5.5. An expanding toolkit to characterise the wheat response to rust fungi

RNA-sequencing has proven to be a powerful tool to enable us to gain a transcriptional-level understanding of the processes being manipulated or altered in wheat during infection with rust fungi. RNA-sequencing has been used to elucidate the transcriptional changes in adult (Hao *et al.*, 2016) and seedling (Dobon *et al.*, 2016) wheat in response to *Puccinia striiformis* f. sp. *tritici* (*Pst*). In both adult and seedlings responding to infection by *Pst,* the expression of photosynthesis-associated genes is downregulated early during infection and then up-regulated during the later stages of infection (Corredor-Moreno *et al.*, 2022; Hao *et al.*, 2016). These results agree with studies performed in model pathosystems which showed that photosynthetic processes are generally supressed early during infection as part of the PTI response (Göhre *et al.*, 2012). For biotrophic pathogens, the up regulation during the later stages of infection may be a result of the need for the pathogen to maintain and manipulate host metabolism to gain key sources of carbon. Increasing our understanding of the host processes being modulated during infection by performing RNA-sequencing can enable the identification of genes important for resistance or susceptibility.

The development of the Targeted Induced Local Lesions In Genome (TILLING) population in wheat opened up opportunities to explore the function of genes identified through RNA-

sequencing in wheat (Krasileva *et al.*, 2017). Mutants in this library have been mutagenised using ethyl methanesulfonate (EMS) across the genome and therefore it is possible to identify single nucleotide polymorphisms (SNPs) that are predicted to result in loss-of-function for a given gene of interest. These gene disruption mutants are available in the two genetic backgrounds of the hexaploid and tetraploid spring wheat varieties Cadenza and Kronos, respectively. This population is maintained in the UK by the Germplasm Resource Unit at the John Innes Centre and available to view and order through Ensembl Plants (Yates *et al.*, 2021). TILLING mutants have been used to study gene function across disciplines, including investigating genes relating to abiotic and biotic stress response (Comastri *et al.*, 2018; Corredor-Moreno *et al.*, 2022). Therefore, the TILLING population presents a valuable resource for studying gene function in wheat in response to pathogens, circumventing the time and cost of generating transgenic lines. The development of user-friendly software to make these data and resources accessible to people with a range of expertise and experience has also accelerated the study of wheat-pathogen interactions. For example, the TILLING library was integrated into the Ensembl Plants database (Yates *et al.*, 2021) so that anyone can search for a gene of interest, identify mutants, and quickly assess their phenotype. Furthermore, as genomic advancements were made in wheat, the release of the Wheat Expression Browser on expVIP and the Wheat electronic fluorescent pictograph (eFP) Broswer (Borrill *et al.*, 2016; Ramírez-González *et al.*, 2018; Winter *et al.*, 2007) provided centralised locations with graphical representations of transcriptomic data from a range of experiments, including from infection with pathogens. Making the vast amount of genomic and gene expression data available makes wheat a much more accessible system to work with and enables the acceleration of new discoveries in a historically challenging system to work with.

1.6. Introduction to the current study

The intimate association between plants and biotrophic fungi is required for the completion of the fungal life cycle. This interaction involves suppression of host immunity, manipulation of metabolic processes and alterations to plant physiology. The chloroplasts sit at the interface of plant immunity and primary and secondary metabolism, making them key targets for manipulation by rust fungi to establish a biotrophic association and ultimately complete the life cycle. As highlighted in this introduction, the development of genetic and technical resources in wheat have expanded the opportunities to study the function of genes previously uncharacterised in the context of plant-pathogen interactions. In recent years, several fungal effectors have been shown to target the wheat chloroplasts, indicating that they are an important component in the wheat response to rust fungi. However, most of the recent

research to date has investigated the wheat chloroplasts from the perspective of the pathogen and focused on the role of effectors. In this thesis, I aimed to explore the ways in which chloroplastic processes may be involved in the wheat response to pathogenic fungi. To this aim, I followed these broad objectives:

1. Use transcriptomic data to identify NGCPs that have expression profiles that are modulated in response to *Pst* infection and that differed between susceptible and resistant interactions.
2. Assess the contribution of these candidate NGCPs to wheat susceptibility to *Pst* by identifying relevant disruption mutants and screening them for alterations in resistance or susceptibility to *Pst*.
3. Functionally characterise any candidate NGCPs showing altered resistance to *Pst* to explore how they contribute to wheat susceptibility to two phytopathogenic fungi, *Pst* and MoT.

2. General methods

2.1. Multiplication of *Pst* isolates

Hexaploid bread wheat (*Triticum aestivum* L.) variety Vuka was used as the standard laboratory susceptible wheat line for multiplication of *Pst* isolates. In this project, the *Pst* isolate 13/14 (Hubbard *et al.*, 2015) was used and propagated on plants to produce enough urediniospores for experiments. Vuka seeds were sterilised, pre-germinated and grown according to Section 2.2. When plants reached approximately 10 cm in height, 25 mL of growth regulator (maleic hydrazide; 0.2 g/ L) was added to the pots to stunt the growth of seedlings. Plants were inoculated with *Pst* when they reached the 2-3 leaf stage. *Pst* urediniospores which had been stored in -20°C or -80°C were heat-activated by incubating at 42°C for 5 mins. Plants were spray inoculated with 1 mg/mL urediniospores suspended in 3M™ Novec™ 7100 Engineered Fluid to facilitate infection. Inoculated plants were kept at 10°C in the dark for 24 h under high relative humidity. Inoculated plants were then placed in cellulose bags and transferred to a glasshouse under long day conditions (16 h light/ 8 h dark, 250 µmol m^{-2} s^{-1} under a 19 °C/14 °C temperature cycle (day/night)) for the duration of infection. Urediniospores were harvested after approximately 3-4 weeks and stored at -80°C.

2.2. Wheat seed sterilisation and plant growth

Seeds of wheat TILLING lines and Vuka were sterilised by gentle shaking in sterile diH2O for 30 s followed by 30 s wash in 50 % (v/v) bleach. Seeds were then rinsed in sterile diH2O twice for 30 s and placed onto wet filter paper in petri dishes for seed imbibition. For lines which had a poor seed germination, an alternative sterilisation protocol was performed by washing seeds in 70 % (v/v) ethanol for 2 mins, then washing twice in sterile diH_2O for 30 s each, followed by 25 mins in 20 % sodium hypochlorite. Seeds were the washed three times with sterile diH_2O for 30 s each and placed onto wet filter paper in petri dishes. Seeds were germinated at 4°C for 24 h followed by 20°C for 48 h. Seeds were sown into the John Innes F2 Starter soil (100% peat, 4 kg/M^3 Dolomitic limestone, 1.2 kg/M^3 osmocote start) in 9 cm pots and placed into containment glasshouses under long day conditions (16 h light/ 8 h dark, 250 µmol m^{-2} s^{-1} under a 19 °C/14 °C temperature cycle (day/night)).

2.2.1. Plant growth for seed multiplication

To shorten the generation time and accelerate the generation of seeds for TILLING mutants, a subset of plants were grown in Speed Breeding conditions (Watson *et al.*, 2018). Seeds were sterilised and pre-germinated according to Methods section 2.2. Plants were grown in a glasshouse under 22 h light (PAR 450-500 µmol m^{-2} s^{-1}), 2 h dark, 22°C/17°C degrees

day/night, respectively. Heads were harvested when grains were filled and plants were fully senesced, after approximately 8-10 weeks. Alternatively, following seed sterilisation and pre-germination in **Section 2.2**, seeds were sown in John Innes F2 Starter soil (100% peat, 4 kg/M^3 Dolomitic limestone, 1.2 kg/M^3 osmocote start) in 9 cm pots and placed into a glasshouse under long-day conditions (16 h light/ 8 h dark). When plants reached the 4-leaf stage they were transplanted into individual 2 L pots containing the John Innes Cereal mix (65% peat, 25% loam, 10% grit, 4 kg/M^3 Dolomitic limestone, 1.2 kg/M^3 osmocote start).

2.3. Standard polymerase chain reaction (PCR) used for molecular biology and genotyping of TILLING lines

PCR was used to genotype a subset of TILLING mutants where KASP™ was not possible. PCR was also used for cloning during the initial amplification of the coding sequence (CDS) and for colony PCRs. For cloning, DreamTaq DNA polymerase (ThermoFisher Scientific, UK) was used for colony PCRs. The high-fidelity and proofreading Platinum™ SuperFi™ (ThermoFisher Scientific, UK) or Phusion® (New England Biolabs, USA) DNA polymerases were used for amplification of fragments used in cloning reactions, and for amplification of the region around the single nucleotide polymorphism (SNP) conferring the TILLING line mutation. For colony PCR, the manufacturer's protocol for DreamTaq DNA polymerase was followed, replacing template DNA with a small amount of colony lifted from the agar plate with a 10 µL tip. Reaction mixtures and thermocycling conditions are outlined below in **Table 2.1**, **Table 2.2**, **Table 2.3**, and **Table 2.4**. PCR products were run on a 1% (w/v) agarose gel containing 1X Gel Red (Biotium, USA) for 30-60 mins at 90-110 V. Products were visualised on a UV transilluminator.

Table 2.1 Reaction mixture components for polymerase chain reaction (PCR) using DreamTaq, Phusion® and Platinum™ SuperFi™ DNA polymerases

	DreamTaq	Phusion	Platinum SuperFi
Buffer	10X DreamTaq green buffer	1X Phusion HF or GC buffer	5X SuperFi™ Buffer
dNTPs (mM)	0.2		
Forward primer (µM)	0.1-1.0	0.5	
Reverse primer (µM)			
Template DNA	10 pg- 1 µg	< 250 ng	5-50 ng
Polymerase (U)	1.25	1	
Nuclease-free water (µL)	To 50		

Table 2.2 Thermocycling conditions for DreamTaq DNA polymerase

Step	Temperature (°C)	Time (s)	Number of cycles
Initial denaturation	95	60-180	1
Denaturation	95	30	25-40
Annealing	Variable	30	
Extension	72	15-30/kb	
Final extension	72	300-900	1

Table 2.3 Thermocycling conditions for Phusion High-Fidelity DNA polymerase

Step	Temperature (°C)	Time (s)	Number of cycles
Initial denaturation	98	30	1
Denaturation	98	5-10	25-35
Annealing	Variable	10-30	
Extension	72	15-30/kb	
Final extension	72	300-600	1

Table 2.4 Thermocycling conditions for Platinum™ SuperFi™ DNA polymerase

Step	Temperature (°C)	Time (s)	Number of cycles
Initial denaturation	98	30	1
Denaturation	98	5-10	25-35
Annealing	Variable	10	
Extension	72	15-30/kb	
Final extension	72	300	1

2.4. Genotyping

2.4.1. DNA extraction

DNA extractions were performed following a protocol adapted from Pallotta *et al.* (2003). From the first leaf of two-week-old seedlings, 2-4 cm of leaf tissue for each plant was placed into a well of a 2 mL 96-well plate. A ball bearing was added to each well along with 500 μL DNA extraction buffer (50 ml 1 M Tris, pH 7.5; 50 mL 0.5 M EDTA, pH 8; 31.25 mL 20 % (v/v) SDS; H_2O to 500 mL) and samples were disrupted in the TissueLyser II (Qiagen, UK) at 3000 rpm for 3 mins. The plate was incubated in a water bath at 65°C for 1 hr. Following incubation, the samples were kept at 4°C for 15 mins then 250 μL 6 M ammonium acetate added. The plates were inverted to mix and the protein precipitated at 4°C for 15 mins. Samples were pelleted by centrifugation at 3434 *g* and 4°C for 15 mins before 600 μL supernatant from each sample in the plate was added to 350 μL ice-cold isopropanol in a different 96-well plate. Samples were

centrifuged at 3434 *g*. Samples were washed with 70 % v/v ethanol by vortexing followed by centrifugation at 3434 *g* at 4°C for 15 mins. Supernatant was discarded and ethanol left to evaporate overnight. To elute the DNA, 100 µL of sterile diH_2O was added, samples were vortexed and centrifuged at 3434 *g* at 4°C for 15 mins. DNA was kept at 4°C for short-term or -20°C for long-term storage.

2.4.2. Genotyping TILLING mutants using Kompetitive Allele Specific PCR (KASP™)

Forward primers with wildtype (WT) or mutant (MUT) SNPs at the 3' end and a common homeologue-specific primer were designed or pre-designed on Ensembl Plants (https://plants.ensembl.org/index.html) for each gene. Primers were designed with a melting temperature of 59- 61°C to amplify a 60-200 bp fragment of the gene with one of the primers capturing the SNP (**Table 2.5**). A primer mix was created for each gene by mixing 100 µM primer stocks in the following volumes: 12 µL of the wildtype primer, 12 µL of the mutant primer, 30 µL of the common primer with 40 µL of diH_2O. KASP™ assays were performed in 5 µL reaction volumes which included 2.5 µL KASP™ 2X mix (LGC Biosearch Technologies, UK), 0.07 µL primer mix and 2.4 µL DNA (approximate concentration 50 ng/ µL), diH_2O (in the non-template control (NTC)) or WT Kronos DNA (for the positive WT control). Reactions were performed in 384 well plates with at least 2 technical replicates, 3 non-template controls (NTCs) and 3 positive controls for each primer set. The KASP™ assay was performed on a thermocycler with the programme outlined in **Table 2.6**.

Table 2.5 Primers used to genotype TILLING mutants using KASP™ with probe sequences highlighted in red.

Gene	Homeologue	TILLING line	WT (Fwd)	Mut (Fwd)	Com (Rvs)
CAS	Traes CS6A02G290600	K2285	gaaggtgaccaagttcatgctgccgcgctgaagatctc	gaaggtcggagtcaacggatttgtgccgcgctgaagatctt	ggttaaaggtcggagaggttag
		K3842	gaaggtgaccaagttcatgctctttccggcccgagaagc	gaaggtcggagtcaacggatttgtttccggcccgagaagt	ctaacctctccgaccttaacc
	Traes CS6B02G320900	K3422	gaaggtgaccaagttcatgctgagttcaaatcttttctcagctgtc	gaaggtcggagtcaacggattgagttcaaatcttttctcagctgtt	tcgcaagcttcttcctggaat
		K2110	gaaggtgaccaagttcatgctacggactcctacaacctctc	gaaggtcggagtcaacggattacggactcctacaacctctt	ctgtccacattcccaggaaga
PsbQ1	Traes CS2A02G344400	K2876	gaaggtgaccaagttcatgcttcatatactacgacttcgacaagc	gaaggtcggagtcaacggatttcatatactacgacttcgacaagt	cgtcatccttggtggtgaca
		K2702	gaaggtgaccaagttcatgctcaggtcaaatgcggagctgc	gaaggtcggagtcaacggattcaggtcaaatgcggagctgt	attcctagagagagagaggcctc
	Traes CS2B02G342000	K2432	gaaggtgaccaagttcatgctgtagatgccgttcttcacaaagg	gaaggtcggagtcaacggattgtagatgccgttcttcacaaaga	caacagtactaccgccactcta
		K2703	gaaggtgaccaagttcatgcttgtcaacaagtacctccgcc	gaaggtcggagtcaacggatttgtcaacaagtacctccgct	cgtcatccttggtggtgacg
PsbQ2	Traes CS6A02G206600	K447	gaaggtgaccaagttcatgctagcccgggctgaccag	gaaggtcggagtcaacggattagcccgggctgaccaa	cacgacatggtctccagaattgg
		K4432	gaaggtgaccaagttcatgctcgcatccggcaaacgg	gaaggtcggagtcaacggattcgcatccggcaaacga	cacgacatggtctccagaattgg
	Traes CS6B02G227900	K651	gaaggtgaccaagttcatgctggaggaggccgcgg	gaaggtcggagtcaacggattggaggaggccgcga	acgacatggtctccagcatc
		K3103	gaaggtgaccaagttcatgctggaggaggccgcgg	gaaggtcggagtcaacggattggaggaggccgcga	acgacatggtctccagcatc
Psah2	Traes CS1A02G392000	K2171	gaaggtgaccaagttcatgctgggccccttcttgatggg	gaaggtcggagtcaacggattgggccccttcttgatgga	gggctgctgctcaaggtc
		K4240	gaaggtgaccaagttcatgctgcagtgggacctgtacgg	gaaggtcggagtcaacggattgcagtgggacctgtacga	accttgagcagcagccct

Table 2.5 Continued

	Traes CS1B02G420100	K3587	gaaggtgaccaagttcatgctgcacagctcgatcgcaatgg	gaaggtcggagtcaacggattgcacagctcgatcgcaatga	taaagtacctgcgggtggag
		K2317	gaaggtgaccaagttcatgctgcagtgggacctgtacgg	gaaggtcggagtcaacggattgcagtgggacctgtacga	accttgagcagcagccc
PRK	Traes CS6A02G267300	K1400	gaaggtgaccaagttcatgctcaatagtgattggcctggcag	gaaggtcggagtcaacggattcaatagtgattggcctggcaa	agcacctccaaacacgctt
		K2188	gaaggtgaccaagttcatgctgtcgggcagcaaacatgg	gaaggtcggagtcaacggattgtcgggcagcaaacatga	cttggttctgcctgaagcca
	Traes CS6B02G294700	K3548	ggatgtgggaaatccaccttgaaggtgaccaagttcatgct	agatgtgggaaatccaccttgaaggtcggagtcaacggatt	caccaccatcccaaactca
		K4557	ggatgtgggaaatccaccttgaaggtgaccaagttcatgct	agatgtgggaaatccaccttgaaggtcggagtcaacggatt	caccaccatcccaaactca
PsbP	Traes CS4A02G101500	K4273	gaaggtgaccaagttcatgcttttgttgtgctgtaaattggcagc	gaaggtcggagtcaacggatttttgttgtgctgtaaattggcagt	gtcatgtgtttccccctcctg
		K4059	gaaggtgaccaagttcatgcttgcagctgcagtctgtccg	gaaggtcggagtcaacggatttgcagctgcagtctgtcca	gtccagaaaatccaggcggaag
	Traes CS4B02G203100	K572	gaaggtgaccaagttcatgctcgatcagcgtgtagtacctcc	gaaggtcggagtcaacggattcgatcagcgtgtagtacctct	tgatcatatgtttcccctttccg
		K355	gaaggtgaccaagttcatgctgacctaggcccaatggatg	gaaggtcggagtcaacggattgacctaggcccaatggata	ggtcagaagaaagggaagacac

Table 2.5 Continued

RSC	Traes CS2A02G067000	C1262	gaaggtgaccaagttcatgctcaatggcggaaggatcagatg	gaaggtcggagtcaacggattcaatggcggaaggatcagata	acgatgatgtgccttgacca
		C1701	gaaggtgaccaagttcatgctgcaagtaagacagggtctcg	gaaggtcggagtcaacggattgcaagtaagacagggtctca	tgagttcagcaaggttggc
	Traes CS2D02G065400	C0117	gaaggtgaccaagttcatgctgcaagtaagacagggtctcg	gaaggtcggagtcaacggattgcaagtaagacagggtctca	cgagtttagcaaggttggc
		C2026	gaaggtgaccaagttcatgctgagaggggtggcaagtaag	gaaggtcggagtcaacggattgagaggggtggcaagtaaa	cgagtttagcaaggttggc
NRIP	Traes CS7A02G545200	K234	gaaggtgaccaagttcatgctctccctccaagtcgagaacc	gaaggtcggagtcaacggattctccctccaagtcgagaact	gtttcacctgctggctcc
		K2524	gaaggtgaccaagttcatgctcaccgaactcaccctccg	gaaggtcggagtcaacggattcaccgaactcaccctcca	tctctgttctctcaacttaactgg
	Traes CS7B02G019600	K4595	gaaggtgaccaagttcatgctcgggttcttggccattcc	gaaggtcggagtcaacggattcgggttcttggccattct	gttgtgtagaacggaggggc
		K3332	gaaggtgaccaagttcatgctccctccaagtcgagaaccc	gaaggtcggagtcaacggattccctccaagtcgagaacct	ctttcacctgccggctct
CL1	Traes CS7A02G568800	K3213	gaaggtgaccaagttcatgctggttggttctactcgctcag	gaaggtcggagtcaacggattggttggttctactcgctcaa	atcaggcttcccttgcgc
		K4268	gaaggtgaccaagttcatgctcggtattccttttcaacagcacg	gaaggtcggagtcaacggattcggtattccttttcaacagcaca	tctcaggtgcttgacaagga
		K2073	gaaggtgaccaagttcatgctggttggttctactcgctcag	gaaggtcggagtcaacggattggttggttctactcgctcaa	atcaggcttcccttgcgc
	Traes CS7B02G489800	K2296	gaaggtgaccaagttcatgctccacggctctggagtagg	gaaggtcggagtcaacggattccacggctctggagtaga	atcaggcttcccttgcgc
		C1045	gaaggtgaccaagttcatgctcgaccgccgtgaaagagg	gaaggtcggagtcaacggattcgaccgccgtgaaagaga	agtgcaggttccatcgcata
CL2	Traes CS5A02G488000	K2536	ccgccacgctgctgccgaagaaggtgaccaagttcatgct	tcgccacgctgctgccgaagaaggtcggagtcaacggatt	gaaggagaagagcatcctg
	Traes CS5B02G501800	K4079	gaaggtgaccaagttcatgctaatggcatcggtggggttcgg	gaaggtcggagtcaacggattaatggcatcggtggggttcga	cctccccgccgtcgacaac
TaCPEP1	Traes CS5A02G523600	K4002	gaaggtgaccaagttcatgcttgagctccctcagagacgtc	gaaggtcggagtcaacggatttgagctccctcagagacgtt	cttgcttgttttctcaactgcgtt

Table 2.5 Continued

	Traes CS2B02G553500	K2206	gaaggtgaccaagttcatgctcagtagggaacgaagaagccc	gaaggtcggagtcaacggattagtagggaacgaagaagcct	cgtctgaacttcagGaaattgtt

Table 2.6 Standard KASP™ thermal cycle programme

Step	Temperature (°C)	Time (s)	Number of cycles per step
Activation	94	900	1
Denaturation	94	20	10
Annealing / Elongation	61 - 55	60 (drop 0.6°C per cycle)	
Denaturation	94	20	26

2.4.3. Genotyping TILLING mutants using Polymerase Chain Reaction (PCR)

Primers were designed in Geneious Prime 2023.0.1 to amplify 100-200 bp either side of the TILLING mutant SNP. PCR was carried out to amplify the target genes using DreamTaq polymerase (ThermoFisher Scientific, UK) according to the protocols outlined in Section 2.3. PCR products were purified using the QIAquick PCR Purification Kit (Qiagen, UK), according to the manufacturers' instructions. Purified PCR products were sequenced by Sanger sequencing at Genewiz (Azenta Life Sciences, Germany) using the same primers that were used for PCR amplification. Chromatograms were visually inspected in Geneious Prime 2023.0.1 and the low-quality sequences trimmed. Genotyping was performed by aligning the PCR product sequence to the reference genome sequence (Zhu *et al.*, 2021) and manually calling the SNP of interest.

2.5. Inoculation of TILLING mutants with *Pst*

Seedlings at the two-leaf stage (approximately 10 days old) were inoculated with 1 mg/mL of urediniospores of *Pst* isolate 13/14 (Hubbard *et al.*, 2015) which had been heat-activated by incubating in a water bath at 42°C for 5 mins. Inoculations were performed by spraying spores resuspended in 3M™ Novec™ 7100 Engineered Fluid. For mock inoculated samples, leaves were sprayed with 3M™ Novec™ 7100 Engineered Fluid without spores. Following inoculation with spores or mock solution, plants were placed at 10°C in the dark with high relative humidity for 24 h and then placed in a Hettich plant growth cabinet and grown at 16 h light/ 8 h dark, 16/20°C. Infection on the second leaf was scored when plants were showing pustule formation on the leaf surface, at around 17-21 dpi. To quantify infections, K-PIE was used to measure the percentage of leaf infected with *Pst* according to the protocol outlined in Bueno-Sancho (2018). Where K-PIE did not work,

infections were quantified by fungal biomass using quantitative real-time PCR (qRT-PCR) as outlined in **Section 2.7**.

2.6. Inoculation with *Magnaporthe oryzae* pathotype *triticum*

The MoT isolate BTJP4-01 (Islam *et al.*, 2016) was grown for 1-to-2 weeks on complete media agar (For 1 L combine 10 g D-glucose, 2 g peptone, 1 g yeast extract, 1 g casamino acids, 6 g $NaNO_3$, 0.52 g KCl, 0.52 g $MgSO_47HOH$, 1.5 g KH_2PO_4, 1 mL trace elements (in 100 ml add 2.2 g $ZnS0_47HOH$, 1.1 g H_3BO_3, 0.5 g $MnCl_24HOH$, 0.5 g $FeSO_47HOH$, 0.17 g $CoCl_26HOH$, 0.16 mg $CuSO_45HOH$, 0.15 mg Na_2MoO_42HOH, 5 g Na_4EDTA), 1 mL vitamin solution (in 100 ml add 0.01 g biotin, 0.01 g pyridoxine, 0.01 g thiamine, 0.01 g riboflavin, 0.01 g PABA (p-aminobenzoic acid) and 0.01 nicotinic acid), adjusted to pH 6.5 with NaOH, and 15 grams of agar for solid media) at 24°C under controlled conditions in a growth cabinet set at 12 h light/12 h dark cycle. Conidia were firmly scraped from the petri dish with 2 mL sterile H_2O using a plastic spreader. Suspended conidia were then filtered through Miracloth (Merck). Conidia were counted using a haemocytometer and diluted to a concentration of $1x10^5$ spores/mL in 0.025% (v/v) tween gelatine. Detached leaves (cut to approximately 10 cm) from wheat at the two-leaf stage were prepared on 1% water agar supplemented with 100 µg/mL penicillin-streptomycin. Spot inoculation was carried out by placing 5 µL of conidial suspension onto the surface of the detached leaves. The droplets were wicked away after 24 h and plants maintained at 23°C 12 h light/12 h dark cycle for 5 days before photographing and sampling by snap freezing tissue in liquid nitrogen.

2.7. RNA extraction, cDNA synthesis and qRT-PCR

2.7.1. RNA extraction and cDNA synthesis

RNA from leaf tissue was isolated using the Qiagen RNeasy Plant Mini Kit (Qiagen, UK) according to the manufacturer's instructions. DNA contamination was removed using Invitrogen™ TURBO DNA-*free*™ Kit (fisherscientific, UK) according to the manufacturer's instructions. RNA integrity was checked and concentration measured using the Qubit Fluorometer 3 (ThermoFisher Scientific, UK). For cDNA synthesis either 3 µg RNA was used as input for cDNA synthesis using SuperScript™ II Reverse Transcriptase (ThermoFisher Scientific, UK) or 1 µg RNA was input into the Verso cDNA Synthesis Kit (ThermoFisher Scientific, UK). cDNA was diluted 1:5 before short-term storage at 4°C or long-term storage at -20°C.

2.7.2. Primer design, efficiency, and qRT-PCR reaction

Primers were designed in Geneious Prime 2023.0.1 to amplify a fragment of 70-200 bp at a melting temperature of between 60 and 63 °C with a GC content of 40-60 %. To test their efficiency, cDNA was diluted in the following proportions: 1, 1:2, 1:4, 1:8, 1:16 and 1:32. qRT-PCR was carried out in 10 µL reactions containing 1X LightCycler 480 SYBR Green I Master Mix (ThermoFisher Scientific, UK) with final concentrations of 0.25 µM for the forward and reverse primers. To each well, 2 µL of cDNA or diH2O (for the non-template controls) were added. Each cDNA dilution was added to separate wells. Reactions were run in three technical replicates on a LightCycler®480 Instrument II (Roche Diagnostics, UK) using the programme in **Table 2.7.** To calculate primer efficiency, which had to be between 80-100% for any primer used, the mean Crossing point (Cp) was calculated for each of the cDNA dilutions and a standard curve was created and the primer efficiency calculated using the following equation:

$$Efficiency\,(\%) = \left(10^{\left(\frac{-1}{slope}\right)} - 1\right) \times 100$$

To determine fungal biomass by qRT-PCR, the expression of the *Pst* housekeeping gene *EF-1* was measured by amplification using forward: 5'- TTCGCCGTCCGTGATATGAGACAA-3' and reverse: 5'-ATGCGTATCATGGTGGTGGAGTGA-3' primers (Liu *et al.*, 2012)). For qRT-PCR relating to VIGS, the expression of *TaCPEP* was measured by amplification using forward: 5'-GCACGACGTCTCTGAGGGAG-3' and reverse: 5'-GGGAACGAAGAAGCCCCAATC-3' primers designed in Geneious Prime 2023.0.1 following standard criteria including (i) primer melting temperature of 60 ± 1° (ii) primer length 18-25 basepairs (bp) (iii) GC content of between 40-60% (iv) PCR product between 60 and 150 bp (Udvardi *et al.*, 2008). The wheat reference gene *UCE-AL* (forward: 5'-ACAAGGTCGAGACGGTGAAC-3', reverse: 5'-GTAAGGATACGCATCGGGCA-3' (Corredor-Moreno, 2019)) was used as the reference gene for all qRT-PCR reactions. Fold change was calculated as $2^{-\Delta\Delta Cp}$. qRT-PCR for VIGS experiments were carried out by Cesaree Morier-Gxoyiya (John Innes Centre).

Table 2.7 Programme used for quantitative real-time polymerase chain reaction (qRT-PCR) on the LightCycler480

Step	Temperature (°C)	Time (s)	Number of cycles per step
Preincubation	95	300	1
Amplification cycles	95	10	45
	60	15	
	72	30	
Melt-curve cooling	To 65		1
	Heating to 97 with five reads per °C		

2.8. Transient expression in *Nicotiana benthamiana*

2.8.1. Cloning

PCR was used to amplify the coding region of *TaCPEP-A* from cDNA synthesised from the wheat variety Cadenza, without the stop codon (forward: 5'- ATGGCGATCGTGGCAGGTC-3', reverse: 5'-GCAATAGAGAACGCCTCCTGA-3'). Amplification was carried out using Platinum™ SuperFI™ polymerase (ThermoFisher Scientific, UK) according to the protocol described in **Section 2.3**. Bands of the correct sizes were cut from the gel and purified using the QiaQuick Gel Extraction Kit (Qiagen, UK) according to the manufacturer's instructions. The purified inserts were cloned into the pENTR/D-TOPO vector using TOPO™ cloning, according to the manufacturer's instructions (ThermoFisher Scientific, UK) and transformed into competent *Escherichia coli* TOP10 cells (ThermoFisher Scientific, UK) according to the manufacturer's instructions. TOP10 cells were spread onto LB agar plates containing 50 µg/mL kanamycin and left to grow overnight at 38°C. After growth overnight, discrete colonies were identified and PCR was used to screen for positive transformants by amplifying from pENTR/D-TOPO with a backbone specific M13 Forward primer (5'-GTAAAACGACGGCCAGT-3') and the gene-specific reverse primer using the DreamTaq DNA polymerase protocol outlined in **Section 2.3**. Colonies that generated amplicons of the correct size were selected and cultured overnight in 10mL liquid LB containing 50 µg/mL kanamycin. Plasmid was purified from 4 mL of liquid culture using the Qiagen Miniprep kit (Qiagen, UK) and the insert was sequenced using Sanger Sequencing from Genewiz (Azenta Life Sciences, Germany). Sequence

chromatograms were visualised using Geneious Prime 2023.0.1 and manually edited to remove low-quality sequence. Alignments of sequenced DNA and *TaCPEP* CDS were performed in Geneious Prime 2023.0.1 using MAFT (Katoh *et al.*, 2017). Verified pENTR/D-TOPO plasmid containing *TaCPEP* CDS was used to transfer the *TaCPEP* CDS into the C-terminal GFP fusion destination *Agrobacterium tumefaciens* expression vector pK7FWG2 (Karimi *et al.*, 2002). The Gateway™ LR Clonase™ II reaction was performed according to the manufacturer's instructions (ThermoFisher Scientific, UK) and reaction product transformed into TOP10 cells (ThermoFisher Scientific, UK) according to the manufacturer's instructions and plated onto LB agar plates containing 100 µg/mL spectinomycin. Screening for colonies carrying pK7FWG2:*TaCPEP* was carried out the same as described above using a gene-specific forward primer and a Green Fluorescent Protein (GFP)-specific reverse primer (5'-GACACGCTGAACTTGTGGCCGTTTACG-3').

2.8.2. Transformation of *Agrobacterium tumefaciens*

Verified pK7FWG2:*TaCPEP* was transformed into the *A. tumefaciens* strain GV3101 by mixing 200 ng of the pK7FWG2:*TaCPEP* vector with 50 µL competent GV3101 cells then placing the mixture into liquid nitrogen for 5 mins. Cells were then thawed at room temperature and 200 µL LB was added before incubating the cells at 28°C for 1-2 h with gentle shaking. Cells were plated onto LB agar containing 100 µg/mL spectinomycin, 100 µg/mL rifampicin and 100 µg/mL gentamycin. Colonies were verified for containing pK7FWG2:*TaCPEP* by PCR using the gene-specific forward and GFP reverse primers, as above.

2.8.3. Transient expression in *N. benthamiana*

A. tumefaciens carrying verified pK7FWG2:*TaCPEP* were grown overnight at 28°C with gentle shaking in LB containing 100 µg/mL spectinomycin, 100 µg/mL rifampicin and 100 µg/mL gentamycin. Cultures were spun at 3434 *g* for 10 mins and the pellet resuspended in 10 mL infiltration buffer (10 mM MES, 10 mM $MgCl_2$, 100 µM acetosyringone, pH 5.6). The OD_{600} was measured and the cultures adjusted to OD 0.3 for localisation or 0.6 for overexpression experiments, using infiltration buffer. Cultures were left for 1 hr with gentle shaking before infiltrating the underside of the two most recently fully emerged leaves of 4-week-old *N. benthamiana* (Bos *et al.*, 2006). For both localisation and *P. infestans* experiments, the leaves were infiltrated until fully saturated. Leaves were left for expression for 3 days before harvesting and use in experiments.

3. Identification of candidate Nuclear Genes encoding Chloroplast Proteins (NGCPs) implicated in wheat susceptibility to *Pst*

3.1. Introduction

Biotrophic fungal pathogens, such as the rust fungi, strike a delicate balance between disruption of chloroplast function to evade immune recognition and maintenance/manipulation of chloroplast processes to gain nutrients and complete their lifecycle. Therefore, understanding how chloroplastic processes change during wheat interaction with rust fungi can provide important insight into the mechanisms of resistance and susceptibility.

Photosynthesis is the process by which atmospheric carbon dioxide and water are converted into chemical energy using sunlight. These processes take place in photosynthetic organelles, which in plants are the chloroplasts. Within the chloroplasts are the thylakoid membranes where the machinery for the light-dependent reactions sits (Vothknecht and Westhoff, 2001). Here, the energy from light is absorbed by pigment molecules which move to an excited state. Electrons pass through the electron transport chain which consists of photosystems I and II, connected by cytochrome b_6f, plastoquinone and plastocyanin (Rantala *et al.*, 2020). The energy generated from this movement is used to create a proton gradient, which then drives the formation of ATP from ADP by ATP-synthase (Kramer *et al.*, 2003). NADPH is also generated through these reactions (Kramer and Evans, 2010). The ATP and NADPH generated by the light-dependent reactions feed into the light-independent reactions in the stroma. Here, atmospheric carbon dioxide is fixed to provide carbon skeletons for the biosynthesis of sugars. The photosynthetic processes are vital for the production of molecules that contribute to the plant response to abiotic and biotic stress, such as the phytohormones SA and JA (Choi, 2024). Below, I explore the role of the chloroplasts and photosynthetic processes in the plant response to pathogens, with a focus on processes that were explored in the current work.

Chloroplastic processes play a central role in the early immune response against pathogens as well in guarding plants against future attacks through SAR (Sowden *et al.*, 2017). During the immune response, signals from the chloroplasts act to initiate and coordinate signalling processes in a process known as retrograde signalling where the production of phytohormones and reactive oxygen species acts to influence nuclear gene expression to initiate transcriptional reprogramming and defence responses (Lewis *et al.*, 2015; Nomura *et al.*, 2012). Anterograde signalling, whereby signals from the nucleus feed back to the chloroplasts, also enables extremely reactive and finely tuned responses to external stimuli (Surpin *et al.*, 2002). The importance of chloroplastic contributions to plant immunity makes them vulnerable to pathogen manipulation, and indeed pathogens from across kingdoms have evolved effectors that target many chloroplast processes that leave the plant's immune system weakened (Littlejohn *et al.*, 2021). As a currently underexplored

area in wheat response to fungal pathogens, expanding our understanding of how the chloroplasts are altered during infection enables us to gain insight into the mechanisms of host manipulation and molecular wheat-*Pst* interactions.

3.1.1. Nuclear genes encoding chloroplast proteins (NGCPs) that function in the light-dependent reactions are targeted by pathogens to manipulate immune responses

The light harvesting machinery, located within the thylakoid membranes, consists of multi-protein complexes that harvest photons of light and convert this light energy into a proton gradient used to drive the synthesis of chemical energy stores in the form of ATP (Rantala *et al.*, 2020). A bi-product of these processes is reactive oxygen species (ROS), in the form of superoxide ($O_2^{\bullet-}$) and hydrogen peroxide (H_2O_2), and components of the photosynthetic electron transport chain (PETC) have in-built mechanisms for maintaining redox status making them remarkably robust to fluctuations in environmental conditions (Asada, 2006). The resilience to change is vital as disequilibrium can result in the production of excess ROS which can damage not only the photosystems themselves but also other cellular components, with the potential to initiate cell death (Liu *et al.*, 2007). The delicate redox balance and potential for ROS to trigger cell death make the chloroplasts highly sensitive and indispensable sensors of stress, as reviewed in Van Breusegem and Dat (2006). Moreover, as comprehensively reviewed in Ballaré (2014), light perception plays an important role in regulating phytohormone levels and the photoreceptor PhyB is a positive regulator of both jasmonate and salicylic acid signalling (Xie *et al.*, 2011).

The NGCPs *PsbP, PsbQ a*nd *PsbO* are subunits of an oxygen evolving enhancer (OEE) protein that binds PSII on the luminal side of the thylakoid membrane and mediates the water splitting reaction (Zabret *et al.*, 2021). Stable silencing of the *PsbP* gene in tobacco resulted in extreme growth reduction and pale green leaves, compared to wildtype plants (Ifuku *et al.*, 2005). ΔPsBP plants were hypersensitive to light and further analysis revealed that they had reduced levels of PSI and electron flow (Ifuku *et al.*, 2005). Similarly, *A. thaliana* mutants in *PsbO* had severely reduced photosynthetic activity (Murakami *et al.*, 2002). In contrast, loss of *PsbQ* has minimal effect on photosynthetic functions in PSII (Allahverdiyeva *et al.*, 2013). With this essential role in photosynthesis and the potential for these Psb proteins to influence the redox state of the photosynthetic electron transport chain, it is perhaps unsurprising that these proteins have been implicated in plant-microbe interactions (de Torres Zabala *et al.*, 2015).

The role of PsbP and PsbO in plant-virus interactions have been well characterised. It was early established that viruses can cause chloroplastic damage and functional disruption. For example, the radish leaf curl virus pathogenicity factor beta C1 (RaCLβC1), rice stripe virus (RSV) disease specific protein (SP) and the alfalfa mosaic virus coat protein (CP) have all been shown to interact with their respective host's PsbP proteins (Balasubramaniam *et al.*, 2014; Gnanasekaran *et al.*, 2019; Kong *et al.*, 2014). RaCLβC1 contributes to pathogenicity by binding to PsbP and reducing its ability to bind to viral DNA (Gnanasekaran *et al.*, 2019). SP and CP binding to PsbP was hypothesised to interfere with PsbP import into the chloroplast thereby disrupting its function in ROS production in immune signalling and enhancing plant susceptibility (Kong *et al.*, 2014; Balasubramaniam *et al.*, 2014). The alternanthera mosaic virus triple gene block 3 (TGB3) protein and the tobacco mosaic virus helicase interact with their host PsbO (Abbink *et al.*, 2002; Jang *et al.*, 2013). It was hypothesised that these interactions may disrupt PSII turnover and maintenance, leading to chloroplastic collapse. The *Nicotiana benthamiana* Kunitz peptidase inhibitor-like protein (KPILP) functions in retrograde signalling during potato virus X (PVX) infection (Ershova *et al.*, 2022). Loss of KPILP leads to a decrease in the total amount of PsbQ in the chloroplasts and it is hypothesised that the viral proteins are interacting with PsbQ to access the chloroplasts for virulence functions (Ershova *et al.*, 2022). In summary, plant-virus interactions provide many examples highlighting the role of the chloroplast in plant immune responses and how pathogens can manipulate the chloroplasts to promote infection.

Beyond their role in plant-virus interactions, there are also examples of PsbP, PsbQ and PsbO being targeted by non-viral plant pathogens. For instance, in the obligate biotrophic oomycete, *Plasmopara viticola,* an RXLR effector RXLR31154 was identified which interacts with PsbP (Liu *et al.*, 2021). Overexpression of PsbP by Liu *et al.* (2021) in *N. benthamiana* increased susceptibility to *P. viticola* whilst silencing increased resistance. Unlike the viral examples above, the interaction between RXLR31154 and the host PsbP occurs in the chloroplasts and causes PsbP stabilisation. The authors hypothesize that the stabilisation of PsbP could enhance susceptibility by reducing the production and accumulation of H_2O_2 whilst promoting the formation of $O_2^{\bullet-}$, an effect that would interfere with cROS production and immune signalling (Liu *et al.*, 2021). Similarly, the type III effector HopN1, from *Pseudomonas syringae*, and the LtGAPR1 effector from *Lasiodiplodia theobromae* (fungal agent of grapevine canker disease) function to suppress defence-related ROS signalling (Huang *et al.*, 2023; Rodríguez-Herva *et al.*, 2012). This effect was found to occur through the interaction of the effectors with PsbQ and a subsequent reduction in ROS signalling, programmed cell death (PCD) and callose deposition. Recent work focussed on the wheat

interaction with *Pst* found that the resistance gene *YR36/WKS1* encodes a protein that phosphorylates PsbO (Wang *et al.*, 2019c). PsbO phosphorylation leads to the dissociation of PsbO from PSII and disruption of photosynthesis. The authors suggest that this could slow initial infection by *Pst* to allow time for ROS signalling and the defence responses to begin, thus promoting pathogen resistance. These studies show that NGCPs are implicated in having positive and negative roles in the plant response to fungal pathogens.

PsaH is another NGCP that functions as a subunit of PSI that is thought to function in energy transfer between PSII and PSI and without it, state transitions are highly reduced (Lunde *et al.*, 2000). Plant PSI complexes are thought to only exist in a monomeric state, which PsaH has been shown to contribute to by restricting the formation of other oligomeric states (Naschberger *et al.*, 2022). In sunflower, the expression of PsaH is downregulated in response to sunflower chlorotic mosaic virus (Rodríguez *et al.*, 2012). The *Pyrenophora tritici-repentis* toxin Ptr ToxA triggers an increase in the total PsaH content in wheat upon infection (Manning *et al.*, 2009).

The above studies show that PsbP, PsbQ and PsbO are common targets for manipulation by viruses, bacteria, fungi, and oomycetes to enhance susceptibility. Although the precise role of PsaH in plant-pathogen interactions has not been fully elucidated, there is some evidence to suggest that it is differentially expressed during infection in two different pathosystems. Together, this evidence shows that NGCPs that encode for proteins involved in the light-dependent photosynthetic processes are key for plant immunity.

3.1.2. NGCPs that function in the light-independent reactions are implicated in the plant response to pathogens

The Calvin-Benson-Bassham (CBB) cycle uses the chemical energy stores ATP and NADPH formed in the light-dependent reactions to drive the fixation of atmospheric carbon for the biosynthesis of organic molecules including starch and sucrose (Geiger and Servaites, 1994; Quick and Neuhaus, 1997; Woodrow and Berry, 1988). Flux through the CBB cycle is regulated at multiple levels, and the mechanisms by which flux is controlled are complex and varied and have been proposed to include post-translational modification of CBB cycle enzymes, enzyme abundance, metabolite concentrations and energetic cofactors (Raines, 2003). The CBB cycle is therefore a highly dynamic and reactive process that ultimately controls the metabolic status of plants in different environmental conditions. Plant biotrophic, hemi-biotrophic and necrotrophic pathogens have evolved different lifestyles to extract nutrients from their host tissue (Rajarammohan, 2021).

All of these lifestyles cause massive host metabolic reprogramming and evidence has suggested that the CBB cycle is a particular target to facilitate these changes (Serag *et al.*, 2023).

One of the most important proteins in the CBB cycle is the NGCP Ribulose-1,5-bisphosphate carboxylase oxygenase (Rubisco) which initiates the CBB cycle by catalysing the carboxylation of ribulose 1,5-bisphosphate (RuBP) (Andersson and Backlund, 2008). Rubisco has long been the subject of intense efforts to engineer more photosynthetically efficient plants for agriculture and biotechnology (Prywes *et al.*, 2023). Several studies from different pathosystems have shown that the partial NGCP *Rubisco small chain* (*RSC*) is differentially regulated or modified during infection. For example, in wheat infected with *Fusarium graminearum* RSC production was upregulated (Shin *et al.*, 2011). Cucumber mosaic virus appears to induce post-translational modification of RSC, although the mechanism and reason for this has not been elucidated (Shimura *et al.*, 2011). Another major enzyme of the CBB cycle, encoded by a NGCP, is Phosphoribulokinase (PRK). PRK uses ATP from the light-dependent reaction to catalyse the phosphorylation of ribulose 5-phosphate (Ru5P) into ribulose 1,5-bisphosphate (RuBP), the CO_2 acceptor molecule for carbon fixation (Avron and Gibbs, 1974). It has been noted in *N. benthamiana* in response to RSV and in oil palm in response to the fungal pathogen *Ganoderma boninense* that PRK expression is decreased and increased, respectively (Bi *et al.*, 2021; Jeffery *et al.*, 2015). Bi *et al.* (2021) hypothesise that downregulation of *PRK* in response to RSV may be a defence response as the decrease in sugars may slow viral infection.

Overall, there is evidence from multiple pathosystems for the targeting of carbon fixation processes to manipulate host metabolism and influence susceptibility. This is particularly relevant to biotrophic pathogens that require the CBB cycle processes to gain sources of carbon whilst evading recognition. These proteins, along with those functioning in the light-dependent reactions, and those involved in chloroplastic movement as outlined in the General Introduction, form interesting candidates for NGCPs involved in plant immunity to *Pst*. These processes are outlined in **Figure 3.1** and form the foundation for investigations in this chapter.

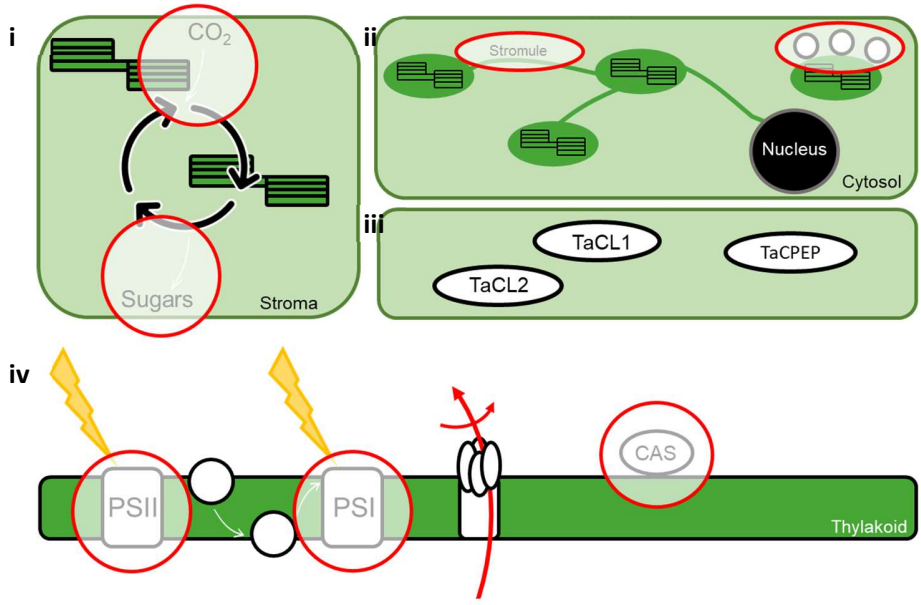

Figure 3.1 Schematic representation of chloroplastic processes implicated in the plant response to microbial pathogens.

Proteins that are chosen for further investigation are highlighted in red from the (**i**) CBB Cycle (**ii**) chloroplast movement in response to pathogens (**iii**) Unknown processes (**iv**) Light-dependent reactions. CBB, Calvin Benson Bassham; RuBisCO, Ribulose-1,5-bisphosphate carboxylase oxygenase; PRK, Phosphoribulokinase; Psb, photosystem II b subunit; CAS, Calcium Sensing receptor; CL, chloroplast localised protein; NRIP, N Receptor interacting protein; CHUP1, Chloroplast Unusual Positioning.

3.1.3. Introduction to the chapter

The aims of this chapter were to identify candidate chloroplastic processes and NGCPs involved in plant immunity to *Pst* for further exploration of this function following the objectives outlined below:

- Use previously published transcriptomic data (Corredor-Moreno *et al.*, 2022) to assess the changes in expression of wheat NGCPs during *Pst* infection to identify candidate genes that are implicated in contributing to susceptibility. Further explore homoeologue expression bias to inform subsequent studies.
- Explore wheat nuclear-chloroplast cross-talk during *Pst* infection by analysing the expression of chloroplast-encoded genes using previously published transcriptomic data (Corredor-Moreno *et al.*, 2022).
- Identify disruption mutants for candidate NGCPs and test their contribution to wheat susceptibility to *Pst* through infection assays.

3.2. Methods

3.2.1. Infection time-course experiment and RNA-sequencing

Prior to the start of this project, Pilar Corredor-Moreno (The John Innes Centre) conducted an infection time-course experiment (Corredor-Moreno *et al.*, 2022). In brief, two-week-old seedlings from the hexaploid wheat varieties Santiago, Solstice and Oakley were spray inoculated with fresh spores of the *Pst* isolates F22 and 13/14 which fall into the genetic groups 1 and 4, respectively (Hubbard *et al.*, 2015). Control plants were sprayed with Novec7000^{TM}. Leaf samples were collected at 0, 1-, 3-, 7- and 11-days post inoculation (dpi). RNA was extracted using the RNeasy Plant Minikit according to the manufacturer's instructions and sent for library preparation and RNA-sequencing by Genewiz (Azenta Life Sciences, Germany). Pilar Corredor-Moreno processed and analysed the RNA-sequencing data which was subsequently made publicly available (Corredor-Moreno *et al.*, 2022).

3.2.2. Analysis of the expression of chloroplast-encoded genes using the ChloroSeq pipeline

The differential expression of chloroplast-encoded genes was analysed following the ChloroSeq pipeline (Castandet *et al.*, 2016). The Chinese Spring chloroplast genome and annotations NC_002762 were downloaded from NCBI. RNA-seq reads from Corredor-Moreno *et al.* (2022) were downloaded from the European Nucleotide Archive (ENA) under the PRJEB50522 accession number. The pipeline was executed by Cesaree Morier-Gxoyiya who also contributed to figure making.

3.2.3. Selection of disruption mutants from the wheat TILLING population for the candidate NGCPs

Disruption mutants from the wheat TILLING population (Krasileva *et al.*, 2017) for the candidate genes were selected from Ensembl Plants (Yates *et al.*, 2021). Gene annotations from RefSeq v2.1 (Zhu *et al.*, 2021) were used to find TILLING lines for the candidate genes with a Sorting Intolerant From Tolerant (SIFT) score of 0. SIFT scores are a prediction of whether an amino acid substitution, or single nucleotide polymorphism (SNP), affect protein function. SIFT scores range from zero (deleterious) to one (tolerated). Where it was not possible to find a line with a SIFT score of zero, the line with a value closest to zero was chosen instead.

3.3. Results

3.3.1. Identification of candidate wheat NGCPs that contribute to wheat susceptibility to *Pst*

To determine how chloroplastic processes might be altered during the wheat interaction with pathogenic fungi, we sought to further explore the role of a subset of NGCPs during the *Pst* infection process. Previous sequence similarity searches had identified homologues of a number of NGCPs that included: (i) *PsbQ1* and *PsbQ2* that are components of the photosystem II complex*,* (ii) *PsaH*, a component of photosystem I, (iii) *RSC*, the small subunit of the enzyme rubisco, (iv) *PRK*, an enzyme that catalyses the reaction of ribulose-5-phosphate into RuBP, (v) *CL1*, *CL2* and *CPEP* that are predicted chloroplast localised proteins of unknown function, (vi) *NRIP* which encodes the wheat homologue of the *Tobacco* N-receptor interacting protein involved in stromule formation and (vii), *CAS,* which encodes the thylakoid localised calcium sensing receptor which mediates Ca^{2+} immune signalling. In addition, I decided to expand this initial set of NGCPs to also include *CHUP1* which is involved in stromule formation with NRIP and the movement of chloroplasts in response to abiotic and biotic stress. To identify homologues of *CHUP1* in wheat I conducted a protein similarity search in Ensembl Plants (Yates *et al.*, 2021) with the *A. thaliana* CHUP1 amino acid sequence obtained from The Arabidopsis Information Resource (TAIR) (Berardini *et al.*, 2015). The top hit corresponded to a gene, *TraesCS1D02G422700*, which had 59.57% sequence identify and an E-value of zero. The gene was also predicted to encode hydroxyproline-rich glycoprotein family protein, the same function as the *A. thaliana* CHUP1 protein. This gene was then used to identify the corresponding homoeologues in the A and B genomes. The wheat homologues of the NGCPs identified in other

systems provide a set of 12 candidate genes for contributing to *Pst* susceptibility that were taken forward for further investigation.

3.3.2. Multiple NGCPs were modulated over the course of *Pst* infection with expression correlating with *Pst* susceptibility

Previous expression profile analysis of NGCPs during a *Pst* infection time-course had identified a general temporal coordination in expression for each gene that differed in later time points dependent on susceptibility of the host variety. Host varieties and their susceptibility to *Pst* isolates used in this study are outlined in **Table 3.1**. Of the 12 candidate genes investigated here, 11 of them followed the pattern of expression outlined in Corredor-Moreno *et al.* (2022) across all homoeologues. These NGCPs were downregulated 1 day post inoculation (dpi), expression then increased at 3 dpi and was correlated with resistance level of the interaction at 7-11 dpi (**Figure 3.2**). However, *NRIP* did not follow this pattern of expression, but appeared to be induced early during infection regardless of the level of susceptibility in the interaction. As NRIP and CHUP1 are functionally linked and both involved in chloroplast movement around the cell in response to stress, I decided to carry both genes forward for further characterisation. Furthermore, *RSC* is only encoded on the A and D subgenomes, with no B homoeologue having been annotated, therefore the expression profile for *RSC* B is absent (**Figure 3.2**).

To expand the analysis of the expression of candidate NGCPs I pulled out individual genes from the RNA-seq data set published in Corredor-Moreno *et al.* (2022). The wheat varieties Oakley, Solstice and Santiago display differing susceptibly to the *Pst* isolate F22, as outlined in **Table 3.1**. I found that the A, B and D homoeologues were expressed at different levels for each of the 12 NGCPs. This difference was particularly apparent in the expression of *RSC* in control samples for which the D homoeologue was expressed 28%, 22% and 22% higher than the A homoeologue across the wheat varieties Oakley, Solstice, and Santiago, respectively. Additionally, the A homoeologue of *CL1* was not expressed at all in Solstice. To further explore this, I used the Wheat Expression Browser (Borrill *et al.*, 2016; Ramírez-González *et al.*, 2018) to assess the homoeologue expression bias for each candidate NGCP in the reference hexaploid wheat variety Chinese Spring, presented in **Table 3.2**. I also assessed the homoeologue expression bias for candidate NGCPs under biotic stress conditions and found that homoeologue expression is dynamic in response to fungal pathogens including *Pst, Zymoseptoria tritici, Fusarium graminearum,* MoT, and *Blumeria graminis* f.sp. *tritici,* with the average percentage of expression coming from the A, B and D homoeologues changing

upon infection. Under controlled conditions there is expression predominantly from the B genome with a small contribution from the A. Upon biotic stress (disease) however, there is a change in this balance with contribution from the A genome increasing by 66% and the contribution from the B genome decreasing by 33% (**Figure 3.3**). Data presented here revealed that the expression of NGCPs is modulated over the course of wheat infection with *Pst* and that this can be used to identify candidate genes whose expression is correlated with susceptibility. Together, these results can be used to inform the selection of candidate NGCPs for investigation with disruption TILLING mutants.

Table 3.1 Infection types for the interactions between wheat varieties Oakley, Solstice and Santiago and the *Pst* isolate F22, as determined by Corredor-Moreno (2019). Oakley with the highest infection score is the most susceptible variety, Solstice infected with F22 is moderately susceptible and Santiago is resistant. Disease scores follow the disease assessment scoring system outlined in McIntosh *et al.* (1995).

	Oakley	Solstice	Santiago
F22	3.8	2.5	0.5

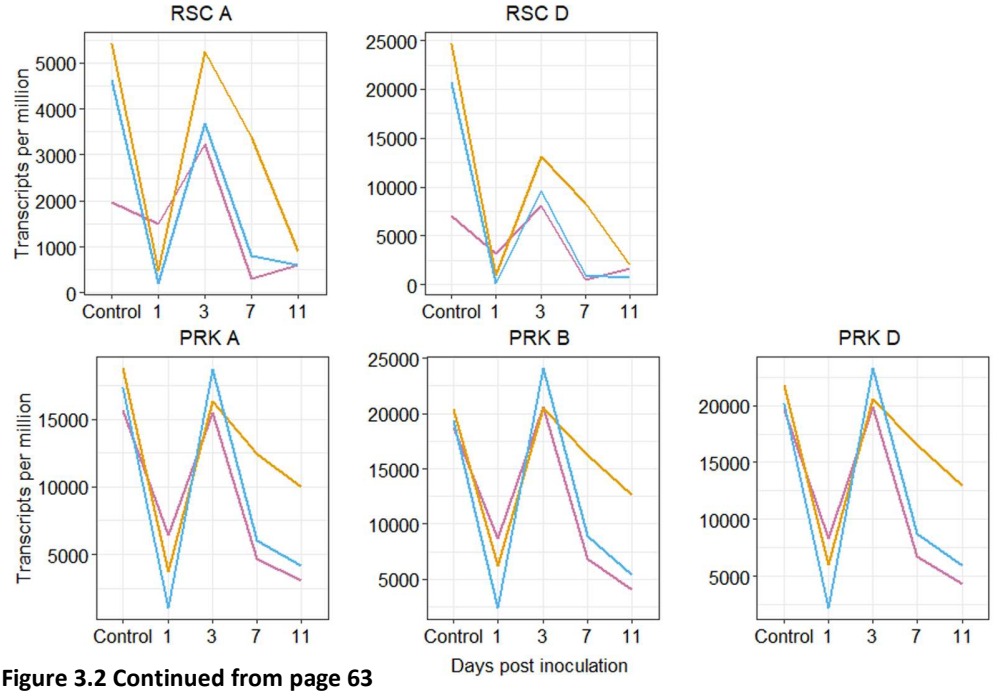

Figure 3.2 Continued from page 63

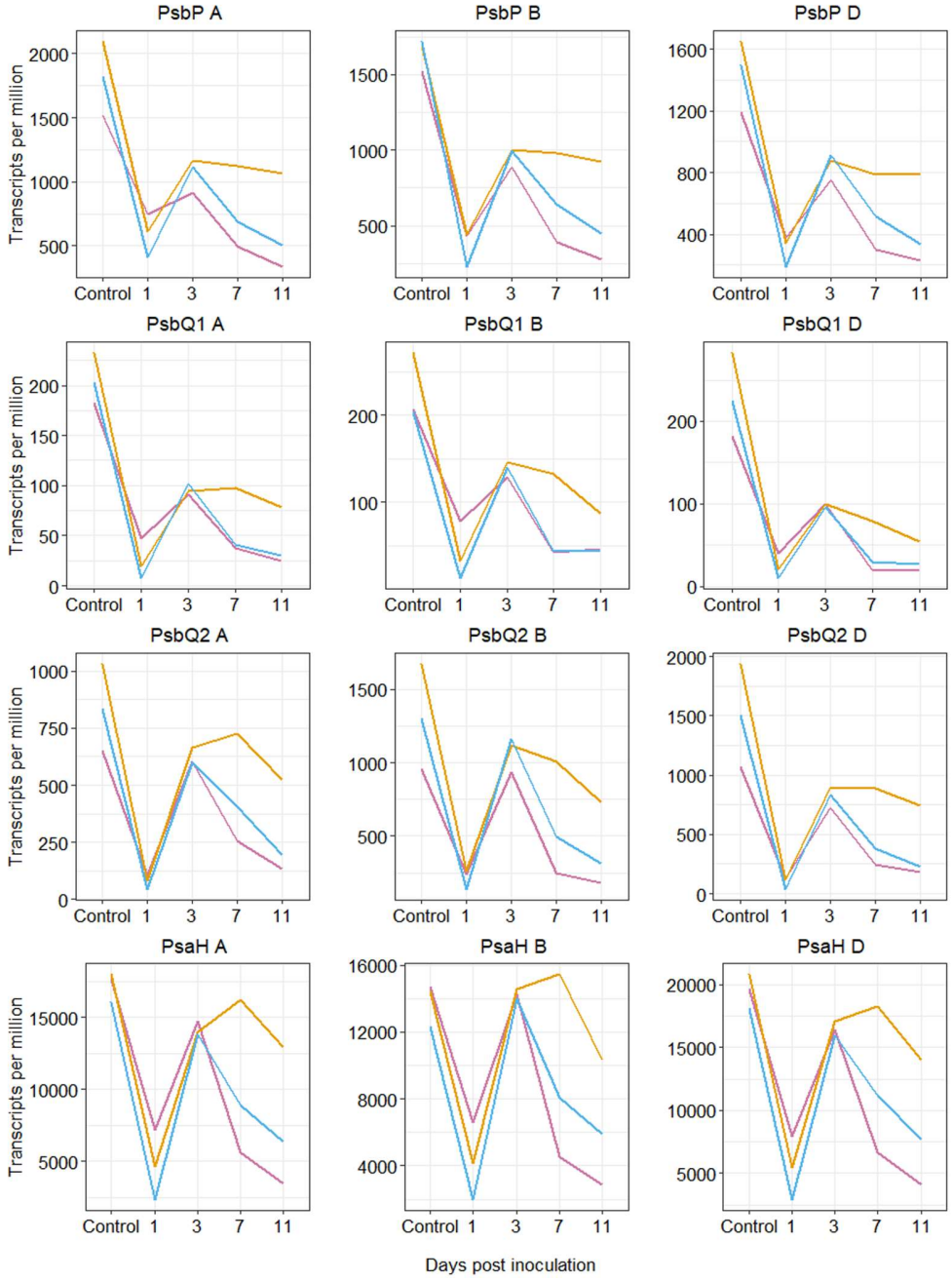

Figure 3.2 Continued from page 63.

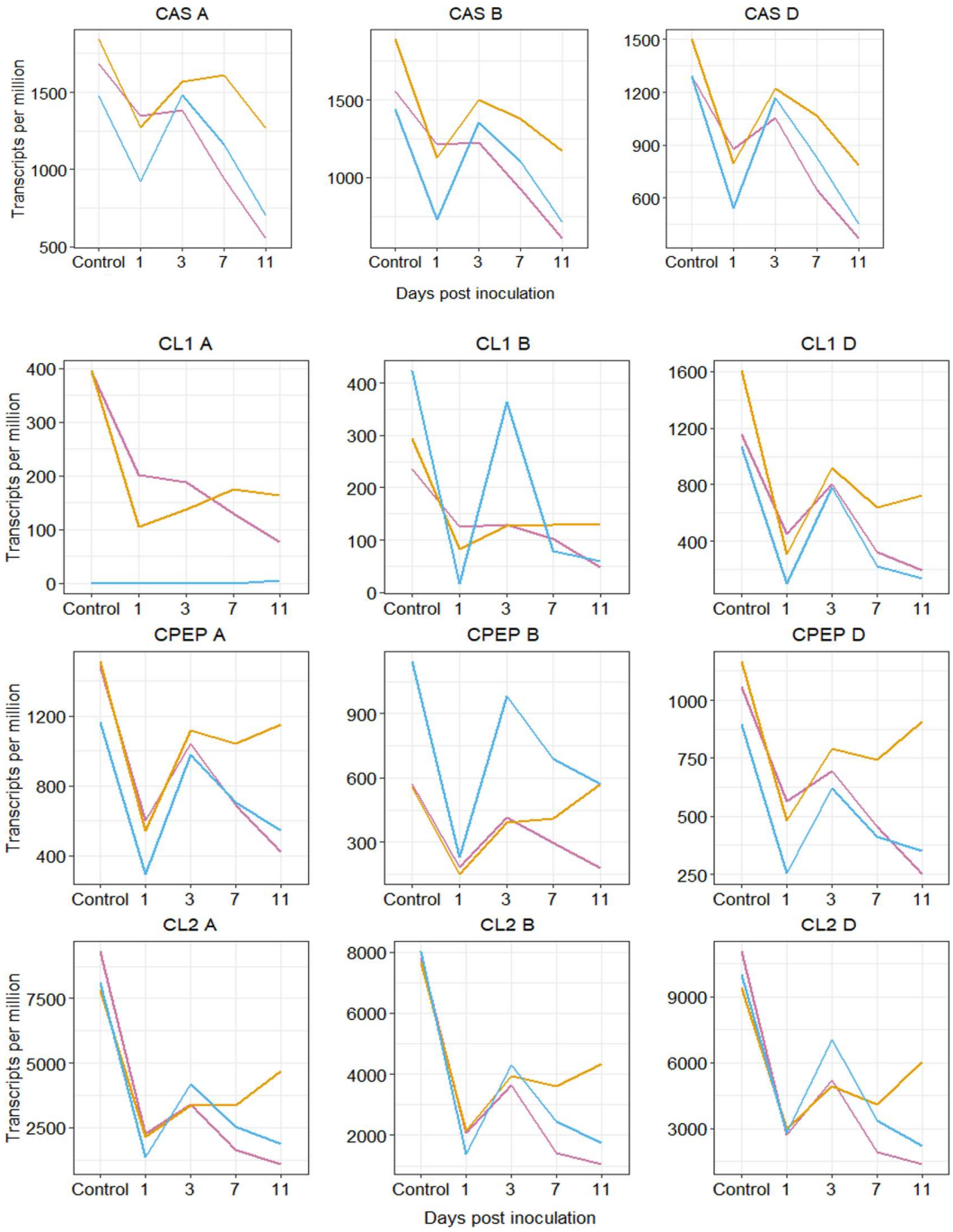

Figure 3.2 Continued from page 63.

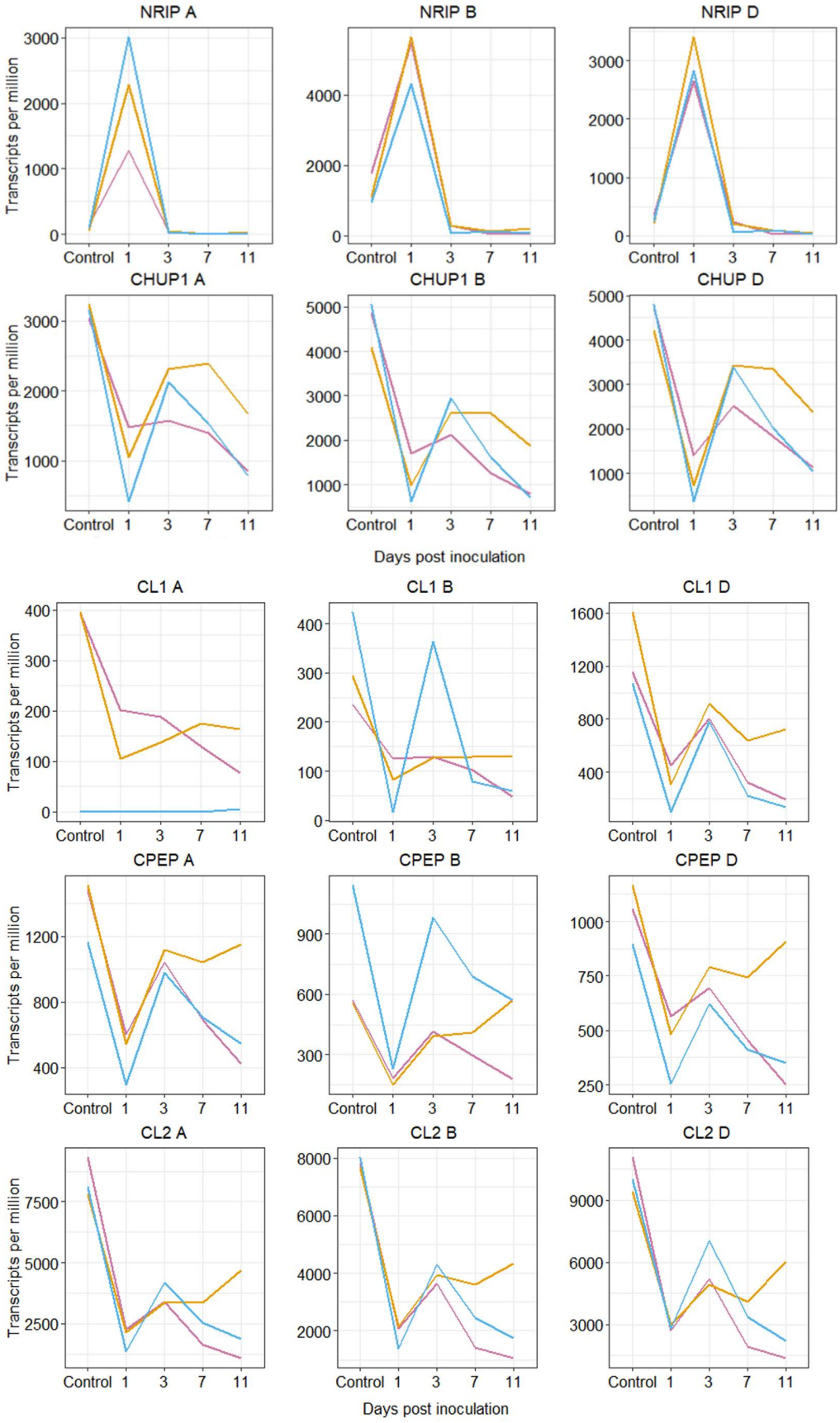
NRIP A
NRIP B
NRIP D
CHUP1 A
CHUP1 B
CHUP D
CL1 A
CL1 B
CL1 D
CPEP A
CPEP B
CPEP D
CL2 A
CL2 B
CL2 D
Transcripts per million
Control 1 3 7 11
Days post inoculation

Figure 3.2 The expression of candidate nuclear genes encoding chloroplast proteins (NGCPs) homoeologues displayed temporally coordinated expression profiles during *Puccinia striiformis* f. sp. *tritici* (*Pst*) infection. Candidate NGCPs which function in the light dependent reactions, the light-independent reactions, unknown function, chloroplast movement and calcium ion sensing in the chloroplast. The gene and homoeologue is labelled at the top of each graph. The expression of each homoeologue from the A, B and D subgenomes was analysed for the candidate NGCPs using RNA-seq data from Corredor-Moreno *et al.* (2022). Coloured lines represent expression levels in the wheat varieties Oakley (pink), Solstice (blue) and Santiago (yellow) infected with the *Pst* isolate F22. Santiago is the most resistant variety, with Oakley and Solstice showing higher susceptibility, as outlined in **Table 3.1.**

Table 3.2 Homoeologue expression bias of candidate nuclear genes encoding chloroplast proteins (NGCPs) is dynamic upon wheat infection with fungal pathogens.

The expression of NGCPs encoded on the A, B and D subgenomes were assessed using publicly available transcriptomic data from the Wheat Expression Browser (Borrill et al., 2016; Ramírez-González et al., 2018). Transcriptomic data from hexaploid wheat variety Chinese Spring infected with fungal pathogens including *Puccinia striiformis* f. sp. *tritici* (*Pst*) (Cantu *et al.* (2013), Zhang *et al.* (2014) and Dobon *et al.* (2016)), *Zymoseptoria tritici* (Yang et al. (2013) and Rudd *et al.* (2015)), *Fusarium graminearum* (Kugler *et al.* (2013) and Schweiger *et al.* (2016)), *Magnaporthe oryzae* pathotype *triticum* (Islam et al. (2016)) and *Blumeria graminis* f. sp. *tritici* (Zhang et al., 2014). Homoeologue-specific expression was unavailable for RSC and NRIP.

Gene	Protein	Percentage overall expression A|B|D (%)	
		Chinese Spring (control)	Stress (disease)
TraesCS4A02G101500 *TraesCS4B02G203100* *TraesCS4D02G204000*	PsbP	36.06|33.98|29.95	36.06|33.98|29.95
TraesCS2A02G344400 *TraesCS2B02G342000* *TraesCS2D02G322700*	PsbQ1	33.90|41.82|24.28	33.14|37.83|29.03

Table 3.2 continued

TraesCS6A02G206600 *TraesCS6B02G227900* *TraesCS4D02G045400*	PsbQ2	53.69|25.65|20.66	47.17|30.54|22.29
TraesCS1A02G392000 *TraesCS1B02G420100* *TraesCS1D02G400100*	Psah2	31.46|32.40|36.14	34.63|23.94|41.43
TraesCS2A02G067000 *TraesCS2D02G065400*	RSC	*	*
TraesCS6A02G267300 *TraesCS6B02G294700* *TraesCS6D02G247400*	PRK	32.34|33.54|34.12	31.04|35.81|33.15
TraesCS7A02G568800 *TraesCS7B02G489800* *TraesCS7D02G543800*	CL1	32.37|35.44|32.19	31.36|26.84|41.80
TraesCS2A02G523600 *TraesCS2B02G553500* *TraesCS2D02G525700*	CPEP	35.31|41.57|23.12	42.39|31.11|26.50
TraesCS5A02G488000 *TraesCS5B02G501800* *TraesCS5D02G502900*	CL2	30.96|39.75|29.29	38.70|29.44|31.86
TraesCS1A02G415200 *TraesCS1B02G445200* *TraesCS1D02G422700*	CHUP1	33.77|31.00|35.24	30.09|32.22|37.70
TraesCS7A02G545200 *TraesCS7B02G019600*	NRIP	*	*

Table 3.2 continued

TraesCS7D02G531600			
TraesCS6A02G290600			
TraesCS6B02G320900	CAS	35.09|38.23|26.67	31.99|41.51|26.50
TraesCS6D02G271900			

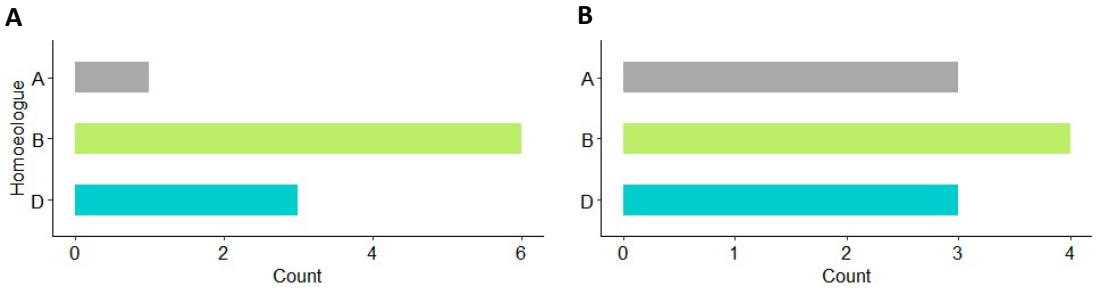

Figure 3.3 Summary of data presented in Table 3.2, using the same data.

Publicly available data from the Wheat Expression Browser (Borrill *et al.*, 2016; Ramírez-González *et al.*, 2018) was used to assess the homoeologue expression bias for each candidate NGCP in the reference wheat variety Chinese Spring under **(A)** control and **(B)** biotic stress (disease). Under controlled conditions, genes are predominantly expressed from the B genome with a small contribution from the A. When under biotic stress the expression bias shifts with an equal contribution from the A and D genome, but still with most genes predominantly expressed from the B genome.

3.3.3. Chloroplast-encoded genes are dynamically modulated during *Pst* infection

Given the modulation in NGCP expression during *Pst* infection, I then decided to examine the expression profiles of genes encoded in the chloroplasts to see if they displayed similar profiles. To explore whether the expression of chloroplast-encoded genes was altered during wheat infection with *Pst*, I re-analysed the existing RNA-seq data from Corredor-Moreno *et al.* (2022). Utilising the Chloroseq pipeline (Castandet *et al.*, 2016), we generated heat maps for chloroplast-encoded genes over the course of wheat infection with the *Pst* isolate F22 (**Figure 3.4**). The response of wheat varieties Oakley, Solstice and Santiago were compared. We found that the expression of chloroplast-encoded genes is dynamic during infection with *Pst*. For example, we found that transcript abundance for genes in the *ndh* operon, which encodes subunits of the NAD(P)H dehydrogenase complex, generally increased during infection in all interactions. This was most substantial at days 7 and 11. We further explored the expression of a subset of genes known to encode proteins of the photosystem complexes, and those involved in energy production in the chloroplast (**Figure 3.5**). I

chose to focus on these genes as they encode for components that have one or more subunits encoded in the nucleus, and function with the NGCPs of interest in this study. For example, *PsbA* encodes a protein (D1) of photosystem II and functions in photoprotection during oxidative stress (Mulo *et al.*, 2012). In the most susceptible interactions, that of Oakley and Solstice, transcript abundance increases in the latter stages of infection, whereas in the most resistant, that of Santiago, transcript abundance remains stable and low. In all varieties the relative abundance of the ATP synthase stalk subunit, *atpF* increases during infection, although the expression of *atpA* remains more stable. Overall, this analysis provides insight into the dynamic transcriptional environment of the chloroplasts during wheat infection with *Pst.*

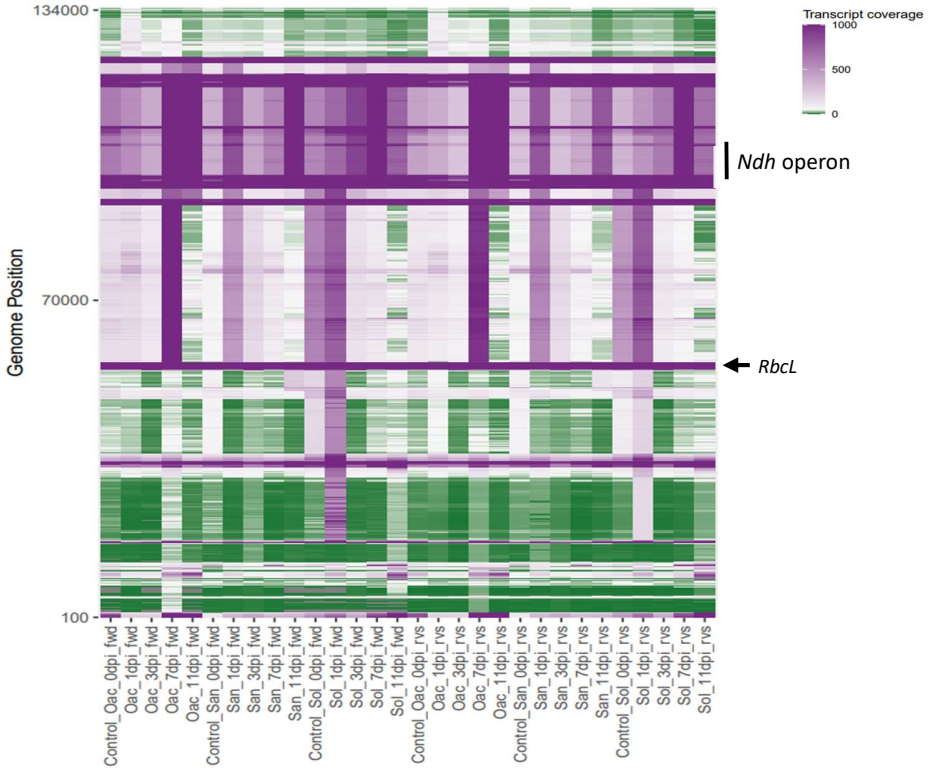

Figure 3.4 Changes in transcript abundance of chloroplast-encoded genes during wheat infection with *Puccinia striiformis* f.sp. *tritici* (*Pst*).

The Chloroseq pipeline (Castandet *et al.*, 2016) was utilised to assess the changes in expression of chloroplast-encoded genes during infection with *Pst.* Heatmap shows the expression of genes in wheat varieties Oakley (Oac), Solstice (Sol) and Santiago (San) infected with *Pst* isolate F22 at 1, 3, 7 and 11 dpi. The window coverage was set to a maximum of 1000. Control (0 dpi); fwd, forward strand; Rvs, reverse strand. *RbcL* is highlighted as a highly expressed control. Highly expressed genes are in purple, with low expression genes in dark green. Genome position refers to the position of the genes on the chloroplast genome.

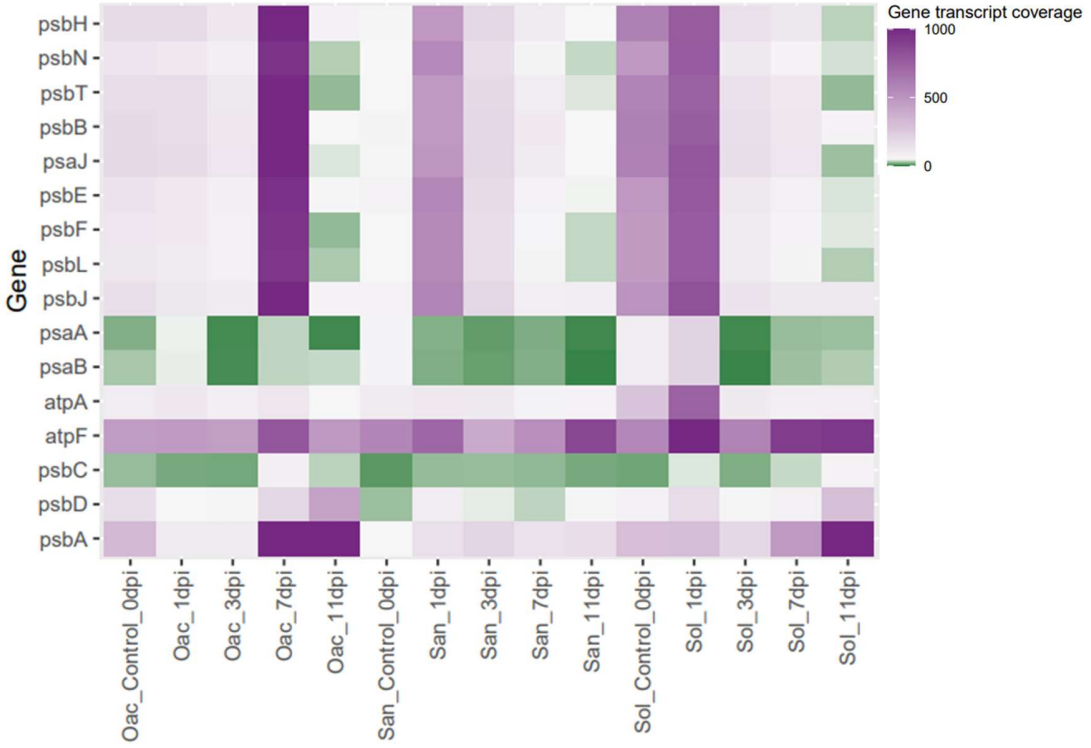

Figure 3.5. Transcript abundance for a subset of chloroplast-encoded genes that encode for energy production and photosystem complex proteins.

Genes in the *psb* and *psa* families encode proteins that function in the multi-protein complexes PSII and PSI. *atpA* and *atpF* encode for the alpha and beta subunits of ATP synthase, respectively. Heatmap shows the expression of genes in wheat varieties Oakley (Oac), Solstice (Sol) and Santiago (San) infected with *Pst* isolate F22 at 1, 3, 7 and 11 dpi. The window coverage was set to a maximum of 1000. Control (0 dpi).

3.3.4. The wheat TILLING population contains disruption mutants for the candidate NGCPs of interest

Having refined the list of candidate NGCPs to take forward based on expression pattern, my next aim was to identify mutants from the TILLING population (Krasileva *et al.*, 2017) to screen with *Pst* to assess their contribution to the *Pst* disease outcome. I searched the Ensembl Plants (Yates *et al.*, 2021) database for the wheat genes in the RefSeq v2.1 reference genome (Zhu *et al.*, 2021) and identified mutants from the TILLING population which fulfilled the following criteria: i) Had a high confidence gene annotation ii) Had a SIFT score of 0-0.1 to ensure the mutation was predicted to cause loss of protein function iii) Had homeologue and chromosome-specific primers available pre-designed for genotyping by KASP or could be designed by hand for genotyping. The generation time

of wheat is approximately four months under optimal conditions, however, the generation time and yield of highly mutagenised TILLING mutants can vary due to genome-wide mutagenesis. Therefore, where possible, I chose TILLING mutants in the spring wheat tetraploid variety Kronos. Although the aim was to identify mutants with the lowest SIFT score, it was still most preferable to obtain mutants which had stop-gained or splice acceptor/donor variant mutations as these are most likely to abolish protein function. However, at the time of obtaining mutants, very few of the genes had stop-gained or splice acceptor/donor mutants available. In this case, I chose missense mutants which had a SIFT score as close to zero as possible. I chose two mutant lines for each homeologue for each gene so that if one failed to germinate or had any developmental defects, then I would still be able to screen the gene. TILLING mutants were genotyped according to Section 2.4 upon receipt to confirm the presence of the mutant SNP. Those plants which were homozygous or heterozygous for the mutant SNP were self-pollinated for one or more generations, until there were sufficient seed for screening. The TILLING population at the John Innes Centre Germplasm Resource Unit is in at least the M6 generation (personal correspondence) and so the seeds received are highly likely to be homozygous for the mutant SNP. In the rare occurrence of performing genotyping and finding plants with the wildtype SNP, these plants were also self-pollinated to act as a control and from herein will be labelled accordingly. The identified mutants for the 12 candidate NGCPs are outlined in **Table 3.3**.

Table 3.3 TILLING lines chosen with high-impact mutations in nuclear genes encoding chloroplast proteins (NGCPs) of interest.

Two TILLING lines with different mutations were chosen for each homoeologue of the candidate genes. Where possible, stop gained or splice region variants were chosen, otherwise, missense mutants with a SIFT score as close to zero as possible were obtained.

Gene	Homoeologue	Subgenome	TILLING line	SNP	Consequence	SIFT
CAS	TraesCS6A02G290600	A	K2285	G/A	Missense	0
			K3842	C/T	Missense	0
	TraesCS6B02G320900	B	K3422	C/T	Missense	0.01
			K2110	G/A	Missense	0
PsbQ1	TraesCS2A02G344400	A	K2876	C/T	Missense	0.01
			K2702	G/A	Missense	0.01
	TraesCS2B02G342000	B	K2432	C/T	Missense	0
			K2703	C/T	Missense	0
PsbQ2	TraesCS6A02G206600	A	K0447	G/A	Missense	0

Table 3.3 continued

			K3622	G/A	Stop gained	0
	TraesCS6B02G227900	B	K0651	G/A	Missense	0.01
			K3103	C/T	Missense	0.01
Psah2	TraesCS1A02G392000	A	K2171	C/T	Missense	0.01
			K4240	G/A	Missense	0
	TraesCS1B02G420100	B	K3587	G/A	Missense	0.01
			K2317	G/A	Missense	0
PRK	TraesCS6A02G267300	A	K1400	C/T	Missense	0
			K2188	G/A	Missense	0.01
			C1325	C/T	Stop gained	0
			C1602	C/T	Splice acceptor variant	0
	TraesCS6B02G294700	B	K3548	G/A	Missense	0
			C0557	G/A	Stop gained	0
PsbP	TraesCS4A02G101500	A	K4273	C/T	Missense/splice region variant	0
			K4059	G/A	Missense	0
	TraesCS4B02G203100	B	K0572	C/T	Missense/splice region variant	0
			K355	C/T	Missense/splice region variant	0.05
RSC	TraesCS2A02G067000	A	C1262	C/T	Missense	0
			C1701	G/A	Missense	0
	TraesCS2D02G065400	D	C0117	G/A	Missense	0
			C2026	G/A	Missense	0
NRIP	TraesCS7A02G545200	A	K0234	G/A	Missense/ splice region variant	0
			K2524	C/T	Missense/splice region variant	0
	TraesCS7B02G019600	B	K4595	G/A	Missense	0
			K3332			
CL1	TraesCS7A02G568800	A	K4268	C/T	Missense	0
			K2073	G/A	Missense	0
	TraesCS7B02G489800	B	C1045	G/A	Splice donor variant	-
CL2	TraesCS5A02G488000	A	K2536	C/T	Missense	0
	TraesCS5B02G501800	B	K4079	C/T	Missense	0
CPEP	TraesCS5A02G523600	A	K4002	C/T	Splice acceptor variant	-

Table 3.3. continued

TraesCS2B02G553500	B	K2206	G/A	Stop gained	-

3.3.5. Assessment of chloroplast transit peptides (cTPs) in the protein sequences of candidate NGCPs

To confirm that the candidate NGCPs encoded for proteins that were predicted to be localised in the chloroplast, I ran the amino acid sequence for each homoeologue of each gene through LOCALIZER 1.0.4 (Sperschneider *et al.*, 2017). All proteins except the D homoeologue of CL1 and CHUP1 were predicted to encode a N terminal chloroplast transit peptide (cTP) (**Table 3.4**.) For each of the NGCPs, I then set out to explore their role more broadly during the *Pst* infection process.

Table 3.4 Final list of candidate nuclear genes encoding chloroplast proteins (NGCPs) of interest with predicted chloroplast transit peptide (cTP).

IWGSC RefSeq v1.1 (Appels *et al.*, 2018) gene name of each of the NGCP homoeologues encoded on the A, B and D genomes of wheat. The predicted functional location of these proteins and the probability and position of a chloroplast transit peptide was assessed.

Gene	Protein	Predicted protein location within chloroplast	Chloroplast transit peptide (probability[i]position[ii])
TraesCS4A02G101500	PsbP	Photosystem II	0.976[i] 1-30[ii]
TraesCS4B02G203100			0.974[i] 1-30[ii]
TraesCS4D02G204000			0.976[i] 1-30[ii]
TraesCS2A02G344400	PsbQ1	Photosystem II	0.998[i] 1-33[ii]
TraesCS2B02G342000			0.991[i] 1-26[ii]
TraesCS2D02G322700			0.992[i] 1-30[ii]
TraesCS6A02G206600	PsbQ2	Photosystem II	1[i] 1-30[ii]
TraesCS6B02G227900			1[i] 1-29[ii]
TraesCS4D02G045400			1[i] 1-30[ii]
TraesCS1A02G392000	Psah2	Photosystem I	0.974[i] 1-41[ii]

Table 3.4 continued

TraesCS1B02G420100			0.986[i] 1-41[ii]
TraesCS1D02G400100			0.974[i] 1-41[ii]
TraesCS2A02G067000	RSC	Stroma	0.999[i] 1-51[ii]
TraesCS2D02G065400			1[i] 1-51[ii]
TraesCS6A02G267300	PRK	Stroma	1[i] 1-41[ii]
TraesCS6B02G294700			1[i] 1-41[ii]
TraesCS6D02G247400			0.999[i] 1-41[ii]
TraesCS7A02G568800	CL1	Unknown	0.989[i] 1-45[ii]
TraesCS7B02G489800			0.999[i] 1-34[ii]
TraesCS7D02G543800			*
TraesCS2A02G523600	CPEP	Unknown	0.983[i] 1-29[ii]
TraesCS2B02G553500			0.957[i] 1-37[ii]
TraesCS2D02G525700			0.927[i] 1-37[ii]
TraesCS5A02G488000	CL2	Thylakoid membrane	0.998[i] 1-32[ii]
TraesCS5B02G501800			0.998[i] 1-32[ii]
TraesCS5D02G502900			0.998[i] 1-29[ii]
TraesCS1A02G415200	CHUP1	Cytosol/ chloroplast outer membrane	*
TraesCS1B02G445200			*
TraesCS1D02G422700			*
TraesCS7A02G545200	NRIP	Nucleus or chloroplast	*
TraesCS7B02G019600			*
TraesCS7D02G531600			*
TraesCS6A02G290600	CAS	Thylakoid membrane	0.989[i] 1-50[ii]
TraesCS6B02G320900			0.993[i] 1-50[ii]
TraesCS6D02G271900			0.98[i] 1-50[ii]

3.3.6. Candidate NGCP disruption mutants were screened with *Pst* to assess their contribution to wheat susceptibility

To assess the contribution of each of the candidate NGCPs to wheat susceptibility to *Pst,* I inoculated the disruption mutants with the *Pst* isolate 13/14, as this isolate is virulent on the wheat varieties Kronos and Cadenza. The disruption mutants for the candidate NGCPs of interest were successfully infected with *Pst* and formed pustules by 21 dpi. Whilst the levels of infection were limited in the variety Kronos, making resistance/susceptibility difficult to score, the infections took and progressed well in the Cadenza background lines. For almost all mutant lines there was no clear effect of the mutation on pathogen resistance (**Figure 3.6**). However, mutants in one gene, *TaCPEP,* did show difference in susceptibility and this phenotype will be presented and explored further in Chapter 4.

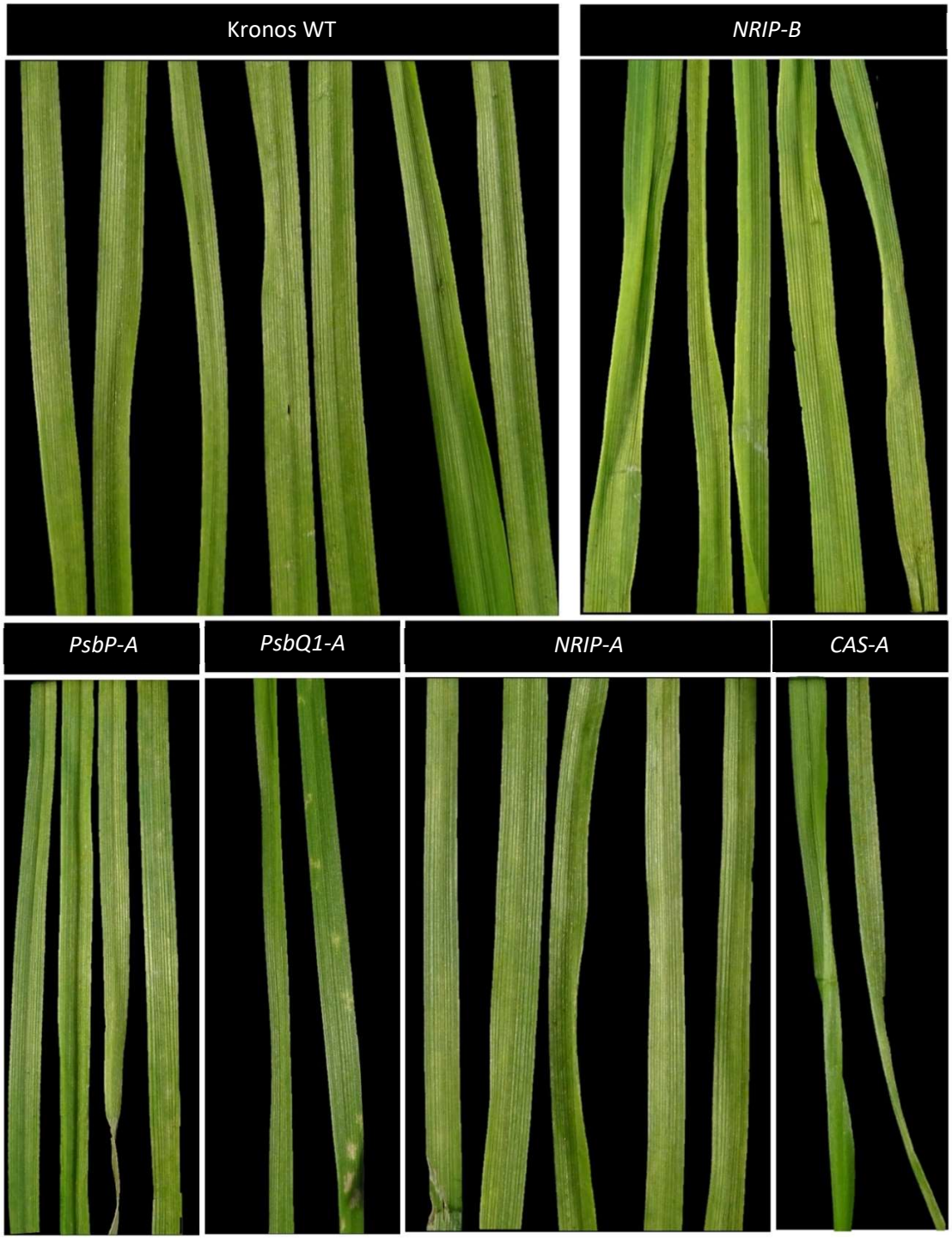

Figure 3.6 continued from page 76.

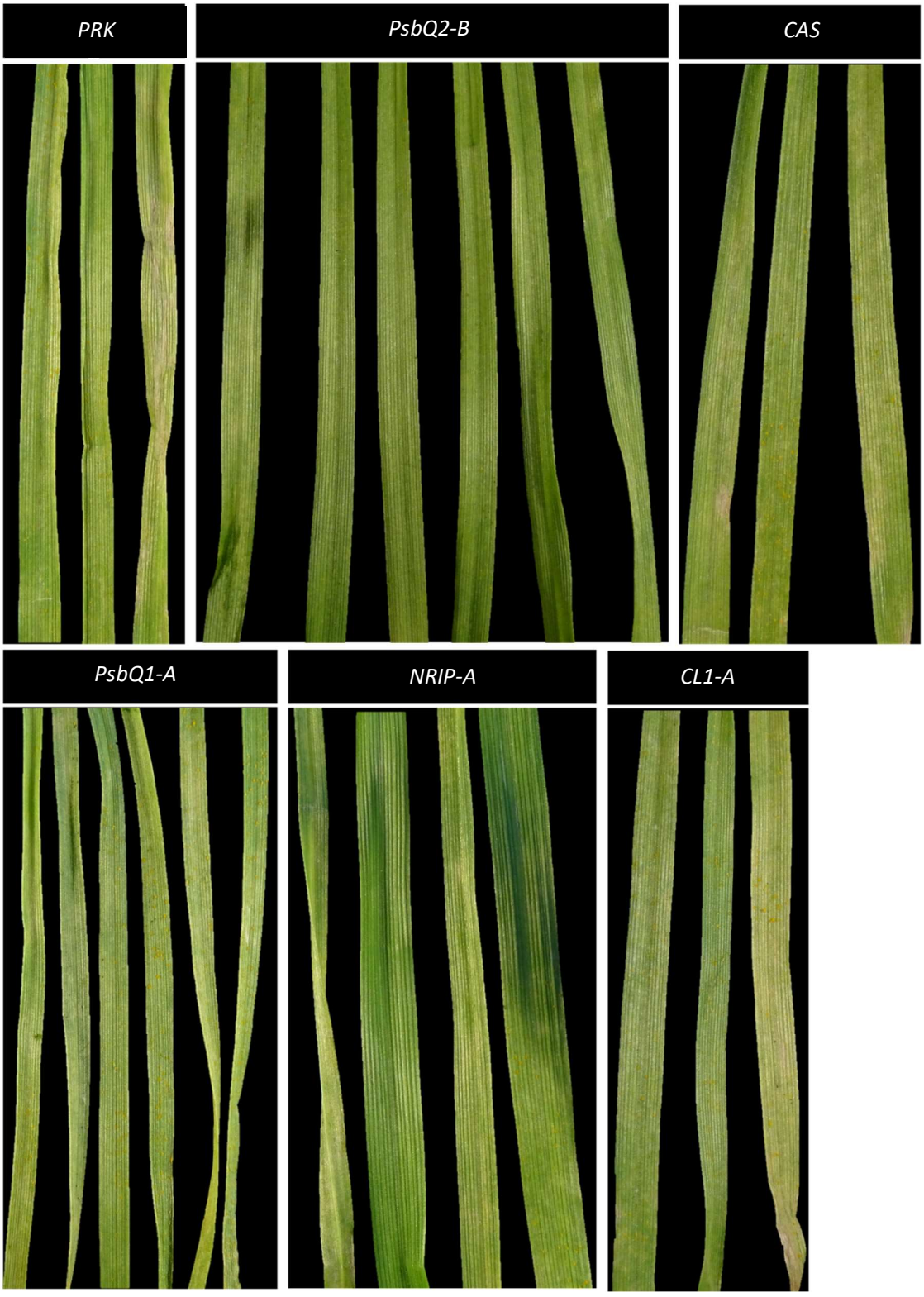

Figure 3.6 continued from page 76.

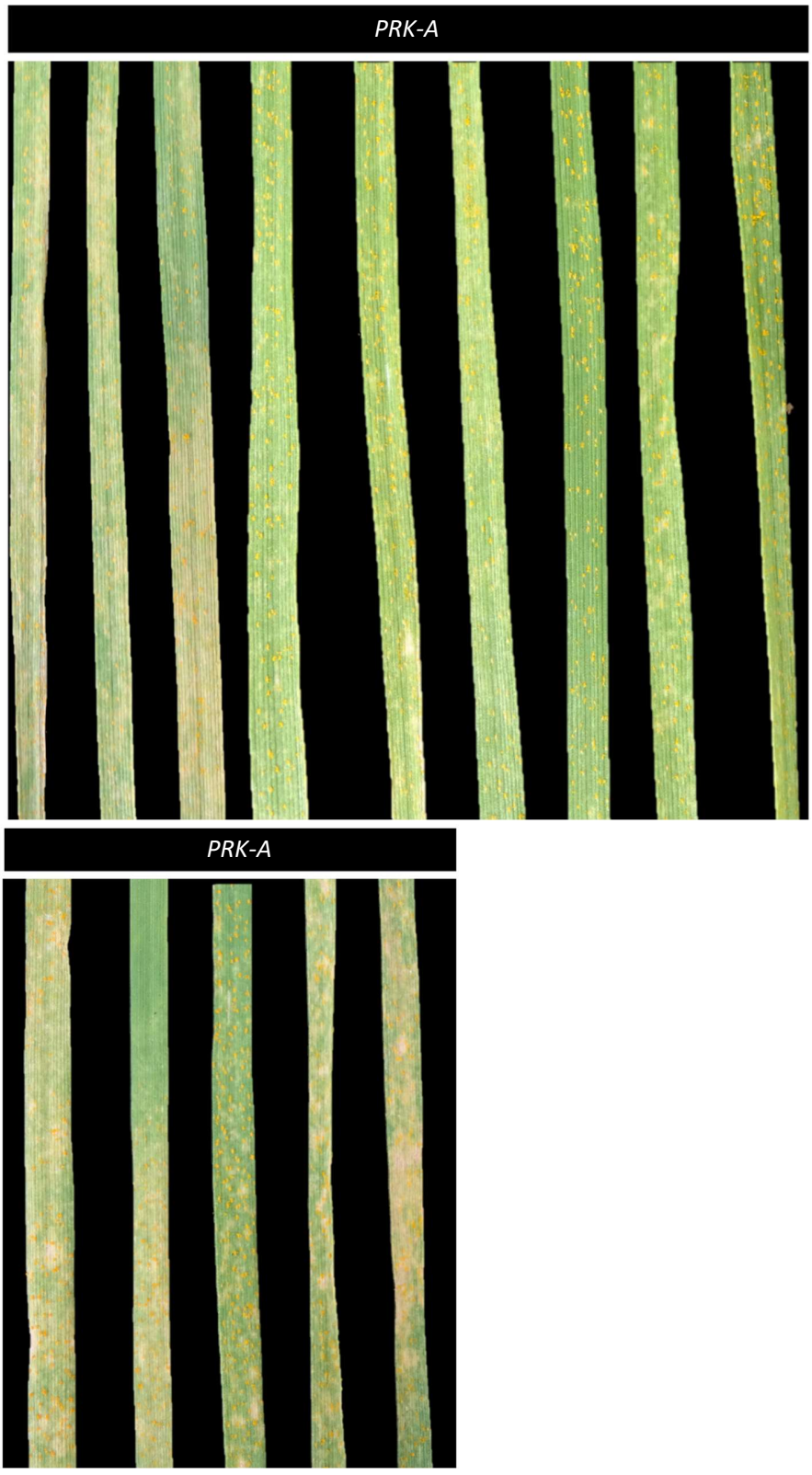

Figure 3.6 Continued from page 76.

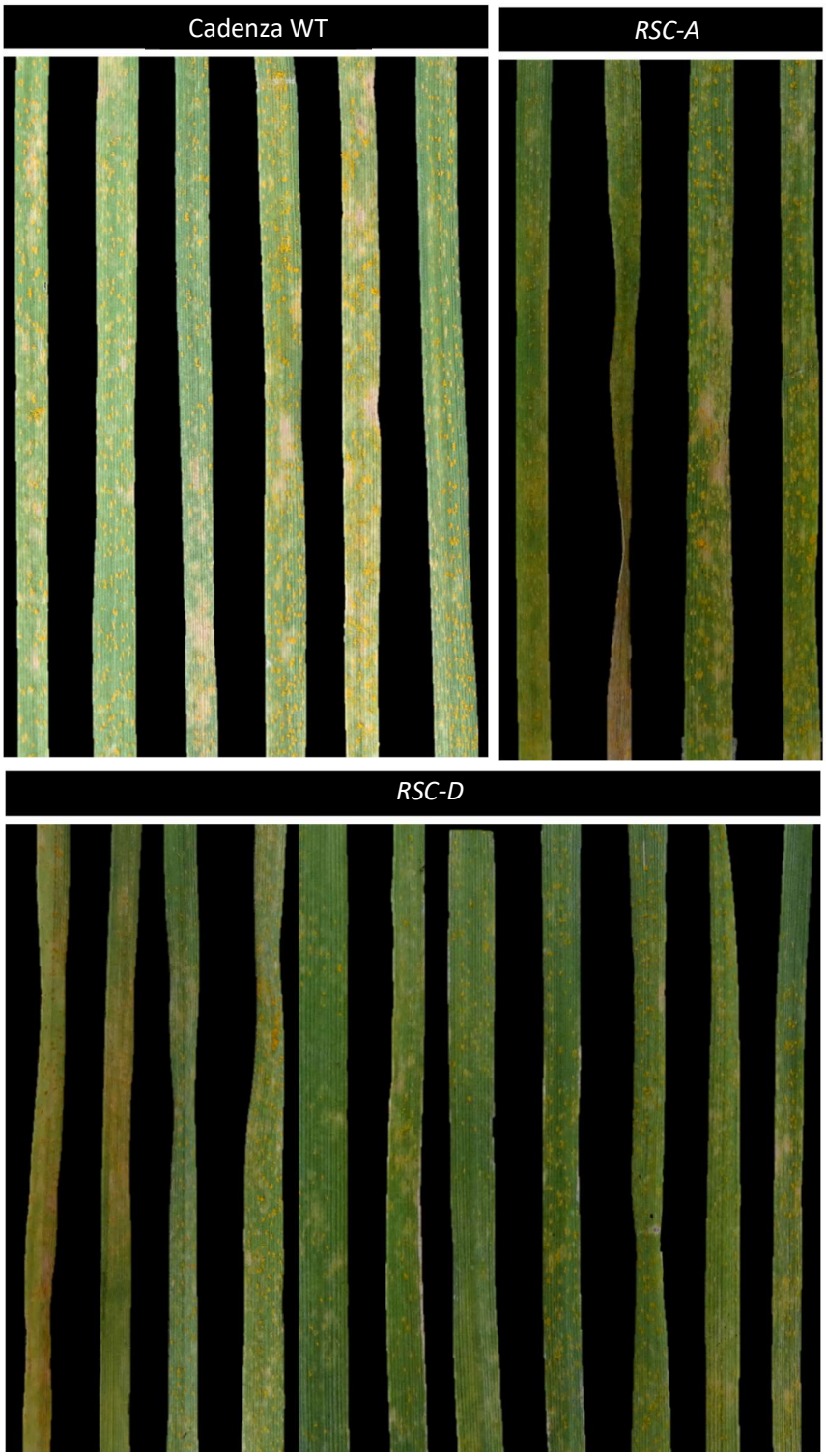

Figure 3.6 NGCP disruption mutants in the Kronos and Cadenza varieties were screened with *Puccinia striiformis* f.sp. *tritici* (*Pst*).

The disruption mutants for 7 candidate NGCPs were infected with the *Pst* isolate 13/14 and images of infection were taken when pustules were formed on the leaf surface, between 14 and 17 dpi.

3.4. Discussion

In this chapter, I utilised existing RNA-sequencing data from an infection time-course to explore the transcriptomic changes occurring for NGCPs during wheat infection with *Pst*. This analysis provided insight into how wheat chloroplastic processes might be affected by infection with *Pst*. Using the RNA-sequencing data I identified candidate NGCPs of interest which showed coordinated modulation of expression which correlated with the level of resistance of the interaction. I further characterised the chloroplastic contributions to the wheat response to *Pst* by assessing the expression of chloroplast-encoded genes. Using a reverse genetics approach, I explored the function of candidate NGCPs in relation to wheat infection with *Pst.* Finally, I identified disruption or missense mutants from the TILLING population and carried out *Pst* infection assays to assess whether there were changes to the level of infection. Those mutants which showed altered levels of susceptibility to *Pst* were taken forward for further investigation.

3.4.1. Previously published RNA-sequencing data was used to identify candidate NGCPs that may function in the wheat response to *Pst*

Using previously published RNA-sequencing time-course data in which resistant and susceptible wheat-*Pst* interactions were compared, I expanded the list of candidate NGCPs to a final subset that had modulated expression correlated with the level of susceptibility of the interaction. Candidate genes had higher expression at the end of infection in the resistant interaction than the susceptible interaction (Corredor-Moreno *et al.*, 2022). The hypothesis was that these genes and the proteins they encode may contribute to supporting *Pst* infection. In this previous study the authors provide a proof-of-concept by testing the contribution of one NGCP, called *TaCsp41-a*, and showing that disruption results in increased resistance to *Pst*, supporting the hypothesis that these genes may function during the wheat-*Pst* interaction (Corredor-Moreno *et al.*, 2022). Additionally, during initial identification of NGCPs, there were several genes which didn't have the pattern of expression associated with the level of resistance (data not shown). This suggests that the expression of NGCPs that is correlated with the level of resistance may be a specific effect for those genes implicated in contributing to susceptibility.

A candidate NGCP identified at the onset of the project was *PsbO*, which is a component of the multiprotein oxygen evolving complex (OEC) of photosystem II (PSII) complex and contributes functionally to water splitting during the light-dependent reactions of photosynthesis (Enami *et al.*,

1998) and regulating the PSII repair cycle (Lundin *et al.*, 2007). Soon after the onset of the current project, a study showed that the yellow rust resistance gene *Yr36* confers resistance to *Pst* through phosphorylation and degradation of PsbO from PSII (Wang *et al.*, 2019c). This study suggests an integral role for PsbO, and wheat photosynthetic processes, in *Yr36*-mediated resistance to *Pst*. This gene was subsequently not included in the set of candidate genes in the current study; however, it may provide support for choosing other NGCPs which are components of the same complex or function within the same processes.

Furthermore, numerous candidate effector proteins from *Pst* have been characterised and are suggested to interact with chloroplastic processes to modulate wheat immunity. For example, the *Pst* candidate effectors Pst_4, Pst_5 and Pst_12806 were shown to supress plant immunity when heterologously expressed in *N. benthamiana* (Wang *et al.*, 2021; Xu *et al.*, 2019). When the candidate effectors were knocked down in *Pst* using RNA interference, *Pst* virulence was attenuated. Further functional characterisation revealed that both candidate effectors interacted with the chloroplastic protein TaISP. TaISP mediates electron transport between PSII and PSI and its inhibition by candidate effectors leads to reduced ROS production and enhanced susceptibility. It is impossible to know from the expression data alone whether NGCPs in the current study are specific targets of *Pst* manipulation or a result of susceptibility/ resistance mechanisms. However, the emerging studies showing how *Pst* targets photosynthetic apparatus and electron transport demonstrates the importance of photosynthetic processes for *Pst* pathogenesis and highlights the potential for the candidate NGCPs in the present study to be implicated in the wheat response to *Pst.*

It has been shown in previous studies in hexaploid wheat and tetraploid *Brassica napus* that there can be bias in the expression of genes from the subgenomes and that this can provide flexibility and elasticity in the adaptability of polyploids to abiotic and biotic stresses (Bhanbhro *et al.*, 2020; de Jong and Adams, 2023; Lee and Adams, 2020; Liu *et al.*, 2015). Additionally, in response to infection by *Fusarium* sp., the expression of homoeologues in wheat changes in a process termed 'homoeologue induction bias'. In this study, genes from the B and D genomes were found to contribute more to the transcriptional response to *Fusarium* sp. (Powell *et al.*, 2017). In the present study, we found that for the NGCPs of interest, the contribution from the A genome increased when under a biotic stress. This may imply that there is also a degree of homoeologue induction bias in the NGCPs. Knowing if there is bias in the expression of homoeologues in wheat in response to pathogens could help to inform the selection and screening of TILLING mutants. If one homoeologue

contributes more to overall gene expression then it could be more appropriate to obtain mutants in that copy to assess the impact of disruption of that NGCP.

There is extensive literature which describes the mechanisms by which the photosynthetic apparatus compensates for loss of photosystem components and in some cases, the loss of subunits has even been shown to enhance photosynthetic rates. For example, An early study revealed that the loss of the PSI-G subunit of photosystem I resulted in no detectable difference in photosynthetic parameters or chlorophyll b content (Jensen *et al.*, 2002). The authors revealed that the loss of PSI-G resulted in a more efficient PSI due to a 48% increase in the reduction of $NADP^+$. Furthermore, studies have shown that, whilst PSI-H (*PsaH*) is required for PSI stability and electron transfer, plants compensate for the loss of PSI-H by increasing P700/chlorophyll ratio by 15% which results in maintenance of the photo-protectant mechanism of non-photochemical quenching (Naver *et al.*, 1999). These studies demonstrate the difficulty in predicting the outcome of the disruption of some of the candidate NGCPs from the current study on photosynthetic processes. Furthermore, as we do not know the mechanisms by which the expression of these NGCPs are manipulated during wheat infection with *Pst*, it is difficult to conclude whether the lack of infection phenotype is due to the protein not being involved in susceptibility, or if an effect would only be seen with the loss of additional protein components. In the future, one approach could be to start with fewer candidate genes and/or focusing on fewer chloroplastic processes which would enable a more rigorous screen to be carried out as less plant material has to be generated. This would also enable candidate genes to be tested in a more targeted way to disrupt gene function, such as CRISPR-Cas9 gene editing or virus-Induced Gene Silencing (VIGS). This would also enable the effects of the loss of multiple components to be tested, as VIGS could be used in combination with the TILLING mutants, or CRISPR-Cas9 could be used to knock-out multiple genes in the same line.

3.4.2. Whole-tissue RNA-seq data can be used to analyse changes to the expression of chloroplast-encoded genes during wheat infection with *Pst*

As the expression of chloroplast- and nuclear-encoded genes are so tightly linked, particularly during development or in response to abiotic and biotic stress (Chan *et al.*, 2016), I retrospectively analysed the whole-tissue RNA-seq data generated by Corredor-Moreno *et al.* (2022). I confirmed that the RNA-seq had captured transcripts encoding for genes in the chloroplasts and that there was enough resolution to detect changes in expression over time and between varieties. The chloroplasts have maintained some characteristics of prokaryotic genome

organisation and have genes organised into functional operons and most are transcribed as polycistronic units (Wicke *et al.*, 2011). Therefore, I could see changes in groups of genes in response to infection and infer their potential function in the wheat-*Pst* interaction.

Compared to the control samples, the expression of *ndh* genes increased in all wheat varieties in response to *Pst* infection. The ndh protein complex sits in the thylakoid membrane and forms a supercomplex with PSI in *A. thaliana* (Peng *et al.*, 2008). This complex functions as an electron acceptor and has been shown to regulate the proton gradient and prevent overreduction of the stroma (Yamori *et al.*, 2011). It has thus been well documented that the ndh complex has an important function in photoprotection under oxidative stress by experiments that showed that loss of function mutants for the ndh complex are more sensitive to oxidative stress (Endo *et al.*, 1999). Studies have also shown that the transcript levels of two genes encoding subunits of the complex, *ndhB* and *ndhF*, increased two-fold in barley in response to ROS in the form of H_2O_2 (Casano *et al.*, 2001). Furthermore, ROS play an important role in the wheat response to *Pst,* with extensive literature illustrating the importance of wheat ROS in susceptibility to *Pst* (Wang *et al.*, 2019c; Wang *et al.*, 2021; Xu *et al.*, 2019; Wang *et al.*, 2022; Zhang *et al.*, 2020). Therefore, it may be that the increase in *ndh* transcript abundance could be due to an increase in oxidative stress during infection with *Pst* resulting from immune responses or *Pst*-induced changes to photosynthesis.

The D1 protein, encoded by the chloroplastic gene *psbA,* has been shown to play a key role in the turnover of photosystem II, with it commonly being damaged under oxidative stress. It has been known for many years that the transcription of *psbA* increases in response to altered energy distribution (Pfannschmidt *et al.*, 1999). There is likely to be extensive alterations in energy demands, in addition to disruption in photosynthetic processes causing oxidative stress, when wheat is infected with *Pst* (as reviewed in Yang and Luo (2021)). Therefore, the increase in transcript abundance in the more susceptible interactions may indicate that these plants are under oxidative stress caused by infection by *Pst.* Furthermore, in the more susceptible interactions, the abundance of transcripts for the gene encoding the stalk component ATP synthase subunit, *atpF*, were increased in the susceptible interactions, and remained low and stable in the resistant interaction. This could be due to an increase in energy demanded from an obligate biotrophic interactions. Studies have shown that ATP accumulates in citrus plants in response to infection by the bacterial pathogen *Candidatus* Liberibacter asiaticus and that this can be seen at the transcriptional level by upregulation of ATP synthase genes (Pitino *et al.*, 2017). The authors found that ATP accumulation increased as disease symptoms increased. Whilst this might indicate possible reasons why *atpF*

transcripts might become more abundant, more work would be required to understand if this is biologically relevant in the wheat-*Pst* system.

By isolating the expression of specific groups of genes, we could hypothesise which processes might be altered during infection. As there is extensive crosstalk between nuclear and chloroplast gene expression in response to stress, we could hypothesise that the changes in expression in chloroplast-encoded genes could reflect global transcriptional responses to *Pst* infection. This provides support for our hypotheses that the chloroplasts are critical players in the wheat response to *Pst.* We were able to perform the ChloroSeq analysis because Corredor-Moreno *et al.* (2022) used both random hexamers and oligo dTs in the synthesis of cDNA from whole-tissue RNA samples which enabled synthesis of chloroplast-encoded genes. However, to further confirm these findings it would be advantageous to use a more targeted method to measure the expression of chloroplast-encoded genes. For example, by performing chloroplast isolation at each infection time-point, followed by RNA-seq, we could gain a much more precise resolution of gene expression changes occurring in the chloroplast during infection. Overall, these results show that the wheat chloroplasts undergo dynamic transcriptional reprogramming in response to *Pst* infection. These results complement our wider knowledge of nuclear transcriptional responses observed for the NGCPs of interest and help us gain insights into the chloroplastic responses of wheat when infected with *Pst.*

4. A NGCP encoding a predicted chloroplast metallopeptidase contributes to wheat susceptibility to *Pst* and MoT

4.1. Introduction

4.1.1. Pathogens employ different strategies to invade and colonise host plants

Fungal and oomycete plant pathogens have evolved different strategies to facilitate the extraction of nutrients from host tissue to complete their life cycle. These strategies have classically been broadly described as biotrophic, hemi-biotrophic and necrotrophic (Liao *et al.*, 2022). Biotrophic pathogens, which can be obligate or non-obligate, require living host cells to survive and complete their lifecycle. The wheat rust fungi are classed as obligate biotrophic pathogens whereby they require a living host to complete each stage of their life cycle. Necrotrophic pathogens kill their host and extract nutrients from dead tissue. Hemi-biotrophic pathogens, such as the fungal pathogen MoT or oomycete *P. infestans* blur the line between biotrophic and necrotrophic characteristics by initially forming a biotrophic interaction with the host then switching to necrotrophy in the later stages of infection (Rajarammohan, 2021). Plants respond to pathogens primarily through phytohormone signalling and these responses differ upon invasion by fungi with biotrophic and necrotrophic strategies. The phytohormone salicylic acid (SA) mainly governs the plant response to biotrophic pathogens, whilst jasmonic acid (JA) and ethylene (ET) mediate the response to pathogens with necrotrophic life-styles, as reviewed in Glazebrook (2005). These hormones can act antagonistically and therefore a delicate balance must be struck to ensure the appropriate response is initiated and maintained to secure plant health (Glazebrook, 2005). Furthermore, these hormones have been shown to have roles during growth and development, leading to a trade-off between defence and plant growth, with important implications in crop breeding (He *et al.*, 2022; van Butselaar and Van den Ackerveken, 2020). This has been demonstrated by the exogenous application of JA or benzothiadiazole (a commercial SA analogue) or the constitutive activation of immune receptors which all result in poor plant growth and significantly smaller plants (Canet *et al.*, 2010; Karasov *et al.*, 2017; Kobayashi *et al.*, 2020). The defence-growth trade-off phenomenon has been the subject of studies for many years, with ROS, resource allocation and constraint, phytohormone triggered transcriptional reprogramming and epigenetic mechanisms all being implicated in contributing to this effect (He *et al.*, 2022). It is therefore of critical importance that, for example, susceptibility or resistance genes against a biotrophic pathogen, don't inadvertently increase susceptibility to hemi-biotrophic or necrotrophic pathogens. Furthermore, any susceptibility or resistance gene must be effective without compromising plant growth and its viability for deployment into the field (Hückelhoven *et al.*, 2013).

4.1.2. Regulation of *Pst* infection in wheat

As biotrophic pathogens, the wheat rusts must form an intimate association with hosts to enable the completion of their life cycle. The life cycle of *Pst* is summarised in **Figure 4.1**. The first stage of the life cycle includes the germination of a Urediniospore on the surface of the leaf (Kang, 1996). This germ tube locates a stoma to enter the plant apoplastic space, and invasive hyphae form in the mesophyll later (Moldenhauer *et al.*, 2006). Haustoria are invaginations of the host cell membrane by invasive hyphae that create a host-pathogen interface for the movement of molecules that are important for fungal growth (Moldenhauer *et al.*, 2006). This includes the secretion of effector proteins that transverse the haustoria to target wheat processes to facilitate infection, for example to supress immunity or to manipulate metabolism (Petre *et al.*, 2014). Both wheat and rust fungi undergo complex and extensive transcriptomic and metabolomic reprogramming during each stage of their infection processes (Dobon *et al.*, 2016). In the wheat-leaf rust interaction, transcriptomic reprogramming in wheat differed depending on the isolate that was infecting (Neugebauer *et al.*, 2018). This study showed isolate specific differential expression of chaperone genes and alanine glyoxylate aminotransferase genes, and that these genes were associated with pathogen virulence. Dobon *et al.* (2016) carried out RNA-sequencing on *Pst*-infected wheat samples and found highly dynamic expression of genes over the 11-day time-course. The expression of wheat genes was modulated according to the stage of the pathogen life cycle. For example, wheat genes differentially expressed at 1 day post inoculation (dpi) included antimicrobial genes, at 3 dpi genes involved in energy production and photosynthesis, and at 11 dpi genes encoding components of stress-induced hormone signalling. In *Pst,* at 7-11 dpi, genes encoding proteins that function in carbohydrate metabolism, nucleic acid metabolism and transcription factors were upregulated. These results from Dobon *et al.* (2016) are an insight into the establishment and maintenance of the biotrophic interaction between wheat and *Pst.*

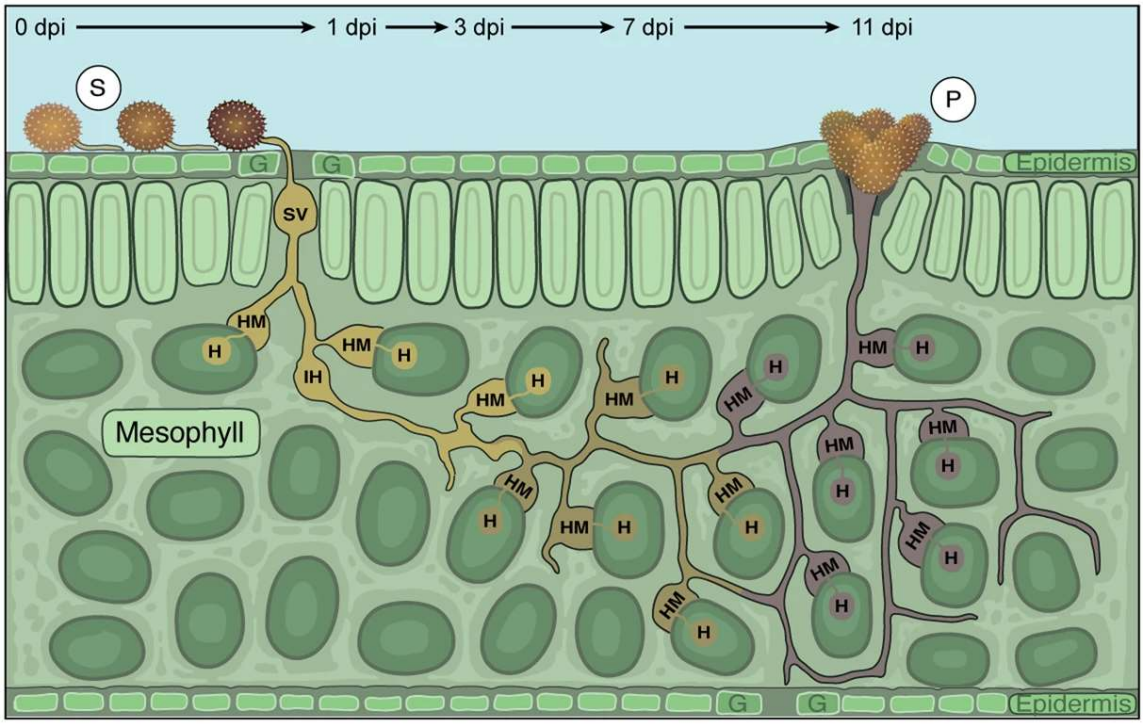

Figure 4.1 The life cycle of *Puccinia striiformis* f.sp. *tritici* (*Pst*) in wheat.

From 0 to 3 days post inoculation (dpi), spores germinate on the surface of the leaf and locate a stoma to gain entry into the leaf. Invasive hyphae grow in the mesophyll layer and haustoria form within cells. Later in infection, days 7-11, fungal proliferation within the plant leads to the completion of the life cycle with the emergence of new spores from pustules in the leaf surface. S, spore; G, guard cell; SV, substomatal vesical; HM, haustorial mother cell; IH, invasive hyphae; H, haustorium; P, pustule. This figure was published in Corredor-Moreno *et al.* (2022) and is reused with permission from copyright holders under the Creative Commons Licence.

4.1.3.Tools for gene disruption in wheat

To characterise genes identified through transcriptomic or genomic studies, molecular tools in wheat have advanced in the past ten years. For example, the development of the TILLING population as a tool for gene disruption (Krasileva *et al.*, 2017) or CRISPR-Cas9 for gene editing. Another method to study gene function is virus-induced gene silencing (VIGS) which exploits the host post-transcriptional gene silencing mechanism to trigger the silencing of endogenous genes. In wheat, barley stripe mosaic virus (BSMV) has been shown to be an effective virus for VIGS (Bennypaul *et al.*, 2012). BSMV carrying sequences from the target gene is inoculated onto seedings. Upon infection, an endogenous RNA-directed RNA polymerase (RDRP) is activated and produces

dsRNA using the target sequences before the dsRNAs are cleaved by Dicer enzymes into siRNAs (Ashfaq *et al.*, 2020). SiRNAs form an RNA-induced silencing complex (RISC) which uses homology between the siRNAs and the target gene to direct degradation of mRNA, effectively silencing gene expression (Ashfaq *et al.*, 2020). Therefore, VIGS in wheat is a highly customisable process which circumvents the time and resource requirements of stable transformation and gene editing in wheat. VIGS has been used to functionally characterise genes involved in the wheat response to pathogenic fungi including *Zymoseptoria tritici,* MoT*, Blumeria graminis* and *Pst* (Corredor-Moreno *et al.*, 2021; Lee *et al.*, 2015; Tufan *et al.*, 2012). A similar tool, viral overexpression (VOX) in wheat, also uses viruses to deliver DNA into plant cells. It has been noted that BSMV vectors become unstable when larger target fragments are used for VOX and this technique is therefore limited to 500 bp target fragments (Bouton *et al.*, 2018). This would limit the size of the protein that could be studied using overexpression to around 150 amino acids, a distinct limitation of this technique. Consequently, VOX in wheat has been developed to instead use foxtail mosaic virus (FoMV) for delivery and overexpression as it can support larger DNA sequences (Bouton *et al.*, 2018). As wheat is a hexaploid with A, B and D subgenomes which can have expression biases, it is important that the VIGS target or VOX gene is chosen appropriately. For VIGS, the siFi software scans all homoeologues of the gene of interest to find regions that can target the A, B and D homoeologues to ensure the most efficient silencing whilst also checking for off-target sequences (Lück *et al.*, 2019). One limitation to VIGS is that gene silencing can be highly variable within a plant and even within an individual leaf, for example a study using VIGS to silence components of the wheat resistance pathway against *Puccinia triticina* achieved silencing between 54% and 83% (Scofield *et al.*, 2005). In the same study, authors found that there was significant variation in the expression of the positive control gene, *Phytoenedesaturase* (*PDS*), and hypothesised that this was due to heterogeneity in silencing within the tissue. Nevertheless, VIGS and VOX have proven to be useful tools in the characterisation of a growing number of genes in wheat.

The aim of this chapter was to assess the contribution of a promising candidate NGCP encoding a predicted chloroplast metallopeptidase, *TaCPEP,* to plant susceptibility to microbial pathogens following these objectives:

- Infect wheat TILLING mutants with *Pst* to determine whether disruption of *TaCPEP* results in a change in infection phenotype.
- In the wheat-*Pst* pathosystem and the model *N. benthamiana-P. infestans* pathosystem, explore the effect of altering the expression of *TaCPEP.*
- Assess whether disruption of *TaCPEP* alters immunity-related transcriptional responses downstream of salicylic acid (SA) signalling, which functions in wheat immune responses to *Pst.*
- Assess whether disruption of *TaCPEP* alters the immune signalling of the ROS burst.

4.2. Methods

4.2.1. Quantification of *TaCPEP* disruption mutants' susceptibility by microscopic analysis of fungal structures

Seeds of the single *TaCPEP* disruption mutants TaCPEP-A^{W135*} and TaCPEP-B^{R100-} and double mutants TaCPEP-A^{W135*}TaCPEP-B^{R100-}, in addition to the mutant with wildtype allele of TaCPEP-B (TaCPEP-B^{WT}) and KWT were sterilised and pre-germinated according to **Section 2.2**. When wheat seedlings reached the 2-3 leaf-stage (approximately 14 days old) they were inoculated with the *Pst* isolate 13/14 according to **Section 2.5**. The first and second leaves of the *Pst*-inoculated wheat lines were harvested at 6 dpi and cut into approximately 2 cm pieces and fixed in 90% ethanol for 2 days. Tissue was transferred to 20% KOH for 2 days, washed in water twice and 1X phosphate buffered saline (PBS) once. Tissue was then transferred to 10 mg/ml Wheat Germ Agglutinin, Alexa Flour™ 488 Conjugate (WGA-AF488) solution for 2 days and stored in this solution at 4°C until imaging. Samples were mounted in water using Carolina observation gel (Carolina®, USA). Fungal infection structures were quantified by counting the number of germinated and ungerminated spores and invasive hyphae on the Zeiss Axio Imager Z2. WGA-AF488 was excited between 450-490 nm and detected at 500-550 nm. Experiments were conducted with five biological replicates (five individual plants per genotype).

4.2.2. VIGS in wheat

Preparation of BSMV constructs The BSMV constructs pCa-γbLIC::msc4D and pCa-γbLIC::*PDS* were obtained from Kostya Kanyuka (Rothamsted Research). pCa-γbLIC::*msc4D* contains an artificial sequence not present in wheat and acts as a negative control and pCa-γbLIC::*PDS* contains a target sequence for the wheat *phytoene desaturase* (*PDS*) gene which causes a bleaching phenotype and acts as a positive control (Lee *et al.*, 2015). The si-Fi software (Lück *et al.*, 2019) was used to identify two regions (fragment 1 and fragment 2) of *TaCPEP* that were predicted to produce the highest number of siRNAs. Primers were designed to amplify this fragment 1 and fragment 2 of *TaCPEP*. Ligation independent cloning (LIC) adaptor sequences were added to the forward and reverse primer sequences which were subsequently ordered. Fragment 1 (Fwd: 5'-AAGGAAGTTTAAGGGGATTGGGGCTTCTTC-3', Rvs: 5'-TGGCCTACCTATCCTGGGAAACCACCACCACCGTT-3') and fragment 2 (Fwd: 5'-AAGGAAGTTTAATACTCTTTGGACATTGG-3', Rvs: 5'- TTCAGGAACCTCTGAAACCACCACCACCGTT-3') were amplified from wheat cDNA using Phusion Polymerase as outlined in section 2.4. PCR products were resolved on a 1% agarose gel and bands of the correct size were excised. Excised bands were purified using the QIAquick PCR Purification kit (Qiagen, UK) according to the manufacturers' instructions. pCa-γbLIC vector was linearised through restriction enzyme digest with ApaI by incubation at 25°C for 5 h followed by inactivation at 65°C for 20 mins. Purified fragments were then cloned into the pCa-γbLIC vector using LIC. In a total volume of 10 µL, 200 ng of purified fragment and 0.6 U of T4 polymerase were incubated with 1X T4 reaction buffer supplemented with 100 ngμL^{-1} bovine serum albumin (BSA) and 5 mM dATP. In parallel, in a total volume of 50 µL, 500 ng of linearised pCa-γbLIC and 3U of T4 polymerase were incubated with 1X T4 reaction buffer supplemented with 100 ng μL^{-1} BSA and 5 mM dTTP. Both reactions were incubated at 22°C for 30 mins and heat inactivated at 75°C for 15 mins. For the ligation reaction, 2 µL of T4 treated pCa-γbLIC and 10 µL of T4 treated fragment were mixed and incubated at 65°C for 2 mins followed by 10 mins at room temperature. A 2 µL aliquot of this reaction mixture was used to transform 50 µL of *Escherichia coli* strain DH5α (ThermoFisher Scientific, UK) cells by heat shock according to the manufacturer's instructions. Cells were plated on LB-Agar containing Kanamycin (50 µg mL^{-1}) and grown overnight at 30°C. Single colonies were selected and subjected to colony PCR as described in section 2.4. Colonies containing plasmids with the correct insert size were grown overnight in LB containing Kanamycin (50 µg mL^{-1}). Plasmid was purified using the Qiagen MiniPrep kit (Qiagen, UK) according to the manufacturers' instructions and the sequence verified via Sanger Sequencing (Genewiz, Germany). Plasmids containing the verified fragment sequence were used to transform

A.tumefaciens strain GV3101 according to methods in **Section 2.8.2**. Cells were plated on LB-Agar containing Gentamycin (25 µg mL^{-1}) and Kanamycin (50 µg mL^{-1}) and grown at 28°C for 4 days. Single colonies were selected, and plasmids verified by colony PCR as described in **Section 2.3**. *A. tumefaciens* containing the BSMV α genome component (RNAα) or the β genome component (RNAβ) were developed by Pilar Corredor-Moreno (John Innes Centre) alongside *A. tumefaciens* containing the control constructs pCa-ɣbLIC::*msc4D* or pCa-ɣbLIC::*PDS*, prior to the start of this project.

Preparation of BSMV-infected *N. benthamiana* Single *A. tumefaciens* colonies containing silencing constructs pCa-ɣbLIC::*msc4D*, pCa-ɣbLIC::*PDS* and pCa-ɣbLIC::*TaCPEP*_fragment_1 or ɣbLIC::TaCPEP_fragment_2 were grown in 5 mL LB containing Gentamycin (25 µg mL^{-1}) and Kanamycin (50 µg mL^{-1}) at 28°C overnight with constant shaking at 220 rpm. Cells were pelleted by centrifugation at 2500 g for 20 mins and then resuspended in infiltration buffer containing 10 mM MgCl2, 10 mM 2-(N-morpholino)ethanesulfonic acid (MES) supplemented with 150 µM acetosyringone to an optical density of 1.5 at 600 nm. Cultures were incubated at room temperature for 3 h. Equal volumes of *A. tumefaciens* containing either pCa-ɣbLIC::*msc4D*, pCa-ɣbLIC::*PDS*, pCa-ɣbLIC::*TaCPEP*_fragment_1 or ɣbLIC::*TaCPEP*_fragment_2 were mixed with *A. tumefaciens* carrying RNAα and RNAβ. Mixtures were then pressure infiltrated using a needleless syringe into the abaxial side of 25–30-day old *N. benthamiana* seedlings. BSMV-inoculated *N. benthamiana* leaves were harvested and snap-frozen in liquid nitrogen at 12 days post viral inoculation (dpvi) or at the onset of viral symptoms.

Inoculation of wheat with BSMV Wildtype seeds of the wheat variety Kronos were sterilised and pre-germinated on plates as described in **Section 2.2**. Germinated seeds were sown in 9 cm pots and grown for approximately 7 days until the second leaf emerged. BSMV-infected *N. benthamiana* leaves were ground in a pestle and mortar with sterile H_2O to create a sap. The first leaf of seedlings was manually inoculated with BSMV-infected *N. benthamiana* sap by moving the leaf between the thumb and middle finger 8 times producing a squeaking sound which indicates the removal of the waxy cuticle. Plants were subsequently left for 10 mins before being sprayed with water, covered, and left in the dark overnight. Inoculated plants were transferred to a growth cabinet under controlled conditions of day/night temperature of 23/20°C, 16 hr photoperiod and light intensity of 120-300 µmol m^{-2} s^{-1} for 2 weeks or until the onset of viral symptoms.

Inoculation of silenced wheat with *Pst* and MoT Inoculations with *Pst* and MoT were carried out according to **Section 2.5** and **2.6**. For MoT, both the second and third leaf were inoculated. For

Pst, the whole plant was inoculated. The second and third leaf of the inoculated plants was harvested and snap-frozen in liquid nitrogen at 24 hpi and 72 hpi for *Pst* and 5 dpi for MoT. RNA extraction, cDNA synthesis and qRT-PCR was carried out according to **Section 2.8**. Fungal biomass and silencing of *TaCPEP* were determined according to **Section 2.7**.

4.2.3. Transient overexpression of *TaCPEP* in *N. benthamiana* and inoculation with *P. infestans*

N. benthamiana plants were infiltrated at 3-to-4 weeks old with *A. tumefaciens* strain GV3101 carrying the pK7FWG2 containing the *TaCPEP-A* CDS (pK7FWG2:*TaCPEP-A*) as outlined in Methods **Section 2.8**. Infiltrated *N. benthamiana* leaves were harvested at three days post-infiltration and placed on plates containing damp paper towel. *P. infestans* isolate 88069 (supplied by Adeline Harant (Kamoun Lab, The Sainsbury Laboratory)) was grown initially on rye agar at room temperature in the dark for 14 days. Plates were then flooded with 5 mL ice-cold sterile water and sporangia harvested by scraping with a plastic spreader. Sporangia were put through 70 µM nylon mesh filter and left at 4°C for 2-6 h and checked regularly under a light microscope for zoospore release. Once zoospores were released, cultures were filtered through 70 µm nylon mesh filter. Zoospores were quantified using a haemacytometer and the concentration was adjusted to 10^5 spores/mL. Abaxial sides of the infiltrated *N. benthamiana* leaves were inoculated with 10 µL droplets of *P. infestans* zoospores. Each leaf was inoculated with 4 droplets. Leaves were placed in 16 h light/ 8 h dark cycle at room temperature (18°C). Infections were monitored and photographed under visible light and UV at 6-14 dpi. Inoculations were repeated with 3 biological replicates (individual leaves from individual plants) in 4 independent experiments.

4.2.4. Luminescence-based reactive oxygen species assays on wheat leaf discs

Seeds of the single *TaCPEP* disruption mutants TaCPEP-A^{W135*} and TaCPEP-B^{R100-} and double mutants TaCPEP-A^{W135*}TaCPEP-B^{R100-} in addition to TaCPEP-B^{WT} and KWT were sterilised and pre-germinated according to the protocol outlined in **Section 2.2**. Plants were grown in controlled conditions of 16 h light/ 8 h dark, 23°C and 60% humidity until the three-leaf stage. Experiments were performed with assistance and reagents (flg22, L-012 and HRP) from Dr Jack Rhodes (The Sainsbury Laboratory). Leaf discs were taken from the middle section of the first and second leaf of 14-day-old seedling from each genotype using a 4 mm biopsy punch. Discs were placed into 100 µL of sterile diH_2O in white flat-bottomed 96-well plates, sealed with clingfilm and left overnight at

room temperature. The following day, plates were placed in the dark for 10 mins before the onset of ROS measurement. Water was removed from the plates and replaced with 100 µL of elicitor solution containing diH_2O, horseradish peroxidase, L-012 and 20 nM Flg22 for treated plants. Negative control samples were treated with a mock solution without flg22 and were assessed in the same plate. Plates were quickly placed into a Varioskan plate reader where measurements of luminescence were taken every 1 min for at least 60 mins. Experiments were repeated with 8 biological replicates.

4.2.5. Measurement of the expression of pathogenesis related genes in *TaCPEP* disruption mutants

Seeds of the single *TaCPEP* disruption mutants TaCPEP-A^{W135*} and TaCPEP-B^{R100-} and double mutants TaCPEP-A^{W135*}TaCPEP-B^{R100-} in addition to TaCPEP-B^{WT} and KWT were grown according to section 2.2. At the two-leaf-stage (approximately 14-day-old seedlings) plants were inoculated with *Pst* isolate 13/14 according to section 2.5. At 24 hours post inoculation (hpi) the first leaf was snap frozen in liquid nitrogen. Samples were processed and used for qRT-PCR according to **Section 2.7**. qRT-PCR was carried out to measure the expression of *PR* genes using the primers listed in **Table 4.1**. Primers to amplify *PR* genes were designed by Pilar Corredor Moreno and SAR genes by Swathy Puthanvila-Surendrababu (John Innes Centre).

Table 4.1 Primer sequences for qRT-PCR to measure the expression of *PR* and SAR genes

Gene	Forward primer (5'-3')	Reverse primer (5'-3')
PR1	CTGGAGCACGAAGCTGCAG	CGAGTGCTGGAGCTTGCAGT
PR2	CTCGACATCGGTAACGACCAG	GCGGCGATGTACTTGATGTTC
PR3	AGAGATAAGCAAGGCCACGTC	GGTTGCTCACCAGGTCCTTC
PR4	CGAGGATCGTGGACCAGTG	GTCGACGAACTGGTAGTTGACG
PR5	ACAGCTACGCCAAGGACGAC	CGCGTCCTAATCTAAGGGCAG
PR9	GAGATTCCACAGATGCAAACGAG	GGAGGCCCTTGTTTCTGAATG
ALD1	AGCCCATACCAAGCATCGTC	TCGGTGTCTCGTATCCCCAT
SARD4	GGCAGGGTGTTCATCGACT	AACGGACTTGAACACGGTGA
ICS1	GGACGACTCGCTTTCTTGGA	AACAGCAAGATCCCAGGACG

4.3. Results

4.3.1. Disruption of *TaCPEP* results in an increase in wheat susceptibility to the pathogenic fungi *Pst* and MoT

To test whether the disruption of *TaCPEP* leads to altered wheat susceptibility to *Pst*, we obtained mutants from the tetraploid wheat population, Kronos. For the A genome, line Kronos4002 encoded an early stop codon mutation at amino acid 135 of TaCPEP (TaCPEP-A^{W135*}). The B genome line, Kronos2206, had a splice acceptor variant at the beginning of the third intron, at amino acid 100 (TaCPEP-B^{R100-}). Additionally, these mutants were crossed to produce a double mutant, TaCPEP-A^{W135*} TaCPEP-B^{R100-}. All lines were compared to a Kronos wildtype (KWT) line. All TILLING lines were genotyped to confirm the presence of the homozygous mutant or wildtype SNP, according to Section 2.4, before every experiment. The confirmed disruption mutants were then inoculated with the *Pst* isolate 13/14 and disease symptoms observed at 14 dpi. The whole second leaf was snap frozen and processed for quantification of fungal biomass by qRT-PCR. The disruption mutants appeared more susceptible to *Pst* with more spores visibly present on the leaf surface of the mutant lines than the KWT lines (**Figure 4.2**). Moreover, whilst the difference was not detected as significant, quantification of fungal biomass indicated a notable increase in fungal presence in the single mutant TaCPEP-A^{W135*} and a more marginal increase in the TaCPEP-$B^{R100-}$and TaCPEP-A^{W135*} TaCPEP-B^{R100-} mutants compared to the KWT lines. Where possible in the future it would be beneficial to perform more replications for fungal biomass measurements. These data suggest that disruption of *TaCPEP* increases wheat susceptibility to *Pst.*

Figure 4.2 Disruption *TaCPEP* mutants appear more susceptible to *Puccinia striiformis* f.sp. *tritici* (*Pst*) isolate 13/14 in the tetraploid Kronos wheat background.

Tetraploid disruption mutants in the A and B copies of *TaCPEP* as well as the double mutants were inoculated with *Pst* isolate 13/14 and representative images of the second leaf of the plants are shown at 14 dpi. The mutants have more pustules formed on the leaf surface. The relative expression in boxplots represents the fungal biomass of these samples as quantified using the expression of the *Pst* elongation factor reference gene normalised to the wheat UCE-AL reference gene. Statistical significance assessed using ANOVA ($P < 0.05$, ns; not significant, for all samples n=4). Boxes signify the upper (Q3) and lower (Q1) quartiles, bars represent median values, and whiskers are located at 1.5 the interquartile range. Experiments were carried out with at least three biological replicates in at least three independent experiments with similar results.

To further assess the impact of the disruption of *TaCPEP* in a different genetic background of wheat and to validate the phenotype obtained in the tetraploid background, I obtained the line Cadenza0703. This line had a glycine (G) to glutamic acid (E) missense mutation at amino acid 141 of TaCPEP-A (TaCPEP-A^{G141E}) which was predicted to cause protein loss of function. Two-week old seedlings of lines TaCPEP-A^{G141E} and Cadenza wildtype were inoculated with the *Pst* isolate 13/14. All lines supported *Pst* infection and phenotypes were observed at 14 dpi. TaCPEP-A^{G141E} plants were more susceptible to *Pst,* compared to the wildtype. This was reflected in the statistically significant higher percentage of leaf infected in TaCPEP-A^{G141E} line compared to Cadenza WT (CWT) plants, as measured with K-PIE (Bueno-Sancho, 2018). However, whilst there was a higher relative expression of *Pst* reference gene *EF-1* in Cadenza0703 compared to wildtype, which implies there is more fungal

biomass is present in the tissue, this increase was not statistically significant (**Figure 4.3**). Nonetheless, these data support the hypothesis that *TaCPEP* disruption mutants have increased susceptibility to *Pst.*

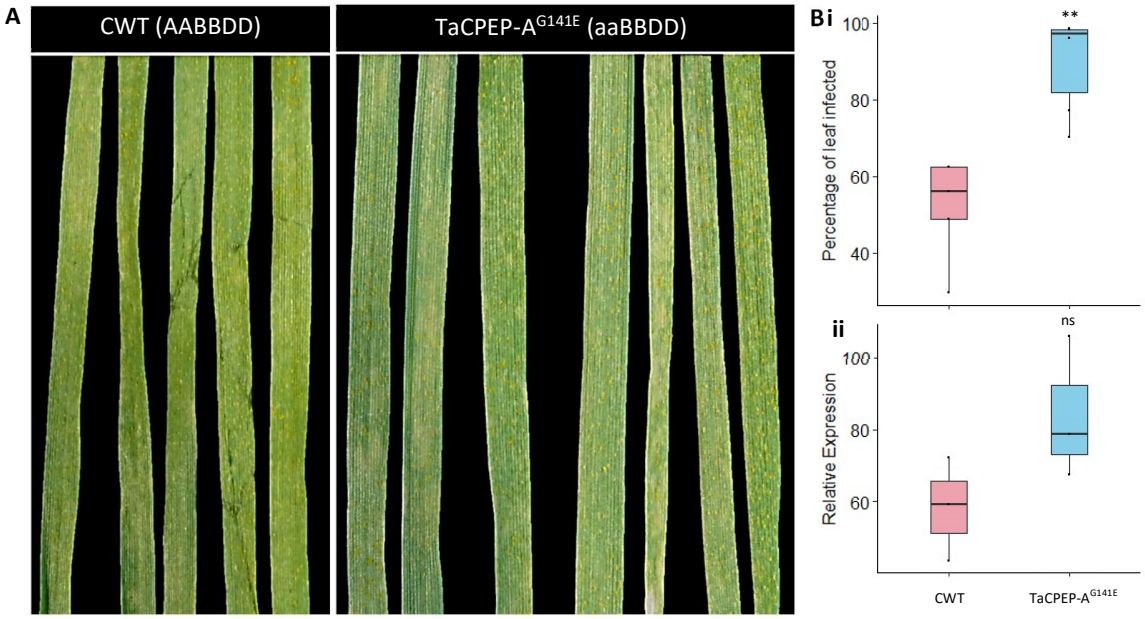

Figure 4.3 Disruption *TaCPEP* mutants in the hexaploid Cadenza wheat background show increased susceptibility to *Puccinia striiformis* f.sp. *tritici* (*Pst*) isolate 13/14.

(**A**) Images showing the macroscopic infection phenotype at 14 dpi and (**B**)(**i**) Boxplot showing the percentage of leaf infected as determined using K-PIE and (**ii**) qRT-PCR data representing fungal biomass. The relative expression in boxplots represents the fungal biomass of these samples as quantified using the expression of the *Pst* elongation factor reference gene normalised to the wheat UCE-AL reference gene. Asterisks indicate significant differences determined using Student's t-test (***p*<0.001; ns, not significant, for all samples n=4). Boxes signify the upper (Q3) and lower (Q1) quartiles, bars represent median values, and whiskers are located at 1.5 the interquartile range. Experiments were carried out with five biological replicates.

To investigate whether the disruption of *TaCPEP* had any impact on disease progression in wheat against a hemi-biotrophic pathogen, I inoculated TaCPEP-A^{W135*}, TaCPEP-B^{R100-}, TaCPEP-A^{W135*} TaCPEP-B^{R100-} and KWT with MoT. The wheat-MoT system is also significantly more tractable than the wheat-*Pst* system, which would facilitate future *in planta* experiments. Therefore, to provide initial investigation of the contribution of *TaCPEP* to wheat susceptibility to MoT, I performed spot inoculations on detached leaves of *TaCPEP* disruption mutants with the MoT isolate BTJP4-01. Infections were assessed at 5 dpi and the lesion length and area measured. Lesion length and area were significantly higher in the single mutants TaCPEP-A^{W135*} and TaCPEP-B^{R100-}, and double mutants

TaCPEP-A^{W135*}TaCPEP-B^{R100}, compared to the wildtype. The length and area also appeared to increase in the double mutant TaCPEP-A^{W135*}TaCPEP-B^{R100} compared to the single mutants TaCPEP-A^{W135*} and TaCPEP-B^{R100-}, although this increase was not statistically significant (**Figure 4.4**).

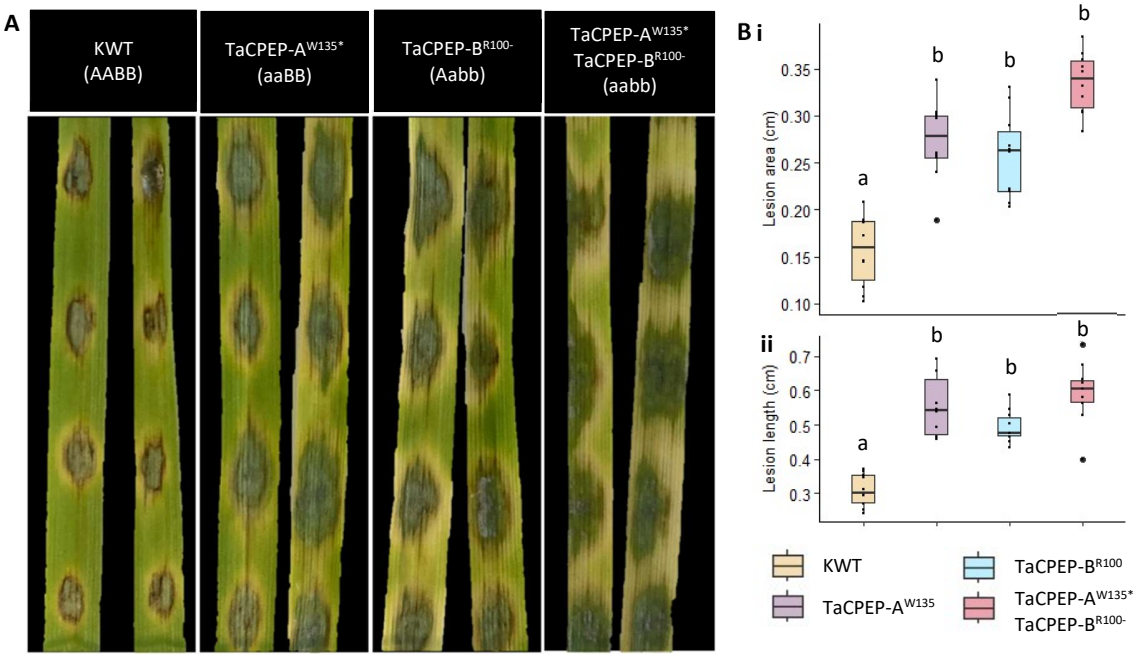

Figure 4.4 Disruption *TaCPEP* mutants are more susceptible to *Magnaporthe oryzae* pathotype *triticum* (MoT).

Disruption *TaCPEP* mutants were inoculated with MoT isolate BTJP4-01 and susceptibility measured at 5 dpi. **(A)** Images displaying infection lesions and **(B)** Boxplots displaying the **(i)** lesion area **(ii)** lesion length. Letters indicate significant differences determined using ANOVA and Tukey post-hoc tests (p<0.05, for all samples n=8). Boxes signify the upper (Q3) and lower (Q1) quartiles, bars represent median values, and whiskers are located at 1.5 the interquartile range. Images are representative of experiments performed in six biological replicates in two independent experiments.

4.3.2. Assessing the formation of internal fungal structures revealed that *TaCPEP* disruption mutants have enhanced susceptibility to *Pst* at 6 dpi

To investigate whether *Pst* infection progression was altered in the disruption *TaCPEP* mutants, I inoculated *TaCPEP* disruption lines with *Pst* and sampled infected tissue at 6 dpi. After clearing the tissue, I stained fungal chitin with WGA-AlexaFluor-488 and visualised fungal structures using fluorescence microscopy. I counted the number of spores with germ tubes and the number of

internal hyphae formed from those initial infection structures (**Figure 4.5**). To analyse the count data, I calculated the number of invasive hyphae relative to the total number of germinated spores to gain a representative overview of the success rate of *Pst.* Overall, there was a significantly higher proportion of IH formed in the TaCPEP-A^{W135*} and TaCPEP-B^{R100-} compared to the wildtypes. TaCPEP-A^{W135*} TaCPEP-B^{R100-} mutants also had a higher proportion of IH compared to the wildtypes, although this was not statistically significant (**Figure 4.5**). This suggests that the mutants more readily allow the formation of invasive hyphae growth *in planta,* and that this enhanced susceptibility has been established by 6 dpi.

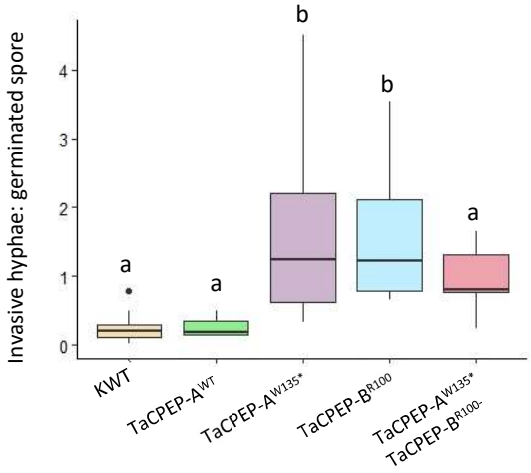

Figure 4.5 *Puccinia striiformis* f.sp. *tritici* (*Pst*) displays increased invasive hyphae growth *in planta* in disruption *TaCPEP* mutants evident in microscopic phenotypes at 6 days post inoculation (dpi).

Internal fungal structures were visualised using fluorescence confocal microscopy. Spores and spores with germ tube and invasive hyphae were counted. Boxplots for the number of invasive hyphae relative to the total number of germinated spores. TaCPEP-A^{WT} are TILLING mutants carrying the wildtype allele of both A and B copies of *TaCPEP* and is used as a control in addition to Kronos wildtype (KWT). Letters indicate significant differences determined using ANOVA and Tukey post-hoc tests (p<0.05, for all samples n=52). Boxes signify the upper (Q3) and lower (Q1) quartiles, bars represent median values, and whiskers are located at 1.5 the interquartile range.

4.3.3. VIGS as a method to investigate the outcome of targeted silencing of *TaCPEP* on the infection progression of *Pst*

To confirm that the change in susceptibility to *Pst* and MoT in *TaCPEP* disruption mutants was due to disruption of *TaCPEP*, I used VIGS by BSMV to silence *TaCPEP* in the tetraploid wheat variety Kronos. To enable the VIGS system to be used in both hexaploid and tetraploid wheat varieties, Cadenza and Kronos, respectively, I used the siFi software (Lück *et al.*, 2019) to predict regions of the A, B and D homoeologues of *TaCPEP* that produce the most efficient small interfering RNAs (siRNAs) (**Figure 4.6**). BSMV can become unstable when larger DNA sequences are used (Scofield *et al.*, 2005), therefore, I split the regions of high siRNA production into two approximately 200 bp fragments (Fragment 1 and Fragment 2). Again using siFi, I confirmed that there were no off-targets for either fragment by submitting fragment 1 and fragment 2 to siFi for a sequence similarity search against the wheat genome. No matching sequences were identified. Fragments 1 and 2 were cloned into separate pCa-ɣbLIC vectors but due to time constraints only fragment 2 was used in experiments.

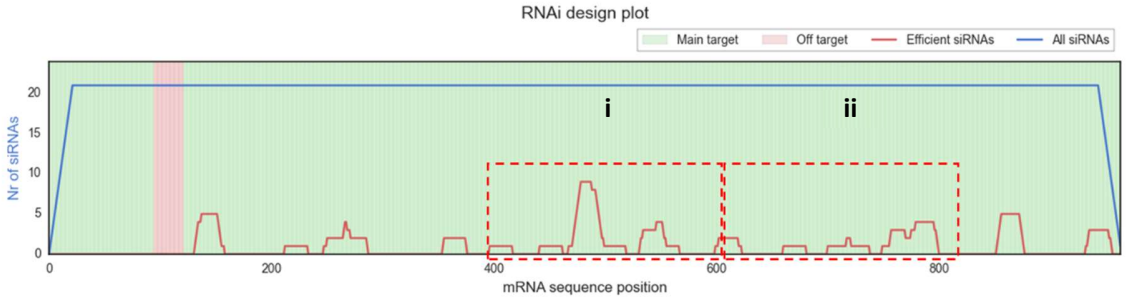

Figure 4.6 Small interfering (si)RNAs were predicted for *TaCPEP*-A, B and D using siFi software.
Regions of efficient siRNA production were predicted across the A, B and D homoeologues of *TaCPEP*. Red lines represent the number of efficient RNAs produced from any given region. Regions chosen were cloned as (i) Fragment 1 and (ii) Fragment 2, as they were regions that were predicted to generate the highest number of efficient siRNAs.

siRNA constructs pCa-ɣbLIC::*msc4D,* pCa-ɣbLIC::*PDS* and pCa-ɣbLIC::*TaCPEP* were transiently expressed in *N. benthamiana* and the viral load built up over 12 days across all leaves. Primary inoculated and systemic *N. benthamiana* leaves were ground together into a sap with water and manually inoculated onto the first leaf of 7-day-old wheat of the tetraploid variety Kronos. Mock inoculated plants were manually inoculated with water and then treated the same as BSMV inoculated plants. The *phytoene desaturase* (*PDS*) gene encodes an enzyme that is involved in the

biosynthesis of carotenoids. The silencing of this gene results in leaves without green carotenoid pigment. Therefore, the onset of bleaching in the leaves inoculated with BSMV carrying pCa-ɣbLIC::*PDS,* at around 10-14 days post viral inoculation (dpvi), was used as an indication that the BSMV inoculation and gene silencing was in effect (**Figure 4.7**). For plants inoculated with all constructs, the leaf that was manually inoculated with BSMV died in the week following inoculation. Therefore, the second and third leaves of the plants were inoculated with either the *Pst* isolate 13/14 or the MoT isolate BTJP4-01. For plants inoculated with *Pst,* leaves were harvested at 24 hpi and 72 hpi (approximately 19 dpvi) and for MoT infection assays, leaves 2 and 3 were harvested at 5 dpi (approximately 21 dpvi). RNA was extracted from samples and cDNA synthesised for an initial RT-PCR to confirm successful inoculation with BSMV by assessing the presence of the BSMV α genome in the tissue. The presence of bands in all samples confirmed that BSMV was successfully inoculated onto the plants and was present in the host tissue (**Figure 4.8**). Assessing resistance between VIGS- and mock-treated plants at 14 dpi revealed that there were no visual differences in the extent of *Pst* infection (**Figure 4.9**). However, MoT infections assessed at 5 dpi appeared highly variable between plants inoculated with the same construct, limiting the ability to visually interpret the data (**Figure 4.11**).

Next, I carried out qRT-PCR to measure the expression of *TaCPEP* and *Pst-EF1* to determine silencing efficiency and fungal biomass, respectively. For all samples, the crossing point (Cp) for amplification of *Pst-EF1* was above the threshold (35 cycles) value set for detection, resulting in relative expression values being extremely low (**Figure 4.10**). This indicates that there is likely no detectable *Pst* in the samples at either 24 or 72 hpi despite high levels of infection seen in macroscopic phenotypes later in infection (**Figure 4.9**). Sampling at 24 and 72 hpi was likely too early to detect *Pst* and therefore these samples were excluded from statistical analysis. With VIGS, we expect the expression of *TaCPEP* to be reduced in plants inoculated with BSMV carrying pCa-ɣbLIC::*TaCPEP*, compared to those carrying the negative control pCa-ɣbLIC::*msc4D* (**Figure 4.10**). We found that at 24 hpi there was a significant reduction in the expression of *TaCPEP* in plants inoculated with BSMV carrying pCa-ɣbLIC::*TaCPEP* or carrying the negative control pCa-ɣbLIC::*msc4D* compared to the mock inoculated and plants inoculated with BSMV carrying pCa-ɣbLIC::*PDS.* However, there was no difference in *TaCPEP* expression in plants inoculated with BSMV carrying pCa-ɣbLIC::*TaCPEP* or pCa-ɣbLIC::*msc4D*. At 72 hpi there was a significant increase in the expression of *TaCPEP* in plants inoculated with BSMV carrying pCa-ɣbLIC::*TaCPEP* compared to pCa-ɣbLIC::*msc4D*. These results indicate variability in *TaCPEP* expression under BSMV mediated VIGS

treatment making it unclear whether silencing was in effect and limiting my ability to assess pathogen susceptibility.

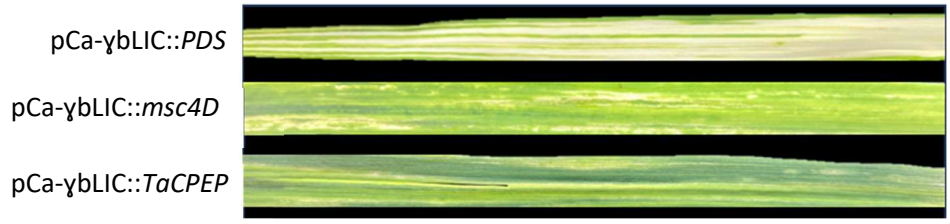

Figure 4.7 Phenotype of barley stripe mosaic virus (BSMV)-inoculated wheat plants.

The first leaf of the wheat variety Kronos was inoculated with BSMV carrying fragments for targeting *phytoene desaturase* (*PDS*), *msc4D* or *TaCPEP*. *PDS* encodes an enzyme that functions in the biosynthesis of carotenoids. When BSMV infection is successful, leaves in which *PDS* is silenced will be lacking green pigment. This is a positive control for BSMV infection. After 10-14 days there were visible viral symptoms on systemic leaves, with the characteristic photobleaching in *PDS*-silenced leaves indicating that BSMV had infected Kronos. For BSMV carrying pCa-γbLIC::*msc4D* or pCa-γbLIC::*TaCPEP,* symptoms presented as mildly chlorotic and striated leaves.

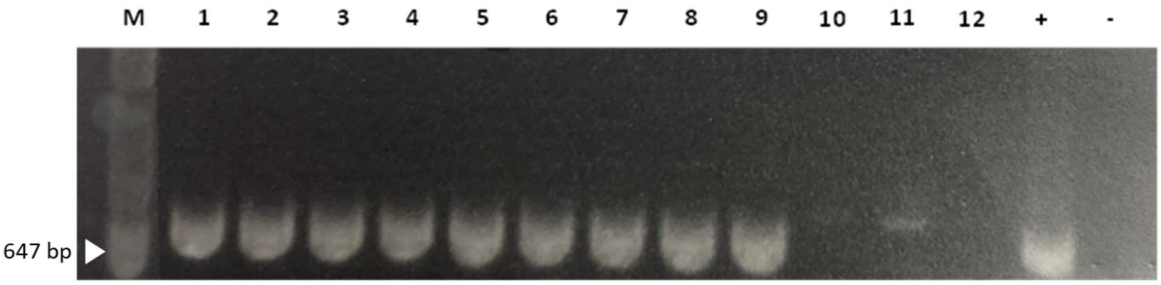

Figure 4.8 Reverse transcriptase polymerase chain reaction (RT-PCR) to verify the presence of barley stripe mosaic virus (BSMV).

Tissue from BSMV and *Pst*-infected virus-induced gene silencing plants was sampled by snap-freezing. RT-PCR was carried out to amplify the alpha component of the BSMV genome to verify the presence of BSMV in the samples before qRT-PCR assays. M, molecular marker; lanes 1-3, samples inoculated with BSMV carrying pCa-γbLIC::*TaCPEP*; lanes 4-6, samples inoculated with pCa-γbLIC::*PDS;* lanes 6-9 samples inoculated with pCa-γbLIC::*4D;* lanes 10-12, samples mock inoculated; +, positive control using pCBS-α as a template; -, negative control using water.

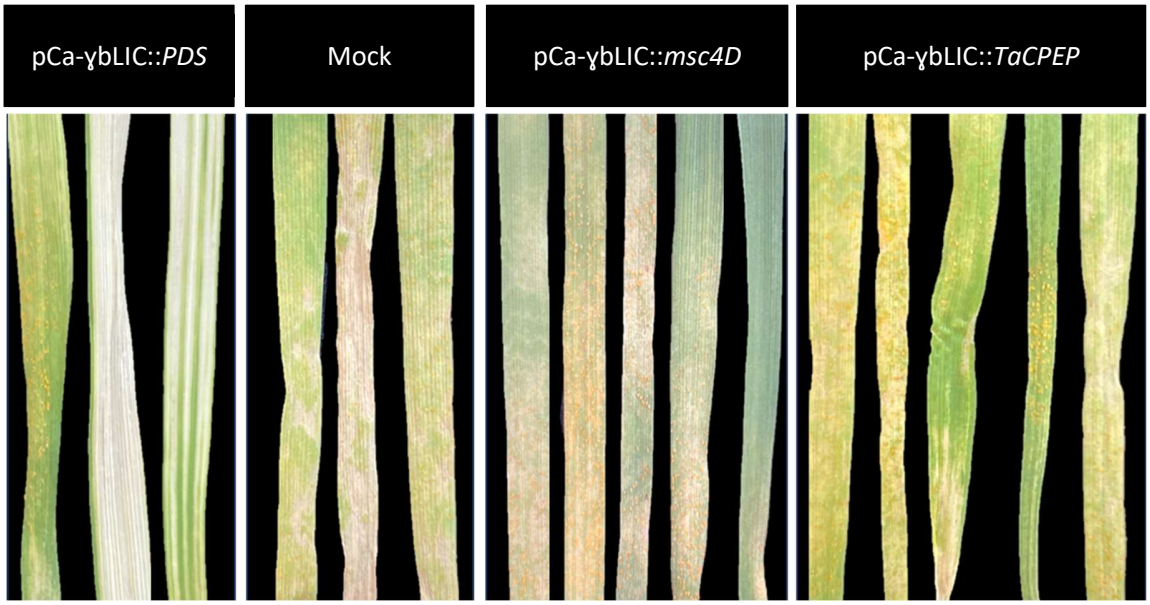

Figure 4.9 Phenotypes of plants that have undergone virus-induced gene silencing (VIGS) inoculated with *Puccinia striiformis* f.sp. *tritici (Pst)* at 14 dpi.

The wheat variety Kronos was inoculated with barley stripe mosaic virus carrying the constructs targeting the wheat *PDS* gene as a positive control for BSMV infection, *msc4D* as a negative control or fragments to target *TaCPEP*. Mock inoculated plants were manually inoculated with only water. All plants were inoculated with the *Pst* isolate 13/14 and infection symptoms observed at 14 dpi. Images are representative of at least 10 biological replicates per construct across four independent experiments that yielded similar results.

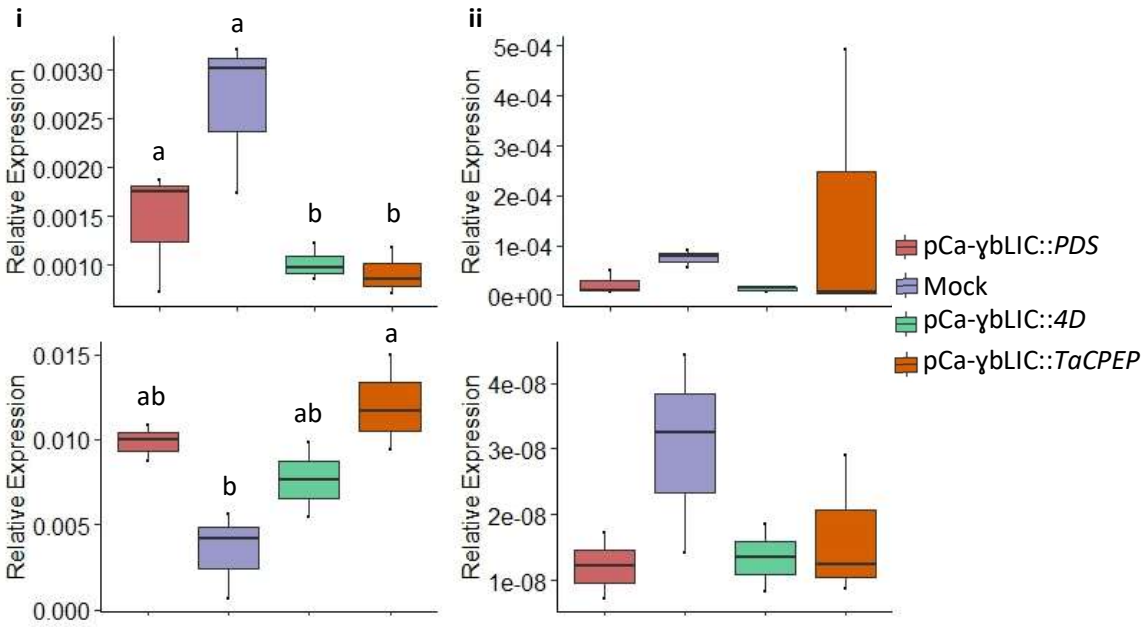

Figure 4.10 Analysis of the expression of *TaCPEP* and *Pst-EF1* in plants inoculated with barley stripe mosaic virus carrying virus-induced gene silencing (VIGS) constructs.

Seedlings of the wheat variety Kronos were inoculated with BSMV carrying constructs pCa-ɣbLIC::*PDS*, pCa-ɣbLIC::msc*4D*, or pCa-ɣbLIC::*TaCPEP*. Mock inoculated plants were rubbed with water and subsequently treated the same as BSMV inoculated plants. At the onset of bleaching in plants inoculated with BSMV carrying pCa-ɣbLIC::*PDS,* all plants were inoculated with the *Pst* isolate 13/14. Boxplots representing the relative expression of **(i)** *TaCPEP* and **(ii)** *EF-1* (to represent fungal biomass) which was measured at 24 (top panel) and 72 (bottom panel) hours post *Pst* inoculation. The crossing point (Cp) values for amplification of *Pst-EF1* exceeded the threshold for all samples, resulting in extremely low relative expression and suggesting no detection of *Pst* in tissue and exclusion from statistical analysis. The expression of *TaCPEP* was not statistically different between pCa-ɣbLIC::msc*4D* or pCa-ɣbLIC::*TaCPEP* at 24 hpi or 72 hpi. Letters indicate significant differences determined using ANOVA and Tukey post-hoc tests ($p<0.05$, n=3). Boxes signify the upper (Q3) and lower (Q1) quartiles, bars represent median values, and whiskers are located at 1.5 the interquartile range. Data are representative of at least 10 biological replicates per construct across four independent experiments that yielded similar results.

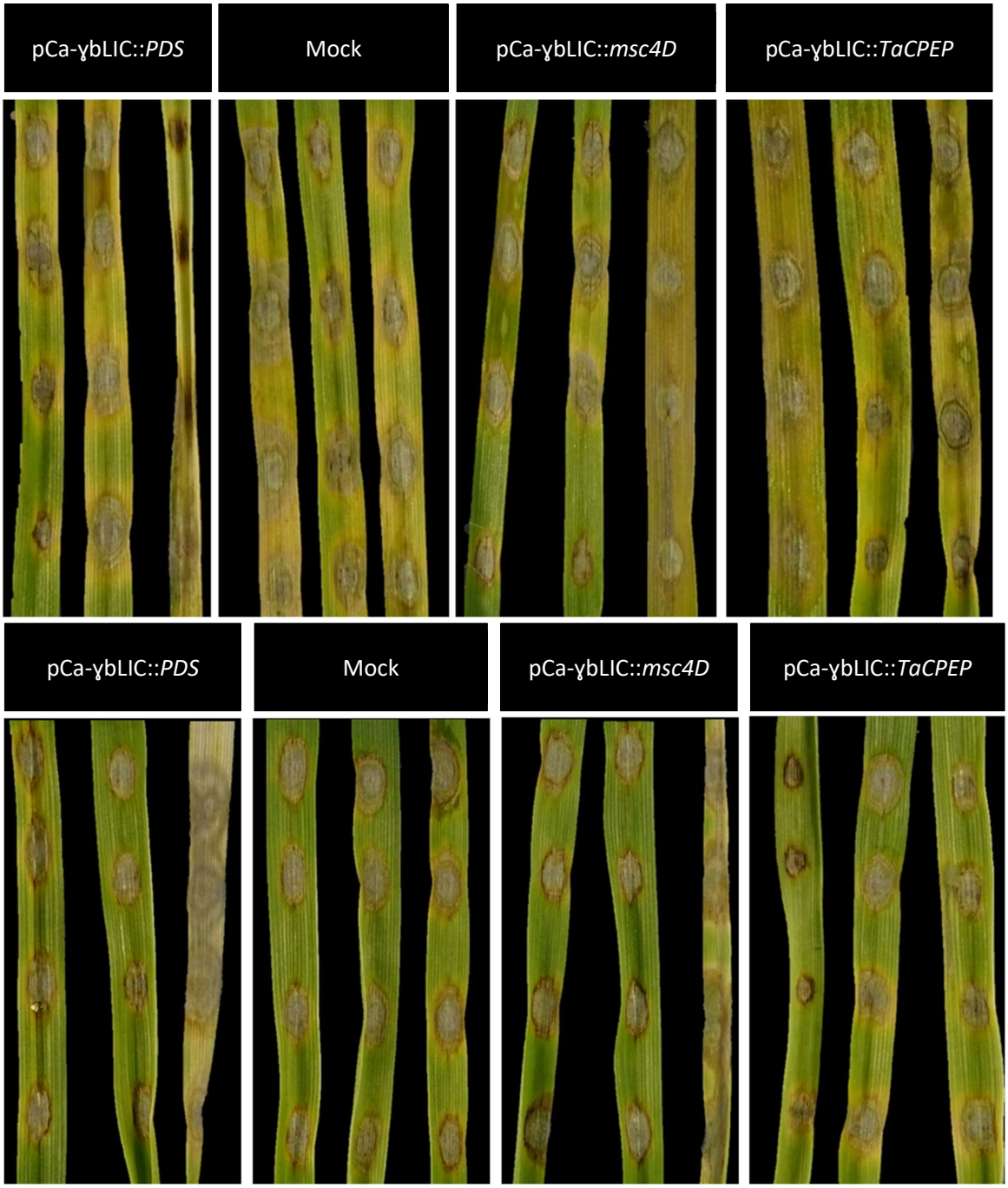

Figure 4.11 Phenotypes of plants that have undergone virus-induced gene silencing (VIGS) inoculated with *Magnaporthe oryzae* pathotype *triticum* (MoT) at 14 dpi.

The wheat variety Kronos was inoculated with BSMV carrying the constructs targeting the wheat *PDS* gene as a positive control for BSMV infection, *msc4D* as a negative control or fragments targeted to silence *TaCPEP*. Mock inoculated plants were manually inoculated with only water. Leaf 2 (top panel) and leaf 3 (bottom panel) were inoculated with the MoT isolate BTJP4-01 and symptoms observed at 5 dpi. Images are representative of at least 10 biological replicates per construct.

As *TaCPEP* disruption led to an enhancement in *Pst* and MoT susceptibility, I then investigated what effect overexpression of *TaCPEP* would have on pathogen resistance. I carried out overexpression of TaCPEP protein in *N. benthamiana* followed by infection with *P. infestans.* I chose to carry out overexpression in this system because the system for viral overexpression in wheat does not allow the expression of genes larger than 500 bp, which *TaCPEP* is. Furthermore, I could use the same overexpression constructs as those used to perform subcellular localisation in Section 5.3, which provided confidence in TaCPEP being expressed and imported into the chloroplasts. Lesion sizes were assessed in *N. benthamiana* by photographing infected leaves under UV light. I found that overexpressing *TaCPEP* generally led to smaller lesions at 6 dpi, compared to the empty vector and un-infiltrated controls (**Figure 4.12**).

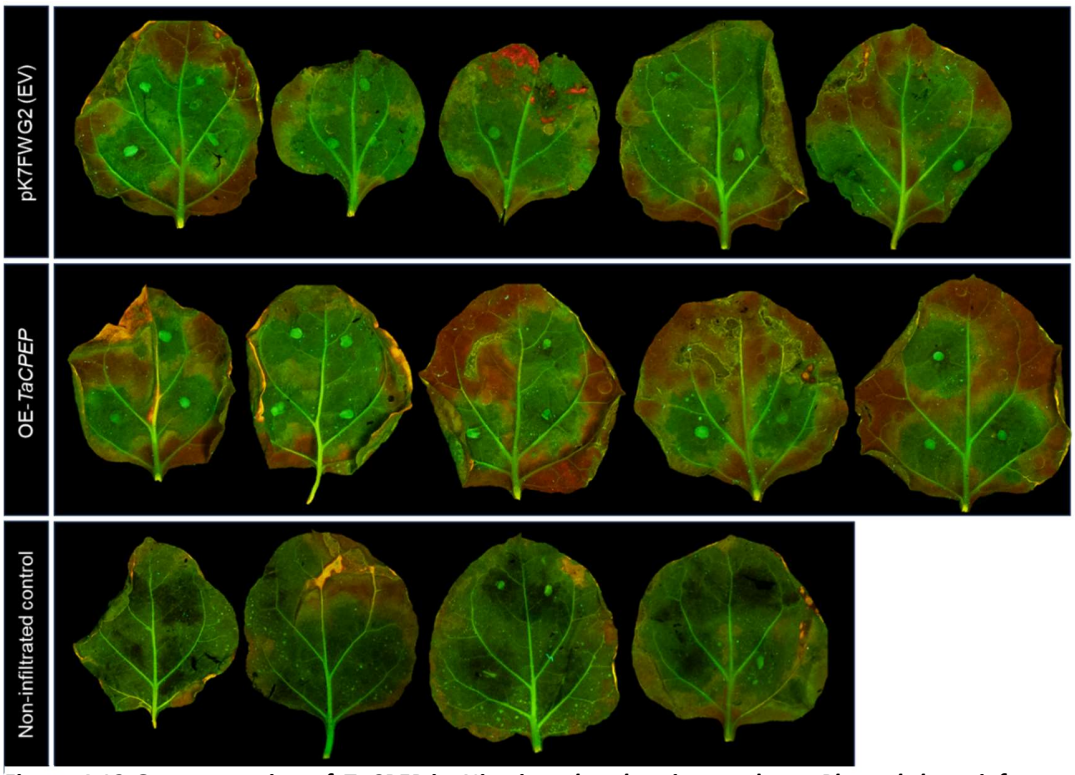

Figure 4.12 Overexpression of *TaCPEP* in *Nicotiana benthamiana* reduces *Phytophthora infestans* lesion size.

N. benthamiana leaves were infiltrated with *A. tumefaciens* GV3101 carrying empty pK7FWG2 (EV) or pK7FWG2::35S::*TaCPEP* (OE-*TaCPEP*) and inoculated with *P. infestans* isolate 88069 after 3 days. Photographs were taken of the infection lesions under UV light at 6 dpi. Photographs were taken by Phil Robinson (JIC photography department). Images are representative of at least six biological replicates across two independent experiments.

4.3.4. The expression of SA-induced *PR* genes is reduced in *TaCPEP* disruption mutants at 24 hpi with *Pst*

Having determined that *TaCPEP* disruption enhances susceptibility to *Pst* and MoT, I next wanted to explore whether this disruption impacts the expression of *pathogenesis related* (*PR*) and systemic acquired resistance (SAR) genes. *PR1, 2, 3, 4, 5* and *9* encode for proteins that have different functions during the plant immune responses to pathogens (**Table 4.2**). SAR equips the whole plant with long-lasting immunity against a broad spectrum of pathogens. *ALD1*, *ICS* and *SARD4* encode for proteins that are required for the biosynthesis of SA, contributing to SAR, and acting as markers for SAR activation, as outlined in **Table 4.2**. As the function of TaCPEP during the wheat response to fungal pathogens is unclear, I decided to analyse the expression of all six of these genes *PR* genes and the three SAR genes *ALD1*, *ICS* and *SARD4* during infection with *Pst.* Disruption mutants and wildtype controls (including KWT and the line TaCPEP-A^{WT}) were inoculated with the *Pst* isolate 13/14. Mock inoculation involved spraying wildtype control plants with 3M™ Novec™ 7100 Engineered Fluid*.* Following mock or *Pst* treatment, the first leaf of the plants was taken at 24 hpi and the expression of genes assessed using qRT-PCR. Analysis of the expression of these genes by qRT-PCR revealed that the expression of the *PR* and SAR marker genes is generally downregulated in TaCPEP-A^{W135*} and TaCPEP-A^{W135*} TaCPEP-B^{R100-}, compared to the wildtype or mock inoculated plants, although this was only statistically significant for *PR4* (**Figure 4.13**; **Table 4.2**). In contrast to this, the expression of *PR* and SAR genes in TaCPEP-B^{R100-} is higher than that of the other single mutant, the double mutant, and the wildtype controls. This data shows that there is a general reduction in *PR* and SAR gene in *TaCPEP* disruption mutants with *PR4* being the most significantly affected.

Table 4.2 Function of *PR* and SAR marker genes and the effect of *TaCPEP* disruption on their expression in response to *Pst.*

Statistical significance was determined using a Wilcoxon rank sum test, asterisk represent statistical significance (p<0.05, for all samples n=4) for reduced expression. TaCPEP-A^{WT} are TILLING mutants carrying the wildtype allele of both A and B copies of TaCPEP and is used as a control in addition to Kronos wildtype (KWT).

Gene	Reference	Protein function	Statistical significance
PR1	(Molina *et al.*, 1999)	Salicylic acid (SA) responsive	Non-significant
PR2	(Ray *et al.*, 2003)	B-1,3-glucanse	
PR3	(Desmond *et al.*, 2005)	Chitinase IV	
PR4	(Bertini *et al.*, 2006)	Antifungal chitin-binding	* (TaCPEP-A^{W135*} vs -TaCPEP-A^{WT}; TaCPEP-A^{W135*} TaCPEP-B^{R100-} vs TaCPEP-A^{WT})
PR5	(Kuwabara *et al.*, 2002)	Thumatin-like protein	Non-significant
PR9	(Ray *et al.*, 2003)	Peroxidase	
ALD1	(Song *et al.*, 2004)	Required for SA accumulation and SAR	
ICS	(Lefevere *et al.*, 2020)		
SARD4	(Ding *et al.*, 2016)		

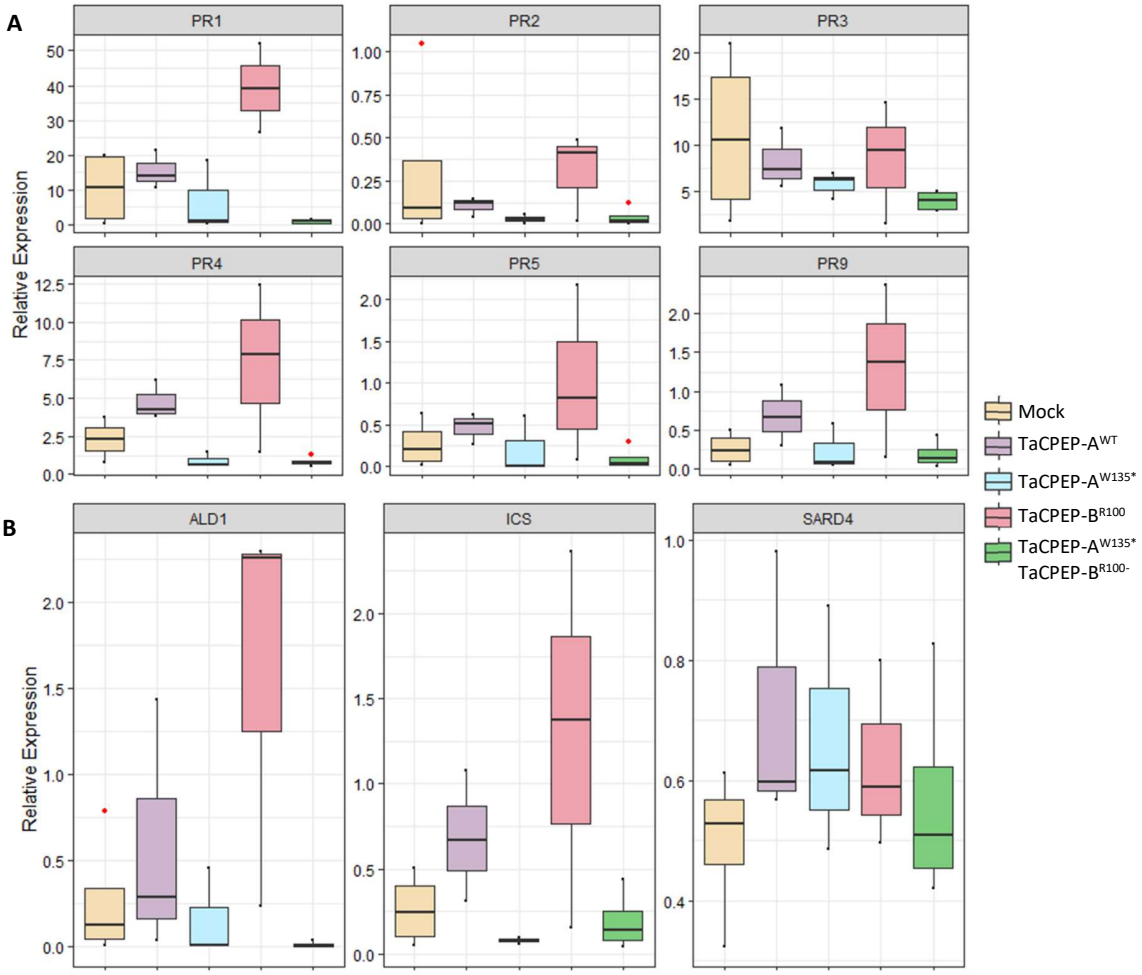

Figure 4.13 Expression of *PR* and SAR genes in disruption *TaCPEP* mutants at 24 hours post inoculation (hpi) with *Puccinia striiformis* f.sp. *tritici (Pst)*.

TaCPEP disruption mutants were inoculated with *Pst* isolate 13/14 and the first leaf was sampled at 24 hpi. Expression of the *PR* and SAR genes *PR1, PR2, PR3, PR4, PR5, PR9, ALD1, ICS* and *SARD4* were measured using qRT-PCR with four biological replicates and 3 technical replicates per genotype. TaCPEP-A^{WT} are TILLING mutants carrying the wildtype allele of both A and B copies of *TaCPEP* and is used as a control in addition to Kronos wildtype (KWT). Boxes signify the upper (Q3) and lower (Q1) quartiles, bars represent median values, and whiskers are located at 1.5 the interquartile range.

4.3.5. Assessment of the elicitor-induced ROS burst in *TaCPEP* disruption mutants

To further understand if other mechanisms of immune signalling were perturbed when *TaCPEP* was disrupted, I carried out leaf-disc ROS burst assays using the bacterial elicitor flg22. This assay detects hydrogen peroxide in the appoplastic space. Due to time constraints, I was only able to carry out the assay for eight biological replicates in one independent experiment and this experiment should be repeated to validate results. Nevertheless, preliminary data suggested that there was an increase in the ROS burst in the single *TaCPEP* mutants compared to the wildtype samples. This effect is notable in the luminescence over time, where the peak and duration of ROS is higher in the single mutants (**Figure 4.14**). When quantified, the cumulative relative luminescence (RLU) was statistically significantly higher in the mutants (**Figure 4.14**). Therefore, these data indicate that *TaCPEP* mutants may display enhanced ROS response during plant immunity.

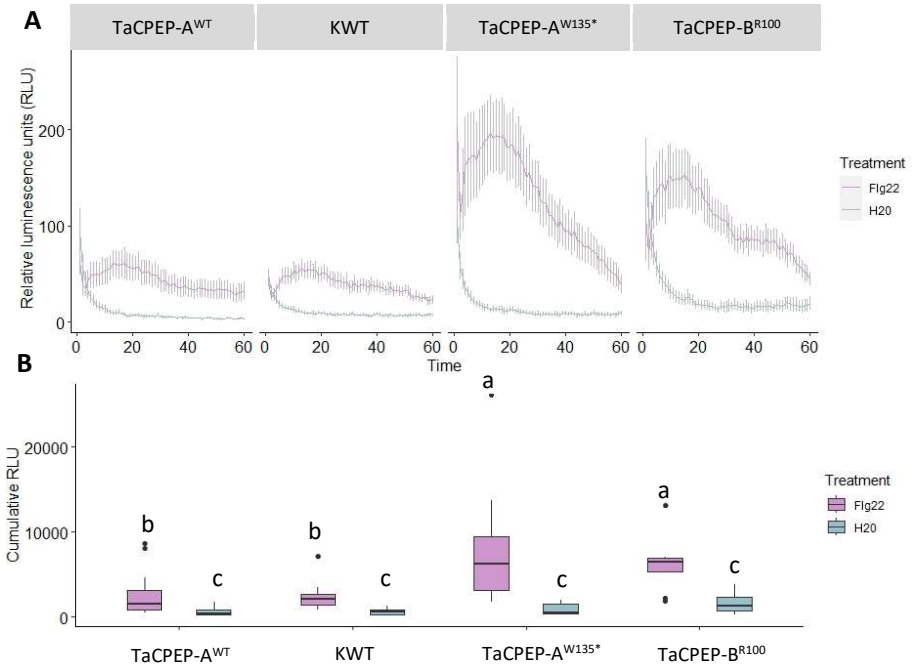

Figure 4.14 Reactive oxygen species (ROS) burst from wheat leaf discs challenged with flg22 were measured in wildtype and *TaCPEP* disruption mutants.

A chemiluminescent method was used to quantify the production of ROS from wheat leaf discs from single *TaCPEP* disruption mutants. **(A)** The production of ROS measured over for 60 mins post elicitor application. **(B)** Cumulative RLU was calculated by integrating the area under the curve. TaCPEP-A^{WT} are TILLING mutants carrying the wildtype allele of both A and B copies of *TaCPEP* and is used as a control in addition to Kronos wildtype (KWT). Letters signify statistical differences determined using the Wilcoxon rank sum test ($p<0.05$, n=8). Boxes signify the upper (Q3) and lower (Q1) quartiles, bars represent median values, and whiskers are located at 1.5 the interquartile range.

4.4. Discussion

In this chapter, I took the candidate NGCP, *TaCPEP*, from the screen carried out in the previous chapter and tested its contribution to susceptibility to the pathogenic fungi *Pst* and MoT. I found that the disruption of this gene led to an increase in wheat susceptibility to both fungi as seen by macroscopic infection phenotypes at the end of the infection cycle. At 6 dpi the disruption of *TaCPEP* resulted in the formation of more internal *Pst* infection structures. I was unable to optimise VIGS to reliably silence *TaCPEP* to enable characterisation, but the increase in susceptibility to *Pst* in tetraploid disruption mutants was also observed in a hexaploid wheat variety, Cadenza. Further investigation showed that overexpressing *TaCPEP* in *N. benthamiana* causes increased resistance to *P. infestans*. To begin to explore the mechanisms behind this change in susceptibility, I assessed the expression of *PR* genes which are known to be responsive to the phytohormone SA which functions in immune signalling during infection with biotrophic pathogens. I also measured the expression of genes involved in SAR, a SA-dependent process that induces long-lasting resistance in distal tissues. Disruption mutants generally had lower expression of all genes, although this was only statistically significant for *PR4*. Overall, the results presented in this chapter indicate that the disruption of *TaCPEP* function leads to an increase in wheat susceptibility to a specific biotrophic and hemi-biotrophic fungal pathogen, and that this increase may be associated with *TaCPEP* function promoting the expression of key genes within wheat immunity.

4.4.1. Overexpression of *TaCPEP* in *N. benthamiana* increases resistance to the oomycete *Phytophthora infestans*

As disruption of *TaCPEP* increased wheat susceptibility to *Pst* and MoT, I wanted to explore the consequence of overexpression of *TaCPEP* with the hypothesis that this could cause the opposite phenotype of increased resistance. To test this, I utilised *A. tumefaciens* to transiently express *TaCPEP* in *N. benthamiana*. In *N. benthamiana, TaCPEP* overexpression generally decreased susceptibility to *P. infestans,* as was reflected in the reduced lesion size imaged under UV light. *P. infestans* is a hemi-biotrophic oomycete closely related to heterokont algae than fungi. However, *P. infestans* does have physiology in common with plant pathogenic fungi such as the secretion of convergently evolved effector proteins to modulate host processes (Wilson and McDowell, 2022). These overlapping mechanisms may explain the correlation between *TaCPEP* function in susceptibility to the evolutionarily diverse pathogens of *Pst* and *P. infestans,* as well as MoT. It was noted that the *P. infestans* resistance phenotype was inconsistent in some of the leaves, which

maybe be due to the developmental stage of the leaf, or different levels of *TaCPEP* overexpression across the leaves and tissues. Furthermore, it was difficult to quantify the size of the lesions by measuring them or through quantification of RGB values, due to lesions overlapping with each other. Repeating this experiment with fewer points of inoculation per leaf should enable further confirmation of the reduction in susceptibility. Nevertheless, these experiments together suggest that *TaCPEP* could play a role in plant defence against pathogens in three different pathosystems.

4.4.2. Investigation of alterations to immune signalling pathways in *TaCPEP* disruption mutants

SA is a well characterised phytohormone known to be involved in immune signalling against biotrophic pathogens, such as the rust fungi (Peng *et al.*, 2021). Part of the role of SA is to trigger downstream responses to pathogen invasion and the activation of defence responses. This is via the non-pathogen response (NPR) transcriptional reprogramming pathway whereby the SA-binding NPR proteins trigger transcriptional activation of defence genes, such as the *PR* genes (Bertini *et al.*, 2003; Liu *et al.*, 2020). As the TILLING mutants that were disrupted for *TaCPEP* had increased susceptibility to *Pst* and MoT one hypothesis was that SA signalling was perturbed in the mutants and that this could be seen at the transcriptional level by reduction in the expression of *PR* and SA-inducible SAR genes. To test this, I measured the expression of *PR* and SAR genes at 24 hpi with *Pst.* I found that all six *PR* genes tested were downregulated in two out of the three mutants compared to the wildtypes. However, this effect was only statistically significant for *PR4.* These results could help us to begin to understand why disruption of *TaCPEP* results in an increase in susceptibility to *Pst* and MoT.

The function of PR1 remains unknown, but the *PR1* gene family is used as a reliable marker for SA and HR activation across plant species. Recent evidence has shown that in wheat, PR1 is targeted by an effector protein from the necrotrophic pathogen *Parastagonospora nodorum,* highlighting its importance in the wheat immune response (Breen *et al.*, 2016). PR2 and PR3 are both involved in recognition and response to fungal pathogens and can function co-ordinately. Previous studies have shown that more susceptible wheat varieties display lower expression of *PR2* at 24 hpi with *Pst* (Esmail *et al.*, 2020). The same study also found that the expression of *PR4* and *PR9* was reduced in the more susceptible wheat varieties. A different study showed that *PR4* was induced in response to triggers of SAR including SA and methyl jasmonate (Bertini *et al.*, 2003). Overall, the general reduction in expression of all 6 *PR* genes tested, but with only statistical

significance for *PR4,* could indicate that *TaCPEP* contributes primarily to inducing a PR4 pathway. In maize, PR4 has been shown to be a fungi-responsive gene that accumulates in response to the fungal pathogen *Fusarium moniliforme* (Bravo *et al.*, 2003). Similarly, in Garlic, *Fusarium* infection resulted in the upregulation of *PR4* (Anisimova *et al.,* 2021). Structural analysis of the wheat PR4 proteins found that they are proteins with anti-fungal activity that can translocate into the fungal cytoplasm, where they disrupt spore germination *in vitro* (Bertini *et al.*, 2009). With the expression of *PR4* seemingly reduced in *TaCPEP* disruption mutants then this anti-fungal function of PR4 could explain why the mutant plants are more susceptible to the fungal pathogens tested in the current study, *Pst* and MoT. Due to time and resource limitations, I was unable to test whether the basal expression of the *PR* genes is altered in disruption mutants, or whether this effect is induced upon pathogen perception. In the future it will be important to experimentally validate this to truly understand how *TaCPEP* disruption might alter wheat perception of *Pst.* Nonetheless, it is clear that *PR* genes play a significant role in plant immunity against fungal pathogens and *TaCPEP* may function to promote this activity potentially explaining why its disruption enhances wheat susceptibility to *Pst* and MoT.

I also measured the expression of the SAR genes *ALD1, ICS* and *SARD4*. *ALD1* encodes the AGD2-LIKE DEFENSE RESPONSE PROTEIN 1 which is an aminotransferase that synthesises pipecolic (Pip) acid from L-lysine, along with the reductase encoded by *SAR-deficient 4* (*SARD4*) (Ding *et al.*, 2016). Pip is converted to *N*-hydroxy-pipecolic acid (NHP), which is the bioactive form of Pip that works in a positive feedback loop with SA, regulated by overlapping transcription factors, to promote SAR (Hartmann and Zeier, 2019). Experiments have shown that pretreatment with NHP provides wheat seedlings with increased resistance to *Fusarium graminearum,* with the upregulation of immune receptors and defence associated genes (Zhang *et al.*, 2021a). *ICS* encodes isochorismate synthase which converts chorismate to isochorismate (IC) in the chloroplasts (Lefevere *et al.*, 2020) and in *A. thaliana* expression of *ICS* rapidly increases upon pathogen perception (Wildermuth *et al.*, 2001). In *A. thaliana*, mutants in *ICS* have severely reduced SA accumulation in response to pathogens. Similarly, barley mutants with suppressed expression of the *ICS* gene are more susceptible to the fungal pathogen *F. graminearum* (Hao *et al.*, 2018). In the current study, the expression of SAR genes was generally reduced in *TaCPEP* mutants, although similarly to *PR* genes *1, 2, 3, 5* and *9,* this was not statistically significant. This could indicate that *TaCPEP* does not strongly contribute to SAR in wheat in response to *Pst.*

In this experiment, the single mutant in the B copy of *TaCPEP* (TaCPEP-B^{R100-}) showed elevated expression of *PR* and SAR genes, which was in contradiction to the other single mutant and

the double mutant. When growing these populations of plants, there was the sporadic appearance of TaCPEP-B^{R100-} plants which had pale green leaves at the seedling stage. This phenotype didn't appear to be associated with environmental conditions during growth, as it was present when plants were grown under controlled conditions and within the glasshouses. It was suspected that these plants may have a background mutation which explained this phenotype and thus plants displaying this phenotype were eliminated from further experimentation. It could be that the elevated *PR* and SAR gene expression seen in some of the TaCPEP-B^{R100-} plants is a result of this putative background mutation. The TaCPEP-B^{R100-} samples generally have much larger variation in the expression data, particularly for the *ALD1* gene. Such variation may have resulted from variation in the zygosity of the background mutations which may have skewed the results of gene expression analysis for this line. In the future, we could analyse the background mutations of these lines to identify any possible mutation that could interfere with *PR* and SAR gene expression. We could also perform targeted gene editing of *TaCPEP* to produce full, targeted knock-outs.

Altogether, these results suggest that the loss of *TaCPEP* function may lead to the reduction of an induced defence response as seen by the downregulation of both *PR* and SAR genes, thus promoting susceptibility to *Pst* and MoT. Future experiments should aim to quantify the total SA level in the mutants to explore the mechanisms of altered *PR* or SAR gene expression in the *TaCPEP* disruption mutants and whether this effect is inducible or constitutive. Furthermore, as the expression of *ICS* is seemingly suppressed upon pathogen perception, it would be interesting to measure the level of chorismate and isochorismate as these compounds are important in the chloroplastic ICS biosynthesis and subsequent SA biosynthetic pathway. These experiments would enable us to discern whether the increase in susceptibility is a result of disruption to *TaCPEP* function during challenge with pathogens, or whether the disruption mutants are primed for enhanced susceptibility.

As the chloroplasts are also a significant contributor to ROS production during the immune response, I explored whether the loss of *TaCPEP* function resulted in altered ROS signalling. The hypothesis was, considering *TaCPEP* disruption increases wheat susceptibility to *Pst* and MoT, that the ROS burst would be diminished in response to elicitors. I chose to carry out ROS burst assays using leaf discs from the *TaCPEP* disruption mutants. The apoplastic ROS burst is one of the earliest immune responses and is indicative of PTI activation, as reviewed in Liu and He (2016). For ROS burst assays, leaf discs are challenged with an elicitor and the amount of ROS in the apoplast is detected by chemiluminescence (Melcher and Moerschbacher, 2016). The higher the signal, the stronger the

ROS burst. These assays can be difficult to optimise in wheat when using the fungal elicitor chitin (personal correspondence). Previous studies that aimed to induce ROS burst in wheat with chitin showed that the wheat varieties they used had absolutely no response to chitin, even at the highest concentrations tested (Hao *et al.*, 2022). Therefore, I chose to use the more reliable bacterial elicitor, flg22, which is a 22 amino acid component of flagella known to induce PTI (Felix *et al.*, 1999). I found that disruption mutants had a larger ROS burst, quantified by the cumulative RLU which was significantly higher in the mutants. These results suggest that, in contrary to our hypothesis, disruption of *TaCPEP* may result in enhanced PTI-associated ROS bursts. In the future, in addition to further validation by independent replicates, it would be beneficial to optimise the assay to use chitin as an elicitor as this is more representative of the wheat-*Pst* system primarily being explored here. Moreover, it would be interesting to use a precise assay to measure ROS production from the chloroplasts to determine whether TaCPEP might specifically function in chloroplastic ROS production, or whether other ROS signalling mechanisms are being altered. To do so, the ROS sensitive dye H_2DCFDA, which has been used to stain chloroplastic ROS in protoplasts (Mubarakshina *et al.*, 2010), could prove valuable. Nonetheless, ROS production appears altered in response to the flg22 elicitor in the *TaCPEP* disruption mutants which may contribute to the association of *TaCPEP* with enhanced susceptibility to *Pst* and MoT.

4.4.3. VIGS in wheat is a valuable tool for functional analysis of genes, but may have limitations depending on the gene being silenced and the pathosystem being investigated

VIGS has been proven to be a useful tool in investigating the function of a broad range of genes in wheat. It has also been used to assess the contribution of genes to wheat defence against pathogenic fungi, including *Pst* and to a lesser amount MoT (Duan *et al.*, 2013; Guo *et al.*, 2013; Tufan *et al.*, 2012; Zhang *et al.*, 2021c). In the current study, I aimed to use VIGS to silence *TaCPEP* to validate the phenotypes observed in the disruption mutants. I was unable to achieve reliable silencing to enable an infection phenotype to be assessed. This could be due to multiple technical difficulties in the experimental approach. To maintain continuity in my experimental set-ups, I aimed to carry out VIGS in the tetraploid wheat variety Kronos and hexaploid wheat variety Cadenza, the same background as the disruption mutants. Firstly, the regions that were chosen as targets were predicted to produce the most siRNAs. The software used to predict the regions of high siRNA production requires an input transcriptome. At the time of the experiment, the most complete and well-annotated transcriptome was the RefSeq v1.2 based on the hexaploid wheat variety Chinese Spring. It is therefore possible that differences in the coding sequences between wheat varieties

could have led to a difference in the siRNA silencing efficiency. In Kronos and Cadenza there could be alternative regions from *TaCPEP* that produce more efficient fragments for VIGS. Recently, there has been the expansion of known genomic sequences in wheat through the GrassRoots project and we can now access high quality genomic resources for Kronos and Cadenza, as well as other commercial wheat varieties of agricultural importance (Bian *et al.*, 2017). In the future, it would be useful to check sequence conservation between the CDS of *TaCPEP* Kronos and Cadenza with the reference genome from Chinese Spring. From there, fragments could be redesigned as necessary to maximise the efficiency of siRNA production and subsequent silencing.

An explanation for the variability in infection phenotypes in MoT-inoculated plants could be that presence of BSMV could induce immune responses in wheat and interfere with subsequent infection phenotypes from *Pst* or MoT. One study found that BSMV carrying a GFP negative control construct caused severe viral symptoms in wheat and triggered an increase in transcript levels of *PR* genes, markers of immune system activation and defence response (Tufan *et al.*, 2011). BSMV infected plants were then inoculated with MoT and *Blumeria graminis* f.sp. *tritici* and the authors found that wheat susceptibility was decreased against MoT, but not *B. graminis* f.sp. *tritici.* Therefore, it is suggested that BSMV-triggered transcription of *PR* genes may prime the immune system, making these plants more resistant to MoT. It is noted that this effect is not seen for *Pst* and therefore appears to be specific to MoT (Tufan *et al.*, 2012). In the present study, the MoT phenotypes in VIGS-treated plants were highly variable which may be explained in part by BSMV-induced immunity. In any case, this variability made data interpretation challenging and limited the ability to use VIGS to assess the role of *TaCPEP* in MoT susceptibility.

Finally, previous findings in the lab suggest that the BSMV-mediated gene silencing becomes limited after approximately five dpi with *Pst* (Corredor-Moreno, 2019). This means that unless the gene of interest functions within the first few days of infection, VIGS may not produce an infection phenotype with *Pst*. In the literature, it is difficult to discern whether this is a challenge for other investigations, as results tend to only be presented for the extent of silencing in the first 72 hours with phenotypes then assessed at 14 dpi without quantifying whether the silencing has been effective during these later critical points of infection (Jianyuan *et al.*, 2017; Zhang *et al.*, 2021b; Zhang *et al.*, 2020). Again, if the gene functions within early infection, for example during spore germination or penetration, then VIGS could remain a useful tool for investigating gene function. For the NGCPs of interest in the current study, however, we can see from the expression data that expression associated with resistance is most prominent at days 7-11 after inoculation. This suggests

that these genes might function during the later stages of infection, and that VIGS in wheat might not be the most suitable means to characterise their function. Overall, in our experience VIGS in wheat is an extremely valuable technique that has been used to study the function of several genes against wheat pathogens. However, in some contexts, like the one of this study, it is more difficult to apply and its limitations become more impactful.

To circumvent the challenges of optimisation of VIGS in wheat for this project, I obtained disruption mutants in the Cadenza background to validate the phenotype in Kronos mutants. Whilst I was limited in time and unable to generate triple mutants in Cadenza, the single mutant in the A copy of the genome was more susceptible to *Pst.* This was evidenced by an increase in fungal biomass and the percentage of leaf infected, although only the percentage of leaf infected was statistically significant. This limited increase in susceptibility could be due to functional redundancy which is particularly prominent in single mutants in the Cadenza background, as they often have two functional copies of genes remaining in the genome which can compensate for the loss of a single gene copy. It is therefore still reassuring that we can see a phenotype in the single Cadenza *TaCPEP* mutants and these results suggest that *TaCPEP* plays an integral role in the wheat response to *Pst.*

5. *TaCPEP* encodes a chloroplast localised predicted metallopeptidase that is required for wheat resistance against *Pst* and MoT

5.1. Introduction

Peptidases are proteolytic enzymes that cleave carbon-nitrogen bonds in proteins and/or peptides. They are distributed in all kingdoms of life and perform essential physiological functions such as in post-translational modification of proteins, regulating protein turnover and degradation and activation of zymogens and DNA repressors (Rawlings and Bateman, 2019; Takechi *et al.*, 2000). Therefore, peptidases are indispensable for maintaining cellular homeostasis and the normal physiological state of organisms (Cerdà-Costa and Xavier Gomis-Rüth, 2014). Peptidases can be classified according to where in the protein or peptide they cleave the peptide bond, with endopeptidases cutting in the middle and exopeptidases cleaving at the end of the peptide chain. They can also be further classified according to their enzymatic mechanism of action and the amino acids and cofactors required for catalysis. Metallopeptidases cleave peptide bonds using a metal ion located within the active site (Rawlings and Barrett, 2004). This metal ion is most commonly zinc but can be cobalt, nickel, or manganese (Auld, 2004). Cleavage of the substrate's peptide bond occurs by metallopeptidases in a single-step reaction following Michaelis-Menten kinetics (Cerdà-Costa and Xavier Gomis-Rüth, 2014). During this, the metal ion functions to activate a water molecule which hydrolyses the nitrogen-carbon bond at the active site. A HEXXH motif is thought to be important for metal ion binding and this motif is indicative of metallopeptidase activity (Jongeneel *et al.*, 1989).

Metallopeptidases can be further classified in the MEROPS database into families according to sequence similarity and evolutionary distance (Rawlings *et al.*, 2017). The M41 family includes ATP-dependent metalloendopeptidases which are a subfamily of ATPases Associated with diverse cellular Activities (AAA proteins) (Janska *et al.*, 2013). One of the most well studied M41 metallopeptidases is the bacterial and organellar Filamentous temperature sensitive H (FtsH). FtsH is conserved in animals and plants in bacterially derived organelles i.e., mitochondria and chloroplasts. *A. thaliana* has 12 orthologues (Sokolenko *et al.*, 2002). Of these orthologues, nine encode a chloroplast transit peptide and are imported into the chloroplasts (Yu *et al.*, 2004). FtsH proteases form homo- or hetero-hexamers that sit within in the thylakoid membrane. The combination of FtsH isoforms confers functional specificity with some functional redundancy (Yu *et al.*, 2004). In *A. thaliana*, FtsH1, 2, 5, and 8 are thylakoidal whilst FtsH7, 9, 11 and 12 localise to the chloroplast envelope (Sun and Jarvis, 2023). For FtsH 1, 2, 5 and 8, transmembrane domains are embedded in the thylakoid membrane, with catalytic domains facing into the stroma (Lindahl *et al.*, 1996). In *A. thaliana,* the *VAR1* and *VAR2* loci encode FtsH2 and FtsH5 proteases, respectively (Chen

et al., 2000; Sakamoto *et al.*, 2002). The first true leaves of *var1* and *var2* mutants are yellow, and as new leaves expand, green islands form and turn white. Green islands are heteroplastidic containing mostly chloroplasts which have underdeveloped lamellae (Takechi *et al.*, 2000; Chen *et al.*, 1999). Further work revealed that the main function of FtsH in *A. thaliana* is in the degradation of the D1 subunit of photosystem II (PSII) during photooxidative stress and damage of D1 (Kato *et al.*, 2009). Without VAR1 and VAR2 plants have reduced maximum yield of photochemistry in PSII and have heightened sensitivity to photoinhibitory light (Bailey *et al.*, 2002). Therefore, FtsH plays an integral role in the maintenance of chloroplast biogenesis and normal photosynthetic functions.

In addition to the FtsH subfamily, there is also a group of FtsH proteases which have mutated or missing zinc binding motifs. This group is known as inactive FtsHs or FtsHis, as the metallopeptidase function is thought to be lost (Sokolenko *et al.*, 2002). Contrary to what the name suggests, these proteases seem to have essential functions, as homozygous null mutants in FtsHis1, 2, 4 and 5 are lethal (Mishra *et al.*, 2019; Lu *et al.*, 2014). Furthermore, knock-down of FtsHis can cause variegated phenotypes, similar to FtsH2 and FtsH5 mutants (Kadirjan-Kalbach *et al.*, 2012). The AAA domains of FtsHis remain active, which is presumed to contribute to the primary function of these proteins. A recent study found that *A. thaliana* mutants in FtsHi5 have temperature-sensitive chloroplastic developmental defects (Li *et al.*, 2022). Li *et al.* (2022) found that proteins are differentially accumulated in FtsHi5 mutants compared to wildtype plants at low temperatures. These results highlight the important role inactive FtsHs can have for regulating the level of proteins within the chloroplasts that are involved in important processes including biogenesis and development, particularly under stress. Overall, both FtsH and FtsHis have been implicated in diverse and fundamental functions in chloroplast biogenesis and development, photosynthesis, and abiotic stress.

PSII produces singlet oxygen ($^1O_2$) as a biproduct of photosynthesis which can cause cellular damage, including to PSII itself. One role of FtsH is in the degradation of damaged PSII components, specifically binding to and cleaving the D1 subunit (Bailey *et al.*, 2002; Lindahl *et al.*, 2000; Kato and Sakamoto, 2009). Upon degradation and removal of damaged D1, new synthesis can occur, maintaining the functionality of PSII (Silva *et al.*, 2003). When plants are under photooxidative stress and the production of $^1O_2$ increases above the threshold for scavenging, damage can occur to FtsH which leads to loss of D1 turnover and lasting damage to PSII (Triantaphylidès *et al.*, 2008; Kato *et al.*, 2009; Dogra and Kim, 2019). Nevertheless, chloroplastic reactive oxygen species (cROS) such as $^1O_2$ and H_2O_2 acts as retrograde signals and are some of the earliest signals of pathogen invasion

required for transcriptional reprogramming during PAMP-triggered immunity (PTI) and effector-triggered immunity (ETI) (de Torres Zabala *et al.*, 2015; Su *et al.*, 2018; Hamel *et al.*, 2016). Perturbation of FtsH activity, therefore, can have far reaching and severe consequences for the immune response. For example, early studies in *A. thaliana* revealed that a gene, *DS9*, encoded the chloroplastic homolog of the bacterial *FtsH* and its expression was linked to the onset of necrosis during infection with tobacco mosaic virus (TMV) (Seo *et al.*, 2000). Seo *et al.* (2000) found that plants with lower DS9 levels had smaller necrotic lesions hypothesised to be caused by accelerated hypersensitive response due to increased production of ROS resulting from deregulation of PSII turnover. Overall, these studies show that FtsH and FtsHi metallopeptidases may be involved in plant immune responses by mediating protein turnover in the chloroplast and contributing to the HR. It is clear that metallopeptidases have important roles in maintaining photosynthetic and chloroplastic processes, which may overlap with immunity.

As *TaCPEP* is predicted to encode a metallopeptidase with unknown function, the aims of this chapter were to use our knowledge of metallopeptidases in the chloroplasts to functionally characterise *TaCPEP* and investigate how its disruption leads to an increase in wheat susceptibility to *Pst* and MoT, following the objectives outlined below:

- Carry out bioinformatic and *in silico* analysis to investigate the function of *TaCPEP,* including analysis of promoter motifs, phylogenetics and structural predictions.
- Investigate the function of *TaCPEP* experimentally by assessing the impact of *TaCPEP* disruption on photosynthetic and chloroplastic processes.

5.2. Methods

5.2.1. Bioinformatic prediction of homoeologue similarity, Gene Ontology (GO), subcellular localisation signals and protein co-expression networks

The amino acid sequence similarity between A, B and D homoeologues of TaCPEP was determined using the MAFT alignment tool (Katoh *et al.*, 2017) in Geneious Prime 2023.0.1 using homoeologous sequences from RefSeq v2.1 (Zhu *et al.*, 2021) obtained from Ensembl Plants (Yates *et al.*, 2021). Using the same amino acid sequences, GO terms were uncovered using Ensembl Plants (Yates *et al.*, 2021) and QuickGO (Binns *et al.*, 2009) and protein subcellular localisation prediction was performed using iPSORT (Bannai *et al.*, 2002), WoLF PSORT (Horton *et al.*, 2007) and Localizer

(Sperschneider *et al.*, 2017). Promoter motifs were predicted from 1000 bp upstream of the coding sequence of the *TaCPEP-A* start site using PlantCARE (Lescot *et al.*, 2002) and MotifSuite (Claeys *et al.*, 2012) using default parameters including all plant species in the database. Finally, the TaCPEP-A amino acid sequence was used to search the STRING database (Szklarczyk *et al.*, 2023) for proteins which were co-expressed with TaCPEP.

5.2.2. Protein phylogeny

A protein BLAST (Altschul *et al.*, 1990) was carried out using the amino acid sequence of TaCPEP-A against the proteome of members of the *Poaceae* family of grasses. The hits were aligned using MAFT (Katoh *et al.*, 2017) before FastTree 2 (Price *et al.*, 2010) was used to create approximately-maximum-likelihood phylogenetic tree in Geneious Prime 2023.0.1 with default parameters which was visualised in iTOL (Letunic and Bork, 2021).

5.2.3. Measurement of leaf gas exchange in the *TaCPEP* TILLING mutants using the LICOR-6800 infrared gas analyser

Seeds for the single *TaCPEP* disruption mutants TaCPEP-A^{W135*} and TaCPEP-B^{R100-} and the double mutants TaCPEP-A^{W135*}TaCPEP-B^{R100-} in addition to Kronos wildtype (KWT) were sterilised, pre-germinated and sown according to the protocol outlined in section 2.2. Plants were grown under controlled conditions in a of 16 h light/ 8 h dark, 23/ 20°C and 60% humidity. Bias in growth conditions was minimised by rotating trays of plants and moving them higher or lower in the growth cabinet every 2 days. Stomatal conductance assimilation (A) and stomatal conductance to water vapor (gsw) were measured in the youngest fully expanded leaf for each *TaCPEP* disruption mutant grown as above. Measurements were conducted from 09:00 to 17:00 over the course of three days under the supervision of Alexader Watson-Lazowski (John Innes Centre). For each measurement, the chamber was set to the following conditions: 23°C, 60% relative humidity, 400 µmol/mol CO_2, head light source 150 µmol m^{-2} s^{-1} with 90:10 (blue:red) light. Leaves were placed in the chamber and A was equilibrated for 10 mins. Once A was stable for each leaf, the IRGA signals were matched and the leaves left to stabilise for 10 mins. A and gsw were measured every 10 s for 2 mins. At least four biological replicates (four separate plants) were measured per genotype.

5.2.4. Quantification of chlorophyll content in the *TaCPEP* disruption mutants

Seeds of the single mutants TaCPEP-A^{W135*} and TaCPEP-B^{R100-} and the double mutants TaCPEP-A^{W135*}TaCPEP-B^{R100-} in addition to TaCPEP-A^{WT} and KWT were sterilised and pre-germinated according to the protocol outlined in section 2.2. Plants were grown in controlled conditions of 16 h light/ 8 h dark, 20/23°C and 60% humidity. Bias in growth conditions was minimised by rotating trays of plants and moving them higher or lower in the growth cabinet every 2 days. Chlorophyll content was measured according to the protocol outlined in Arnon (1949). Briefly, for each genotype, leaf sections of approximately 2 cm were harvested, weighed, and placed in 1.75 mL 80% acetone. Samples were incubated in the dark at 4 °C for 3 days. Chlorophyll a and b and total chlorophyll were measured using the BMG Omega Plate Reader by measuring the UV-vis of the acetone solution at wavelengths 645 nm and 663 nm. Values for chlorophyll a, b and total chlorophyll were obtained using resources from Alexander Watson-Lazowski (John Innes Centre). Measurements were performed with four biological replicates (four separate plants) per experiment in three independent experiments.

5.2.5. Isolation of mesophyll cells and imaging of chloroplasts

Seeds of single mutants TaCPEP-A^{W135*} and TaCPEP-B^{R100-} and the double mutant TaCPEP-A^{W135*}TaCPEP-B^{R100-} in addition to TaCPEP-A^{WT} and KWT were sterilised pre-germinated and sown according to the protocol outlined in 2.2. Plants were grown in controlled conditions of 16 h light/ 8 h dark, 23°C and 60% humidity. The most recently fully emerged leaf of each plant at the 3-leaf stage was sectioned into 2 mm pieces and fixed in 10 % formalin in 1x phosphate buffered solution (PBS) overnight. Formalin was replaced with 0.1 M Na_2EDTA (pH 9) and samples were shaken at 100 rpm for 2 h at 60°C. Samples were stored at 4°C in the dark until imaging. Individual 2 mm pieces were mounted in water. A cover slip was placed on top and gently tapped to release single cells. Cover slips were sealed with nail varnish. From each isolated cell, chlorophyll autofluorescence was imaged using the Zeiss LSM860 confocal microscope with excitation at 614 nm and emission detected at 600-750 nm. A custom Python script was written by Dr. Sergio Lopez (JIC Bioimaging department) to detect individual chloroplasts in the 2D images and measure their length. I generated and prepared the material, isolated the mesophyll cells, and mounted the samples. Dr Sergio Lopez (JIC Bioimaging department) performed confocal microscopy and wrote the Python script for size analysis. I further quantified the size of chloroplasts to complement the data

generated using the Python script. The mesophyll isolation protocol was provided with guidance by Dr Lara Esch (John Innes Centre).

5.3. Results

5.3.1. *In silico* and bioinformatic characterisation of *TaCPEP*

To begin to understand the possible functions of *TaCPEP*, GO terms associated with the molecular function, cellular component and biological process were obtained via Ensembl Plants (Yates *et al.*, 2021) and QuickGO (Binns *et al.*, 2009). Each homoeologue had the same GO terms predicted. These GO terms included ATP-dependent peptidase activity (GO:004176), metalloendopeptidase activity (GO:004222) and ATP binding (GO:005524) for the molecular function, chloroplast thylakoid (GO:0009534) and integral component of membrane (GO:0016021) for cellular component and proteolysis (GO:006508) for biological process. The prediction of having chloroplastic ATP-dependent metallopeptidase function is in agreement with results from InterPro (Paysan-Lafosse *et al.*, 2022), LOCALIZER (Sperschneider *et al.*, 2017) and WoLF PSORT (Horton *et al.*, 2007). LOCALIZER predicts that amino acids 1-29 of the C-terminal end of TaCPEP encode the chloroplast transit peptide (cTP) (**Table 5.1**). Protein domain predictions by InterPro indicate likely metallopeptidase and/or FtsH-like domains at the N-terminal end of the protein (**Figure 5.1**). Integral membrane protein and transmembrane domains for the chloroplast thylakoid were also predicted using WoLFPSORT for which the top three hits with the lowest distance in localisation features from the query sequence were chloroplast proteins, either localised to the thylakoid or associated with PSII and PSI.

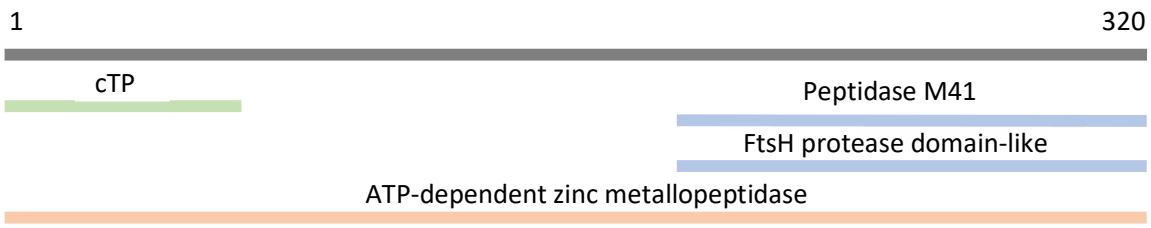

Figure 5.1 Protein domains and localisation as predicted using InterPro and LOCALIZER.
The amino acid sequence of TaCPEP was used to predict localisation and domain features. The protein was identified as having a C-terminal chloroplast transit peptide (cTP) and N-terminal functional domains in the M41 family of FtsH-like metallopeptidases. Adapted from InterPro (Paysan-Lafosse *et al.*, 2022).

Table 5.1 Prediction of subcellular localisation of TaCPEP-A using WoLF PSORT (Horton *et al.*, 2007)

Protein	Distance	Identity	Organism	Comments
Chlorophyll a-b binding protein of LHCII type I, chloroplastic	225.5	19.1%	*Dunaliella tertiolecta*	Chloroplast thylakoid membrane.
Low molecular mass early light-inducible protein HV90, chloroplastic	296.8	16.9%	*Hordeum vulgare*	Chloroplast. Associated with both photosystems I and II.
Inner membrane ALBINO3-like protein 1, chloroplastic	313.3	15%	*Chlamydomonas reinhardtii*	Integral membrane protein. Chloroplast thylakoid membrane.

Next, I analysed the sequence similarity between the homoeologous copies at the nucleotide and amino acid sequence level. There is a high degree of similarity between both the nucleotide and amino acid sequences, between 92.8-94.3% and 94.8-97.8%, respectively (**Table 5.2**). For all subsequent analysis unless otherwise stated, the A copy of the gene or the protein was used and it was assumed that there would be functional conservation between all three copies.

Table 5.2 Distance matrix showing the percentage sequence identify for the [i]nucleotide and [ii]amino acid sequence for *TaCPEP* as calculated using Geneious Prime 2023.0.1

	TraesCS2A02G523600	TraesCS2B02G553500	TraesCS2D02G525700
TraesCS2A02G523600		92.9[i] 94.8[ii]	92.8[i] 96.3[ii]
TraesCS2B02G553500	92.9[i] 94.8[ii]		94.2[i] 97.8[ii]
TraesCS2D02G525700	92.8[i] 96.3[ii]	94.2[i] 97.8[ii]	

To confirm subcellular localisation, I fused Green Fluorescent Protein (GFP) to the C-terminus of TaCPEP-A by cloning the coding sequence (CDS) of *TaCPEP-A* into the p7FWG2. TaCPEP:GFP was transiently expressed in *N. benthamiana.* Chlorophyll autofluorescence was used to mark chloroplasts. We found that the GFP signal and the chlorophyll autofluorescence signals overlap, which indicated a clear subcellular localisation of TaCPEP in the chloroplasts (**Figure 5.3**). In addition to confirming chloroplast localisation, I also found that there was potentially the formation of a stromule. As highlighted in **Figure 5.3**, this stromule lacks a signal from chlorophyll autofluorescence but displays a GFP signal, which is in agreement with the literature that states that thylakoids containing chlorophyll cannot pass into the stromules, but proteins tagged with GFP can (Hanson and Conklin, 2020).

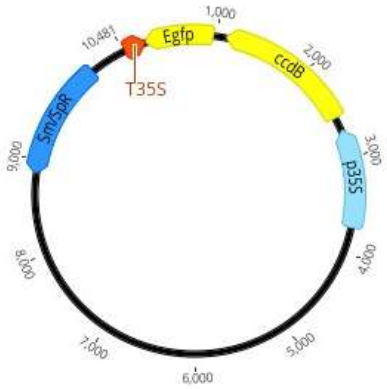

Figure 5.2. p7FWG2 vector used for the fusion of Green Fluorescent Protein to the C-terminus of TaCPEP-A.

The coding sequence of *TaCPEP-A* was cloned into the p7FWG2 vector and transiently expressed in *Nicotiana benthamiana* for subcellular localisation studies.

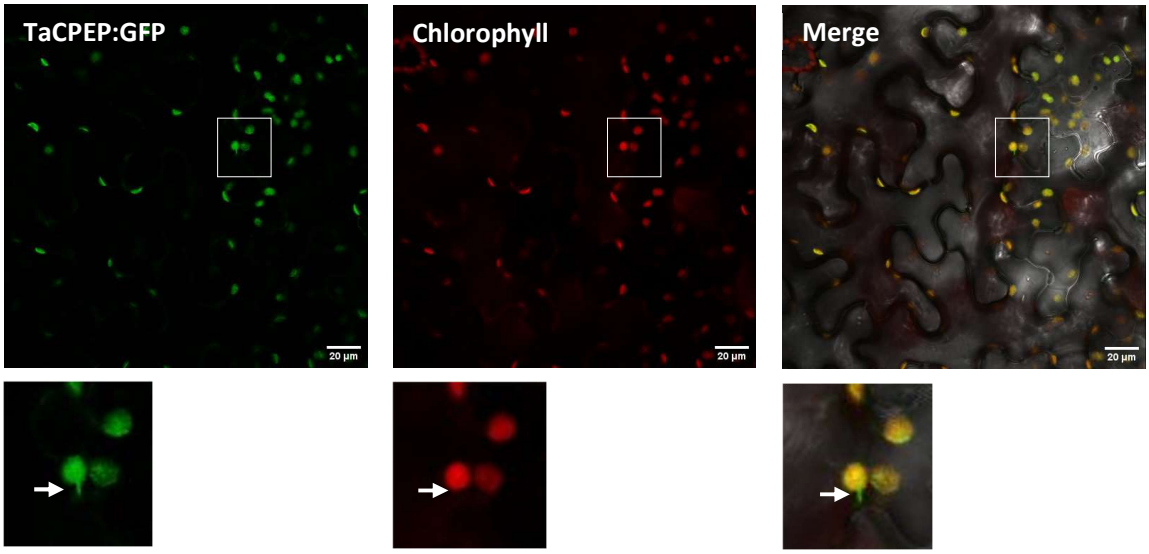

Figure 5.3 TaCPEP-A is localised to the chloroplasts in *Nicotiana benthamiana*.

TaCPEP-A was C-terminally tagged with Green Fluorescent Protein (GFP) and transiently expressed in *N. benthamiana.* Confocal microscopy was carried out 3 days after infiltration. GFP signal was excited at 488 nm and detected at 510 nm; Chlorophyll autofluorescence detected between 660-695 nm. Zoomed images show the formation of a putative stromule (white arrow) with GFP signal but lacking chlorophyll autofluorescence. Scale bars, 20 µm.

5.3.2. *In silico* analysis shows that the *TaCPEP-A* promoter region contains transcription factor-binding and cis-acting regulatory elements

To further explore the possible function of *TaCPEP* during infection with pathogenic fungi, an *in-silico* analysis was performed to determine whether the promoter region contains any stress-response motifs. To do this, the 1 kb upstream sequence of the *TaCPEP-A* translational start site was submitted to the PlantCARE tool to identify conserved motifs. The region was found to contain 23 motifs including AAGAA-motifs (n=1), ABRE (n=2), ARE (n=1), CAAT-box (n=5), CCAAT-box (n=2), CGTCA-motif (n=1), DRE-core (n=2), G-box (2), GC-motif (n=1), LTR (n=1), MYB recognition site (n=2), MYC recognition site (n=2), STRE (n=4), Sp1 (n=4), TCA (n=1), TGA-element (n=2), TGACG-motif (n=1), unnamed motifs (n=28), as-1 (n=1) and d0CT (n=1) (**Figure 5.4**). Of those promoters, a subset is of particular interest as they may be indicative of the function of *TaCPEP-A* and are involved in the response to abiotic and biotic stress. Such motifs include those for responsiveness to abscisic acid (ABRE) and auxin (TGA-element), key plant hormones in growth and development. Also included are motifs for light-responsiveness (G-box and Sp1) and response to oxygen availability (ARE and GC-

motif), in addition to the oxidative stress response motif as-1 element. Furthermore, there were motifs present for responsiveness to salicylic acid and jasmonic acid, important hormones in the plant immune response (**Table 5.3**).

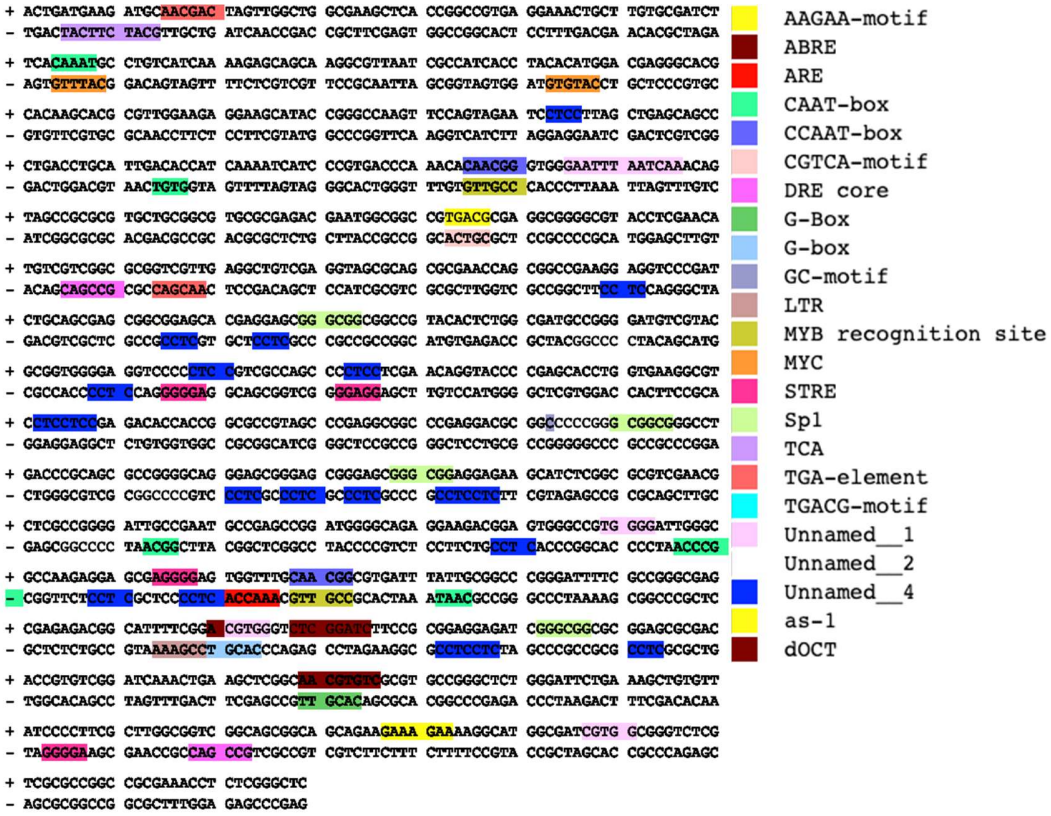

Figure 5.4 Promoter motif prediction for *TaCPEP-A*.

The 1000 bp upstream region of *TaCPEP-A* was submitted to PlantCARE to predict the TF binding or cis-acting regulatory motifs present. Overall, 23 motifs were identified, 20 of which were known and 3 were unnamed.

Table 5.3 The promoter region of *TaCPEP-A* contains motifs that function in the response to abiotic and biotic stress.

The 1 kb region upstream of the *TaCPEP* translation start site was submitted to PlantCARE and conserved motifs were predicted. Motifs identified were known to be involved in abiotic and biotic stress response, with four being responsive to phytohormones that function in biotic stress responses and five being responsive to abiotic stresses.

Motif	Organism	Sequence	Function
ABRE	*Arabidopsis thaliana*	ACGTG	Abscisic acid-responsiveness
	Hordeum vulgare	GCAACGTGTC	

Table 5.3 continued

ARE	*Zea mays*	AAACA	Anaerobic induction
CCAAT-box	*Hordeum vulgare*	CAACGG	MYBHv1 binding
TGACG-motif	*Hordeum vulgare*	TGACG	MeJA-responsiveness
CGTCA-motif		CGTCA	
G-box	*Pisum sativum*	CACGTT	Light responsiveness
	Zea mays	CACGTC	
Sp1	*Oryzae sativa*	GGGCGG	
GC-motif	*Zea mays*	CCCCG	Anoxic specific inducibility
LTR	*Hordeum vulgare*	CCGAAA	Low-temperature responsiveness
STRE	*Arabidopsis thaliana*	AGGGG	Stress-response element
TCA	*Pisum sativum*	TCATCTTCAT	Salicylic acid-responsiveness
TGA-element	*Brassica oleracea*	AACGAC	Auxin-responsiveness element
as-1 element	*Arabidopsis thaliana*	TGACG	Oxidative stress response

To explore which processes TaCPEP might be associated with in wheat, the TaCPEP-A amino acid sequence was entered into the STRING database which identifies functional protein networks within a species (Szklarczyk *et al.*, 2023) and proteins with a high confidence interaction score (over 0.7) were extracted. Ten proteins were identified as being co-expressed or co-regulated with TaCPEP-A, although most of these interactions were based off homologous proteins in other plant species (**Figure 5.5**). Proteins were predicted to be involved in plastid translation (GO:0032544), protein peptidyl-prolyl isomerization (GO:0000413), circadian rhythm (GO:0007623), positive regulation of translation (GO:0045727), regulation of translation (GO:0006417), chloroplast organization (GO:0009658) and defence response to bacterium (GO:0042742).

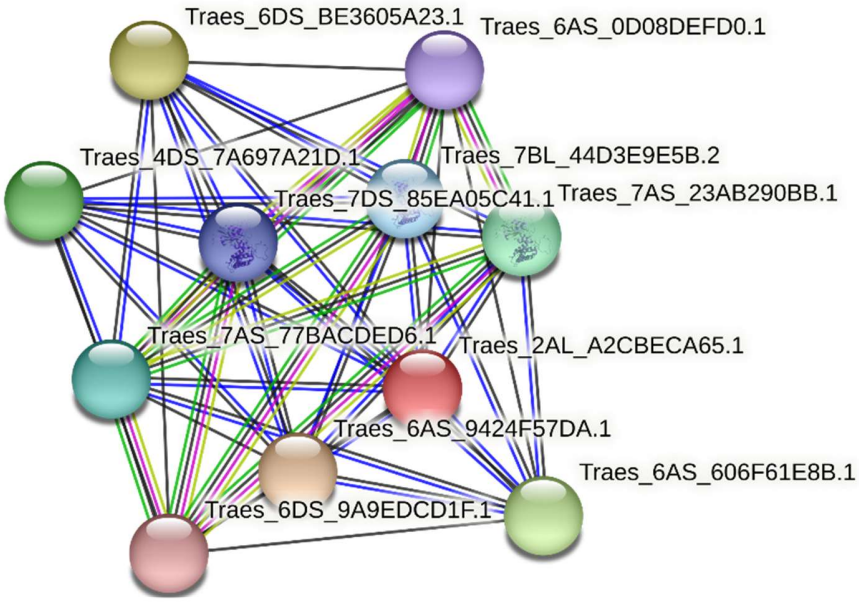

Figure 5.5 STRING database revealed the co-regulation or co-expression of TaCPEP-A with other proteins in wheat which function in the chloroplasts and are associated with the defence response.

Proteins with high confidence, above 0.7, were chosen. Each node represents a protein with the lines showing the evidence used to predict the association between them. Green line: neighbourhood association; blue line: cooccurrence evidence; yellow: textmining evidence; black line: coexpression evidence.

5.3.3. Using structural predictions to further our understanding of TaCPEP-A

To further explore the role of TaCPEP, I used Alphafold2 to predict the structural conformation of TaCPEP (**Figure 5.6**). Using this structure, I carried out a 3D structural similarity search using Uniprot (The UniProt Consortium, 2022) and the top hits were annotated as being metallopeptidases in the M48 or M41 family (

Table 5.4). To further investigate the structural homology of TaCPEP, I submitted the protein databank (PDB) file obtained by protein structure prediction using AlphaFold2 to the Dali Protein Structure Comparison Server. This server didn't support wheat as a target organism; therefore, the rice proteome was used (

Table 5.4). The top hits were unannotated proteins which through further analysis were associated with the GO terms ATP-dependent peptidase activity (GO:0004176), metalloendopeptidase activity (GO:0004222), ATP binding (GO:0005524), proteolysis (GO:0006508) and membrane (GO:0016020). Across the top five hits from both UniProt and the Dali Server, seven were predicted to be chloroplastic or mitochondrial metallopeptidases of the FtsH family.

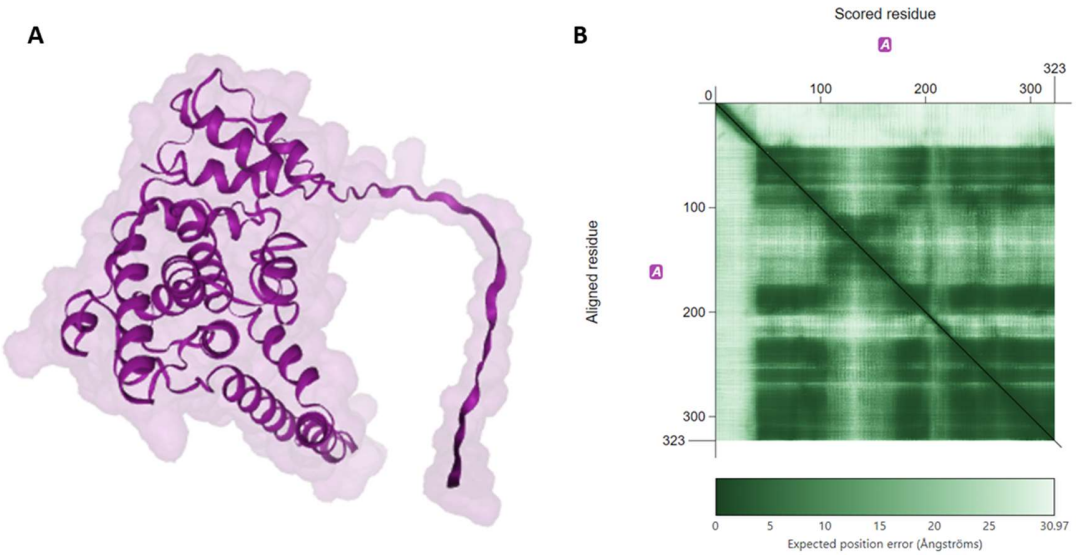

Figure 5.6 AlphaFold2 structural prediction of TaCPEP.

The amino acid sequence of TaCPEP-A was submitted to the AlphaFold2 server and the resulting (A) structure and (B) Average Predicted Aligned Error were viewed using the PAE Viewer.

Table 5.4 Top hits from UniProt and Dali Server structural similarity searches of TaCPEP-A protein.

The amino acid sequence or PDB file was submitted to the UniProt BLAST tool or Dali Server, respectively. For the Dali Server, structures were searched against the rice proteome. The top five hits from each search are listed below.

UniProt ID	Server	Organism	Metallopeptidase family
A0A3B6CFB2	UniProt BLAST	*Triticum aestivum*	M48
A0A3B6DMR8			M48
A0A453DA14		*Aegilops tauschii*	M41
A0A7H4LPL1		*Triticum aestivum*	M41
A0A453D9W7		*Aegilops tauschii*	M41
A0A0P0V2T0	Dali Protein Structure Comparison Server	*Oryza sativa*	unknown
A0A0P0WFM3			unknown
B9F395			unknown
FTSH9			M41
FTSH4			M41

5.3.4. Protein phylogeny of TaCPEP suggests that within wheat there are highly related proteins with similar function

To explore the molecular evolution of TaCPEP in the hexaploid wheat species *Triticum aestivum*, a protein phylogeny was carried out. A protein sequence similarity search against the wheat proteome using TaCPEP-A amino acid sequence as a reference was performed. This search returned six proteins (two new sets of A, B and D genome homoeologous proteins) from chromosomes 6 and 7 with similarity to TaCPEP (TraesCS6A02G166300, TraesCS6B02G193700, TraesCS6D02G154900, TraesCS7A02G375700, TraesCS7B02G277300 and TraesCS7D02G375700). The phylogenetic tree shows that the homoeologous proteins TraesCS7A02G375700, TraesCS7B02G277300 and TraesCS7D02G375700 are most closely related to TaCPEP homoeologues (**Figure 5.7**). A domain prediction revealed that all the proteins share N-terminal M41 family metallopeptidase functional domains and have the same associated GO Terms for proteolysis (GO:0006508), ATP-dependent peptidase activity (GO:0004176), metalloendopeptidase activity (GO:0004222) and ATP binding (GO:0005524). They all have a conserved HEXXH zinc-binding motif at residues 263-267, although the TaCPEP homoeologues have an alanine in residue four, which is substituted for a glycine in the BLAST hits (**Figure 5.7**). TraesCS6A02G166300, TraesCS6B02G193700 and TraesCS6D02G154900 are predicted to have both nuclear and chloroplast localisation signals.

TraesCS7A02G375700, TraesCS7B02G277300 and TraesCS7D02G375700 were predicted to contain no transit peptide and therefore most likely remains cytosolic.

To understand whether these genes may also be involved in the wheat response to *Pst*, I analysed their expression over the course of *Pst* isolate F22 infection in the wheat varieties Oakley, Solstice and Santiago, using the RNA-seq data from Corredor-Moreno *et al.* (2022). In the later stages of infection, the expression profile of each of these genes approximately matched those for the NGCPs identified in Chapter 3. That is, these genes generally showed increased expression to day 11 in the most resistant line, Santiago, but reduced expression in the more susceptible lines. The A homoeologue of each set of genes follows this more closely, with downregulation at 1 dpi, increase in expression at 3 dpi and then Santiago having the highest expression at the end of infection. The homoeologues proteins more closely related to TaCPEP also followed the NGCP expression pattern more closely, with the most resistant interaction (wheat variety Santiago) having the highest expression of these genes at the end of infection. TraesCS6A02G166300, TraesCS6B02G193700 and TraesCS6D02G154900 had a larger evolutionary distance from TaCPEP homoeologues and the expression profiles also diverged from that of the other NGCPs presented, as the increase in expression peaked at around 7 dpi, as opposed to 3 dpi. Additionally, the heightened expression in Santiago at the end of the time-course was less pronounced than in other NGCPs (**Figure 5.7**).

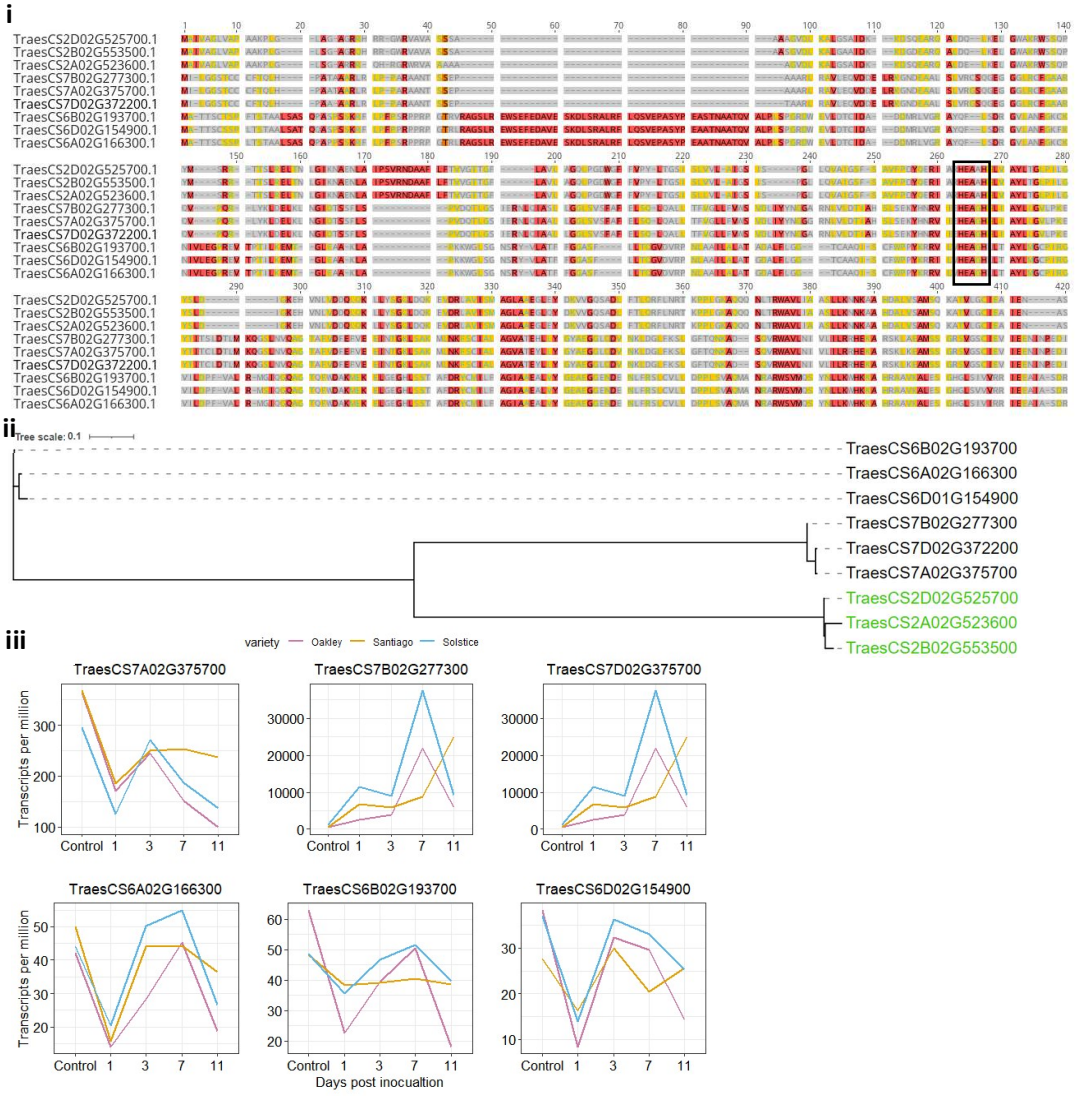

Figure 5.7 Sequence similarity searches for TaCPEP in wheat at the protein level reveals two sets of highly related and functionally conserved proteins that approximately follow the NGCP expression pattern.

(i) Amino acid sequence alignment for the wheat TaCPEP homoeologues with the six hits identified through sequence similarity search (BLAST). The metallopeptidase HEXXA motif is highlighted in black at residues 263-267. **(ii)** Phylogenetic analysis was carried out using a multiple sequence alignment (MSA) of TaCPEP amino acid sequences (highlighted in green) and the BLAST hits. The tree was made using Approximately-Maximum-Likelihood model in FastTree (Price *et al.*, 2010). Scale bar represents amino acid substitutions per site. **(iii)** Gene expression profiles across a *Pst* infection time-course for the six most closely related wheat genes to TaCPEP identified through an amino acid sequence similarity search against TaCPEP. Gene expression lines in pink, orange and blue correspond to Oakley, Santiago and Solstice infected with the *Puccinia striiformis* f. sp. *tritici Pst* isolate F22, respectively and used data generated from Corredor-Moreno *et al.* (2022).

To understand the evolutionary history of TaCPEP within the *Poaceae* family of grasses, a protein phylogeny was constructed. For this, I performed a MSA of sequences identified through an amino sequence similarity search and used this to construct a protein phylogenetic tree. The tree is split into two clades, Clade I and II. Every species is represented in both Clade I and II, including *A. thaliana* which was included as a highly diverged plant species from outside the Poaceae family. The wheat TaCPEP is in Clade II and was clustered with proteins from other wheat species, barley, and the progenitor of the wheat D genome, *Aegilops tauschii* (**Figure 5.8**). I noticed that the proteins had either alanine (A) or glycine (G) amino acids in position four of the metal binding HEXXH motif and upon annotation found that the clades were largely split by the identity of this amino acid within the HEXXH motif. Proteins in Clade II primarily had A in this position, including TaCPEP, whereas in Clade I proteins primarily possessed G in position four of the HEXXH motif (**Figure 5.8**).

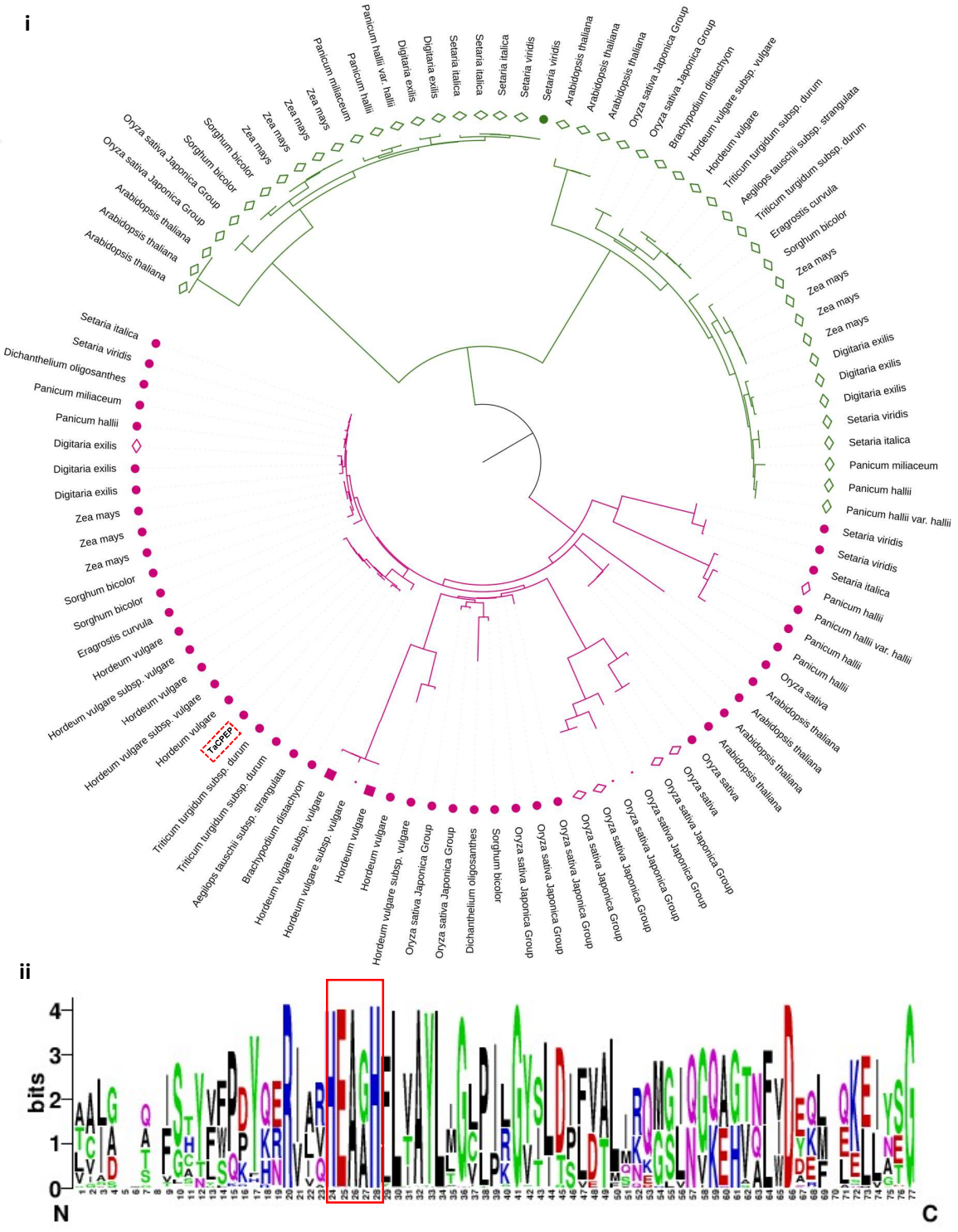
i
Panicum hallii var. hallii
Digitaria exilis
Digitaria exilis
Setaria italica
Setaria italica
Setaria italica
Setaria viridis
Setaria viridis
Arabidopsis thaliana
Arabidopsis thaliana
Arabidopsis thaliana
Oryza sativa Japonica Group
Oryza sativa Japonica Group
Brachypodium distachyon
Hordeum vulgare subsp. vulgare
Hordeum vulgare
Triticum turgidum subsp. durum
Aegilops tauschii subsp. strangulata
Triticum turgidum subsp. durum
Eragrostis curvula
Sorghum bicolor
Zea mays
Zea mays
Zea mays
Zea mays
Digitaria exilis
Digitaria exilis
Digitaria exilis
Setaria viridis
Setaria italica
Panicum miliaceum
Panicum hallii
Panicum hallii var. hallii
Setaria viridis
Setaria viridis
Setaria italica
Panicum hallii
Panicum hallii var. hallii
Panicum hallii
Panicum hallii
Oryza sativa
Arabidopsis thaliana
Arabidopsis thaliana
Arabidopsis thaliana
Oryza sativa
Oryza sativa Japonica Group
Oryza sativa Japonica Group
Oryza sativa Japonica Group
Oryza sativa Japonica Group
Oryza sativa Japonica Group
Oryza sativa Japonica Group
Oryza sativa Japonica Group
Sorghum bicolor
Dichanthelium oligosanthes
Oryza sativa Japonica Group
Oryza sativa Japonica Group
Hordeum vulgare
Hordeum vulgare subsp. vulgare
Hordeum vulgare subsp. vulgare
Brachypodium distachyon
Aegilops tauschii subsp. strangulata
Triticum turgidum subsp. durum
Triticum turgidum subsp. durum
TaCPEF
Hordeum vulgare
Hordeum vulgare subsp. vulgare
Hordeum vulgare
Hordeum vulgare subsp. vulgare
Hordeum vulgare
Sorghum bicolor
Sorghum bicolor
Zea mays
Zea mays
Zea mays
Eragrostis curvula
Hordeum vulgare
Hordeum vulgare subsp. vulgare
Dichanthelium oligosanthes
Panicum miliaceum
Panicum hallii
Digitaria exilis
Digitaria exilis
Digitaria exilis
Zea mays
Setaria italica
Setaria viridis
ii
bits
4
3
2
1
0
N
C

Figure 5.8 Orthologues of TaCPEP are present in the *Poaceae* family and are split into two clades that contain proteins with conserved HEXXH motifs.

(i) A MSA of TaCPEP amino acid sequence and proteins from members of the *Poaceae* family identified through sequence similarity search was used to construct the phylogenetic tree. The tree is divided into Clade I and Clade II, with branches in pink and green, respectively. TaCPEP is in Clade II, highlighted in red dashed box. The symbols represent the presence of either the amino acid alanine (circle), glycine (diamond) or neither (small dot) in position four of the metal binding HEXXH motif. The tree was made using Approximately-Maximum-Likelihood model in FastTree (Price *et al.*, 2010). Scale bar represents amino acid substitutions per site. **(ii)** Amino acid sequence conservation in the HEXXH motif and flanking sequence between proteins from the MSA used to generate the protein phylogeny. The amino acid sequences were extracted from the MSA and input into the WebLogo software (Crooks *et al.*, 2004). The HEXXH motif is located at residues 24-28.

5.3.5. Disruption of *TaCPEP* has no apparent effect on assimilation, or starch density but may alter chlorophyll content and chloroplast size

As *TaCPEP* is predicted to encode a metallopeptidase in the M41 family, and other chloroplast-localised metallopeptidases in that family are vital for photosynthesis and chloroplast biogenesis, I examined photosynthetic processes and chloroplast morphology in *TaCPEP* disruption mutants. Firstly, to assess whether there was a difference in the activity of the light-dependent or light-independent processes, I measured resting assimilation which is the rate at which atmospheric carbon dioxide is fixed and converted into organic compounds such as amino acids and carbohydrates (Smith and Zeeman, 2020). These measurements were taken in the most recently fully emerged leaves of *TaCPEP* disruption mutants and wildtype controls at the two-leaf stage (approximately 10 days old). There was no statistically significant difference in resting assimilation rates between TaCPEP-A^{W135*}, TaCPEP-B^{R100}, TaCPEP-A^{W135*}TaCPEP-B^{R100-} or KWT (**Figure 5.9**).

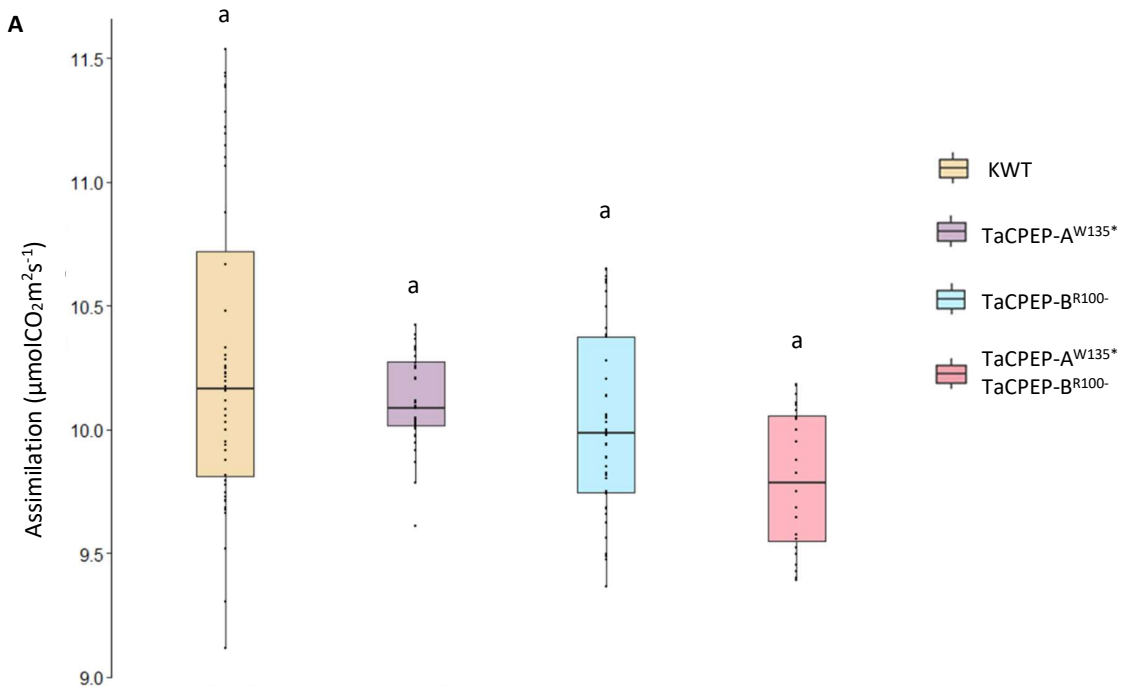

Figure 5.9 There is no statistical difference in the resting assimilation rate in *TaCPEP* disruption mutants compared to a wildtype control line.

The infrared gas analyser LICOR-6800 was used to measure the resting assimilation in the most recently fully emerged leaf of *TaCPEP* disruption mutants. There was no statistically significant difference between genotypes, as determined using the Wilcoxon signed-rank test (p<0.05). Boxes signify the upper (Q3) and lower (Q1) quartiles, bars represent median values, and whiskers are located at 1.5 the interquartile range**.** Data represent four biological replicates.

To further assess the impact of TaCPEP disruption on photosynthetic processes, I measured the chlorophyll *a*, *b*, and total chlorophyll content. TaCPEP-A^{W135*} had significantly lower chlorophyll a, b and total chlorophyll content compared to TaCPEP-B^{R100-}, TaCPEP-A^{W135*}TaCPEP-B^{R100-}, TaCPEP-A^{WT} and KWT (**Figure 5.10**).

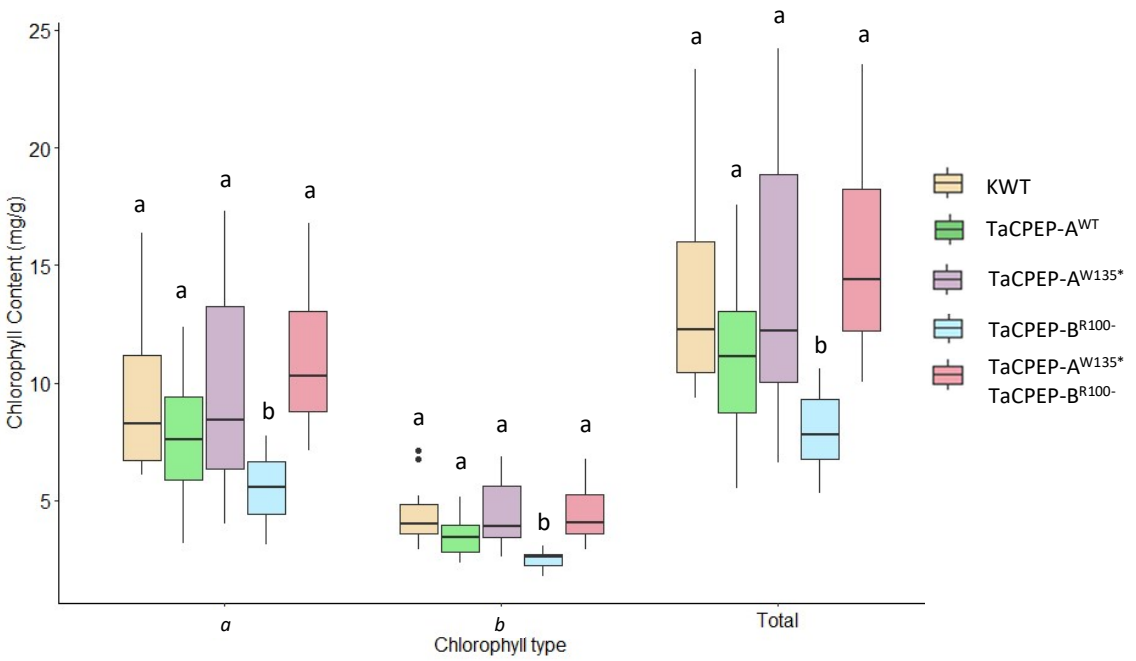

Figure 5.10 Chlorophyll *a*, *b* and total chlorophyll measured in *TaCPEP* disruption mutants.

The content, by total leaf weight, of chlorophyll *a*, *b* and total chlorophyll was measured in *TaCPEP* disruption mutants and wildtype control lines using spectrophotometry by measuring absorbance at 645 nm and 663 nm. An approximately 2 cm section of the second leaf of each plant was sampled, weighed, and placed in 80% acetone for 3 days. Absorbance at 645 nm and 663 nm was measured using the BMG Labtech FLUOstar Omega plate reader. TaCPEP-A^{W135*} had significantly lower chlorophyll a, b and total chlorophyll content compared to TaCPEP-B^{R100-}, TaCPEP-A^{W135*}TaCPEP-B^{R100-} , TaCPEP-A^{WT} and KWT. Letters indicate significant differences determined using ANOVA and Tukey post-hoc tests (p<0.05). Measurements were taken for 16 biological reps per genotype across three independent experiments. TaCPEP-A^{WT} are TILLING mutants carrying the wildtype allele of both A and B copies of *TaCPEP* and is used as a control in addition to Kronos wildtype (KWT). Boxes signify the upper (Q3) and lower (Q1) quartiles, bars represent median values, and whiskers are located at 1.5 the interquartile range.

To evaluate the impact of loss of *TaCPEP* function on photosynthesis and photoassimilate production, I carried out starch staining on *TaCPEP* disruption mutants. I sampled the first leaf of plants just prior to the end of the day cycle for maximum starch accumulation. I cleared the leaf tissue in ethanol for three days and then stained the leaves with Lugols iodine stain. This showed that starch accumulation and distribution in the leaves was comparable between TaCPEP-A^{W135*}, TaCPEP-B^{R100-}, TaCPEP-A^{W135*}TaCPEP-B^{R100-}, TaCPEP-A^{WT} and KWT as there was no observable difference in the distribution or density of the stain (**Figure 5.11**). To explore whether the

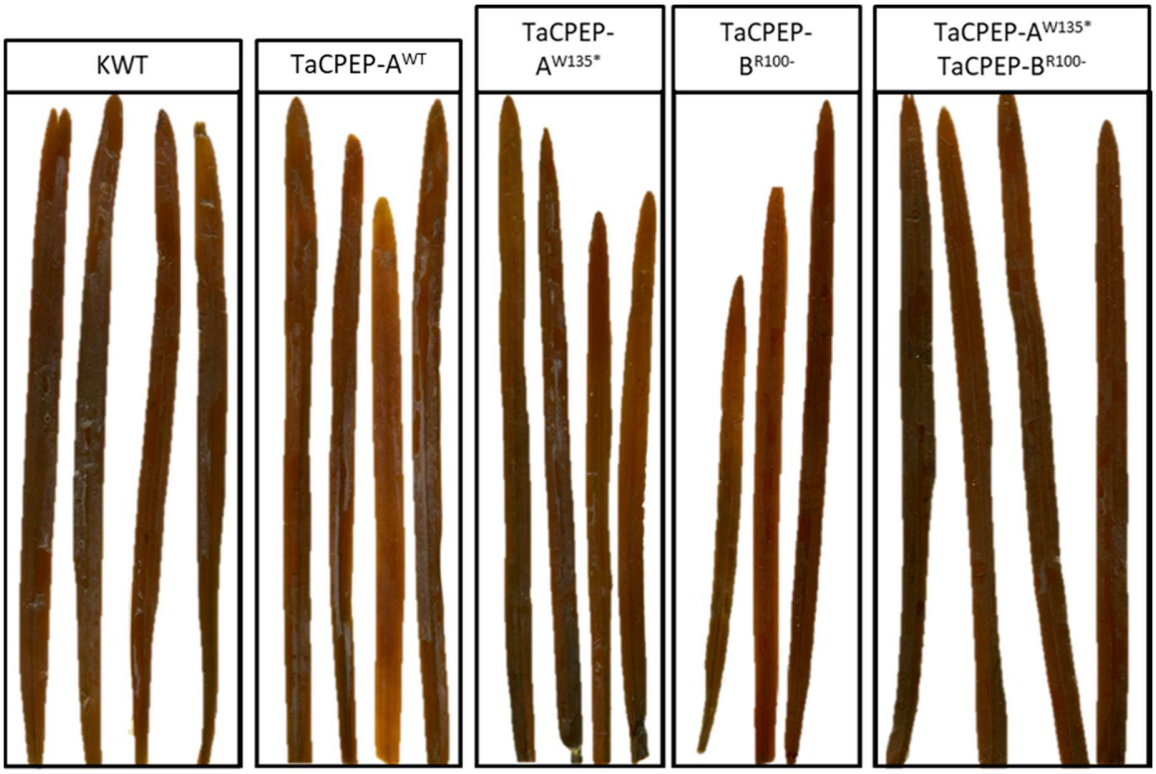

Figure 5.11 Starch accumulation and distribution in *TaCPEP* disruption mutants.

Lugol's Iodine stain was used to stain starch in the first leaf of plants. Staining suggests that the accumulation and distribution of starch is comparable between genotypes with no clear difference in the distribution or darkness of the starch stain of leaves between the lines TaCPEP-A^{W135*}, TaCPEP-B^{R100-}, TaCPEP-A^{W135*}TaCPEP-B^{R100-}, TaCPEP-A^{WT} and KWT. TaCPEP-A^{WT} are TILLING mutants carrying the wildtype allele of both A and B copies of *TaCPEP* and is used as a control in addition to Kronos wildtype (KWT). The experiment was carried out with four biological replicates.

chloroplasts of *TaCPEP* disruption mutants had any changes in morphology, I isolated single mesophyll cells from the most recently fully emerged leaves of *TaCPEP* disruption mutants at the three-leaf stage (approximately 14 days old). Cells were fixed and released from the tissue by gentle tapping. Samples were mounted in water and immediately imaged using confocal microscopy.

Chlorophyll autofluorescence was used to visualise chloroplasts in individual mesophyll cells using confocal microscopy (**Figure 5.13**). To quantify chloroplast size, Dr. Sergio Lopez (JIC Bioimaging facility) wrote a custom Python script to automate the measurement of chloroplast length and area in each of the mesophyll cells. This script included size exclusion to ensure that artefacts were not aberrantly measured. With manual curation, 28 % of measurements were discarded and 516 individual chloroplasts were taken forward for analysis (TaCPEP-A^{WT}; n=122, KWT; n= 210, TaCPEP-A^{W135*}; n= 37, TaCPEP-B^{R100-}; n= 56, TaCPEP-A^{W135*}TaCPEP-B^{R100-}; n= 91) (**Figure 5.12**). Pairwise comparisons revealed that chloroplasts in the genotypes TaCPEP-B^{R100-} and TaCPEP-A^{W135*}TaCPEP-B^{R100} had significantly lower area and length compared to TaCPEP-B^{WT} (**Figure 5.14**).

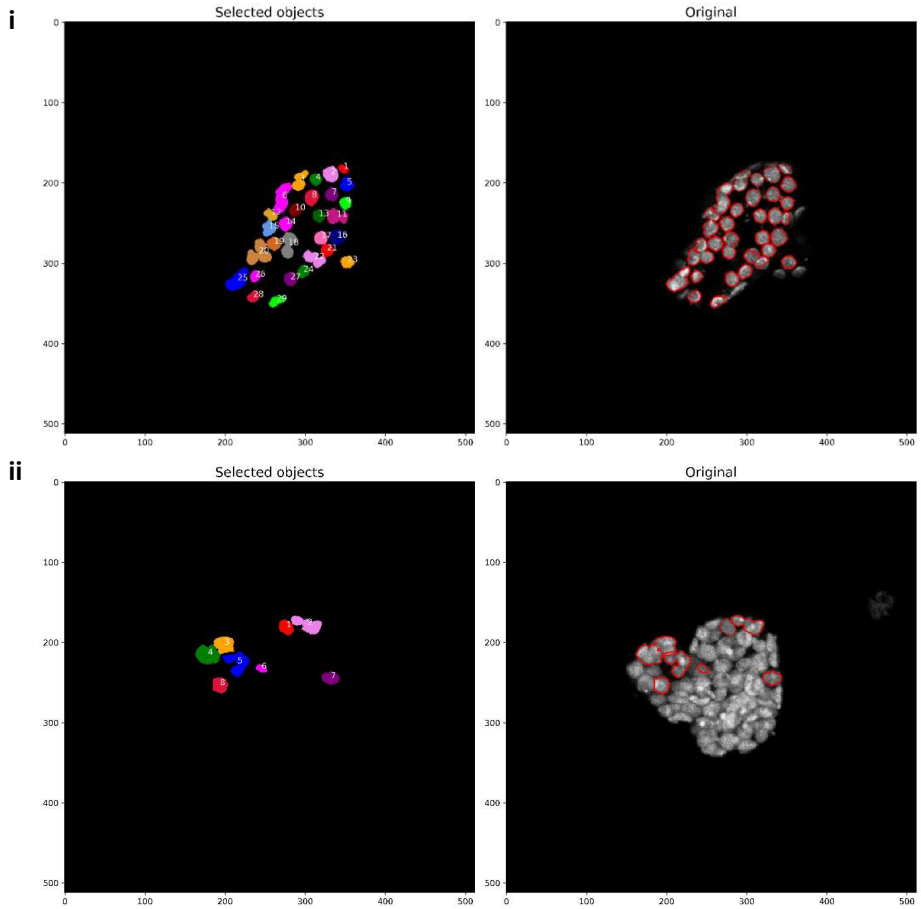

Figure 5.12 Phyton script detects chloroplasts from single mesophyll cells and automates the measurement of area and length.

Examples of the detection of chloroplasts from the original images acquired by confocal microscopy. Chloroplasts detected and measured are highlighted in colours in the left panels and the original chloroplasts from the confocal images in the right panels. (**i**) Shows an example where 29 of the chloroplasts were detected and measured, with chloroplasts 1, 6, 11, 15, 20 and 25 being manually discarded for incorrect detection and (**ii**) where the confocal image enabled only 8 chloroplasts to be detected, with 2, 3, 4, 5 and 6 being manually discarded for incorrect detection.

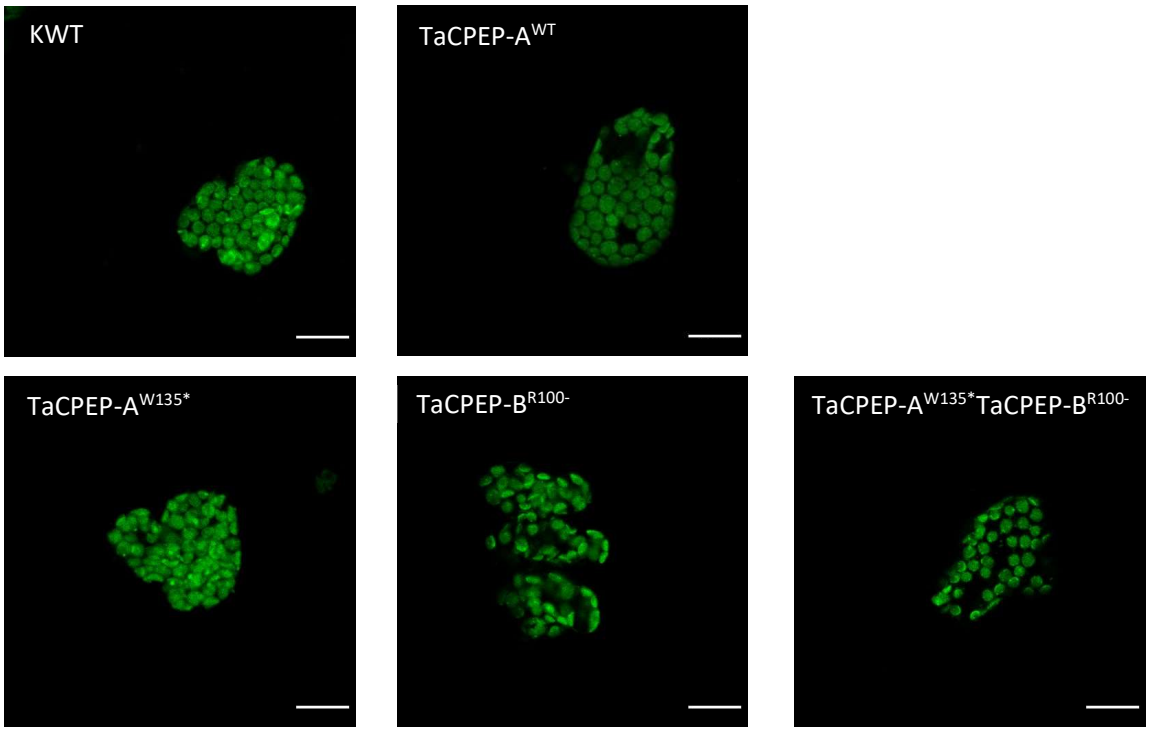

Figure 5.13 Single mesophyll cells from *TaCPEP* disruption mutants were isolated and the chloroplasts imaged using confocal microscopy.

The chloroplasts from single mesophyll cells isolated from the most recently fully emerged leaf from wildtype and *TaCPEP* disruption mutant seedlings were imaged by confocal microscopy using chlorophyll autofluorescence, as shown in green. Each genotype was sampled with four biological replicates. TaCPEP-A^{WT} are TILLING mutants carrying the wildtype allele of both A and B copies of *TaCPEP* and is used as a control in addition to Kronos wildtype (KWT). Scale bar represents 22 µm.

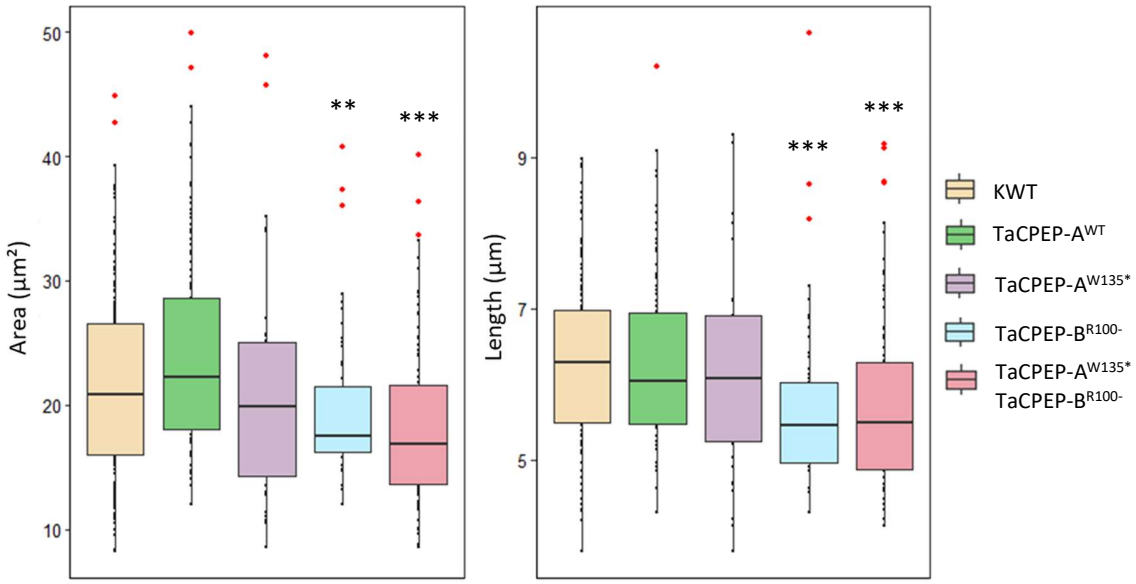

Figure 5.14 Automated quantification of chloroplast area and length in *TaCPEP* disruption mutants shows that single and double mutants have smaller chloroplasts.

The quantification of chloroplast area and length from single mesophyll cells imaged using confocal microscopy suggest that mutants TaCPEP-B^{R100-} and TaCPEP-A^{W135*}TaCPEP-B^{R100-} have significantly smaller chloroplasts with lower area and length compared to the TaCPEP-A^{WT} control (asterisks denote statistically significant values; *** P<0.001, ** P <0.01, Wilcoxon rank-sum test). TaCPEP-A^{WT} are TILLING mutants carrying the wildtype allele of both A and B copies of *TaCPEP* and is used as a control in addition to Kronos wildtype (KWT). Boxes signify the upper (Q3) and lower (Q1) quartiles, bars represent median values, and whiskers are located at 1.5 the interquartile range.

5.4. Discussion

In this chapter, I performed *in silico* analysis of *TaCPEP* and found that the promoter region of *TaCPEP* may contain pathogen-response *cis*-acting regulatory regions and TF-binding sites. Additionally, String cluster analysis also implicates TaCPEP in the response against pathogens by being co-expressed and regulated with other genes involved in the immune response. I further characterised photosynthetic properties of the *TaCPEP* mutants, including chlorophyll content, starch density and distribution, and chloroplast morphology. I found that, whilst there was a reduction in the content of chlorophyll in one of the single *TaCPEP* disruption mutants, starch density and distribution as well as assimilation was unaltered. There was a difference in the length and area of chloroplasts in the single and double mutant. Together, these results suggest that TaCPEP is unlikely to play a key role in the light-dependent or light-independent processes.

However, as there was a reduction in chlorophyll content, chloroplast length and area in the mutants, TaCPEP function could be linked to these processes. Therefore, TaCPEP might function in both photosynthetic processes as well as plant immunity.

5.4.1. *In silico* investigation of *TaCPEP* shows that it may be a stress-responsive gene that is co-regulated with others involved in the response to pathogens

As the results thus far suggested that *TaCPEP* encodes a chloroplastic protein that when disrupted leads to an increase in wheat susceptibility to *Pst* and MoT, I wanted to investigate whether we could enhance our understanding of the function of *TaCPEP* using bioinformatic tools. Analysis of co-regulatory networks for *TaCPEP* suggested that *TaCPEP* was co-expressed and co-regulated with other genes predicted to be involved in chloroplastic processes and plant immunity against bacteria. Promoter sequences can contain elements that enable transcriptional responses to certain stimuli including abiotic and biotic stress. To analyse the promoter region of *TaCPEP*, I carried out prediction of TF- binding and *cis* acting regulatory motifs. I found that the 1 kb region upstream of the *TaCPEP* translational start site contained motifs that function in the plant response to abiotic and biotic stresses. For example, the TGACG motif has been shown to be required for the SARD4 response to SA (Ding *et al.*, 2018b). In support of this, studies also showed that TGACG-BINDING FACTOR 1 (TGA1) positively regulate SA biosynthesis and that TGA4 is also required for full SARD4 expression during PTI (Sun *et al.*, 2018). Additionally, it has been shown that the MYB1 transcription factor, for which the promoter of *TaCPEP* also has a binding site, regulates the drought stress response in barley (Alexander *et al.*, 2019). Alexander *et al.* (2019) showed that overexpression of MYB1 caused constitutive expression of ROS scavenging enzymes and a reduction in the presence of ROS. Overall, promoter analysis suggests that expression of *TaCPEP* may be involved in responses to numerous abiotic and biotic stresses. This adds further evidence supporting the hypothesis that *TaCPEP* is involved in the wheat response to pathogens. Future experiments could help explore whether this promoter analysis reflects biological significance. For example, it could be informative to test the expression of *TaCPEP* in response to different exogenous stimuli including SA and ROS. Moreover, we could analyse the response of *TaCPEP* disruption mutants under abiotic stresses such as drought and high/low light. Coupling such experiments with the data presented here would help elucidate the mechanisms behind TaCPEP regulation and function in biotic and abiotic stress responses.

5.4.2. Protein phylogeny was used to gain insight into TaCPEP evolution and its potential function

To further investigate the function of *TaCPEP*, I carried out phylogenetic studies to reconstitute its evolutionary history in the *Poaceae* family and understand whether there might be functional conservation between species. Further to this, I also constructed a phylogenetic tree based on an amino acid MSA between TaCPEP and the top BLAST hits from the wheat genome. I found that the *Poaceae* phylogenetic tree is divided into two clades, with the wheat TaCPEP being in Clade II. Wheat TaCPEP was most closely grouped with proteins from the grasses *Triticum turgidum* subspecies *durum* and *Hordeum vulgare*. All except one protein in Clade I had HEAGH metallopeptidase motifs whilst Clade II comprises almost exclusively of proteins that have a HEAAH metallopeptidase motif. This suggests that there may have been functional divergence of this protein and the motifs early in the evolution of the *Poaceae* family. Furthermore, using a sequence similarity search, I found that within the wheat genome there were six other proteins encoded by genes *TraesCS6A02G166300, TraesCS6B02G193700, TraesCS6D02G154900, TraesCS7A02G375700, TraesCS7B02G277300* and *TraesCS7D02G375700* (two sets of A, B and D homoeologues) that were found to be highly similar to TaCPEP at the protein level. A MSA and subsequent construction of a phylogenetic tree revealed that TraesCS7A02G375700, TraesCS7B02G277300 and TraesCS7D02G375700 were most closely related to TaCPEP. All these wheat proteins had the same functional annotations and were predicted to encode for ATP-dependent metallopeptidases in the M41 family which suggests that there could be functional redundancy. Such redundancy could mean that disrupting *TaCPEP* and those closely related genes could result in more marked phenotypes than those reported in *TaCPEP* disruption mutants alone in pathogen resistance or *PR* gene expression in Chapter 4. As TraesCS7A02G375700, TraesCS7B02G277300 and TraesCS7D02G375700 were not predicted to have a subcellular localisation signal and therefore are likely to localise in the cytosol, it could be that differing subcellular localisation may spatially separate the function of these proteins from TaCPEP which may limit the potential for functional redundancy with TaCPEP. Extensive characterisation of the metallopeptidase HEXXH motif has found that the motif can be expanded to more stringently select for metallopeptidases and to place them into certain families (Hooper, 1994). TaCPEP does not have an expanded motif and therefore cannot be placed more specifically in the metallopeptidase family. Without experimental validation of the HEXXH motif and its functionality, the contribution of this motif to metal binding and the relevance of the amino acid substitution to function is unknown. In the future, it may be important to further explore the

biochemical function of TaCPEP. For example, by confirming the metallopeptidase activity of TaCPEP and exploring its protein targets we may move a step closer to understanding how this protein contributes to the wheat response to pathogens. We could do this using comparative proteomics of isolated chloroplasts from infected and non-infected *TaCPEP* disruption mutants and wildtypes, following a technique such as the one used by He *et al.* (2013).

5.4.3.TaCPEP is a chloroplast-localised protein

TaCPEP is an uncharacterised gene with unknown protein function. By performing *in silico* analyses, it was predicted that *TaCPEP* encodes a metalloprotease with a chloroplast transit peptide (cTP) at the C-terminal. Further investigation supports this with the top hits from WoLF PSORT being 'chloroplast thylakoid membrane', 'chloroplast associated with photosystem I and II' and 'integral membrane protein in the chloroplast thylakoid'. Together, these results suggest that *TaCPEP* is a NGCP that functions in the chloroplast. To confirm this, I conducted subcellular localisation by transiently overexpressing a GFP-tagged TaCPEP in *N. benthamiana* and observing localisation using confocal microscopy. I confirmed chloroplast localisation by observing GFP signals overlapping with chlorophyll autofluorescence although the precise sub-chloroplast location could not be determined. The function of proteins within the chloroplast is tightly linked to location. For example, proteins involved in light-dependent reactions are located on the thylakoid membranes and those involved in metabolism can cluster into plastoglobules (Wang *et al.*, 2023b). M41 metallopeptidases of the FtsH family are known to localise and function in the thylakoid membrane and there are M48 metallopeptidases thought to function in plastoglobules. As there are conflicting predictions of which metallopeptidase family TaCPEP belongs to based on structural searches in UniProt and the Dali Server, knowing the sub-chloroplast localisation of TaCPEP may provide more insight into its function. Sub-chloroplast localisation could be achieved by chloroplast fractionation and proteomics or through fluorescent microscopy (Bruley *et al.*, 2012). Recently, there was a *Chlamydomonas* protein localisation atlas published whereby 1034 candidate chloroplast proteins were experimentally localised to the sub-chloroplast level (Wang *et al.*, 2023b). The authors also predicted protein-protein interactions and created a library of mutants. These data were published on the *Chlamydomonas* Library Project (CLiP). A search for *TaCPEP* orthologues via the Ensemble Plants database, and a BLAST search of the protein, led to the *Chlamydomonas* genes *Cre08.g379175* and *Cre08.g379200* being identified as orthologues of *TaCPEP* at the gene and protein level. With the aim to use Chlamydomonas as a model to study *TaCPEP*, for example in complementation assays, sub-chloroplast localisation or for phenotypic studies, I searched the CLiP

databases for mutants, sub-chloroplast localisation and protein-protein interaction networks. Unfortunately, neither Cre08.g379175 or Cre08.g379200 were represented in any of the libraries (Li *et al.*, 2019). Through personal correspondence with the Chlamydomonas Resource Centre it is most likely that mutagenesis didn't generate mutants in these genes, or that the mutations were lethal. These results suggest that TaCPEP may play an integral role in a chloroplast function, making a *Chlamydomonas* mutants in orthologues unviable. However, as there is limited information on *Cre08.g379175* and *Cre08.g379200* this does not exclude the possibility that these genes and the proteins they encode are functionally diverged as there is significant evolutionary time between *Chlamydomonas* and wheat.

Additionally, from the subcellular localisation studies I also noticed that there was a GFP signal in a small 'tail' emanating from one of the chloroplasts. This could be the beginning of the formation of a stromule, a structure that is typically stress-induced and projects from the chloroplast containing stroma and published images of *N. benthamiana* stromules strongly resemble that in **Figure 5.3** (Brunkard *et al.*, 2015). Studies suggest that thylakoid membranes, containing chlorophyll, are unable to translocate into the stromules (Hanson and Sattarzadeh, 2011). However, some GFP-tagged proteins can move into the stromules. This may suggest that TaCPEP is not restricted to the thylakoid membranes, contrary to predictions from WoLF PSORT. Further investigation is required to ascertain whether TaCPEP can move into the stromules, or whether the loss or overexpression of TaCPEP causes any differences in stromule formation. To this end, it would be interesting to overexpress GFP-tagged TaCPEP in *N. benthamiana* and infect with *P. infestans,* as was carried out in Chapter 4, to compare stromule formation in infected and uninfected samples. These studies, along with sub-chloroplast localisation, may help us to further understand the function of TaCPEP in the chloroplasts.

5.4.4. Loss of *TaCPEP* function leads to smaller chloroplasts without compromising photosynthetic processes

In Chapter 4, I found that the disruption of *TaCPEP* in wheat leads to an increase in susceptibility to *Pst* and MoT. Overexpression of *TaCPEP* in *N. benthamiana* increased resistance against *P. infestans.* Furthermore, mutants had reduced expression of the *PR* gene *PR4,* which is required for resistance against fungal pathogens (Bertini *et al.*, 2009; Bertini *et al.*, 2006; Bertini *et al.*, 2003). These results suggest that the TaCPEP protein might function in response to fungal infection, although the mechanism for this remains elusive. One hypothesis was that the loss of

TaCPEP, a chloroplast metalloprotease, may negatively impact chloroplast morphology, chlorophyll content, starch density and distribution in source tissue, or photosynthetic processes, which may diminish the immune response. To test this, I carried out a series of experiments to investigate the above processes. I found that there was no difference in resting assimilation, or starch distribution and density. However, chlorophyll content was reduced in the single *TaCPEP* disruption mutant and whilst there were no dramatic differences in chloroplast morphology, there was a significant decrease in chloroplast area and length in the mutants.

Chloroplasts, like their prokaryotic ancestors, divide by binary fission. This involves the coordinated effort of multiple proteins, some of which are bacterial homologs, that create a contractile ring on the inner and outer membranes which pinches off the new chloroplast (Chen *et al.*, 2017a). There are various environmental and developmental reasons for aberrant chloroplast size. Studies have shown that mutations in proteins involved in forming the contractile ring can cause chloroplasts to develop different sizes. For example, *FtsZ* mutants form larger and fewer chloroplasts (Strepp *et al.*, 1998). It is possible that *TaCPEP* mutants have smaller chloroplasts because they are undergoing increased rates of chloroplast division. In the future, we could modify the Python script to enable determination of chloroplast number. If mutants had more but smaller chloroplasts then that might suggest that TaCPEP disruption impacts chloroplast division. However, as we found no statistically significantly differences in assimilation, it seems that any difference in chloroplast size does not result in any changes to photosynthetic processes. In *A. thaliana,* studies have shown that fewer, larger chloroplasts results in no difference in chlorophyll a or b content, but does result in a decrease in photosynthetic efficiency seen in lower assimilation compared to plants which had normal chloroplast size (Xiong *et al.*, 2017). Therefore, it is probable that if there was a biologically significant reduction in chloroplast size in the TaCPEP mutants, that this would have translated to a reduction in assimilation.

It could be that limitations to the methods and analyses led to an artefactual result for chloroplast size. To isolate the mesophyll cells, I took tissue from the middle of the most fully emerged leaf. Chloroplast biogenesis, division and size differs depending on the developmental stage of the plant. It is therefore possible that subtle differences in developmental stages that were not obvious when sampling led to *TaCPEP* mutant samples containing smaller chloroplasts. Furthermore, a major limitation of the quantification of chloroplast size lies in the 2D confocal images. A study found that 2D images severely underestimated the number of chloroplasts in cells, compared to analysis of 3D images (Kubínová *et al.*, 2013). In agreement, Harwood *et al.* (2020) also

found that in wheat mesophyll cells, chloroplast area was underestimated in 2D images compared to 3D. According to the literature, Serial Block Face Scanning Electron Microscopy (SBF-SEM) is a better tool for measuring the size and volume of chloroplasts in mesophyll cells. This technique, however, requires extensive resources and time, which was limited in the current study. In the future, if we wanted to validate the results of the 2D image analysis, then SBF-SEM could be utilised. However, to elucidate the function of TaCPEP, I believe that biochemical assays that enable determination of enzyme substrates would yield more information on protein function and its contribution to the wheat response to pathogenic fungi.

Overall, in this chapter, I characterised potential functions for *TaCPEP* through assessing photosynthetic processes in disruption mutants, performing *in silico* analyses, and assessing protein localisation. I found that there was limited impact of disruption of *TaCPEP* function on photosynthetic processes, including starch distribution and density and assimilation. Chlorophyll content was lower for one of the lines carrying a mutation in *TaCPEP-B* and whilst the chloroplasts in *TaCPEP* disruption mutants appeared smaller, further investigations are needed to validate these results. I experimentally confirmed computational predictions of chloroplast localisation by fluorescently tagging TaCPEP and transiently expressing it in *N. benthamiana.* Investigation of TaCPEP's evolutionary history showed that there is potentially a functional divergence of TaCPEP relatives within the *Poaceae* family, with two clades containing proteins that have different residues in the HEXXH motif. Whilst closely related proteins to TaCPEP were identified within the wheat genome, it is unclear whether they could overlap in function as some of these proteins are predicted to localise outside of the chloroplasts. Altogether, this chapter bought us closer to understanding the contribution of TaCPEP to the response against pathogens and its broader function in wheat chloroplasts. It will be significant to now experimentally validate the biochemical function of TaCPEP to help understand how it might be involved in wheat susceptibility to pathogenic fungi.

6. General Discussion

6.1. Expanding our means of crop protection through the identification of robust sources of resistance

There are many challenges facing our ability to control cereal diseases caused by pathogenic fungi, both current and emerging. These challenges include fungicide bans, fungicide resistance and climate change altering pathogen populations in more unpredictable ways (Fones *et al.*, 2020). Additionally, wheat is highly monogenic after intensive selection for desirable traits during its domestication and this lack of genetic diversity increases the risk posed by genetic resistance being quickly overcome by fast-evolving pathogens (Wulff and Dhugga, 2018). It will take multiple approaches to ensure the future of our crops is secure. One strategy that could contribute to the solution to these challenges includes utilising new genetic tools and genomic data to identify host elements that contribute to promoting resistance in our crops (Minter and Saunders, 2023). By understanding these mechanisms, we could enhance wheat resistance to pathogens using traditional or modern techniques to alter the wheat response to pathogens. This has been shown to be a successful approach with the publication of *TaBCAT* and *TaCsp41a* as genes in wheat that, when they are functionally disrupted, can enhance resistance in wheat against rust fungi (Corredor-Moreno *et al.*, 2022; Corredor-Moreno *et al.*, 2021). These genes have the potential to expand our means of crop protection and contribute to the future of food security. However, to provide our crops with robust resistance we need multiple approaches and resources. The chloroplasts are known to be important components of the plant immune response, being the location for the biosynthesis of significant immune signalling molecules such as SA and ROS (Littlejohn *et al.*, 2021). These signals are important for both local and distal immune signalling, further highlighting the role of the chloroplasts and its signalling functions in plant immunity and its potential for crop protection. To explore this potential for *Pst,* we needed to increase our understanding of how these processes are involved in the infection biology and interaction between wheat and *Pst.*

6.1.1. Identification of candidate NGCPs as targets for investigation into the molecular mechanism of wheat susceptibility

To begin to uncover putative chloroplastic mechanisms of wheat susceptibility to pathogenic fungi, in Chapter 3 of this thesis I used previously published transcriptomic data to assess the expression of interesting NGCPs to identify those which have modulated expression correlated with susceptibility level to *Pst*. By utilising genetic resources in wheat such as ExpVIP (Borrill *et al.*, 2016; Krasileva *et al.*, 2017; Ramírez-González *et al.*, 2018), I also explored the expression of NGCPs of

interest during infection with other fungal pathogens of wheat. I hypothesised that the genes *PsbP, PsbQ1, PsbQ2, Psah2, Rubisco Small Chain, Phosphoribulokinase, N Receptor-Interacting protein, Chloroplast Unusual Positioning 1,* the uncharacterised genes (Chloroplast Localised) *1* and *2*, and *TaCPEP* may contribute to the outcome of wheat infection with *Pst* (Corredor-Moreno *et al.*, 2022). I also investigated the homoeologue expression bias for these genes to enable a more targeted approach to investigating gene function. However, there was no drastic expression bias in these genes, which might indicate functional redundancy among the homoeologues. Whilst such genetic redundancy could limit the impact to detect phenotypes in investigations here, this property can be beneficial for crop development as maintaining some gene function in mutants can limit the risk of pleiotropic and detrimental effects. For the recently identified chloroplastic *TaCsp41a* gene, disruption of a single copy encoded on the B genome was sufficient to enhance resistance to *Pst* (Corredor-Moreno *et al.*, 2022).

6.1.2. The future of NGCPs as candidate susceptibility genes

A significant focus in plant biology is on enhancing photosynthetic processes to increase yield, enable plants to respond to changing atmospheric composition or to produce sustainable sources of fuel. Scientists have been working towards solutions to these problems for decades, tackling it from many different angles, from altering components of the light-dependent reactions to modifying plants to carry out a more efficient version of photosynthesis (as reviewed in Orr *et al.* (2017)). Within these broad aims are many individual approaches with varying rates of success. Some of the NGCPs identified within the current study have been a target for improving photosynthesis. When attempting to functionally characterise the role of these NGCPs during wheat infection with *Pst* there are lessons to be learnt from previous attempts to engineer better photosynthesis. As noted in the recent review of efforts of improve photosynthesis by Leister (2023) '*it is necessary to acknowledge the formidable complexity involved in efforts to enhance such a complex process as photosynthesis, which is intimately intertwined with so many other plant processes*'. For the NGCPs identified in the current study, trying to understand how these processes contribute to wheat susceptibility to a biotrophic pathogen with the potential to utilise them in breeding would be an incredible challenge.

6.2. Elucidating the function of *TaCPEP* to fully understand its place in wheat immunity

In Chapters 4 and 5, I explored the function of a predicted chloroplastic metallopeptidase which was found to contribute to the wheat response to pathogenic fungi including *Pst* and MoT. Disrupting the function of *TaCPEP* in wheat led to an increase in susceptibility to both pathogens. Further investigation outlined in Chapter 5 suggested that the disruption of *TaCPEP* does not lead to a reduction in photosynthetic capacity of the plant or starch density or distribution within the leaf, although there may be an alteration in chlorophyll content and chloroplast size. Preliminary data uncovered that *TaCPEP* might contribute to modulated chloroplastic immune processes. We found that there was a general reduction in *Pst*-induced expression of *pathogenesis-related* (*PR*) and SAR genes in *TaCPEP* disruption mutants, although this reduction was only statistically significant for the expression of the fungal response gene *PR4*. In contrast, preliminary data showed that the ROS burst might be enhanced when *TaCPEP* function is disrupted. These two results are in contradiction to each other, as the increase in ROS is usually associated with enhanced resistance against pathogens whilst *TaCPEP* disruption results in reduced resistance. A summary model for the mechanism of the proposed mechanism TaCPEP function is outlined in **Figure 6.1**. Further validation of these results will help to better understand the contribution of *TaCPEP* to wheat susceptibility to *Pst.* Metallopeptidases have diverse functions and by understanding the function of *TaCPEP*, we could greatly enhance our understanding of how metallopeptidases might function within the context of wheat immunity against pathogens.

TaCPEP encodes a predicted metallopeptidase of the M41 family. Other members of the M41 family include the FtsH proteins (Kato and Sakamoto, 2018). These proteins have prokaryotic origins and therefore are exclusively localised to the plastids, both in the mitochondria and chloroplasts (Adam *et al.*, 2001). TaCPEP localises to the chloroplasts and some evidence suggests it is a putative metallopeptidase in the M41 family. Therefore, to begin to understand the potential function of *TaCPEP* in wheat we can look to the function of well characterised FtsHs that function in the chloroplasts. FtsH proteases span the thylakoid membrane and function in the turnover of the photosystem II complex (Kato *et al.*, 2009; Kato and Sakamoto, 2009). This function is integral to the maintenance of photosynthetic function, and mutations in FtsH has dramatic consequences for photosynthesis and leaf phenotypes. For example, mutations in FtsH2 in *A. thaliana* led to a variegated phenotype where the green sectors contain only chloroplasts that have higher levels of other FtsHs that compensate for the loss of FtsH2 (Kato *et al.*, 2009). The functional redundancy

present in the FtsH family reflects what we see in *TaCPEP* from the protein phylogeny which suggests that *TaCPEP* may have close relatives with similar functions in the wheat genome. Although, the fact that we see an infection phenotype by the disruption of a single copy suggests that any functional redundancy may not influence the mechanism of TaCPEP action during immunity. Furthermore, there was no difference in assimilation in disruption mutants for *TaCPEP*. Together with *TaCPEP* having little sequence similarity to FtsH at the nucleotide and amino acid level (data not shown), and the prediction that these closely related genes might function in different subcellular compartments, it appears that *TaCPEP* might not function in the same processes as canonical FtsH in the chloroplast.

In *A. thaliana*, a group of M3 metallopeptidases called Thimet oligopeptidases have been shown to function in regulating chloroplast-mediated immune signalling. Using a protein microarray (PMA) and probing with a SA analogue, it was shown that the thimet oligopeptidases TOP1 and its homologue TOP2 are SA binding proteins, with TOP1 having a higher SA affinity than TOP2 (Moreau *et al.*, 2013). SA binding triggers the homo- and hetero-dimerization of TOP1 and TOP2 (Westlake *et al.*, 2015). Structural analysis showed that TOP1 and TOP2 are zinc metallopeptidase with the metal binding motif, HEXXH, expanded to HEXXGH (Al-Mohanna *et al.*, 2021). Furthermore, whilst TOP1 preferentially binds Zn^{2+}, it was shown that TOP2 has structural differences that enable it to bind an expanded set of divalent cations including Co^{2+}, Zn^{2+}, Mn^{2+} and Cu^{2+} (Wang *et al.*, 2014). Further structural analysis in the same study uncovered that TOP1 and TOP2 were redox sensitive with their activity increasing under oxidising conditions. TOP1 is localised to the chloroplasts and mitochondria and TOP2, lacking any signal peptide, localises to the cytosol (Moreau *et al.*, 2013). Furthermore, mutations in TOP1 and TOP2 made plants less responsive to SA application, and drastically reduced both PTI and ETI (Moreau *et al.*, 2013; Al-Mohanna *et al.*, 2021). Additionally, TOP1 and TOP2 are required for systemic acquired resistance (SAR) in a chloroplast localised NADPH-dependent thioredoxin reductase C (NTRC)-dependent manner (Al-Mohanna *et al.*, 2021). Overall, TOP1 and TOP2 function as redox sensitive, SA binding metallopeptidases that regulate plant immunity at the interface between chloroplastic and cytosolic ROS and SA signalling. TOP1 is hypothesised to positively regulate SA signalling and negatively regulate ROS from the chloroplasts (Westlake *et al.*, 2015). The model for TOP1 and TOP2 activity and function in plant immunity is summarised in **Figure 6.2.** We can see similarities between the presumed function of TOP1 and TaCPEP. In Chapter 4, preliminary data suggested that disruption *TaCPEP* mutants show a suppressed SA responses with a reduction of expression of *PR* and SAR genes. The general effect of *TaCPEP* disruption in reducing SA-inducible genes with roles in plant immunity may explain why *TaCPEP* mutants have increased

susceptibility to *Pst.* Furthermore, like TOP1, preliminary ROS assays showed that *TaCPEP* may negatively impact ROS production as an increase in the flg22 elicitor-induced ROS burst was detected in *TaCPEP* disruption mutants. Moreover, in Chapter 5 I found that in wheat there is a closely related and functionally conserved gene with no subcellular localisation signal, suggesting it is cytosolic. This resembles the relationship between chloroplastic TOP1 and cytosolic TOP2. The TOP proteins require the chloroplastic NADH thioredoxin reductase (NTRC) for function (Al-Mohanna *et al.*, 2021). In Chapter 3, I found that the expression of chloroplastic NAD(P)H genes were altered during wheat infection with rust fungi, suggesting that the redox state of wheat chloroplasts could be altered during *Pst* infection. This could provide the right conditions for NTRC and TOP-like proteins to function. However, *TaCPEP* shares little sequence similarity at both the nucleotide and amino acid level to the wheat TOP1 and TOP2 orthologues (data not shown). Additionally, they are predicted to be members of different metallopeptidase families. So, although there are some preliminary functional similarities between TaCPEP and the *A. thaliana* TOP1 proteins, the potential for TaCPEP to function like TOP1 remains unclear. Further experimental work investigating TaCPEP function would help clarify its activity *in planta* and any similarities to that of TOP1.

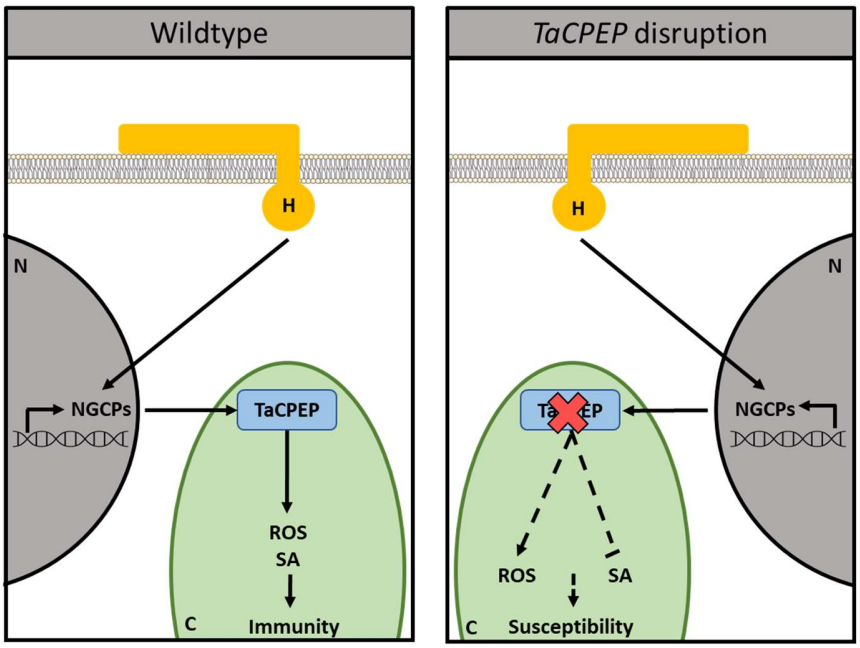

Figure 6.1 Summary model for the mechanism of *TaCPEP* function in wheat during fungal pathogen infection.

In wildtype plants, infection by *Pst* leads to the modulation of nuclear genes encoding chloroplast proteins (NGCPs), including the predicted metallopeptidase *TaCPEP.* TaCPEP functions in the chloroplasts to modulate SA and ROS signalling upstream of plant immunity. When *TaCPEP* is disrupted, there is potentially a perturbation in immune processes contributed by the chloroplasts, leading to reduced SA signalling and increased ROS bursts during infection. Ultimately, this *TaCPEP* disruption results in wheat which has a higher susceptibility to pathogenic fungi. Dashed lined represent unknown mechanisms. H, haustorium; N, nucleus; NGCP, nuclear genes encoding chloroplast proteins; C, chloroplast; ROS, reactive oxygen species; SA, salicylic acid.

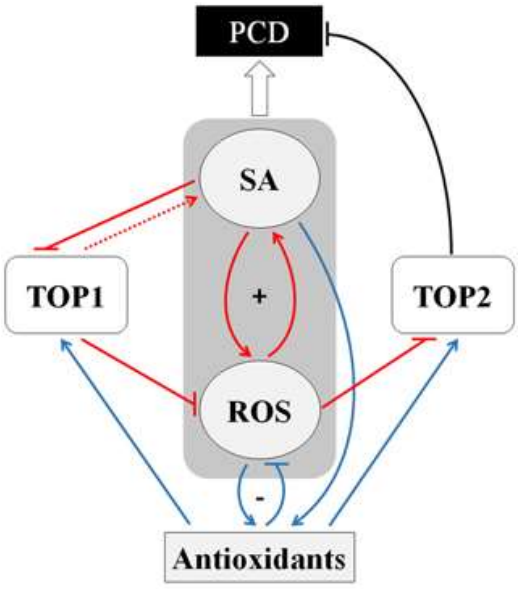

Figure 6.2 Summary model of the activity and function of TOP1 and TOP2 in plant immunity. Computational and experimental evidence suggests that the *A. thaliana* TOP1 and TOP2 are metallopeptidases that contribute to both SA and ROS signalling during immunity. TOP1 is localised to the chloroplasts and is hypothesised to positively regulate SA signalling and negatively regulate ROS. TOP2 localises in the cytosol and is negatively regulated by ROS. The lines in black represent the programmed cell death pathway, red the SA pathway and blue the antioxidant pathway. The dashed line shows the hypothetical signalling component. '+' shows positive feedback loop and '- 'a negative feedback loop. PCD, programmed cell death; SA, salicylic acid; TOP1, thimet oligopeptidase 1; TOP2, thimet oligopeptidase 2; ROS, reactive oxygen species. This figure was published in Westlake *et al.* (2015) and is reused with permission from copyright holders under the Creative Commons Licence.

6.2.1. Future work to characterise the function of *TaCPEP*

To further understand the function of TaCPEP at the protein level, we could perform *in silico* experiments to explore its structural properties and assess whether there is any similarity to characterised metallopeptidases. Firstly, the AlphaFold2 (Jumper *et al.*, 2021) algorithm AlphaFill (Hekkelman *et al.*, 2023) could be used to model the binding of predicted ligands of TaCPEP, including Zn^{2+} and ATP/ADP. This would bring us closer to confirming the ATP-dependent zinc metallopeptidase function of TaCPEP. TaCPEP is predicted to be in the M41 family of metallopeptidases. We know that other members of the M41 family that function in the chloroplasts

include the FtsH family (Kato and Sakamoto, 2018). The ligand of FtsH is the D1 subunit of photosystem II, so if TaCPEP has a similar function to FtsH then we could expect it to also be able to bind the D1 subunit (Lindahl *et al.*, 2000). Alphafold2 can make predictions of the ability for protein-ligand binding and therefore could be a quick way to test whether TaCPEP and FtsH might function similarly. An initial structural similarity search on the Dali Server (Holm *et al.*, 2023) agreed with previous predictions that TaCPEP is most similar to uncharacterised M41 metallopeptidases. We could further interrogate the similarity by comparing the structures of TaCPEP with other characterised M41 metallopeptidases. Furthermore, we could use this approach to assess the differences in the structure of TaCPEP and the similar proteins identified in Chapter 5, and to determine whether the differences in HEXXH motifs result in any structural differences that could influence metal binding, as with TOP1 and TOP2 (Wang *et al.*, 2014). By knowing if TaCPEP shares structural similarity with other metallopeptidases, we could move forward in understanding how TaCPEP might be contributing to wheat susceptibility to pathogens.

Fundamentally, the function of metallopeptidases is to cleave target peptides. In the case of TaCPEP, it is possible that its function is to regulate the levels of proteins that are important for chloroplast-derived immune processes. To test this, an untargeted approach could be used to assess the changes in the chloroplast proteome. By isolating the chloroplasts of infected and uninfected *TaCPEP* disruption mutants and comparing these to wildtype plants, we could analyse differential protein expression to infer changes to protein abundance between samples. I hypothesise that *TaCPEP* disruption mutants would have a different abundance of proteins that function in chloroplast mediated immune processes. As the expression of *PR4* was significantly reduced in disruption mutants (Chapter 4), then TaCPEP could be involved in the regulation of processes that lead to *PR4* induction, such as SA and SAR signalling. It would be wise to also carry out metabolomics to quantify the total amount of SA precursors in the TaCPEP disruption mutants to assess whether the reduction in *PR* gene expression is due to a difference in SA biosynthesis or downstream in SA signalling. These methods have been established and used previously to conduct comparative chloroplast proteomics and whole plant metabolomics in wheat and have provided insight into chloroplastic responses to salt stress and the function of a susceptibility factor to *Pst* (Corredor-Moreno *et al.*, 2021; Xu *et al.*, 2016). As outlined above, the role of metallopeptidases in chloroplast protein turnover and plant immunity has been well characterised. In this work, I found an uncharacterised putative chloroplast metallopeptidase that seemed to be involved in how wheat responds to pathogens. Overall, building a better understanding of how TaCPEP may function could offer insight into new mechanisms of wheat susceptibility to fungal pathogens.

6.3. Protecting plant health in a global food system, future work for candidate susceptibility factors

In this thesis, the focus was largely on the response of wheat to pathogenic fungi, mainly the rust fungi. We identified a gene, *TaCPEP*, which could contribute to the wheat response to *Pst* and another fungal pathogen, MoT. Moving forward, it is important to contextualise these results in the wider view of global crop protection. Our crops do not exist in the confines of a single stress. They are exposed to a multitude of microbes, both pathogenic and beneficial. Crops are also increasingly exposed to unpredictable weather including fluctuations in water availability, light, and nutrients. Furthermore, these variables will differ between geographical locations. It is important then that when we work on one aspect of plant pathology that we integrate individual approaches into a global picture of plant health (Jeger *et al.*, 2021).

Firstly, many of the genes identified in the current study are at the interface of overlapping processes including immunity, photosynthesis, growth, and development. For example, ROS has been shown to be produced as a result of damage to the photosystems under heat and high light stress (Yamamoto *et al.*, 2008). The phytohormone SA which is pivotal to the immune response, was also found to reduce the negative effects of high temperature and light stress in tomato (Shah Jahan *et al.*, 2019) and alfalfa (Wassie *et al.*, 2020). Furthermore, a recent review into the effect of heat stress in wheat highlighted the dynamic effects of heat on wheat photosynthetic processes at different stages of growth (Posch *et al.*, 2019). Together these studies highlight the importance of testing the effect of NGCP disruption, including that of *TaCPEP*, on wheat under various stresses at different stages of development. This will also enable us to predict the effect of gene disruption in a global context, by understanding how the plants might behave if grown in different parts of the world. This is particularly important as fungal pathogens like the wheat rusts are found in all wheat growing areas. As presented in Chapter 5 with *TaCPEP,* we can assess whether disruption of candidate NGCPs results in alteration in photosynthetic processes by measuring the rate of assimilation using a LI-6800, assessing chlorophyll biosynthesis and visualising starch density and distribution. These are all valuable methods which could also be used to take measurements in other NGCP disruption mutants across a developmental time-course or under confounding stresses. Doing so would allow a broader assessment of the plant phenotype and performance which will be valuable when considering such mutants as tools for crop protection in diverse geographical regions. Making such assessments can help make informed decisions on crop protection tools, which is particularly important for those with limited access to fungicides.

Plants live in a complex and dynamic environment where they encounter pathogens and microbes with different lifestyles. As discussed in Chapter 4, pathogens with different lifestyles elicit distinct molecular responses in the host, and these processes can often be antagonistic. Furthermore, activation of defences can cause a trade-off with growth. Therefore, candidate susceptibility factors should be thoroughly integrated into the bigger picture of plant health and crop protection. This should include testing susceptibility factors against a range of pathogens to assess whether increased resistance against one group of pathogens is not accompanied by increased susceptibility to others. In the current study, this could be done using infection assays with necrotrophic fungal pathogens of wheat such as *Parastagonospora nodorum* or bacterial pathogens of wheat such as *Burkholderia cepacia.* Once it is known whether these susceptibility factors could be used for protection against a range of pathogens and don't inadvertently increase susceptibility to any, then they could be taken forward as promising candidates to protect plant health.

6.4. Concluding statement

The pursuit of new and robust sources of resistance to protect one of our most valuable food crops from diseases is not straightforward. To begin to achieve crop protection, we must increase our knowledge of infection processes and the establishment of infection. To do this for diseases caused by obligate biotrophic pathogens like *Pst* adds layers of complexity that take time to unravel. Recent advances in resources available to study wheat at the genetic and experimental levels alleviates some of the burden of working with this system. However, the wheat rusts remain a challenge to study with a limited molecular toolkit available for their investigation. This leaves us many questions yet to be answered surrounding wheat-rust interactions. Despite this, in Chapter 3 I progressed in the identification of NGCPs that had modulated expression during wheat infection with *Pst,* with the expression being associated with the level of susceptibility. In Chapters 4 and 5, I explored the function of one of these genes, a yet uncharacterised metallopeptidase that shows promise for being a key part of how the chloroplasts function in wheat susceptibility to disease-causing fungi. In the coming years, more tools and methods will be established that facilitate key investigations into the elusive interactions between wheat and rust fungi. Such tools could help shed light on the genes investigated in this work alongside other mechanisms operating at the interface

of plant immunity between wheat and devastating rust fungi. This work could reveal new targets for enhancing wheat resistance and ensuring plant health.

7. References

Abbass, K., Qasim, M. Z., Song, H., Murshed, M., Mahmood, H. & Younis, I. 2022. A review of the global climate change impacts, adaptation, and sustainable mitigation measures. *Environmental Science and Pollution Research,* 29**,** 42539-42559.

Abbink, T. E. M., Peart, J. R., Mos, T. N. M., Baulcombe, D. C., Bol, J. F. & Linthorst, H. J. M. 2002. Silencing of a Gene Encoding a Protein Component of the Oxygen-Evolving Complex of Photosystem II Enhances Virus Replication in Plants. *Virology,* 295**,** 307-319.

Adachi, H., Derevnina, L. & Kamoun, S. 2019. NLR singletons, pairs, and networks: evolution, assembly, and regulation of the intracellular immunoreceptor circuitry of plants. *Current Opinion in Plant Biology,* 50**,** 121-131.

Adachi, H. & Kamoun, S. 2022. NLR receptor networks in plants. *Essays in Biochemistry,* 66**,** 541-549.

Adam, Z., Adamska, I., Nakabayashi, K., Ostersetzer, O., Haussuhl, K., Manuell, A., Zheng, B., Vallon, O., Rodermel, S. R., Shinozaki, K. & Clarke, A. K. 2001. Chloroplast and Mitochondrial Proteases in Arabidopsis. A Proposed Nomenclature1. *Plant Physiology,* 125**,** 1912-1918.

Al-Mohanna, T., Nejat, N., Iannetta, A. A., Hicks, L. M., Popescu, G. V. & Popescu, S. C. 2021. Arabidopsis thimet oligopeptidases are redox-sensitive enzymes active in the local and systemic plant immune response. *Journal of Biological Chemistry,* 296.

Alexander, R. D., Wendelboe-Nelson, C. & Morris, P. C. 2019. The barley transcription factor HvMYB1 is a positive regulator of drought tolerance. *Plant Physiology and Biochemistry,* 142**,** 246-253.

Allahverdiyeva, Y., Suorsa, M., Rossi, F., Pavesi, A., Kater, M. M., Antonacci, A., Tadini, L., Pribil, M., Schneider, A., Wanner, G., Leister, D., Aro, E.-M., Barbato, R. & Pesaresi, P. 2013. Arabidopsis plants lacking PsbQ and PsbR subunits of the oxygen-evolving complex show altered PSII super-complex organization and short-term adaptive mechanisms. *The Plant Journal,* 75**,** 671-684.

Altschul, S. F., Gish, W., Miller, W., Myers, E. W. & Lipman, D. J. 1990. Basic local alignment search tool. *J Mol Biol,* 215**,** 403-10.

Anastassiadou, M., Arena, M., Auteri, D., Brancato, A., Bura, L., Carrasco Cabrera, L., Chaideftou, E., Chiusolo, A., Court Marques, D., Crivellente, F., De Lentdecker, C., Egsmose, M., Fait, G., Greco, L., Ippolito, A., Istace, F., Jarrah, S., Kardassi, D., Leuschner, R., Lostia, A., Lythgo, C., Magrans, O., Mangas, I., Miron, I., Molnar, T., Padovani, L., Parra Morte, J. M., Pedersen, R., Reich, H., Santos, M., Serafimova, R., Sharp, R., Stanek, A., Sturma, J., Szentes, C., Terron, A., Tiramani, M., Vagenende, B. & Villamar-Bouza, L. 2020. Peer review of the pesticide risk assessment of the active substance benalaxyl. *EFSA Journal,* 18**,** e05985.

Andersson, I. & Backlund, A. 2008. Structure and function of Rubisco. *Plant Physiology and Biochemistry,* 46**,** 275-291.

Anisimova, O. K., Shchennikova, A. V., Kochieva, E. Z. & Filyushin, M. A. 2021. Pathogenesis-Related Genes of PR1, PR2, PR4, and PR5 Families Are Involved in the Response to Fusarium Infection in Garlic (Allium sativum L.). *International Journal of Molecular Sciences,* 22**,** 6688.

Appels, R., Eversole, K., Stein, N., Feuillet, C., Keller, B., Rogers, J., Pozniak, C. J., Choulet, F., Distelfeld, A., Poland, J., Ronen, G., Sharpe, A. G., Barad, O., Baruch, K., Keeble-Gagnère, G., Mascher, M., Ben-Zvi, G., Josselin, A.-A., Himmelbach, A., Balfourier, F., Gutierrez-Gonzalez, J., Hayden, M., Koh, C., Muehlbauer, G., Pasam, R. K., Paux, E., Rigault, P., Tibbits, J., Tiwari, V., Spannagl, M., Lang, D., Gundlach, H., Haberer, G., Mayer, K. F. X., Ormanbekova, D., Prade, V., Šimková, H., Wicker, T., Swarbreck, D., Rimbert, H., Felder, M., Guilhot, N., Kaithakottil, G., Keilwagen, J., Leroy, P., Lux, T., Twardziok, S., Venturini, L., Juhász, A., Abrouk, M., Fischer, I., Uauy, C., Borrill, P., Ramirez-Gonzalez, R. H., Arnaud, D., Chalabi, S., Chalhoub, B., Cory, A., Datla, R., Davey, M. W., Jacobs, J., Robinson, S. J., Steuernagel, B.,

Van Ex, F., Wulff, B. B. H., Benhamed, M., Bendahmane, A., Concia, L., Latrasse, D., Bartoš, J., Bellec, A., Berges, H., Doležel, J., Frenkel, Z., Gill, B., Korol, A., Letellier, T., Olsen, O.-A., Singh, K., Valárik, M., Van Der Vossen, E., Vautrin, S., Weining, S., Fahima, T., Glikson, V., Raats, D., Číhalíková, J., Toegelová, H., Vrána, J., Sourdille, P., Darrier, B., Barabaschi, D., Cattivelli, L., Hernandez, P., Galvez, S., Budak, H., Jones, J. D. G., Witek, K., Yu, G., Small, I., et al. 2018. Shifting the limits in wheat research and breeding using a fully annotated reference genome. *Science,* 361**,** eaar7191.

Arena, M., Auteri, D., Barmaz, S., Bellisai, G., Brancato, A., Brocca, D., Bura, L., Byers, H., Chiusolo, A., Court Marques, D., Crivellente, F., De Lentdecker, C., Egsmose, M., Erdos, Z., Fait, G., Ferreira, L., Goumenou, M., Greco, L., Ippolito, A., Istace, F., Jarrah, S., Kardassi, D., Leuschner, R., Lythgo, C., Magrans, J. O., Medina, P., Miron, I., Molnar, T., Nougadere, A., Padovani, L., Parra Morte, J. M., Pedersen, R., Reich, H., Sacchi, A., Santos, M., Serafimova, R., Sharp, R., Stanek, A., Streissl, F., Sturma, J., Szentes, C., Tarazona, J., Terron, A., Theobald, A., Vagenende, B., Verani, A. & Villamar-Bouza, L. 2018. Peer review of the pesticide risk assessment of the active substance chlorothalonil. *EFSA Journal,* 16**,** e05126.

Arnon, D. I. 1949. Copper Enzymes In Isolated Chloroplasts Polyphenoloxidase in *Beta vulgaris*. *Plant Physiol,* 24**,** 1-15.

Asada, K. 2006. Production and Scavenging of Reactive Oxygen Species in Chloroplasts and Their Functions. *Plant Physiology,* 141**,** 391-396.

Ashfaq, M. A., Dinesh Kumar, V., Soma Sekhar Reddy, P., Anil Kumar, C., Sai Kumar, K., Narasimha Rao, N., Tarakeswari, M. & Sujatha, M. 2020. Post-transcriptional gene silencing: Basic concepts and applications. *Journal of Biosciences,* 45**,** 128.

Auld, D. S. 2004. Catalytic mechanisms for metallopeptidases. *In:* BARRETT, A. J., RAWLINGS, N. D. & WOESSNER, J. F. (eds.) *Handbook of Proteolytic Enzymes (Second Edition).* London: Academic Press.

Avron, M. & Gibbs, M. 1974. Properties of Phosphoribulokinase of Whole Chloroplasts 1. *Plant Physiology,* 53**,** 136-139.

Bailey, S., Thompson, E., Nixon, P. J., Horton, P., Mullineaux, C. W., Robinson, C. & Mann, N. H. 2002. A Critical Role for the Var2 FtsH Homologue of Arabidopsis thaliana in the Photosystem II Repair Cycle >in Vivo. *Journal of Biological Chemistry,* 277**,** 2006-2011.

Bakkeren, G. & Szabo, L. J. 2020. Progress on Molecular Genetics and Manipulation of Rust Fungi. *Phytopathology®,* 110**,** 532-543.

Balasubramaniam, M., Kim, B.-S., Hutchens-Williams, H. M. & Loesch-Fries, L. S. 2014. The Photosystem II Oxygen-Evolving Complex Protein PsbP Interacts With the Coat Protein of Alfalfa mosaic virus and Inhibits Virus Replication. *Molecular Plant-Microbe Interactions®,* 27**,** 1107-1118.

Balint-Kurti, P. 2019. The plant hypersensitive response: concepts, control and consequences. *Molecular Plant Pathology,* 20**,** 1163-1178.

Ballaré, C. L. 2014. Light Regulation of Plant Defense. *Annual Review of Plant Biology,* 65**,** 335-363.

Bannai, H., Tamada, Y., Maruyama, O., Nakai, K. & Miyano, S. 2002. Extensive feature detection of N-terminal protein sorting signals. *Bioinformatics,* 18**,** 298-305.

Bari, R. & Jones, J. D. G. 2009. Role of plant hormones in plant defence responses. *Plant Molecular Biology,* 69**,** 473-488.

Barka, E. A., Lahlali, R. & Mauch-Mani, B. 2022. Editorial: Elicitors, secret agents at the service of the plant kingdom. *Frontiers in Plant Science,* 13.

Bennypaul, H. S., Mutti, J. S., Rustgi, S., Kumar, N., Okubara, P. A. & Gill, K. S. 2012. Virus-induced gene silencing (VIGS) of genes expressed in root, leaf, and meiotic tissues of wheat. *Functional & Integrative Genomics,* 12**,** 143-156.

Bentham, A. R., De La Concepcion, J. C., Mukhi, N., Zdrzałek, R., Draeger, M., Gorenkin, D., Hughes, R. K. & Banfield, M. J. 2020. A molecular roadmap to the plant immune system. *Journal of Biological Chemistry,* 295**,** 14916-14935.

Berardini, T. Z., Reiser, L., Li, D., Mezheritsky, Y., Muller, R., Strait, E. & Huala, E. 2015. The arabidopsis information resource: Making and mining the "gold standard" annotated reference plant genome. *genesis,* 53**,** 474-485.

Bertini, L., Caporale, C., Testa, M., Proietti, S. & Caruso, C. 2009. Structural basis of the antifungal activity of wheat PR4 proteins. *FEBS Letters,* 583**,** 2865-2871.

Bertini, L., Cascone, A., Tucci, M., D'amore, R., Berardino, I. D., Buonocore, V., Caporale, C. & Caruso, C. 2006. Molecular and functional analysis of new members of the wheat PR4 gene family. *Biological Chemistry,* 387**,** 1101-1111.

Bertini, L., Leonardi, L., Caporale, C., Tucci, M., Cascone, N., Di Berardino, I., Buonocore, V. & Caruso, C. 2003. Pathogen-responsive wheat PR4 genes are induced by activators of systemic acquired resistance and wounding. *Plant Science,* 164**,** 1067-1078.

Bhanbhro, N., Xiao, B., Han, L., Lu, H., Wang, H. & Yang, C. 2020. Adaptive strategy of allohexaploid wheat to long-term salinity stress. *BMC Plant Biology,* 20**,** 210.

Bi, G., Su, M., Li, N., Liang, Y., Dang, S., Xu, J., Hu, M., Wang, J., Zou, M., Deng, Y., Li, Q., Huang, S., Li, J., Chai, J., He, K., Chen, Y.-H. & Zhou, J.-M. 2021. The ZAR1 resistosome is a calcium-permeable channel triggering plant immune signaling. *Cell,* 184**,** 3528-3541.e12.

Bian, X., Tyrrell, S. & Davey, R. 2017. The Grassroots life science data infrastructure. Earlham Institute. https://grassroots. tools.

Bigeard, J., Colcombet, J. & Hirt, H. 2015. Signaling mechanisms in pattern-triggered immunity (PTI). *Molecular plant,* 8**,** 521-539.

Binns, D., Dimmer, E., Huntley, R., Barrell, D., O'donovan, C. & Apweiler, R. 2009. QuickGO: a web-based tool for Gene Ontology searching. *Bioinformatics,* 25**,** 3045-3046.

Borrill, P., Ramirez-Gonzalez, R. & Uauy, C. 2016. expVIP: a Customizable RNA-seq Data Analysis and Visualization Platform *Plant Physiology,* 170**,** 2172-2186.

Bos, J. I., Kanneganti, T. D., Young, C., Cakir, C., Huitema, E., Win, J., Armstrong, M. R., Birch, P. R. & Kamoun, S. 2006. The C-terminal half of Phytophthora infestans RXLR effector AVR3a is sufficient to trigger R3a-mediated hypersensitivity and suppress INF1-induced cell death in Nicotiana benthamiana. *The Plant Journal,* 48**,** 165-176.

Bouton, C., King, R. C., Chen, H., Azhakanandam, K., Bieri, S., Hammond-Kosack, K. E. & Kanyuka, K. 2018. Foxtail mosaic virus: A Viral Vector for Protein Expression in Cereals. *Plant Physiology,* 177**,** 1352-1367.

Bouvet, L., Holdgate, S., James, L., Thomas, J., Mackay, I. J. & Cockram, J. 2022. The evolving battle between yellow rust and wheat: implications for global food security. *Theoretical and Applied Genetics,* 135**,** 741-753.

Bravo, J. M., Campo, S., Murillo, I., Coca, M. & San Segundo, B. 2003. Fungus- and wound-induced accumulation of mRNA containing a class II chitinase of the pathogenesis-related protein 4 (PR-4) family of maize. *Plant Molecular Biology,* 52**,** 745-759.

Breen, S., Williams, S. J., Winterberg, B., Kobe, B. & Solomon, P. S. 2016. Wheat PR-1 proteins are targeted by necrotrophic pathogen effector proteins. *The Plant Journal,* 88**,** 13-25.

Bruley, C., Dupierris, V., Salvi, D., Rolland, N. & Ferro, M. 2012. AT_CHLORO: A Chloroplast Protein Database Dedicated to Sub-Plastidial Localization. *Frontiers in Plant Science,* 3.

Brunkard, J. O., Runkel, A. M. & Zambryski, P. C. 2015. Chloroplasts extend stromules independently and in response to internal redox signals. *Proceedings of the National Academy of Sciences,* 112**,** 10044-10049.

Bueno-Sancho, V. 2018. K-PIE: using K-mean algorithm for Percentage Infection symptoms Estimation. *Zenodo*.

Calderon, R. H. & Strand, Å. 2021. How retrograde signaling is intertwined with the evolution of photosynthetic eukaryotes. *Current Opinion in Plant Biology,* 63**,** 102093.

Callaway, E. 2016. Devastating wheat fungus appears in Asia for first time. *Nature,* 532**,** 421-422.

Canet, J. V., Dobón, A., Ibáñez, F., Perales, L. & Tornero, P. 2010. Resistance and biomass in Arabidopsis: a new model for Salicylic Acid perception. *Plant Biotechnology Journal,* 8**,** 126-141.

Cantu, D., Segovia, V., Maclean, D., Bayles, R., Chen, X., Kamoun, S., Dubcovsky, J., Saunders, D. G. O. & Uauy, C. 2013. Genome analyses of the wheat yellow (stripe) rust pathogen Puccinia striiformis f. sp. triticireveal polymorphic and haustorial expressed secreted proteins as candidate effectors. *BMC Genomics,* 14**,** 270.

Cao, Y., Liang, Y., Tanaka, K., Nguyen, C. T., Jedrzejczak, R. P., Joachimiak, A. & Stacey, G. 2014. The kinase LYK5 is a major chitin receptor in Arabidopsis and forms a chitin-induced complex with related kinase CERK1. *eLife,* 3**,** e03766.

Caplan, Jeffrey l., Kumar, Amutha s., Park, E., Padmanabhan, Meenu s., Hoban, K., Modla, S., Czymmek, K. & Dinesh-Kumar, Savithramma p. 2015. Chloroplast Stromules Function during Innate Immunity. *Developmental Cell,* 34**,** 45-57.

Caplan, J. L., Mamillapalli, P., Burch-Smith, T. M., Czymmek, K. & Dinesh-Kumar, S. P. 2008. Chloroplastic Protein NRIP1 Mediates Innate Immune Receptor Recognition of a Viral Effector. *Cell,* 132**,** 449-462.

Carmona, M., Sautua, F., Pérez-Hérnandez, O. & Reis, E. M. 2020. Role of Fungicide Applications on the Integrated Management of Wheat Stripe Rust. *Frontiers in Plant Science,* 11.

Carmona, M. A., Sautua, F. J., Pérez-Hernández, O., Grosso, C., Vettorello, L., Milanesio, B., Corvi, E., Almada, G. & Hovmøller, M. S. 2019. Rapid emergency response to yellow rust epidemics caused by newly introduced lineages of Puccinia striiformis f. sp. tritici in Argentina. *Tropical Plant Pathology,* 44**,** 385-391.

Casano, L. M., MartíN, M. & Sabater, B. 2001. Hydrogen Peroxide Mediates the Induction of Chloroplastic Ndh Complex under Photooxidative Stress in Barley1. *Plant Physiology,* 125**,** 1450-1458.

Castandet, B., Hotto, A. M., Strickler, S. R. & Stern, D. B. 2016. ChloroSeq, an Optimized Chloroplast RNA-Seq Bioinformatic Pipeline, Reveals Remodeling of the Organellar Transcriptome Under Heat Stress. *G3 (Bethesda),* 6**,** 2817-27.

Cavalier-Smith, T. 2000. Membrane heredity and early chloroplast evolution. *Trends in Plant Science,* 5**,** 174-182.

Cavalier-Smith, T. 2002. Chloroplast Evolution: Secondary Symbiogenesis and Multiple Losses. *Current Biology,* 12**,** R62-R64.

Cerdà-Costa, N. & Xavier Gomis-Rüth, F. 2014. Architecture and function of metallopeptidase catalytic domains. *Protein Science,* 23**,** 123-144.

Ceresini, P. C., Castroagudín, V. L., Rodrigues, F. Á., Rios, J. A., Aucique-Pérez, C. E., Moreira, S. I., Croll, D., Alves, E., De Carvalho, G., Maciel, J. L. N. & Mcdonald, B. A. 2019. Wheat blast: from its origins in South America to its emergence as a global threat. *Molecular Plant Pathology,* 20**,** 155-172.

Chaloner, T. M., Gurr, S. J. & Bebber, D. P. 2021. Plant pathogen infection risk tracks global crop yields under climate change. *Nature Climate Change,* 11**,** 710-715.

Chamberlain, K., Pickett, J. A. & Woodcock, C. M. 2000. Plant signalling and induced defence in insect attack. *Molecular Plant Pathology,* 1**,** 67-72.

Chan, K. X., Phua, S. Y., Crisp, P., Mcquinn, R. & Pogson, B. J. 2016. Learning the Languages of the Chloroplast: Retrograde Signaling and Beyond. *Annual Review of Plant Biology,* 67**,** 25-53.

Chanda, B., Xia, Y., Mandal, M. K., Yu, K., Sekine, K. T., Gao, Q.-M., Selote, D., Hu, Y., Stromberg, A., Navarre, D., Kachroo, A. & Kachroo, P. 2011. Glycerol-3-phosphate is a critical mobile inducer of systemic immunity in plants. *Nature Genetics,* 43**,** 421-427.

Chaturvedi, R., Venables, B., Petros, R. A., Nalam, V., Li, M., Wang, X., Takemoto, L. J. & Shah, J. 2012. An abietane diterpenoid is a potent activator of systemic acquired resistance. *The Plant Journal,* 71**,** 161-172.

Chen, C., Maccready, J. S., Ducat, D. C. & Osteryoung, K. W. 2017a. The Molecular Machinery of Chloroplast Division. *Plant Physiology,* 176**,** 138-151.

Chen, J., Upadhyaya, N. M., Ortiz, D., Sperschneider, J., Li, F., Bouton, C., Breen, S., Dong, C., Xu, B., Zhang, X., Mago, R., Newell, K., Xia, X., Bernoux, M., Taylor, J. M., Steffenson, B., Jin, Y., Zhang, P., Kanyuka, K., Figueroa, M., Ellis, J. G., Park, R. F. & Dodds, P. N. 2017b. Loss of AvrSr50 by somatic exchange in stem rust leads to virulence for Sr50 resistance in wheat. *Science,* 358**,** 1607-1610.

Chen, M., Choi, Y., Voytas, D. F. & Rodermel, S. 2000. Mutations in the Arabidopsis VAR2 locus cause leaf variegation due to the loss of a chloroplast FtsH protease. *The Plant Journal,* 22**,** 303-313.

Chen, M., Jensen, M. & Rodermel, S. 1999. The yellow variegated mutant of Arabidopsis is plastid autonomous and delayed in chloroplast biogenesis. *Journal of Heredity,* 90**,** 207-214.

Chen, W., Wellings, C., Chen, X., Kang, Z. & Liu, T. 2014. Wheat stripe (yellow) rust caused by Puccinia striiformis f. sp. tritici. *Molecular Plant Pathology,* 15**,** 433-446.

Chen, Y.-E., Cui, J.-M., Su, Y.-Q., Yuan, S., Yuan, M. & Zhang, H.-Y. 2015. Influence of stripe rust infection on the photosynthetic characteristics and antioxidant system of susceptible and resistant wheat cultivars at the adult plant stage. *Frontiers in Plant Science,* 6.

Chinchilla, D., Zipfel, C., Robatzek, S., Kemmerling, B., Nürnberger, T., Jones, J. D. G., Felix, G. & Boller, T. 2007. A flagellin-induced complex of the receptor FLS2 and BAK1 initiates plant defence. *Nature,* 448**,** 497-500.

Choi, H. W. 2024. From the Photosynthesis to Hormone Biosynthesis in Plants. *Plant Pathol J,* 40**,** 99-105.

Claeys, M., Storms, V., Sun, H., Michoel, T. & Marchal, K. 2012. MotifSuite: workflow for probabilistic motif detection and assessment. *Bioinformatics,* 28**,** 1931-1932.

Comastri, A., Janni, M., Simmonds, J., Uauy, C., Pignone, D., Nguyen, H. T. & Marmiroli, N. 2018. Heat in Wheat: Exploit Reverse Genetic Techniques to Discover New Alleles Within the Triticum durum sHsp26 Family. *Frontiers in Plant Science,* 9.

Consortium, T. U. 2022. UniProt: the Universal Protein Knowledgebase in 2023. *Nucleic Acids Research,* 51**,** D523-D531.

Corredor-Moreno, P. 2019. *Deciphering host responses to wheat yellow rust* Doctor of Philosophy University of East Anglia.

Corredor-Moreno, P., Badgami, R., Jones, S. & Saunders, D. G. O. 2022. Temporally coordinated expression of nuclear genes encoding chloroplast proteins in wheat promotes Puccinia striiformis f. sp. tritici infection. *Communications Biology,* 5**,** 853.

Corredor-Moreno, P., Minter, F., Davey, P. E., Wegel, E., Kular, B., Brett, P., Lewis, C. M., Morgan, Y. M. L., Macías Pérez, L. A., Korolev, A. V., Hill, L. & Saunders, D. G. O. 2021. The branched-chain amino acid aminotransferase TaBCAT1 modulates amino acid metabolism and positively regulates wheat rust susceptibility. *The Plant Cell,* 33**,** 1728-1747.

Couto, D. & Zipfel, C. 2016. Regulation of pattern recognition receptor signalling in plants. *Nature Reviews Immunology,* 16**,** 537-552.

Crawford, T., Lehotai, N. & Strand, Å. 2017. The role of retrograde signals during plant stress responses. *Journal of Experimental Botany,* 69**,** 2783-2795.

Crooks, G. E., Hon, G., Chandonia, J. M. & Brenner, S. E. 2004. WebLogo: a sequence logo generator. *Genome Res,* 14**,** 1188-90.

Cruz, C. D., Peterson, G. L., Bockus, W. W., Kankanala, P., Dubcovsky, J., Jordan, K. W., Akhunov, E., Chumley, F., Baldelomar, F. D. & Valent, B. 2016. The 2NS Translocation from Aegilops

ventricosa Confers Resistance to the Triticum Pathotype of Magnaporthe oryzae. *Crop Science,* 56**,** 990-1000.

Cruz, C. D. & Valent, B. 2017. Wheat blast disease: danger on the move. *Tropical Plant Pathology,* 42**,** 210-222.

Daniell, H., Lin, C. S., Yu, M. & Chang, W. J. 2016. Chloroplast genomes: diversity, evolution, and applications in genetic engineering. *Genome Biol,* 17**,** 134.

De Jong, G. W. & Adams, K. L. 2023. Subgenome-dominant expression and alternative splicing in response to Sclerotinia infection in polyploid Brassica napus and progenitors. *The Plant Journal,* 114**,** 142-158.

De Torres Zabala, M., Littlejohn, G., Jayaraman, S., Studholme, D., Bailey, T., Lawson, T., Tillich, M., Licht, D., Bölter, B., Delfino, L., Truman, W., Mansfield, J., Smirnoff, N. & Grant, M. 2015. Chloroplasts play a central role in plant defence and are targeted by pathogen effectors. *Nature Plants,* 1**,** 15074.

Dean, J. V., Mohammed, L. A. & Fitzpatrick, T. 2005. The formation, vacuolar localization, and tonoplast transport of salicylic acid glucose conjugates in tobacco cell suspension cultures. *Planta,* 221**,** 287-296.

Derevnina, L., Contreras, M. P., Adachi, H., Upson, J., Vergara Cruces, A., Xie, R., Skłenar, J., Menke, F. L. H., Mugford, S. T., Maclean, D., Ma, W., Hogenhout, S. A., Goverse, A., Maqbool, A., Wu, C.-H. & Kamoun, S. 2021. Plant pathogens convergently evolved to counteract redundant nodes of an NLR immune receptor network. *PLOS Biology,* 19**,** e3001136.

Desmond, O. J., Edgar, C. I., Manners, J. M., Maclean, D. J., Schenk, P. M. & Kazan, K. 2005. Methyl jasmonate induced gene expression in wheat delays symptom development by the crown rot pathogen Fusarium pseudograminearum. *Physiological and Molecular Plant Pathology,* 67**,** 171-179.

Dietz, K.-J., Turkan, I. & Krieger-Liszkay, A. 2016. Redox- and Reactive Oxygen Species-Dependent Signaling into and out of the Photosynthesizing Chloroplast *Plant Physiology,* 171**,** 1541-1550.

Ding, P., Rekhter, D., Ding, Y., Feussner, K., Busta, L., Haroth, S., Xu, S., Li, X., Jetter, R., Feussner, I. & Zhang, Y. 2016. Characterization of a Pipecolic Acid Biosynthesis Pathway Required for Systemic Acquired Resistance. *The Plant Cell,* 28**,** 2603-2615.

Ding, Y., Sun, T., Ao, K., Peng, Y., Zhang, Y., Li, X. & Zhang, Y. 2018a. Opposite roles of salicylic acid receptors NPR1 and NPR3/NPR4 in transcriptional regulation of plant immunity. *Cell,* 173**,** 1454-1467. e15.

Ding, Y., Sun, T., Ao, K., Peng, Y., Zhang, Y., Li, X. & Zhang, Y. 2018b. Opposite Roles of Salicylic Acid Receptors NPR1 and NPR3/NPR4 in Transcriptional Regulation of Plant Immunity. *Cell,* 173**,** 1454-1467.e15.

Dobon, A., Bunting, D. C. E., Cabrera-Quio, L. E., Uauy, C. & Saunders, D. G. O. 2016. The host-pathogen interaction between wheat and yellow rust induces temporally coordinated waves of gene expression. *BMC Genomics,* 17**,** 380.

Dodds, P. N. & Rathjen, J. P. 2010. Plant immunity: towards an integrated view of plant–pathogen interactions. *Nature Reviews Genetics,* 11**,** 539-548.

Dogra, V. & Kim, C. 2019. Chloroplast protein homeostasis is coupled with retrograde signaling. *Plant Signaling & Behavior,* 14**,** 1656037.

Douglas, S. E. 1998. Plastid evolution: origins, diversity, trends. *Current Opinion in Genetics & Development,* 8**,** 655-661.

Dracatos, P. M., Lu, J., Sánchez-Martín, J. & Wulff, B. B. H. 2023. Resistance that stacks up: engineering rust and mildew disease control in the cereal crops wheat and barley. *Plant Biotechnology Journal,* 21**,** 1938-1951.

Duan, X., Wang, X., Fu, Y., Tang, C., Li, X., Cheng, Y., Feng, H., Huang, L. & Kang, Z. 2013. TaEIL1, a wheat homologue of AtEIN3, acts as a negative regulator in the wheat–stripe rust fungus interaction. *Molecular Plant Pathology,* 14**,** 728-739.

Durrant, W. E. & Dong, X. 2004. Systemic acquired resistance. *Annual Review of Phytopathology,* 42**,** 185-209.

Enami, I., Kamo, M., Ohta, H., Takahashi, S., Miura, T., Kusayanagi, M., Tanabe, S., Kamei, A., Motoki, A., Hirano, M., Tomo, T. & Satoh, K. 1998. Intramolecular Cross-linking of the Extrinsic 33-kDa Protein Leads to Loss of Oxygen Evolution but Not Its Ability of Binding to Photosystem II and Stabilization of the Manganese Cluster*. *Journal of Biological Chemistry,* 273**,** 4629-4634.

Endo, T., Shikanai, T., Takabayashi, A., Asada, K. & Sato, F. 1999. The role of chloroplastic NAD(P)H dehydrogenase in photoprotection. *FEBS Letters,* 457**,** 5-8.

Erenstein, O., Jaleta, M., Mottaleb, K. A., Sonder, K., Donovan, J. & Braun, H.-J. 2022. Global Trends in Wheat Production, Consumption and Trade. *In:* REYNOLDS, M. P. & BRAUN, H.-J. (eds.) *Wheat Improvement: Food Security in a Changing Climate.* Cham: Springer International Publishing.

Eriksson, J. 1894. *Ueber die Specialisirung des Parasitismus bei den Getreiderostpilzen*, G. Borntraeger.

Ershova, N., Sheshukova, E., Kamarova, K., Arifulin, E., Tashlitsky, V., Serebryakova, M. & Komarova, T. 2022. Nicotiana benthamiana Kunitz peptidase inhibitor-like protein involved in chloroplast-to-nucleus regulatory pathway in plant-virus interaction. *Frontiers in Plant Science,* 13.

Esmail, S. M., Aboulila, A. A. & El-Moneim, D. A. 2020. Variation in several pathogenesis - Related (PR) protein genes in wheat (Triticum aestivum) involved in defense against Puccinia striiformis f. sp. tritici. *Physiological and Molecular Plant Pathology,* 112**,** 101545.

Felix, G., Duran, J. D., Volko, S. & Boller, T. 1999. Plants have a sensitive perception system for the most conserved domain of bacterial flagellin. *Plant J,* 18**,** 265-76.

Felix, G., Regenass, M. & Boller, T. 1993. Specific perception of subnanomolar concentrations of chitin fragments by tomato cells: induction of extracellular alkalinization, changes in protein phosphorylation, and establishment of a refractory state. *The Plant Journal,* 4**,** 307-316.

Figueroa, M., Hammond-Kosack, K. E. & Solomon, P. S. 2018. A review of wheat diseases—a field perspective. *Molecular Plant Pathology,* 19**,** 1523-1536.

Figueroa, M., Ortiz, D. & Henningsen, E. C. 2021. Tactics of host manipulation by intracellular effectors from plant pathogenic fungi. *Current Opinion in Plant Biology,* 62**,** 102054.

Fones, H. N., Bebber, D. P., Chaloner, T. M., Kay, W. T., Steinberg, G. & Gurr, S. J. 2020. Threats to global food security from emerging fungal and oomycete crop pathogens. *Nature Food,* 1**,** 332-342.

Förderer, A., Li, E., Lawson, A. W., Deng, Y.-N., Sun, Y., Logemann, E., Zhang, X., Wen, J., Han, Z., Chang, J., Chen, Y., Schulze-Lefert, P. & Chai, J. 2022. A wheat resistosome defines common principles of immune receptor channels. *Nature,* 610**,** 532-539.

Fu, Z. Q., Yan, S., Saleh, A., Wang, W., Ruble, J., Oka, N., Mohan, R., Spoel, S. H., Tada, Y., Zheng, N. & Dong, X. 2012. NPR3 and NPR4 are receptors for the immune signal salicylic acid in plants. *Nature,* 486**,** 228-232.

Gaupp, F., Hall, J., Hochrainer-Stigler, S. & Dadson, S. 2020. Changing risks of simultaneous global breadbasket failure. *Nature Climate Change,* 10**,** 54-57.

Geiger, D. R. & Servaites, J. C. 1994. Diurnal regulation of photosynthetic carbon metabolism in C3 plants. *Annual review of plant biology,* 45**,** 235-256.

Glazebrook, J. 2005. Contrasting Mechanisms of Defense Against Biotrophic and Necrotrophic Pathogens. *Annual Review of Phytopathology,* 43**,** 205-227.

Gnanasekaran, P., Ponnusamy, K. & Chakraborty, S. 2019. A geminivirus betasatellite encoded βC1 protein interacts with PsbP and subverts PsbP-mediated antiviral defence in plants. *Molecular Plant Pathology,* 20**,** 943-960.

Göhre, V., Jones, A. M. E., Sklenář, J., Robatzek, S. & Weber, A. P. M. 2012. Molecular Crosstalk Between PAMP-Triggered Immunity and Photosynthesis. *Molecular Plant-Microbe Interactions®,* 25**,** 1083-1092.

Gong, B.-Q., Guo, J., Zhang, N., Yao, X., Wang, H.-B. & Li, J.-F. 2019. Cross-microbial protection via priming a conserved immune co-receptor through juxtamembrane phosphorylation in plants. *Cell Host & Microbe,* 26**,** 810-822. e7.

Goulart, A. C. P., Sousa, P. G. & Urashima, A. S. 2007. Damages in wheat caused by infection of Pyricularia grisea. *Summa Phytopathologica,* 33**,** 358-363.

Grote, U., Fasse, A., Nguyen, T. T. & Erenstein, O. 2021. Food Security and the Dynamics of Wheat and Maize Value Chains in Africa and Asia. *Frontiers in Sustainable Food Systems,* 4.

Guedes, M. E. M., Richmond, S. & Kuć, J. 1980. Induced systemic resistance to anthracnose in cucumber as influenced by the location of the inducer inoculation with Colletotrichum lagenarium and the onset of flowering and fruiting. *Physiological Plant Pathology,* 17**,** 229-233.

Guerillot, P., Salamov, A., Louet, C., Morin, E., Frey, P., Grigoriev, I. V. & Duplessis, S. 2023. A Remarkable Expansion of Oligopeptide Transporter Genes in Rust Fungi (Pucciniales) Suggests a Specialization in Nutrient Acquisition for Obligate Biotrophy. *Phytopathology®,* 113**,** 252-264.

Guo, J., Bai, P., Yang, Q., Liu, F., Wang, X., Huang, L. & Kang, Z. 2013. Wheat zinc finger protein TaLSD1, a negative regulator of programmed cell death, is involved in wheat resistance against stripe rust fungus. *Plant Physiology and Biochemistry,* 71**,** 164-172.

Hamel, L.-P., Sekine, K.-T., Wallon, T., Sugiwaka, Y., Kobayashi, K. & Moffett, P. 2016. The Chloroplastic Protein THF1 Interacts with the Coiled-Coil Domain of the Disease Resistance Protein N′ and Regulates Light-Dependent Cell Death *Plant Physiology,* 171**,** 658-674.

Han, S., Tang, R., Anderson, L. K., Woerner, T. E. & Pei, Z.-M. 2003. A cell surface receptor mediates extracellular Ca2+ sensing in guard cells. *Nature,* 425**,** 196-200.

Hanson, M. R. & Conklin, P. L. 2020. Stromules, functional extensions of plastids within the plant cell. *Current Opinion in Plant Biology,* 58**,** 25-32.

Hanson, M. R. & Sattarzadeh, A. 2011. Stromules: recent insights into a long neglected feature of plastid morphology and function. *Plant Physiol,* 155**,** 1486-92.

Hao, G., Tiley, H. & Mccormick, S. 2022. Chitin Triggers Tissue-Specific Immunity in Wheat Associated With Fusarium Head Blight. *Frontiers in Plant Science,* 13.

Hao, Q., Wang, W., Han, X., Wu, J., Lyu, B., Chen, F., Caplan, A., Li, C., Wu, J., Wang, W., Xu, Q. & Fu, D. 2018. Isochorismate-based salicylic acid biosynthesis confers basal resistance to Fusarium graminearum in barley. *Molecular Plant Pathology,* 19**,** 1995-2010.

Hao, Y., Wang, T., Wang, K., Wang, X., Fu, Y., Huang, L. & Kang, Z. 2016. Transcriptome Analysis Provides Insights into the Mechanisms Underlying Wheat Plant Resistance to Stripe Rust at the Adult Plant Stage. *PLOS ONE,* 11**,** e0150717.

Hartmann, M. & Zeier, J. 2019. N-hydroxypipecolic acid and salicylic acid: a metabolic duo for systemic acquired resistance. *Current Opinion in Plant Biology,* 50**,** 44-57.

Hartmann, M., Zeier, T., Bernsdorff, F., Reichel-Deland, V., Kim, D., Hohmann, M., Scholten, N., Schuck, S., Bräutigam, A. & Hölzel, T. 2018. Flavin monooxygenase-generated N-hydroxypipecolic acid is a critical element of plant systemic immunity. *Cell,* 173**,** 456-469. e16.

Harwood, R., Goodman, E., Gudmundsdottir, M., Huynh, M., Musulin, Q., Song, M. & Barbour, M. M. 2020. Cell and chloroplast anatomical features are poorly estimated from 2D cross-sections. *New Phytologist,* 225**,** 2567-2578.

He, Z.-H., Li, H.-W., Shen, Y., Li, Z.-S. & Mi, H. 2013. Comparative analysis of the chloroplast proteomes of a wheat (Triticum aestivum L.) single seed descent line and its parents. *Journal of Plant Physiology,* 170**,** 1139-1147.

He, Z., Webster, S. & He, S. Y. 2022. Growth–defense trade-offs in plants. *Current Biology,* 32**,** R634-R639.

Hekkelman, M. L., De Vries, I., Joosten, R. P. & Perrakis, A. 2023. AlphaFill: enriching AlphaFold models with ligands and cofactors. *Nature Methods,* 20**,** 205-213.

Holm, L., Laiho, A., Törönen, P. & Salgado, M. 2023. DALI shines a light on remote homologs: One hundred discoveries. *Protein Science,* 32**,** e4519.

Hooper, N. M. 1994. Families of zinc metalloproteases. *FEBS Lett,* 354**,** 1-6.

Horton, P., Park, K.-J., Obayashi, T., Fujita, N., Harada, H., Adams-Collier, C. J. & Nakai, K. 2007. WoLF PSORT: protein localization predictor. *Nucleic Acids Research,* 35**,** W585-W587.

Hovmøller, M. S., Rodriguez-Algaba, J., Thach, T., Justesen, A. F. & Hansen, J. 2019. Report for Puccinia striiformis race analyses/molecular genotyping, GRRC, Flakkebjerg, DK-4200 Slagelse, Denmark. *GRRC, Aarhus University. Denmark*.

Huai, B., Yang, Q., Qian, Y., Qian, W., Kang, Z. & Liu, J. 2019. ABA-Induced Sugar Transporter TaSTP6 Promotes Wheat Susceptibility to Stripe Rust1 [OPEN]. *Plant Physiology,* 181**,** 1328-1343.

Huai, B., Yang, Q., Wei, X., Pan, Q., Kang, Z. & Liu, J. 2020. TaSTP13 contributes to wheat susceptibility to stripe rust possibly by increasing cytoplasmic hexose concentration. *BMC Plant Biology,* 20**,** 49.

Huai, B., Yuan, P., Ma, X., Zhang, X., Jiang, L., Zheng, P., Yao, M., Chen, Z., Chen, L., Shen, Q., Kang, Z. & Liu, J. 2022. Sugar transporter TaSTP3 activation by TaWRKY19/61/82 enhances stripe rust susceptibility in wheat. *New Phytologist,* 236**,** 266-282.

Huang, C., Peng, J., Zhang, W., Chethana, T., Wang, X., Wang, H. & Yan, J. 2023. LtGAPR1 Is a Novel Secreted Effector from Lasiodiplodia theobromae That Interacts with NbPsQ2 to Negatively Regulate Infection. *Journal of Fungi,* 9**,** 188.

Hubbard, A., Lewis, C. M., Yoshida, K., Ramirez-Gonzalez, R. H., De Vallavieille-Pope, C., Thomas, J., Kamoun, S., Bayles, R., Uauy, C. & Saunders, D. G. O. 2015. Field pathogenomics reveals the emergence of a diverse wheat yellow rust population. *Genome Biology,* 16**,** 23.

Hückelhoven, R., Eichmann, R., Weis, C., Hoefle, C. & Proels, R. K. 2013. Genetic loss of susceptibility: a costly route to disease resistance? *Plant Pathology,* 62**,** 56-62.

Ifuku, K., Yamamoto, Y., Ono, T.-A., Ishihara, S. & Sato, F. 2005. PsbP Protein, But Not PsbQ Protein, Is Essential for the Regulation and Stabilization of Photosystem II in Higher Plants. *Plant Physiology,* 139**,** 1175-1184.

Igarashi, S. 1986. Pyricularia em trigo. 1. Ocorrencia de Pyricularia sp noestado do Parana. *Fitopatol. Bras,* 11**,** 351-352.

Inoue, Y., Vy, T. T. P., Yoshida, K., Asano, H., Mitsuoka, C., Asuke, S., Anh, V. L., Cumagun, C. J. R., Chuma, I., Terauchi, R., Kato, K., Mitchell, T., Valent, B., Farman, M. & Tosa, Y. 2017. Evolution of the wheat blast fungus through functional losses in a host specificity determinant. *Science,* 357**,** 80-83.

Ishiga, Y., Watanabe, M., Ishiga, T., Tohge, T., Matsuura, T., Ikeda, Y., Hoefgen, R., Fernie, A. R. & Mysore, K. S. 2017. The SAL-PAP Chloroplast Retrograde Pathway Contributes to Plant Immunity by Regulating Glucosinolate Pathway and Phytohormone Signaling. *Molecular Plant-Microbe Interactions®,* 30**,** 829-841.

Islam, M. T., Croll, D., Gladieux, P., Soanes, D. M., Persoons, A., Bhattacharjee, P., Hossain, M. S., Gupta, D. R., Rahman, M. M., Mahboob, M. G., Cook, N., Salam, M. U., Surovy, M. Z., Sancho, V. B., Maciel, J. L. N., Nhanijúnior, A., Castroagudín, V. L., Reges, J. T. D. A., Ceresini, P. C., Ravel, S., Kellner, R., Fournier, E., Tharreau, D., Lebrun, M.-H., Mcdonald, B. A., Stitt, T., Swan, D., Talbot, N. J., Saunders, D. G. O., Win, J. & Kamoun, S. 2016. Emergence of wheat

blast in Bangladesh was caused by a South American lineage of Magnaporthe oryzae. *BMC Biology,* 14**,** 84.

Jan, M., Liu, Z., Rochaix, J.-D. & Sun, X. 2022. Retrograde and anterograde signaling in the crosstalk between chloroplast and nucleus. *Frontiers in Plant Science,* 13.

Jang, C., Seo, E.-Y., Nam, J., Bae, H., Gim, Y. G., Kim, H. G., Cho, I. S., Lee, Z.-W., Bauchan, G., Hammond, J. & Lim, H.-S. 2013. Insights into Alternanthera mosaic virus TGB3 Functions: Interactions with Nicotiana benthamiana PsbO Correlate with Chloroplast Vesiculation and Veinal Necrosis Caused by TGB3 Over-Expression. *Frontiers in Plant Science,* 4.

Janska, H., Kwasniak, M. & Szczepanowska, J. 2013. Protein quality control in organelles — AAA/FtsH story. *Biochimica et Biophysica Acta (BBA) - Molecular Cell Research,* 1833**,** 381-387.

Jeffery, D., Leona, D., Ooi, T. E. K., Ithnin, N., Mohd Yusof, H., Kulaveerasingam, H., Abdul Majid, N. & Karsani, S. A. 2015. Comparative proteomic analysis of oil palm leaves infected with Ganoderma boninense revealed changes in proteins involved in photosynthesis, carbohydrate metabolism, and immunity and defense. *ELECTROPHORESIS,* 36**,** 1699-1710.

Jeger, M., Beresford, R., Bock, C., Brown, N., Fox, A., Newton, A., Vicent, A., Xu, X. & Yuen, J. 2021. Global challenges facing plant pathology: multidisciplinary approaches to meet the food security and environmental challenges in the mid-twenty-first century. *CABI Agriculture and Bioscience,* 2**,** 20.

Jensen, P. E., Rosgaard, L., Knoetzel, J. & Scheller, H. V. 2002. Photosystem I activity is increased in the absence of the PSI-G subunit. *Journal of Biological Chemistry,* 277**,** 2798-2803.

Jianyuan, L., Xiaodong, W., Lirong, Z., Qingfang, M., Na, Z., Wenxiang, Y. & Daqun, L. 2017. A wheat NBS-LRR gene TaRGA19 participates in Lr19-mediated resistance to Puccinia triticina. *Plant Physiology and Biochemistry,* 119**,** 1-8.

Jin, Z., Wan, L., Zhang, Y., Li, X., Cao, Y., Liu, H., Fan, S., Cao, D., Wang, Z., Li, X., Pan, J., Dong, M.-Q., Wu, J. & Yan, Z. 2022. Structure of a TOC-TIC supercomplex spanning two chloroplast envelope membranes. *Cell,* 185**,** 4788-4800.e13.

Jones, J. D. G. & Dangl, J. L. 2006. The plant immune system. *Nature,* 444**,** 323-329.

Jongeneel, C. V., Bouvier, J. & Bairoch, A. 1989. A unique signature identifies a family of zinc-dependent metallopeptidases. *FEBS Letters,* 242**,** 211-214.

Jumper, J., Evans, R., Pritzel, A., Green, T., Figurnov, M., Ronneberger, O., Tunyasuvunakool, K., Bates, R., Žídek, A., Potapenko, A., Bridgland, A., Meyer, C., Kohl, S. a. A., Ballard, A. J., Cowie, A., Romera-Paredes, B., Nikolov, S., Jain, R., Adler, J., Back, T., Petersen, S., Reiman, D., Clancy, E., Zielinski, M., Steinegger, M., Pacholska, M., Berghammer, T., Bodenstein, S., Silver, D., Vinyals, O., Senior, A. W., Kavukcuoglu, K., Kohli, P. & Hassabis, D. 2021. Highly accurate protein structure prediction with AlphaFold. *Nature,* 596**,** 583-589.

Jung, H. W., Tschaplinski, T. J., Wang, L., Glazebrook, J. & Greenberg, J. T. 2009. Priming in Systemic Plant Immunity. *Science,* 324**,** 89-91.

Kadirjan-Kalbach, D. K., Yoder, D. W., Ruckle, M. E., Larkin, R. M. & Osteryoung, K. W. 2012. FtsHi1/ARC1 is an essential gene in Arabidopsis that links chloroplast biogenesis and division. *The Plant Journal,* 72**,** 856-867.

Kang, Z. 1996. Ultrastructure of plant pathogenic fungi. *China Science and Technology Press: Beijing, China***,** 7-11.

Karasov, T. L., Chae, E., Herman, J. J. & Bergelson, J. 2017. Mechanisms to Mitigate the Trade-Off between Growth and Defense. *The Plant Cell,* 29**,** 666-680.

Karimi, M., Inzé, D. & Depicker, A. 2002. GATEWAY vectors for Agrobacterium-mediated plant transformation. *Trends Plant Sci,* 7**,** 193-5.

Kato, Y., Miura, E., Ido, K., Ifuku, K. & Sakamoto, W. 2009. The Variegated Mutants Lacking Chloroplastic FtsHs Are Defective in D1 Degradation and Accumulate Reactive Oxygen Species. *Plant Physiology,* 151**,** 1790-1801.

Kato, Y. & Sakamoto, W. 2009. Protein Quality Control in Chloroplasts: A Current Model of D1 Protein Degradation in the Photosystem II Repair Cycle. *The Journal of Biochemistry,* 146**,** 463-469.

Kato, Y. & Sakamoto, W. 2018. FtsH Protease in the Thylakoid Membrane: Physiological Functions and the Regulation of Protease Activity. *Frontiers in Plant Science,* 9.

Katoh, K., Rozewicki, J. & Yamada, K. D. 2017. MAFFT online service: multiple sequence alignment, interactive sequence choice and visualization. *Briefings in Bioinformatics,* 20**,** 1160-1166.

Kim, D. B., Na, C., Hwang, I. & Lee, D. W. 2022. Understanding protein translocation across chloroplast membranes: translocons and motor proteins. *Journal of Integrative Plant Biology,* n/a.

Kobayashi, Y., Fukuzawa, N., Hyodo, A., Kim, H., Mashiyama, S., Ogihara, T., Yoshioka, H., Matsuura, H., Masuta, C., Matsumura, T. & Takeshita, M. 2020. Role of salicylic acid glucosyltransferase in balancing growth and defence for optimum plant fitness. *Molecular Plant Pathology,* 21**,** 429-442.

Kong, L., Wu, J., Lu, L., Xu, Y. & Zhou, X. 2014. Interaction between Rice stripe virus Disease-Specific Protein and Host PsbP Enhances Virus Symptoms. *Molecular Plant,* 7**,** 691-708.

Kramer, D. M., Cruz, J. A. & Kanazawa, A. 2003. Balancing the central roles of the thylakoid proton gradient. *Trends in Plant Science,* 8**,** 27-32.

Kramer, D. M. & Evans, J. R. 2010. The Importance of Energy Balance in Improving Photosynthetic Productivity *Plant Physiology,* 155**,** 70-78.

Krasileva, K. V., Vasquez-Gross, H. A., Howell, T., Bailey, P., Paraiso, F., Clissold, L., Simmonds, J., Ramirez-Gonzalez, R. H., Wang, X., Borrill, P., Fosker, C., Ayling, S., Phillips, A. L., Uauy, C. & Dubcovsky, J. 2017. Uncovering hidden variation in polyploid wheat. *Proceedings of the National Academy of Sciences,* 114**,** E913-E921.

Kubínová, Z., Janáček, J., Lhotáková, Z., Kubínová, L. & Albrechtová, J. 2013. Unbiased estimation of chloroplast number in mesophyll cells: advantage of a genuine three-dimensional approach. *Journal of Experimental Botany,* 65**,** 609-620.

Kugler, K. G., Siegwart, G., Nussbaumer, T., Ametz, C., Spannagl, M., Steiner, B., Lemmens, M., Mayer, K. F. X., Buerstmayr, H. & Schweiger, W. 2013. Quantitative trait loci-dependent analysis of a gene co-expression network associated with Fusarium head blight resistance in bread wheat (Triticum aestivumL.). *BMC Genomics,* 14**,** 728.

Kumar, A. S., Park, E., Nedo, A., Alqarni, A., Ren, L., Hoban, K., Modla, S., Mcdonald, J. H., Kambhamettu, C., Dinesh-Kumar, S. P. & Caplan, J. L. 2018. Stromule extension along microtubules coordinated with actin-mediated anchoring guides perinuclear chloroplast movement during innate immunity. *eLife,* 7**,** e23625.

Kuwabara, C., Takezawa, D., Shimada, T., Hamada, T., Fujikawa, S. & Arakawa, K. 2002. Abscisic acid- and cold-induced thaumatin-like protein in winter wheat has an antifungal activity against snow mould, Microdochium nivale. *Physiologia Plantarum,* 115**,** 101-110.

Kwok, E. Y. & Hanson, M. R. 2004. Plastids and stromules interact with the nucleus and cell membrane in vascular plants. *Plant Cell Reports,* 23**,** 188-195.

Lamkanfi, M. & Dixit, Vishva m. 2014. Mechanisms and Functions of Inflammasomes. *Cell,* 157**,** 1013-1022.

Lata, C., Manjul, A. S., Prasad, P., Gangwar, O. P., Adhikari, S., Sonu, Kumar, S., Bhardwaj, S. C., Singh, G., Samota, M. K., Choudhary, M., Bohra, A. & Varshney, R. K. 2023. Unraveling the diversity and functions of sugar transporters for sustainable management of wheat rust. *Functional & Integrative Genomics,* 23**,** 213.

Latorre, S. M., Were, V. M., Foster, A. J., Langner, T., Malmgren, A., Harant, A., Asuke, S., Reyes-Avila, S., Gupta, D. R., Jensen, C., Ma, W., Mahmud, N. U., Mehebub, M. S., Mulenga, R. M., Muzahid, A. N. M., Paul, S. K., Rabby, S. M. F., Rahat, A. a. M., Ryder, L., Shrestha, R.-K., Sichilima, S., Soanes, D. M., Singh, P. K., Bentley, A. R., Saunders, D. G. O., Tosa, Y., Croll, D.,

Lamour, K. H., Islam, T., Tembo, B., Win, J., Talbot, N. J., Burbano, H. A. & Kamoun, S. 2023. Genomic surveillance uncovers a pandemic clonal lineage of the wheat blast fungus. *PLOS Biology,* 21**,** e3002052.

Lee, J. S. & Adams, K. L. 2020. Global insights into duplicated gene expression and alternative splicing in polyploid Brassica napus under heat, cold, and drought stress. *The Plant Genome,* 13**,** e20057.

Lee, W.-S., Rudd, J. J. & Kanyuka, K. 2015. Virus induced gene silencing (VIGS) for functional analysis of wheat genes involved in Zymoseptoria tritici susceptibility and resistance. *Fungal Genetics and Biology,* 79**,** 84-88.

Lefevere, H., Bauters, L. & Gheysen, G. 2020. Salicylic Acid Biosynthesis in Plants. *Frontiers in Plant Science,* 11.

Leister, D. 2023. Enhancing the light reactions of photosynthesis: Strategies, controversies, and perspectives. *Molecular Plant,* 16**,** 4-22.

Lescot, M., Déhais, P., Thijs, G., Marchal, K., Moreau, Y., Van De Peer, Y., Rouzé, P. & Rombauts, S. 2002. PlantCARE, a database of plant cis-acting regulatory elements and a portal to tools for in silico analysis of promoter sequences. *Nucleic Acids Research,* 30**,** 325-327.

Letunic, I. & Bork, P. 2021. Interactive Tree Of Life (iTOL) v5: an online tool for phylogenetic tree display and annotation. *Nucleic Acids Research,* 49**,** W293-W296.

Lewis, C. M., Persoons, A., Bebber, D. P., Kigathi, R. N., Maintz, J., Findlay, K., Bueno-Sancho, V., Corredor-Moreno, P., Harrington, S. A., Kangara, N., Berlin, A., García, R., Germán, S. E., Hanzalová, A., Hodson, D. P., Hovmøller, M. S., Huerta-Espino, J., Imtiaz, M., Mirza, J. I., Justesen, A. F., Niks, R. E., Omrani, A., Patpour, M., Pretorius, Z. A., Roohparvar, R., Sela, H., Singh, R. P., Steffenson, B., Visser, B., Fenwick, P. M., Thomas, J., Wulff, B. B. H. & Saunders, D. G. O. 2018. Potential for re-emergence of wheat stem rust in the United Kingdom. *Communications Biology,* 1**,** 13.

Lewis, L. A., Polanski, K., De Torres-Zabala, M., Jayaraman, S., Bowden, L., Moore, J., Penfold, C. A., Jenkins, D. J., Hill, C., Baxter, L., Kulasekaran, S., Truman, W., Littlejohn, G., Prusinska, J., Mead, A., Steinbrenner, J., Hickman, R., Rand, D., Wild, D. L., Ott, S., Buchanan-Wollaston, V., Smirnoff, N., Beynon, J., Denby, K. & Grant, M. 2015. Transcriptional Dynamics Driving MAMP-Triggered Immunity and Pathogen Effector-Mediated Immunosuppression in Arabidopsis Leaves Following Infection with Pseudomonas syringae pv tomato DC3000. *The Plant Cell,* 27**,** 3038-3064.

Li, B. & Zheng, Y. 2018. Dynamic evolution and phylogenomic analysis of the chloroplast genome in Schisandraceae. *Scientific Reports,* 8**,** 9285.

Li, J.-Y., Sun, J.-L., Tian, Y.-Y. & Liu, J.-X. 2022. The FtsH-Inactive Protein FtsHi5 Is Required for Chloroplast Development and Protein Accumulation in Chloroplasts at Low Ambient Temperature in Arabidopsis. *Frontiers in Plant Science,* 12.

Li, X., Patena, W., Fauser, F., Jinkerson, R. E., Saroussi, S., Meyer, M. T., Ivanova, N., Robertson, J. M., Yue, R., Zhang, R., Vilarrasa-Blasi, J., Wittkopp, T. M., Ramundo, S., Blum, S. R., Goh, A., Laudon, M., Srikumar, T., Lefebvre, P. A., Grossman, A. R. & Jonikas, M. C. 2019. A genome-wide algal mutant library and functional screen identifies genes required for eukaryotic photosynthesis. *Nature Genetics,* 51**,** 627-635.

Liao, C.-J., Hailemariam, S., Sharon, A. & Mengiste, T. 2022. Pathogenic strategies and immune mechanisms to necrotrophs: Differences and similarities to biotrophs and hemibiotrophs. *Current Opinion in Plant Biology,* 69**,** 102291.

Lindahl, M., Spetea, C., Hundal, T., Oppenheim, A. B., Adam, Z. & Andersson, B. 2000. The Thylakoid FtsH Protease Plays a Role in the Light-Induced Turnover of the Photosystem II D1 Protein. *The Plant Cell,* 12**,** 419-431.

Lindahl, M., Tabak, S., Cseke, L., Pichersky, E., Andersson, B. & Adam, Z. 1996. Identification, Characterization, and Molecular Cloning of a Homologue of the Bacterial FtsH Protease in Chloroplasts of Higher Plants *. *Journal of Biological Chemistry,* 271**,** 29329-29334.

Littlejohn, G. R., Breen, S., Smirnoff, N. & Grant, M. 2021. Chloroplast immunity illuminated. *New Phytologist,* 229**,** 3088-3107.

Liu, J., Zhang, Q., Chang, Q., Zhuang, H., Huang, L.-L. & Kang, Z.-S. 2012. Cloning and characterization of the actin gene from Puccinia striiformis f. sp. tritici. *World Journal of Microbiology and Biotechnology,* 28**,** 2331-2339.

Liu, R., Chen, T., Yin, X., Xiang, G., Peng, J., Fu, Q., Li, M., Shang, B., Ma, H., Liu, G., Wang, Y. & Xu, Y. 2021. A Plasmopara viticola RXLR effector targets a chloroplast protein PsbP to inhibit ROS production in grapevine. *The Plant Journal,* 106**,** 1557-1570.

Liu, Y. & He, C. 2016. Regulation of plant reactive oxygen species (ROS) in stress responses: learning from AtRBOHD. *Plant Cell Reports,* 35**,** 995-1007.

Liu, Y., Ren, D., Pike, S., Pallardy, S., Gassmann, W. & Zhang, S. 2007. Chloroplast-generated reactive oxygen species are involved in hypersensitive response-like cell death mediated by a mitogen-activated protein kinase cascade. *The Plant Journal,* 51**,** 941-954.

Liu, Y., Sun, T., Sun, Y., Zhang, Y., Radojičić, A., Ding, Y., Tian, H., Huang, X., Lan, J., Chen, S., Orduna, A. R., Zhang, K., Jetter, R., Li, X. & Zhang, Y. 2020. Diverse Roles of the Salicylic Acid Receptors NPR1 and NPR3/NPR4 in Plant Immunity. *The Plant Cell,* 32**,** 4002-4016.

Liu, Z., Xin, M., Qin, J., Peng, H., Ni, Z., Yao, Y. & Sun, Q. 2015. Temporal transcriptome profiling reveals expression partitioning of homeologous genes contributing to heat and drought acclimation in wheat (Triticum aestivum L.). *BMC Plant Biology,* 15**,** 152.

Lobell, D. B. & Field, C. B. 2007. Global scale climate–crop yield relationships and the impacts of recent warming. *Environmental Research Letters,* 2**,** 014002.

Lolle, S., Stevens, D. & Coaker, G. 2020. Plant NLR-triggered immunity: from receptor activation to downstream signaling. *Current Opinion in Immunology,* 62**,** 99-105.

Lorrain, C., Gonçalves Dos Santos, K. C., Germain, H., Hecker, A. & Duplessis, S. 2019. Advances in understanding obligate biotrophy in rust fungi. *New Phytologist,* 222**,** 1190-1206.

Loudya, N., Maffei, D. P. F., Bédard, J., Ali, S. M., Devlin, P. F., Jarvis, R. P. & López-Juez, E. 2022. Mutations in the chloroplast inner envelope protein TIC100 impair and repair chloroplast protein import and impact retrograde signaling. *The Plant Cell,* 34**,** 3028-3046.

Lu, X., Zhang, D., Li, S., Su, Y., Liang, Q., Meng, H., Shen, S., Fan, Y., Liu, C. & Zhang, C. 2014. FtsHi4 Is Essential for Embryogenesis Due to Its Influence on Chloroplast Development in Arabidopsis. *PLOS ONE,* 9**,** e99741.

Lück, S., Kreszies, T., Strickert, M., Schweizer, P., Kuhlmann, M. & Douchkov, D. 2019. siRNA-Finder (si-Fi) Software for RNAi-Target Design and Off-Target Prediction. *Frontiers in Plant Science,* 10.

Luderer, R. & Joosten, M. H. a. J. 2001. Avirulence proteins of plant pathogens: determinants of victory and defeat. *Molecular Plant Pathology,* 2**,** 355-364.

Lunde, C., Jensen, P. E., Haldrup, A., Knoetzel, J. & Scheller, H. V. 2000. The PSI-H subunit of photosystem I is essential for state transitions in plant photosynthesis. *Nature,* 408**,** 613-615.

Lundin, B., Thuswaldner, S., Shutova, T., Eshaghi, S., Samuelsson, G., Barber, J., Andersson, B. & Spetea, C. 2007. Subsequent events to GTP binding by the plant PsbO protein: Structural changes, GTP hydrolysis and dissociation from the photosystem II complex. *Biochimica et Biophysica Acta (BBA) - Bioenergetics,* 1767**,** 500-508.

Macioszek, V. K., Jęcz, T., Ciereszko, I. & Kononowicz, A. K. 2023. Jasmonic Acid as a Mediator in Plant Response to Necrotrophic Fungi. *Cells,* 12**,** 1027.

Manning, V. A., Chu, A. L., Steeves, J. E., Wolpert, T. J. & Ciuffetti, L. M. 2009. A Host-Selective Toxin of Pyrenophora tritici-repentis, Ptr ToxA, Induces Photosystem Changes and Reactive

Oxygen Species Accumulation in Sensitive Wheat. *Molecular Plant-Microbe Interactions®,* 22**,** 665-676.
Mcintosh, R., Wellings, C. & Park, R. 1995. *Wheat Rusts*.
Mehrabi, Z. 2020. Food system collapse. *Nature Climate Change,* 10**,** 16-17.
Melcher, R. L. J. & Moerschbacher, B. M. 2016. An improved microtiter plate assay to monitor the oxidative burst in monocot and dicot plant cell suspension cultures. *Plant Methods,* 12**,** 5.
Minter, F. & Saunders, D. G. O. 2023. Safeguarding wheat yields from cereal fungal invaders in the postgenomic era. *Current Opinion in Microbiology,* 73**,** 102310.
Mishra, L. S., Mielke, K., Wagner, R. & Funk, C. 2019. Reduced expression of the proteolytically inactive FtsH members has impacts on the Darwinian fitness of Arabidopsis thaliana. *Journal of Experimental Botany,* 70**,** 2173-2184.
Moldenhauer, J., Moerschbacher, B. M. & Van Der Westhuizen, A. J. 2006. Histological investigation of stripe rust (Puccinia striiformis f.sp. tritici) development in resistant and susceptible wheat cultivars. *Plant Pathology,* 55**,** 469-474.
Molina, A., Görlach, J., Volrath, S. & Ryals, J. 1999. Wheat Genes Encoding Two Types of PR-1 Proteins Are Pathogen Inducible, but Do Not Respond to Activators of Systemic Acquired Resistance. *Molecular Plant-Microbe Interactions®,* 12**,** 53-58.
Moore, J. W., Loake, G. J. & Spoel, S. H. 2011. Transcription Dynamics in Plant Immunity. *The Plant Cell,* 23**,** 2809-2820.
Moreau, M., Westlake, T., Zampogna, G., Popescu, G., Tian, M., Noutsos, C. & Popescu, S. 2013. The Arabidopsis oligopeptidases TOP1 and TOP2 are salicylic acid targets that modulate SA-mediated signaling and the immune response. *The Plant Journal,* 76**,** 603-614.
Mubarakshina, M. M., Ivanov, B. N., Naydov, I. A., Hillier, W., Badger, M. R. & Krieger-Liszkay, A. 2010. Production and diffusion of chloroplastic H2O2 and its implication to signalling. *Journal of Experimental Botany,* 61**,** 3577-3587.
Mulo, P., Sakurai, I. & Aro, E.-M. 2012. Strategies for psbA gene expression in cyanobacteria, green algae and higher plants: From transcription to PSII repair. *Biochimica et Biophysica Acta (BBA) - Bioenergetics,* 1817**,** 247-257.
Murakami, R., Ifuku, K., Takabayashi, A., Shikanai, T., Endo, T. & Sato, F. 2002. Characterization of an Arabidopsis thaliana mutant with impaired psbO, one of two genes encoding extrinsic 33-kDa proteins in photosystem II. *FEBS Letters,* 523**,** 138-142.
Naschberger, A., Mosebach, L., Tobiasson, V., Kuhlgert, S., Scholz, M., Perez-Boerema, A., Ho, T. T. H., Vidal-Meireles, A., Takahashi, Y., Hippler, M. & Amunts, A. 2022. Algal photosystem I dimer and high-resolution model of PSI-plastocyanin complex. *Nature Plants,* 8**,** 1191-1201.
Návarová, H., Bernsdorff, F., Döring, A.-C. & Zeier, J. 2012. Pipecolic Acid, an Endogenous Mediator of Defense Amplification and Priming, Is a Critical Regulator of Inducible Plant Immunity. *The Plant Cell,* 24**,** 5123-5141.
Naver, H., Haldrup, A. & Scheller, H. V. 1999. Cosuppression of Photosystem I Subunit PSI-H in Arabidopsis thaliana: efficient electron transfer and stability of photosystem I is dependent upon the PSI-H subunit. *Journal of Biological Chemistry,* 274**,** 10784-10789.
Nawrath, C., Heck, S., Parinthawong, N. & MéTraux, J.-P. 2002. EDS5, an Essential Component of Salicylic Acid–Dependent Signaling for Disease Resistance in Arabidopsis, Is a Member of the MATE Transporter Family. *The Plant Cell,* 14**,** 275-286.
Neugebauer, K. A., Bruce, M., Todd, T., Trick, H. N. & Fellers, J. P. 2018. Wheat differential gene expression induced by different races of Puccinia triticina. *PLOS ONE,* 13**,** e0198350.
Ngou, B. P. M., Ahn, H.-K., Ding, P. & Jones, J. D. G. 2021. Mutual potentiation of plant immunity by cell-surface and intracellular receptors. *Nature,* 592**,** 110-115.
Nomura, H., Komori, T., Uemura, S., Kanda, Y., Shimotani, K., Nakai, K., Furuichi, T., Takebayashi, K., Sugimoto, T., Sano, S., Suwastika, I. N., Fukusaki, E., Yoshioka, H., Nakahira, Y. & Shiina, T.

2012. Chloroplast-mediated activation of plant immune signalling in Arabidopsis. *Nature Communications,* 3**,** 926.

Norris, K. 2008. Agriculture and biodiversity conservation: opportunity knocks. *Conservation Letters,* 1**,** 2-11.

Op Den Camp, R. G. L., Przybyla, D., Ochsenbein, C., Laloi, C., Kim, C., Danon, A., Wagner, D., Hideg, E. V., GöBel, C., Feussner, I., Nater, M. & Apel, K. 2003. Rapid Induction of Distinct Stress Responses after the Release of Singlet Oxygen in Arabidopsis[W]. *The Plant Cell,* 15**,** 2320-2332.

Orr, D. J., Pereira, A. M., Da Fonseca Pereira, P., Pereira-Lima Í, A., Zsögön, A. & Araújo, W. L. 2017. Engineering photosynthesis: progress and perspectives. *F1000Res,* 6**,** 1891.

Orton, E. S., Lewis, C. M., Davey, P. E., Radhakrishnan, G. V. & Saunders, D. G. O. 2019. Stem rust (Puccina graminis) identified on spring barley in the UK adjacent to infected Berberis vulgaris. *New Disease Reports,* 40**,** 11-11.

Pallotta, M. A., Asayama, S., Reinheimer, J. M., Davies, P. A., Barr, A. R., Jefferies, S. P., Chalmers, K. J., Lewis, J., Collins, H. M., Roumeliotis, S., Logue, S. J., Coventry, S. J., Lance, R. C. M., Karakousis, A., Lim, P., Verbyla, A. P. & Eckermann, P. J. 2003. Mapping and QTL analysis of the barley population Amagi Nijo × WI2585. *Australian Journal of Agricultural Research,* 54**,** 1141-1144.

Paysan-Lafosse, T., Blum, M., Chuguransky, S., Grego, T., Pinto, B. L., Salazar, Gustavo a., Bileschi, Maxwell l., Bork, P., Bridge, A., Colwell, L., Gough, J., Haft, Daniel h., Letunić, I., Marchler-Bauer, A., Mi, H., Natale, Darren a., Orengo, Christine a., Pandurangan, Arun p., Rivoire, C., Sigrist, C. J. A., Sillitoe, I., Thanki, N., Thomas, P. D., Tosatto, S. C. E., Wu, Cathy h. & Bateman, A. 2022. InterPro in 2022. *Nucleic Acids Research,* 51**,** D418-D427.

Peng, L., Shimizu, H. & Shikanai, T. 2008. The Chloroplast NAD(P)H Dehydrogenase Complex Interacts with Photosystem I in Arabidopsis*. *Journal of Biological Chemistry,* 283**,** 34873-34879.

Peng, Y., Yang, J., Li, X. & Zhang, Y. 2021. Salicylic Acid: Biosynthesis and Signaling. *Annual Review of Plant Biology,* 72**,** 761-791.

Pequeno, D. N., Hernandez-Ochoa, I. M., Reynolds, M., Sonder, K., Moleromilan, A., Robertson, R. D., Lopes, M. S., Xiong, W., Kropff, M. & Asseng, S. 2021. Climate impact and adaptation to heat and drought stress of regional and global wheat production. *Environmental Research Letters,* 16**,** 054070.

Petre, B., Joly, D. L. & Duplessis, S. 2014. Effector proteins of rust fungi. *Frontiers in Plant Science,* 5.

Petre, B., Saunders, D. G. O., Sklenar, J., Lorrain, C., Krasileva, K. V., Win, J., Duplessis, S. & Kamoun, S. 2016. Heterologous Expression Screens in Nicotiana benthamiana Identify a Candidate Effector of the Wheat Yellow Rust Pathogen that Associates with Processing Bodies. *PLOS ONE,* 11**,** e0149035.

Pfannschmidt, T., Nilsson, A., Tullberg, A., Link, G. & Allen, J. F. 1999. Direct Transcriptional Control of the Chloroplast Genes psbA and psaAB Adjusts Photosynthesis to Light Energy Distribution in Plants. *IUBMB Life,* 48**,** 271-276.

Pitino, M., Armstrong, C. M. & Duan, Y. 2017. Molecular mechanisms behind the accumulation of ATP and H2O2 in citrus plants in response to 'Candidatus Liberibacter asiaticus' infection. *Horticulture Research,* 4.

Posch, B. C., Kariyawasam, B. C., Bramley, H., Coast, O., Richards, R. A., Reynolds, M. P., Trethowan, R. & Atkin, O. K. 2019. Exploring high temperature responses of photosynthesis and respiration to improve heat tolerance in wheat. *Journal of Experimental Botany,* 70**,** 5051-5069.

Powell, J. J., Fitzgerald, T. L., Stiller, J., Berkman, P. J., Gardiner, D. M., Manners, J. M., Henry, R. J. & Kazan, K. 2017. The defence-associated transcriptome of hexaploid wheat displays homoeolog expression and induction bias. *Plant Biotechnology Journal,* 15**,** 533-543.

Price, M. N., Dehal, P. S. & Arkin, A. P. 2010. FastTree 2 – Approximately Maximum-Likelihood Trees for Large Alignments. *PLOS ONE,* 5**,** e9490.

Prywes, N., Phillips, N. R., Tuck, O. T., Valentin-Alvarado, L. E. & Savage, D. F. 2023. Rubisco Function, Evolution, and Engineering. *Annual Review of Biochemistry,* 92**,** 385-410.

Qi, T., Guo, J., Liu, P., He, F., Wan, C., Islam, M. A., Tyler, B. M., Kang, Z. & Guo, J. 2019. Stripe rust effector PstGSRE1 disrupts nuclear localization of ROS-promoting transcription factor TaLOL2 to defeat ROS-induced defense in wheat. *Molecular Plant,* 12**,** 1624-1638.

Quick, W. P. & Neuhaus, H. E. 1997. The regulation and control of photosynthetic carbon assimilation. *A Molecular Approach to Primary Metabolism in Higher Plants,* 41**,** 62.

Radhakrishnan, G. V., Cook, N. M., Bueno-Sancho, V., Lewis, C. M., Persoons, A., Mitiku, A. D., Heaton, M., Davey, P. E., Abeyo, B., Alemayehu, Y., Badebo, A., Barnett, M., Bryant, R., Chatelain, J., Chen, X., Dong, S., Henriksson, T., Holdgate, S., Justesen, A. F., Kalous, J., Kang, Z., Laczny, S., Legoff, J.-P., Lesch, D., Richards, T., Randhawa, H. S., Thach, T., Wang, M., Hovmøller, M. S., Hodson, D. P. & Saunders, D. G. O. 2019. MARPLE, a point-of-care, strain-level disease diagnostics and surveillance tool for complex fungal pathogens. *BMC Biology,* 17**,** 65.

Raines, C. A. 2003. The Calvin cycle revisited. *Photosynthesis research,* 75**,** 1-10.

Rajarammohan, S. 2021. Redefining Plant-Necrotroph Interactions: The Thin Line Between Hemibiotrophs and Necrotrophs. *Frontiers in Microbiology,* 12.

Ramírez-González, R. H., Borrill, P., Lang, D., Harrington, S. A., Brinton, J., Venturini, L., Davey, M., Jacobs, J., Van Ex, F., Pasha, A., Khedikar, Y., Robinson, S. J., Cory, A. T., Florio, T., Concia, L., Juery, C., Schoonbeek, H., Steuernagel, B., Xiang, D., Ridout, C. J., Chalhoub, B., Mayer, K. F. X., Benhamed, M., Latrasse, D., Bendahmane, A., Consortium, I. W. G. S., Wulff, B. B. H., Appels, R., Tiwari, V., Datla, R., Choulet, F., Pozniak, C. J., Provart, N. J., Sharpe, A. G., Paux, E., Spannagl, M., Bräutigam, A., Uauy, C., Korol, A., Sharpe, A. G., Juhász, A., Rohde, A., Bellec, A., Distelfeld, A., Akpinar, B. A., Keller, B., Darrier, B., Gill, B., Chalhoub, B., Steuernagel, B., Feuillet, C., Chaudhary, C., Uauy, C., Pozniak, C., Ormanbekova, D., Xiang, D., Latrasse, D., Swarbreck, D., Barabaschi, D., Raats, D., Sergeeva, E., Salina, E., Paux, E., Cattonaro, F., Choulet, F., Kobayashi, F., Keeble-Gagnere, G., Kaur, G., Muehlbauer, G., Kettleborough, G., Yu, G., Šimková, H., Gundlach, H., Berges, H., Rimbert, H., Budak, H., Handa, H., Small, I., Bartoš, J., Rogers, J., Doležel, J., Keilwagen, J., Poland, J., Melonek, J., Jacobs, J., Wright, J., Jones, J. D. G., Gutierrez-Gonzalez, J., Eversole, K., Nilsen, K., Mayer, K. F. X., Kanyuka, K., Singh, K., Gao, L., Concia, L., Venturini, L., Cattivelli, L., Spannagl, M., Mascher, M., Hayden, M., et al. 2018. The transcriptional landscape of polyploid wheat. *Science,* 361**,** eaar6089.

Rantala, M., Rantala, S. & Aro, E.-M. 2020. Composition, phosphorylation and dynamic organization of photosynthetic protein complexes in plant thylakoid membrane. *Photochemical & Photobiological Sciences,* 19**,** 604-619.

Rasmussen, J. B., Hammerschmidt, R. & Zook, M. N. 1991. Systemic Induction of Salicylic Acid Accumulation in Cucumber after Inoculation with Pseudomonas syringae pv syringae 1. *Plant Physiology,* 97**,** 1342-1347.

Rawlings, N. D. & Barrett, A. J. 2004. Introduction: metallopeptidases and their clans. *In:* BARRETT, A. J., RAWLINGS, N. D. & WOESSNER, J. F. (eds.) *Handbook of Proteolytic Enzymes (Second Edition).* London: Academic Press.

Rawlings, N. D., Barrett, A. J., Thomas, P. D., Huang, X., Bateman, A. & Finn, R. D. 2017. The MEROPS database of proteolytic enzymes, their substrates and inhibitors in 2017 and a comparison with peptidases in the PANTHER database. *Nucleic Acids Research,* 46**,** D624-D632.

Rawlings, N. D. & Bateman, A. 2019. Origins of peptidases. *Biochimie,* 166**,** 4-18.

Ray, S., Anderson, J. M., Urmeev, F. I. & Goodwin, S. B. 2003. Rapid induction of a protein disulfide isomerase and defense-related genes in wheat in response to the hemibiotrophic fungal pathogen Mycosphaerella graminicola. *Plant Molecular Biology,* 53**,** 741-754.

Rodríguez-Herva, J. J., González-Melendi, P., Cuartas-Lanza, R., Antúnez-Lamas, M., Río-Alvarez, I., Li, Z., López-Torrejón, G., Díaz, I., Del Pozo, J. C., Chakravarthy, S., Collmer, A., Rodríguez-Palenzuela, P. & López-Solanilla, E. 2012. A bacterial cysteine protease effector protein interferes with photosynthesis to suppress plant innate immune responses. *Cellular Microbiology,* 14**,** 669-681.

Rodríguez, M., Muñoz, N., Lenardon, S. & Lascano, R. 2012. The chlorotic symptom induced by Sunflower chlorotic mottle virus is associated with changes in redox-related gene expression and metabolites. *Plant Science,* 196**,** 107-116.

Rudd, J. J., Kanyuka, K., Hassani-Pak, K., Derbyshire, M., Andongabo, A., Devonshire, J., Lysenko, A., Saqi, M., Desai, N. M., Powers, S. J., Hooper, J., Ambroso, L., Bharti, A., Farmer, A., Hammond-Kosack, K. E., Dietrich, R. A. & Courbot, M. 2015. Transcriptome and Metabolite Profiling of the Infection Cycle of Zymoseptoria tritici on Wheat Reveals a Biphasic Interaction with Plant Immunity Involving Differential Pathogen Chromosomal Contributions and a Variation on the Hemibiotrophic Lifestyle Definition *Plant Physiology,* 167**,** 1158-1185.

Sakamoto, W., Tamura, T., Hanba-Tomita, Y., Sodmergen & Murata, M. 2002. The VAR1 locus of Arabidopsis encodes a chloroplastic FtsH and is responsible for leaf variegation in the mutant alleles. *Genes to Cells,* 7**,** 769-780.

Salcedo, A., Rutter, W., Wang, S., Akhunova, A., Bolus, S., Chao, S., Anderson, N., De Soto, M. F., Rouse, M., Szabo, L., Bowden, R. L., Dubcovsky, J. & Akhunov, E. 2017. Variation in the AvrSr35 gene determines Sr35 resistance against wheat stem rust race Ug99. *Science,* 358**,** 1604-1606.

Savage, Z., Duggan, C., Toufexi, A., Pandey, P., Liang, Y., Segretin, M. E., Yuen, L. H., Gaboriau, D. C. A., Leary, A. Y., Tumtas, Y., Khandare, V., Ward, A. D., Botchway, S. W., Bateman, B. C., Pan, I., Schattat, M., Sparkes, I. & Bozkurt, T. O. 2021. Chloroplasts alter their morphology and accumulate at the pathogen interface during infection by Phytophthora infestans. *The Plant Journal,* 107**,** 1771-1787.

Savary, S., Willocquet, L., Pethybridge, S. J., Esker, P., Mcroberts, N. & Nelson, A. 2019. The global burden of pathogens and pests on major food crops. *Nature Ecology & Evolution,* 3**,** 430-439.

Schweiger, W., Steiner, B., Vautrin, S., Nussbaumer, T., Siegwart, G., Zamini, M., Jungreithmeier, F., Gratl, V., Lemmens, M., Mayer, K. F. X., Bérgès, H., Adam, G. & Buerstmayr, H. 2016. Suppressed recombination and unique candidate genes in the divergent haplotype encoding Fhb1, a major Fusarium head blight resistance locus in wheat. *Theoretical and Applied Genetics,* 129**,** 1607-1623.

Schwessinger, B. 2017. Fundamental wheat stripe rust research in the 21st century. *New Phytologist,* 213**,** 1625-1631.

Scofield, S. R., Huang, L., Brandt, A. S. & Gill, B. S. 2005. Development of a Virus-Induced Gene-Silencing System for Hexaploid Wheat and Its Use in Functional Analysis of the Lr21-Mediated Leaf Rust Resistance Pathway. *Plant Physiology,* 138**,** 2165-2173.

Selin, C., De Kievit, T. R., Belmonte, M. F. & Fernando, W. G. D. 2016. Elucidating the Role of Effectors in Plant-Fungal Interactions: Progress and Challenges. *Frontiers in Microbiology,* 7.

Seo, S., Okamoto, M., Iwai, T., Iwano, M., Fukui, K., Isogai, A., Nakajima, N. & Ohashi, Y. 2000. Reduced Levels of Chloroplast FtsH Protein in Tobacco Mosaic Virus–Infected Tobacco Leaves Accelerate the Hypersensitive Reaction. *The Plant Cell,* 12**,** 917-932.

Serag, A., Salem, M. A., Gong, S., Wu, J.-L. & Farag, M. A. 2023. Decoding Metabolic Reprogramming in Plants under Pathogen Attacks, a Comprehensive Review of Emerging Metabolomics Technologies to Maximize Their Applications. *Metabolites,* 13**,** 424.

Serrano, M., Wang, B., Aryal, B., Garcion, C., Abou-Mansour, E., Heck, S., Geisler, M., Mauch, F., Nawrath, C. & Métraux, J.-P. 2013. Export of Salicylic Acid from the Chloroplast Requires the Multidrug and Toxin Extrusion-Like Transporter EDS5 *Plant Physiology,* 162**,** 1815-1821.

Shah Jahan, M., Wang, Y., Shu, S., Zhong, M., Chen, Z., Wu, J., Sun, J. & Guo, S. 2019. Exogenous salicylic acid increases the heat tolerance in Tomato (Solanum lycopersicum L) by enhancing photosynthesis efficiency and improving antioxidant defense system through scavenging of reactive oxygen species. *Scientia Horticulturae,* 247**,** 421-429.

Shibuya, N., Kaku, H., Kuchitsu, K. & Maliarik, M. J. 1993. Identification of a novel high-affinity binding site for N-acetylchitooligosaccharide elicitor in the membrane fraction from suspension-cultured rice cells. *FEBS Letters,* 329**,** 75-78.

Shields, A., Shivnauth, V. & Castroverde, C. D. M. 2022. Salicylic Acid and N-Hydroxypipecolic Acid at the Fulcrum of the Plant Immunity-Growth Equilibrium. *Frontiers in Plant Science,* 13.

Shimura, H., Pantaleo, V., Ishihara, T., Myojo, N., Inaba, J.-I., Sueda, K., Burgyán, J. & Masuta, C. 2011. A Viral Satellite RNA Induces Yellow Symptoms on Tobacco by Targeting a Gene Involved in Chlorophyll Biosynthesis using the RNA Silencing Machinery. *PLOS Pathogens,* 7**,** e1002021.

Shin, K.-H., Kamal, A. H. M., Cho, K., Choi, J.-S., Yu, J., Nam-Chon, P., Lee, Y. W., Lee, J. K., Park, J.-C., Kim, H.-T. & Woo, S. H. 2011. Defense proteins are induced in wheat spikes exposed to Fusarium graminearum. *Plant Omics,* 4**,** 270-277.

Silva, P., Thompson, E., Bailey, S., Kruse, O., Mullineaux, C. W., Robinson, C., Mann, N. H. & Nixon, P. J. 2003. FtsH Is Involved in the Early Stages of Repair of Photosystem II in Synechocystis sp PCC 6803 [W]. *The Plant Cell,* 15**,** 2152-2164.

Singh, P. K., Gahtyari, N. C., Roy, C., Roy, K. K., He, X., Tembo, B., Xu, K., Juliana, P., Sonder, K., Kabir, M. R. & Chawade, A. 2021. Wheat Blast: A Disease Spreading by Intercontinental Jumps and Its Management Strategies. *Frontiers in Plant Science,* 12.

Smith, A. M. & Zeeman, S. C. 2020. Starch: A Flexible, Adaptable Carbon Store Coupled to Plant Growth. *Annual Review of Plant Biology,* 71**,** 217-245.

Sokolenko, A., Pojidaeva, E., Zinchenko, V., Panichkin, V., Glaser, V. M., Herrmann, R. G. & Shestakov, S. V. 2002. The gene complement for proteolysis in the cyanobacterium Synechocystis sp. PCC 6803 and Arabidopsis thaliana chloroplasts. *Current Genetics,* 41**,** 291-310.

Song, J. T., Lu, H., Mcdowell, J. M. & Greenberg, J. T. 2004. A key role for ALD1 in activation of local and systemic defenses in Arabidopsis. *The Plant Journal,* 40**,** 200-212.

Sowden, Robert g., Watson, Samuel j. & Jarvis, P. 2017. The role of chloroplasts in plant pathology. *Essays in Biochemistry,* 62**,** 21-39.

Sperschneider, J., Catanzariti, A.-M., Deboer, K., Petre, B., Gardiner, D. M., Singh, K. B., Dodds, P. N. & Taylor, J. M. 2017. LOCALIZER: subcellular localization prediction of both plant and effector proteins in the plant cell. *Scientific Reports,* 7**,** 44598.

Sperschneider, J., Dodds, P. N., Gardiner, D. M., Manners, J. M., Singh, K. B. & Taylor, J. M. 2015. Advances and Challenges in Computational Prediction of Effectors from Plant Pathogenic Fungi. *PLOS Pathogens,* 11**,** e1004806.

Strepp, R., Scholz, S., Kruse, S., Speth, V. & Reski, R. 1998. Plant nuclear gene knockout reveals a role in plastid division for the homolog of the bacterial cell division protein FtsZ, an ancestral tubulin. *Proceedings of the National Academy of Sciences,* 95**,** 4368-4373.

Su, J., Yang, L., Zhu, Q., Wu, H., He, Y., Liu, Y., Xu, J., Jiang, D. & Zhang, S. 2018. Active photosynthetic inhibition mediated by MPK3/MPK6 is critical to effector-triggered immunity. *PLOS Biology,* 16**,** e2004122.

Sun, T., Busta, L., Zhang, Q., Ding, P., Jetter, R. & Zhang, Y. 2018. TGACG-BINDING FACTOR 1 (TGA1) and TGA4 regulate salicylic acid and pipecolic acid biosynthesis by modulating the expression of SYSTEMIC ACQUIRED RESISTANCE DEFICIENT 1 (SARD1) and CALMODULIN-BINDING PROTEIN 60g (CBP60g). *New Phytologist,* 217**,** 344-354.

Sun, Y. & Jarvis, R. P. 2023. Chloroplast Proteostasis: Import, Sorting, Ubiquitination, and Proteolysis. *Annual Review of Plant Biology,* 74**,** null.

Surpin, M., Larkin, R. M. & Chory, J. 2002. Signal Transduction between the Chloroplast and the Nucleus. *The Plant Cell,* 14**,** S327-S338.

Susek, R. E., Ausubel, F. M. & Chory, J. 1993. Signal transduction mutants of arabidopsis uncouple nuclear CAB and RBCS gene expression from chloroplast development. *Cell,* 74**,** 787-799.

Szklarczyk, D., Kirsch, R., Koutrouli, M., Nastou, K., Mehryary, F., Hachilif, R., Gable, A. L., Fang, T., Doncheva, N. T., Pyysalo, S., Bork, P., Jensen, L. J. & Von Mering, C. 2023. The STRING database in 2023: protein-protein association networks and functional enrichment analyses for any sequenced genome of interest. *Nucleic Acids Res,* 51**,** D638-d646.

Takechi, K., Sodmergen, Murata, M., Motoyoshi, F. & Sakamoto, W. 2000. The YELLOW VARIEGATED (VAR2) Locus Encodes a Homologue of FtsH, an ATP-Dependent Protease in Arabidopsis. *Plant and Cell Physiology,* 41**,** 1334-1346.

Tang, L., Yang, G., Ma, M., Liu, X., Li, B., Xie, J., Fu, Y., Chen, T., Yu, Y., Chen, W., Jiang, D. & Cheng, J. 2020. An effector of a necrotrophic fungal pathogen targets the calcium-sensing receptor in chloroplasts to inhibit host resistance. *Molecular Plant Pathology,* 21**,** 686-701.

Tateda, C., Zhang, Z., Shrestha, J., Jelenska, J., Chinchilla, D. & Greenberg, J. T. 2014. Salicylic Acid Regulates Arabidopsis Microbial Pattern Receptor Kinase Levels and Signaling *The Plant Cell,* 26**,** 4171-4187.

Tembo, B., Mulenga, R. M., Sichilima, S., M'siska, K. K., Mwale, M., Chikoti, P. C., Singh, P. K., He, X., Pedley, K. F., Peterson, G. L., Singh, R. P. & Braun, H. J. 2020. Detection and characterization of fungus (Magnaporthe oryzae pathotype Triticum) causing wheat blast disease on rain-fed grown wheat (Triticum aestivum L.) in Zambia. *PLOS ONE,* 15**,** e0238724.

Thomma, B. P. H. J., Nürnberger, T. & Joosten, M. H. a. J. 2011. Of PAMPs and Effectors: The Blurred PTI-ETI Dichotomy. *The Plant Cell,* 23**,** 4-15.

Toruño, T. Y., Stergiopoulos, I. & Coaker, G. 2016. Plant-Pathogen Effectors: Cellular Probes Interfering with Plant Defenses in Spatial and Temporal Manners. *Annual Review of Phytopathology,* 54**,** 419-441.

TriantaphylidèS, C., Krischke, M., Hoeberichts, F. A., Ksas, B., Gresser, G., Havaux, M., Van Breusegem, F. & Mueller, M. J. 2008. Singlet Oxygen Is the Major Reactive Oxygen Species Involved in Photooxidative Damage to Plants. *Plant Physiology,* 148**,** 960-968.

Tsuda, K., Sato, M., Stoddard, T., Glazebrook, J. & Katagiri, F. 2009. Network Properties of Robust Immunity in Plants. *PLOS Genetics,* 5**,** e1000772.

Tufan, H. A., Mcgrann, G. R. D., Maccormack, R. & Boyd, L. A. 2012. TaWIR1 contributes to post-penetration resistance to Magnaporthe oryzae, but not Blumeria graminis f. sp. tritici, in wheat. *Molecular Plant Pathology,* 13**,** 653-665.

Tufan, H. A., Stefanato, F. L., Mcgrann, G. R. D., Maccormack, R. & Boyd, L. A. 2011. The Barley stripe mosaic virus system used for virus-induced gene silencing in cereals differentially affects susceptibility to fungal pathogens in wheat. *Journal of Plant Physiology,* 168**,** 990-994.

Udvardi, M. K., Czechowski, T. & Scheible, W.-R. D. 2008. Eleven Golden Rules of Quantitative RT-PCR. *The Plant Cell,* 20**,** 1736-1737.

Van Breusegem, F. & Dat, J. F. 2006. Reactive Oxygen Species in Plant Cell Death. *Plant Physiology,* 141**,** 384-390.

Van Butselaar, T. & Van Den Ackerveken, G. 2020. Salicylic Acid Steers the Growth-Immunity Tradeoff. *Trends in Plant Science,* 25**,** 566-576.

Vernooij, B., Friedrich, L., Morse, A., Reist, R., Kolditz-Jawhar, R., Ward, E., Uknes, S., Kessmann, H. & Ryals, J. 1994. Salicylic Acid Is Not the Translocated Signal Responsible for Inducing Systemic Acquired Resistance but Is Required in Signal Transduction. *The Plant Cell,* 6**,** 959-965.

Vleeshouwers, V. G. a. A., Rietman, H., Krenek, P., Champouret, N., Young, C., Oh, S.-K., Wang, M., Bouwmeester, K., Vosman, B., Visser, R. G. F., Jacobsen, E., Govers, F., Kamoun, S. & Van Der Vossen, E. a. G. 2008. Effector Genomics Accelerates Discovery and Functional Profiling of Potato Disease Resistance and Phytophthora Infestans Avirulence Genes. *PLOS ONE,* 3**,** e2875.

Voegele, R. T. & Mendgen, K. 2003. Rust haustoria: nutrient uptake and beyond. *New Phytologist,* 159**,** 93-100.

Vothknecht, U. C. & Soll, J. 2005. Chloroplast membrane transport: Interplay of prokaryotic and eukaryotic traits. *Gene,* 354**,** 99-109.

Vothknecht, U. C. & Westhoff, P. 2001. Biogenesis and origin of thylakoid membranes. *Biochimica et Biophysica Acta (BBA) - Molecular Cell Research,* 1541**,** 91-101.

Wang, F., Yu, G. & Liu, P. 2019a. Transporter-Mediated Subcellular Distribution in the Metabolism and Signaling of Jasmonates. *Frontiers in Plant Science,* 10.

Wang, J., Hu, M., Wang, J., Qi, J., Han, Z., Wang, G., Qi, Y., Wang, H.-W., Zhou, J.-M. & Chai, J. 2019b. Reconstitution and structure of a plant NLR resistosome conferring immunity. *Science,* 364**,** eaav5870.

Wang, J., Song, W. & Chai, J. 2023a. Structure, biochemical function, and signaling mechanism of plant NLRs. *Molecular Plant,* 16**,** 75-95.

Wang, L., Patena, W., Van Baalen, K. A., Xie, Y., Singer, E. R., Gavrilenko, S., Warren-Williams, M., Han, L., Harrigan, H. R., Hartz, L. D., Chen, V., Ton, V. T. N. P., Kyin, S., Shwe, H. H., Cahn, M. H., Wilson, A. T., Onishi, M., Hu, J., Schnell, D. J., Mcwhite, C. D. & Jonikas, M. C. 2023b. A chloroplast protein atlas reveals punctate structures and spatial organization of biosynthetic pathways. *Cell,* 186**,** 3499-3518.e14.

Wang, N., Fan, X., He, M., Hu, Z., Tang, C., Zhang, S., Lin, D., Gan, P., Wang, J., Huang, X., Gao, C., Kang, Z. & Wang, X. 2022. Transcriptional repression of TaNOX10 by TaWRKY19 compromises ROS generation and enhances wheat susceptibility to stripe rust. *The Plant Cell,* 34**,** 1784-1803.

Wang, R., Rajagopalan, K., Sadre-Bazzaz, K., Moreau, M., Klessig, D. F. & Tong, L. 2014. Structure of the Arabidopsis thaliana TOP2 oligopeptidase. *Acta Crystallogr F Struct Biol Commun,* 70**,** 555-9.

Wang, S., Li, Q.-P., Wang, J., Yan, Y., Zhang, G.-L., Yan, Y., Zhang, H., Wu, J., Chen, F., Wang, X., Kang, Z., Dubcovsky, J. & Gou, J.-Y. 2019c. YR36/WKS1-Mediated Phosphorylation of PsbO, an Extrinsic Member of Photosystem II, Inhibits Photosynthesis and Confers Stripe Rust Resistance in Wheat. *Molecular Plant,* 12**,** 1639-1650.

Wang, X., Zhai, T., Zhang, X., Tang, C., Zhuang, R., Zhao, H., Xu, Q., Cheng, Y., Wang, J., Duplessis, S., Kang, Z. & Wang, X. 2021. Two stripe rust effectors impair wheat resistance by suppressing import of host Fe–S protein into chloroplasts. *Plant Physiology,* 187**,** 2530-2543.

Wassie, M., Zhang, W., Zhang, Q., Ji, K., Cao, L. & Chen, L. 2020. Exogenous salicylic acid ameliorates heat stress-induced damages and improves growth and photosynthetic efficiency in alfalfa (Medicago sativa L.). *Ecotoxicology and Environmental Safety,* 191**,** 110206.

Watson, A., Ghosh, S., Williams, M. J., Cuddy, W. S., Simmonds, J., Rey, M.-D., Asyraf Md Hatta, M., Hinchliffe, A., Steed, A., Reynolds, D., Adamski, N. M., Breakspear, A., Korolev, A., Rayner, T., Dixon, L. E., Riaz, A., Martin, W., Ryan, M., Edwards, D., Batley, J., Raman, H., Carter, J., Rogers, C., Domoney, C., Moore, G., Harwood, W., Nicholson, P., Dieters, M. J., Delacy, I. H., Zhou, J., Uauy, C., Boden, S. A., Park, R. F., Wulff, B. B. H. & Hickey, L. T. 2018. Speed breeding is a powerful tool to accelerate crop research and breeding. *Nature Plants,* 4**,** 23-29.

Westlake, T. J., Ricci, W. A., Popescu, G. V. & Popescu, S. C. 2015. Dimerization and thiol sensitivity of the salicylic acid binding thimet oligopeptidases TOP1 and TOP2 define their functions in redox-sensitive cellular pathways. *Frontiers in Plant Science,* 6.

Weyers, J. D. B. & Paterson, N. W. 2001. Plant hormones and the control of physiological processes. *New Phytologist,* 152**,** 375-407.

White, R. 1979. Acetylsalicylic acid (aspirin) induces resistance to tobacco mosaic virus in tobacco. *Virology,* 99**,** 410-412.

Wicke, S., Schneeweiss, G. M., Depamphilis, C. W., Müller, K. F. & Quandt, D. 2011. The evolution of the plastid chromosome in land plants: gene content, gene order, gene function. *Plant Molecular Biology,* 76**,** 273-297.

Wildermuth, M. C., Dewdney, J., Wu, G. & Ausubel, F. M. 2001. Isochorismate synthase is required to synthesize salicylic acid for plant defence. *Nature,* 414**,** 562-565.

Wilson, R. A. & Mcdowell, J. M. 2022. Recent advances in understanding of fungal and oomycete effectors. *Current Opinion in Plant Biology,* 68**,** 102228.

Winter, D., Vinegar, B., Nahal, H., Ammar, R., Wilson, G. V. & Provart, N. J. 2007. An "Electronic Fluorescent Pictograph" Browser for Exploring and Analyzing Large-Scale Biological Data Sets. *PLOS ONE,* 2**,** e718.

Woodrow, I. E. & Berry, J. 1988. Enzymatic regulation of photosynthetic CO2, fixation in C3 plants. *Annual Review of Plant Physiology and Plant Molecular Biology,* 39**,** 533-594.

Woodson, Jesse d., Perez-Ruiz, Juan m. & Chory, J. 2011. Heme Synthesis by Plastid Ferrochelatase I Regulates Nuclear Gene Expression in Plants. *Current Biology,* 21**,** 897-903.

Wu, C.-H., Abd-El-Haliem, A., Bozkurt, T. O., Belhaj, K., Terauchi, R., Vossen, J. H. & Kamoun, S. 2017. NLR network mediates immunity to diverse plant pathogens. *Proceedings of the National Academy of Sciences,* 114**,** 8113-8118.

Wu, C.-H. & Derevnina, L. 2023. The battle within: How pathogen effectors suppress NLR-mediated immunity. *Current Opinion in Plant Biology,* 74**,** 102396.

Wu, G.-Z. & Bock, R. 2021. GUN control in retrograde signaling: How GENOMES UNCOUPLED proteins adjust nuclear gene expression to plastid biogenesis. *The Plant Cell,* 33**,** 457-474.

Wulff, B. B. H. & Dhugga, K. S. 2018. Wheat—the cereal abandoned by GM. *Science,* 361**,** 451-452.

Xi, L., Wu, X. N., Gilbert, M. & Schulze, W. X. 2019. Classification and Interactions of LRR Receptors and Co-receptors Within the Arabidopsis Plasma Membrane – An Overview. *Frontiers in Plant Science,* 10.

Xiao, Y., Savchenko, T., Baidoo, Edward e. K., Chehab, Wassim e., Hayden, Daniel m., Tolstikov, V., Corwin, Jason a., Kliebenstein, Daniel j., Keasling, Jay d. & Dehesh, K. 2012. Retrograde Signaling by the Plastidial Metabolite MEcPP Regulates Expression of Nuclear Stress-Response Genes. *Cell,* 149**,** 1525-1535.

Xie, X.-Z., Xue, Y.-J., Zhou, J.-J., Zhang, B., Chang, H. & Takano, M. 2011. Phytochromes regulate SA and JA signaling pathways in rice and are required for developmentally controlled resistance to Magnaporthe grisea. *Molecular Plant,* 4**,** 688-696.

Xiong, D., Huang, J., Peng, S. & Li, Y. 2017. A few enlarged chloroplasts are less efficient in photosynthesis than a large population of small chloroplasts in Arabidopsis thaliana. *Scientific Reports,* 7**,** 5782.

Xu, Q., Tang, C., Wang, X., Sun, S., Zhao, J., Kang, Z. & Wang, X. 2019. An effector protein of the wheat stripe rust fungus targets chloroplasts and suppresses chloroplast function. *Nature Communications,* 10**,** 5571.

Xu, W., Lv, H., Zhao, M., Li, Y., Qi, Y., Peng, Z., Xia, G. & Wang, M. 2016. Proteomic comparison reveals the contribution of chloroplast to salt tolerance of a wheat introgression line. *Scientific Reports,* 6**,** 32384.

Yamamoto, Y., Aminaka, R., Yoshioka, M., Khatoon, M., Komayama, K., Takenaka, D., Yamashita, A., Nijo, N., Inagawa, K., Morita, N., Sasaki, T. & Yamamoto, Y. 2008. Quality control of photosystem II: impact of light and heat stresses. *Photosynthesis Research,* 98**,** 589-608.

Yamori, W., Sakata, N., Suzuki, Y., Shikanai, T. & Makino, A. 2011. Cyclic electron flow around photosystem I via chloroplast NAD(P)H dehydrogenase (NDH) complex performs a significant physiological role during photosynthesis and plant growth at low temperature in rice. *The Plant Journal,* 68**,** 966-976.

Yang, F., Li, W. & Jørgensen, H. J. L. 2013. Transcriptional Reprogramming of Wheat and the Hemibiotrophic Pathogen Septoria tritici during Two Phases of the Compatible Interaction. *PLOS ONE,* 8**,** e81606.

Yang, H. & Luo, P. 2021. Changes in Photosynthesis Could Provide Important Insight into the Interaction between Wheat and Fungal Pathogens. *International Journal of Molecular Sciences,* 22**,** 8865.

Yang, Q., Huai, B., Lu, Y., Cai, K., Guo, J., Zhu, X., Kang, Z. & Guo, J. 2020. A stripe rust effector Pst18363 targets and stabilises TaNUDX23 that promotes stripe rust disease. *New Phytologist,* 225**,** 880-895.

Yates, Andrew d., Allen, J., Amode, R. M., Azov, A. G., Barba, M., Becerra, A., Bhai, J., Campbell, Lahcen i., Carbajo martinez, M., Chakiachvili, M., Chougule, K., Christensen, M., Contreras-Moreira, B., Cuzick, A., Da rin fioretto, L., Davis, P., De silva, Nishadi h., Diamantakis, S., Dyer, S., Elser, J., Filippi, C. V., Gall, A., Grigoriadis, D., Guijarro-Clarke, C., Gupta, P., Hammond-Kosack, Kim e., Howe, K. L., Jaiswal, P., Kaikala, V., Kumar, V., Kumari, S., Langridge, N., Le, T., Luypaert, M., Maslen, G. L., Maurel, T., Moore, B., Muffato, M., Mushtaq, A., Naamati, G., Naithani, S., Olson, A., Parker, A., Paulini, M., Pedro, H., Perry, E., Preece, J., Quinton-Tulloch, M., Rodgers, F., Rosello, M., Ruffier, M., Seager, J., Sitnik, V., Szpak, M., Tate, J., Tello-Ruiz, Marcela k., Trevanion, Stephen j., Urban, M., Ware, D., Wei, S., Williams, G., Winterbottom, A., Zarowiecki, M., Finn, Robert d. & Flicek, P. 2021. Ensembl Genomes 2022: an expanding genome resource for non-vertebrates. *Nucleic Acids Research,* 50**,** D996-D1003.

Yu, F., Park, S. & Rodermel, S. R. 2004. The Arabidopsis FtsH metalloprotease gene family: interchangeability of subunits in chloroplast oligomeric complexes. *The Plant Journal,* 37**,** 864-876.

Yuan, M., Jiang, Z., Bi, G., Nomura, K., Liu, M., Wang, Y., Cai, B., Zhou, J.-M., He, S. Y. & Xin, X.-F. 2021. Pattern-recognition receptors are required for NLR-mediated plant immunity. *Nature,* 592**,** 105-109.

Yuan, P., Tanaka, K. & Poovaiah, B. W. 2022. Calcium/Calmodulin-Mediated Defense Signaling: What Is Looming on the Horizon for AtSR1/CAMTA3-Mediated Signaling in Plant Immunity. *Frontiers in Plant Science,* 12.

Zabret, J., Bohn, S., Schuller, S. K., Arnolds, O., Möller, M., Meier-Credo, J., Liauw, P., Chan, A., Tajkhorshid, E., Langer, J. D., Stoll, R., Krieger-Liszkay, A., Engel, B. D., Rudack, T., Schuller, J. M. & Nowaczyk, M. M. 2021. Structural insights into photosystem II assembly. *Nature Plants,* 7**,** 524-538.

Zhang, E. T., Zhang, H. & Tang, W. 2021a. Transcriptomic Analysis of Wheat Seedling Responses to the Systemic Acquired Resistance Inducer N-Hydroxypipecolic Acid. *Frontiers in Microbiology,* 12.

Zhang, H., Yang, Y., Wang, C., Liu, M., Li, H., Fu, Y., Wang, Y., Nie, Y., Liu, X. & Ji, W. 2014. Large-scale transcriptome comparison reveals distinct gene activations in wheat responding to stripe rust and powdery mildew. *BMC Genomics,* 15**,** 898.

Zhang, N., Yuan, S., Zhao, C., Park, R. F., Wen, X., Yang, W., Zhang, N. & Liu, D. 2021b. TaNAC35 acts as a negative regulator for leaf rust resistance in a compatible interaction between common wheat and Puccinia triticina. *Molecular Genetics and Genomics,* 296**,** 279-287.

Zhang, Q., Zhang, X., Zhuang, R., Wei, Z., Shu, W., Wang, X. & Kang, Z. 2020. TaRac6 Is a Potential Susceptibility Factor by Regulating the ROS Burst Negatively in the Wheat–Puccinia striiformis f. sp. tritici Interaction. *Frontiers in Plant Science,* 11.

Zhang, Y., Geng, H., Cui, Z., Wang, H. & Liu, D. 2021c. Functional Analysis of Wheat NAC Transcription Factor, TaNAC069, in Regulating Resistance of Wheat to Leaf Rust Fungus. *Frontiers in Plant Science,* 12.

Zhang, Y., Liang, Z., Zong, Y., Wang, Y., Liu, J., Chen, K., Qiu, J.-L. & Gao, C. 2016. Efficient and transgene-free genome editing in wheat through transient expression of CRISPR/Cas9 DNA or RNA. *Nature Communications,* 7**,** 12617.

Zhao, J., Bi, W., Zhao, S., Su, J., Li, M., Ma, L., Yu, X. & Wang, X. 2021. Wheat Apoplast-Localized Lipid Transfer Protein TaLTP3 Enhances Defense Responses Against Puccinia triticina. *Frontiers in Plant Science,* 12.

Zheng, W., Huang, L., Huang, J., Wang, X., Chen, X., Zhao, J., Guo, J., Zhuang, H., Qiu, C., Liu, J., Liu, H., Huang, X., Pei, G., Zhan, G., Tang, C., Cheng, Y., Liu, M., Zhang, J., Zhao, Z., Zhang, S., Han, Q., Han, D., Zhang, H., Zhao, J., Gao, X., Wang, J., Ni, P., Dong, W., Yang, L., Yang, H., Xu, J.-R., Zhang, G. & Kang, Z. 2013. High genome heterozygosity and endemic genetic recombination in the wheat stripe rust fungus. *Nature Communications,* 4**,** 2673.

Zhu, T., Wang, L., Rimbert, H., Rodriguez, J. C., Deal, K. R., De Oliveira, R., Choulet, F., Keeble-Gagnère, G., Tibbits, J., Rogers, J., Eversole, K., Appels, R., Gu, Y. Q., Mascher, M., Dvorak, J. & Luo, M.-C. 2021. Optical maps refine the bread wheat Triticum aestivum cv. Chinese Spring genome assembly. *The Plant Journal,* 107**,** 303-314.

Zurbriggen, M. D., Carrillo, N., Tognetti, V. B., Melzer, M., Peisker, M., Hause, B. & Hajirezaei, M.-R. 2009. Chloroplast-generated reactive oxygen species play a major role in localized cell death during the non-host interaction between tobacco and Xanthomonas campestris pv. vesicatoria. *The Plant Journal,* 60**,** 962-973.